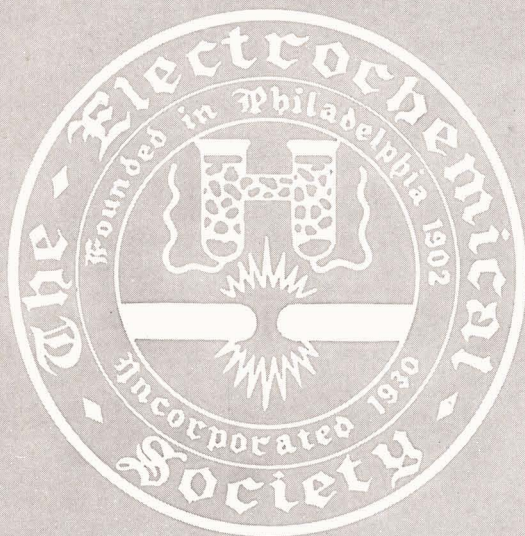


JOURNAL OF THE

Electrochemical Society

. 110, No. 6

June 1963 in Two Sections—Section II



Passivity Symposium Transactions

EDITORIAL STAFF

C. L. Faust, Chairman, Publication Committee
Cecil V. King, Editor
Norman Hackerman, Technical Editor
Ruth G. Sterns, Managing Editor
H. W. Salzberg, Book Review Editor
Daniel J. Immediato, Assistant Editor

DIVISIONAL EDITORS

W. C. Vosburgh, Battery
Paul C. Milner, Battery
G. A. Marsh, Corrosion
A. C. Makrides, Corrosion
Morris Cohen, Corrosion
Harry C. Gatos, Corrosion—Semiconductors
Louis J. Frisco, Electric Insulation
Seymour Senderoff, Electrodeposition
H. C. Froelich, Electronics
Ephraim Banks, Electronics
Charles S. Peet, Jr., Electronics—Semiconductors
D. R. Frankl, Electronics—Semiconductors
Sherlock Swann, Jr., Electro-Organic
Stanley Wawzonek, Electro-Organic
John M. Blocher, Jr., Electrothermics and Metallurgy
J. H. Westbrook, Electrothermics and Metallurgy
H. Barclay Morley, Industrial Electrolytic
C. W. Tobias, Theoretical Electrochemistry
A. J. deBethune, Theoretical Electrochemistry
R. M. Hurd, Theoretical Electrochemistry

ADVERTISING OFFICE

ECS
30 East 42 St., New York 17, N. Y.

ECS OFFICERS

W. J. Hamer, President
National Bureau of Standards,
Washington, D. C.
Lyle I. Gilbertson, Vice-President
Aerospace Placement Corp.,
1518 Walnut St.,
Philadelphia 2, Pa.
E. B. Yeager, Vice-President
Western Reserve University,
Cleveland, Ohio
H. J. Read, Vice-President
Dept. of Metallurgy,
Pennsylvania State University,
University Park, Pa.
Ernest G. Enck, Treasurer
Windrush,
Chatham, Mass.
Ivor E. Campbell, Secretary
National Steel Corp., Weirton, W. Va.
Robert K. Shannon, Executive Secretary
National Headquarters, The ECS,
30 East 42 St., New York 17, N. Y.

Manuscripts submitted to the Journal should be sent, in triplicate, to the Editorial Office at 30 East 42 St., New York 17, N. Y. They should conform to the revised Instructions to Authors published on pp. i-ii of this issue. Manuscripts so submitted become the property of The Electrochemical Society and may not be published elsewhere, in whole or in part, unless permission is requested of and granted by the Editor. The Electrochemical Society does not maintain a supply of reprints of papers appearing in its Journal. A photoprint copy of any particular paper, however, may be obtained by corresponding direct with the Engineering Societies Library, 345 E. 47 St., New York, N. Y.

Inquiries re positive microfilm copies of volumes should be addressed to University Microfilms, Inc., 313 N. First St., Ann Arbor, Mich. Walter J. Johnson, Inc., 111 Fifth Ave., New York 3, N. Y., have reprint rights to out-of-print volumes of the Journal, and also have available for sale back volumes and single issues, with the exception of the current calendar year. Anyone interested in securing back copies should correspond direct with them.

Journal of the Electrochemical Society

JUNE 1963

VOL. 110 • NO. 6

Section II

CONTENTS

Introduction. <i>M. Cohen, N. Hackerman, and H. H. Uhlig</i>	596
Technical Papers	
A General Thermodynamic Theory of the Potential of Passive Electrodes and Its Influence on Passive Corrosion. <i>K. J. Vetter</i>	597
Anodic Passivation of Nickel in Sulfuric Acid Solutions. <i>N. Sato and G. Okamoto</i>	605
The Initiation of Pores in Anodic Oxide Films Formed on Aluminum in Acid Solutions. <i>T. P. Hoar and J. Yahalom</i>	614
The Corrosion of 1100 Aluminum in Oxygen-Saturated Water at 70°C. <i>J. E. Draley, S. Mori, and R. E. Loess</i>	622
Contribution to the Electrochemical Behavior of Chromium and Iron-Chromium Alloys in the Transpassive Region. <i>Th. Heumann and H. S. Panesar</i>	628
The Passivity of Iron-Chromium Alloys. <i>G. Aronowitz and N. Hackerman</i>	633
The Influence of Film Thickness on the Thermodynamic Properties of Thin Oxide Layers on Iron. <i>K. G. Weil</i>	640
Ion-Exchange Properties of the Film on Passive Iron and Steel. <i>G. H. Cartledge and D. H. Spahrbrter</i>	644
Corrosion and Passivity of Molybdenum-Nickel Alloys in Hydrochloric Acid. <i>H. H. Uhlig, P. Bond, and H. Feller</i>	650
Optical Studies of the Formation and Breakdown of Passive Films Formed on Iron Single Crystal Surfaces in Inorganic Inhibitor Solutions. <i>J. Kruger</i>	654
Investigation into the Nature of Anodic Passive and Barrier Coatings. <i>K. Schwabe</i>	663
The Anodic Oxidation of Iron in a Neutral Solution, II. Effect of Ferrous Ion and pH on the Behavior of Passive Iron. <i>M. Nagayama and M. Cohen</i>	670
Valency Changes in the Surface Oxide Films on Metals. <i>H. S. Isaacs and J. S. Llewellyn Leach</i>	680
The Growth of Thin Passivating Layers on Metallic Surfaces. <i>M. Fleischmann and H. R. Thirsk</i>	688
Throwing Power of the Current in Anodic and Cathodic Protection. <i>W. A. Mueller</i>	698
On the Passivity of Manganese in Acid Solutions. <i>K. E. Heusler</i>	703

Published monthly by The Electrochemical Society, Inc., at 215 Canal St., Manchester, N. H.; Executive Offices, Editorial Office and Circulation Dept., and Advertising Office at 30 East 42 St., New York 17, N. Y., combining the JOURNAL and TRANSACTIONS OF THE ELECTROCHEMICAL SOCIETY. Statements and opinions given in articles and papers in the JOURNAL OF THE ELECTROCHEMICAL SOCIETY are those of the contributors, and The Electrochemical Society assumes no responsibility for them. Subscription to members as part of membership service; subscription to nonmembers \$24.00 plus \$1.50 for postage outside U.S. and Canada. Single copies \$1.70 to members, \$2.25 to nonmembers. © 1963 by The Electrochemical Society, Inc. Entered as second-class matter at the Post Office at Manchester, N. H., under the act of August 24, 1912.

Introduction

The First International Symposium on Passivity in 1957 grew out of conversations at the San Francisco meeting of the Society in 1956. The late Dr. K. F. Bonhoeffer, then Director of the Max Planck Institut für Physikalische Chemie at Göttingen and in whose laboratory research on passivity had received great emphasis, was attracted to the proposal of exchanging ideas on an international level. With characteristic enthusiasm, he set about to organize the meeting after obtaining the generous financial support of the Deutsche Bunsen Gesellschaft. The Board of Directors of The Electrochemical Society voted to co-sponsor the meeting, and this action was followed by similar sponsorship of the Faraday Society. Upon the untimely death of Dr. Bonhoeffer early in 1957, Dr. U. F. Franck took over the final arrangements. The Symposium was held in the relaxing surroundings of Schloss Heiligenberg located along the old Roman road running through a wooded area near Darmstadt. Fruitful exchange of ideas continued for 5½ days, with running translations between German and English, and the meeting was an outstanding success.

The Second International Symposium was organized under the same auspices of the three societies mentioned above, and was held at the University of Toronto, September 3-7, 1962. The National Research Council of Canada made available a major grant in support of the Symposium; this was followed by additional grants from the Corrosion Handbook Fund of The Electrochemical Society, and also from The American Society for Testing Materials. Fifty-eight participants from 7 countries met on the attractive University campus to hear a total of 27 papers, each followed by active discussions. Most of these papers have now been assembled and appear in this special issue as a further contribution to the science of passivity in metals and alloys. The present issue parallels the previous special issue of *The Zeitschrift für Elektrochemie*, Vol. 62, 619-827 (1958), which contains all the papers of the First Symposium.

It is quite obvious on reading these reports that some questions still remain unanswered, and that, despite the impressive advances made during the past 10 years, further research is needed. In particular, the exact structure of the passive film remains elusive. Further knowledge is needed regarding conditions which establish passivity in alloys, of which perhaps stainless steels are an outstanding example. As in many parallel fields of science, application has run ahead of theory. There can be little question, however, that once theory more nearly catches up with experiment, practice will be enabled to move ahead so much the faster. Symposia like the one presently recorded are a major factor in both supplying and inspiring the much needed understanding.

March 25, 1963

M. Cohen
N. Hackerman
H. H. Uhlig

A General Thermodynamic Theory of the Potential of Passive Electrodes and Its Influence on Passive Corrosion

K. J. Vetter

Fritz-Haber-Institut of the Max-Planck-Gesellschaft, Berlin-Dahlem, Germany

ABSTRACT

A theory of the electrode potential of nonstoichiometric electron conductive metal oxides MeO_n on a foreign metal is presented. When the oxygen ions of the oxide are in equilibrium with the electrolyte the oxide electrode potential is $e_n = (1/2F) \cdot d\Delta G(n)/dn - 0.059 \cdot \text{pH}$ with the free enthalpy $\Delta G(n)$ for the reaction $\text{Me} + n\text{H}_2\text{O} \rightarrow \text{MeO}_n + n\text{H}_2$ as a function of the degree of oxidation n . The oxide electrode potential for the case of an equilibrium of the metal ions between the oxide and the electrolyte is also derived. The condition of equilibrium between the oxide MeO_n and the electrolyte with dissolved z -valent metal ions ($z \neq 2n$) is given. The "equilibrium oxide" relative to its parent metal and the corresponding potential are discussed. The potential of a passive electrode depends only on the surface oxide in contact with the electrolyte and is independent of the construction of the passive layer.

The effect of the corrosion rate and of the current density on the passive potential and on the construction and composition of the inner layer are discussed. The establishment of a stationary layer is explained. The experimental pH dependence of the corrosion current density of equal surface oxides of Ni, Fe, and Cr are analyzed. For this reason passive potentials against the hydrogen electrode at the same pH value are compared.

In electrolytic solutions the passivity of metals is caused by a porefree (1) oxidic layer, which prevents the direct contact of the metal and the electrolyte. The behavior of the passive metal depends on the properties of this passive layer, especially on the thickness, chemical composition, rate of dissolution in the electrolyte, and the electronic and ionic conductivity. In most cases of clear¹ passivity the electronic conductivity is good. The rate of dissolution of the passive layer in the electrolyte is a function of the chemical composition at the interface passive layer/electrolyte. After a stationary state of this layer has been reached, the rate of dissolution is equal to the remaining corrosion rate of the metal in the passive state. Therefore the corrosion rate is one of the most important properties of the passive metal.

The chemical composition and thickness of the passive layer depend on the potential. The stationary thickness is regulated by the ionic current through the layer, which depends on the electrical field strength in the layer. The field strength and therefore the ionic current increase with increasing potential difference in the layer and decrease with increasing layer thickness. By changing the layer thickness the ionic current density can become equal to the corrosion current density. At this point, the stationary state of the layer will be reached. In this case the anodic rate of formation of passive oxide will be equal to the dissolution rate in the electrolyte.

In this paper the composition of a nonstoichiometric inhomogeneous passive layer shall be discussed according to Vetter (2) as a function of the

potential, corrosion rate, pH-value, and electrolyte concentration of ions of the passive metal on the basis of thermodynamic considerations.

Potential of an Oxide Electrode with a Nonstoichiometric Oxide with Electronic Conductivity

Oxide on a Foreign Metal. Oxygen Ion Equilibrium Oxide/Electrolyte

Single-phase (homogeneous) oxide.—This problem will be worked out most simply for the case of an arbitrary nonstoichiometric oxide, oxyhydrate, or hydroxide $\text{MeO}_n \cdot m\text{H}_2\text{O}$ on a foreign metal other than the parent metal Me in the oxide. Later these considerations will be extended to the case of an oxide in contact with its parent metal Me. It may be assumed that the foreign metal is completely insoluble in the oxide. In this case the metal simply acts as an electron carrier. Figure 1 represents the phase scheme for this case. At the phase boundaries the equilibrium of the electrons $\beta(1,2)$ and of the oxygen ions $\beta(2,3)$ O^{2-} (oxide) + 2H^+ (electrolyte) $\rightleftharpoons \text{H}_2\text{O}$ (electrolyte) are established (straight lines). All other reactions are assumed to be completely inhibited (dotted lines). Later, this restriction will be

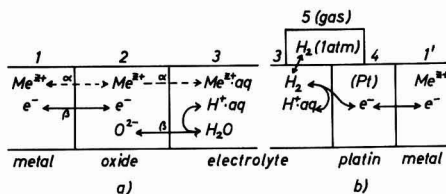
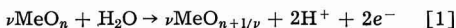


Fig. 1. (a) Phase scheme of an oxide electrode in contact with a foreign metal; (b) hydrogen reference electrode.

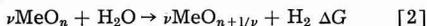
¹ The definition of passivity is very difficult. A definition which is satisfactory in all cases cannot be found as yet.

removed to a certain extent. Instead of reaction $\beta(2,3)$ the reaction $\beta'(2,3)$ O^{2-} (oxide) + H^+ (electrolyte) \rightleftharpoons OH^- (oxide) can occur. Both reactions are thermodynamically equivalent. Therefore only the first one $\beta(2,3)$ shall be discussed further.

By an anodic current O^{2-} ions will be taken up, and for each O^{2-} ion two electrons of the own metal ions will be delivered to the foreign metal. If the anodic current is so small that the equilibrium potential differences at the two phase boundaries 1,2 and 2,3 are not appreciably disturbed, both phase boundary reactions occur reversibly. Therefore, the total electrode process is a thermodynamically reversible absorption of oxygen atoms by the oxide MeO_n or $MeO_n \cdot mH_2O$.² Through this process the degree of oxidation n will be increased by a small amount. In the case $\beta'(2,3)$ protons H^+ will be emitted in a thermodynamically reversible manner. The assumption is that the phase width is large enough that no further oxide phase is formed. For ν moles MeO_n and $2F$ coulombs the reversible overall electrode reaction is



Against a hydrogen electrode in the same electrolyte (same pH value, Fig. 1) the reversible cell reaction is



with the electrode reaction valency 2 and the free enthalpy of the reaction^{2*} ΔG . The reversible cell voltage becomes $\epsilon = +\Delta G/2F$.

This free enthalpy of the reaction ΔG can be calculated from the values of free enthalpies of formation $\Delta G(n)$ and $\Delta G(n+1/\nu)$ for the oxides MeO_n and $MeO_{n+1/\nu}$ according to



Therefore ΔG amounts to

$$\Delta G = \nu \cdot [\Delta G(n+1/\nu) - \Delta G(n)] \\ = \frac{\Delta G(n+1/\nu) - \Delta G(n)}{1/\nu} \quad [5]$$

For the limiting case when $\Delta n = 1/\nu \rightarrow 0$ one gets

$$\lim_{\nu \rightarrow \infty} \Delta G = \lim_{\Delta n \rightarrow 0} \Delta G = \frac{d\Delta G(n)}{dn} \quad [6]$$

Therefore the reversible cell voltage against the hydrogen electrode of the same pH value can be expressed by the differential quotient of the free enthalpy of formation of the oxide MeO_n to the degree of oxidation n

$$E_o = + \frac{1}{2F} \cdot \frac{d\Delta G(n)}{dn} \quad [7]$$

Against the standard hydrogen electrode the potential ϵ_h of the oxide electrode on a foreign metal is (at 25°C)

$$\epsilon_h = \frac{1}{2F} \cdot \frac{d\Delta G(n)}{dn} - 0.059 \cdot pH \quad [8]$$

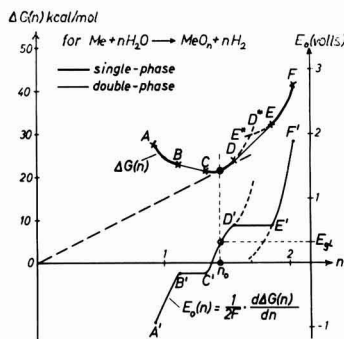


Fig. 2. Free reaction enthalpy $\Delta G(n)$ and the deviated oxide electrode potential E_o (Eq. [8]) as function of the degree of oxidation n (arbitrary assumed values).

If an oxide $MeO_n \cdot mH_2O$ is considered, the value of $\Delta G(n)$ corresponds to the reaction $Me + (n+m)H_2O \rightleftharpoons MeO_n \cdot mH_2O + nH_2$. Equations [5] to [8] are likewise valid. However, the value of the potential ϵ_h depends on the content m of water, which can be a function $m = f(n)$ of n . In Fig. 2 $\Delta G(n)$ is represented as a function of the degree of oxidation n by assuming arbitrary values for $\Delta G(n)$. Equations [7] or [8] are first of all only applicable to one of the three ranges of homogeneous solid solution series of the oxide, which are assumed in Fig. 2.

For a nonhydrated ($m = 0$) oxide MeO_n Eq. [7] and [8] can also be formulated by using the standard free enthalpy of formation of the oxide from the elements $\Delta G_o(n)$ following the paper of Bell and Huber (3). From the relation

$$\Delta G(n) = \Delta G_o(n) - n \cdot \Delta G_o(H_2O)$$

with the free enthalpy of formation of water $\Delta G_o(H_2O)$ according to $H_2 + 1/2 O_2 \rightarrow H_2O$, Eq. [7] transforms into

$$E_o = \frac{1}{2F} \cdot \frac{d\Delta G_o(n)}{dn} - \frac{1}{2F} \Delta G_o(H_2O) \quad [9]$$

The term $-(1/2F) \cdot \Delta G_o(H_2O) = +1.23v$ is the potential of the reversible standard oxygen electrode.

For a hydrated oxide $MeO_n \cdot mH_2O$ with a water content $m = f(n)$ depending on the degree of oxidation n the relation

$$\Delta G(n) = \Delta G_o(n) - (n+m) \cdot \Delta G_o(H_2O) \quad [10]$$

is valid. Therefore the standard oxide potential E_o , according to the formulation of Bell and Huber (3), becomes

$$E_o = \frac{1}{2F} \cdot \frac{d\Delta G_o(n)}{dn} - (1 + dm/dn) \cdot \frac{1}{2F} \cdot \Delta G_o(H_2O) \quad [11]$$

Regarding $\Delta G_o(n,m)$ as a function of two independent variables n and m , $d\Delta G_o(n)/dn$ can be formulated as

$$\frac{d\Delta G_o(n,m)}{dn} = \frac{\partial \Delta G_o(n,m)}{\partial n} + \frac{\partial \Delta G_o(n,m)}{\partial m} \cdot \frac{dm}{dn}$$

Using this relation, Eq. [11] changes to

$$E_o = \frac{1}{2F} \cdot \frac{\partial \Delta G_o(n,m)}{\partial n}$$

² Instead of $MeO_n \cdot mH_2O$ the abbreviated formula for the oxide MeO_n shall be used in the following part. The same treatment may also be applied to $MeO_n \cdot mH_2O$.

^{2*} Change of Gibbs free energy ΔG .

$$+ \frac{1}{2F} \cdot \left[\frac{\partial \Delta G_o(n, m)}{\partial m} - \Delta G_o(\text{H}_2\text{O}) \right] \cdot \frac{dm}{dn} - \frac{1}{2F} \cdot \Delta G_o(\text{H}_2\text{O}) \quad [12]$$

The bracket in the second term represents the free enthalpy of association of the crystal water.

In the special case of the frequently observed oxide series $\text{Me}(\text{OH})_2 \rightarrow \text{MeO}(\text{OH}) \rightarrow \text{MeO}_2$ which mostly form series of mixed crystals without miscibility gap, the water content m is $m = a - n$ (here $2 - n$). Because $m = 2 - n$ is $dm/dn = -1$ and Eq. [11] simplifies to

$$E_o = \frac{1}{2F} \cdot \frac{d\Delta G_o(n)}{dn} = \frac{1}{2F} \cdot \frac{d\Delta G(n)}{dn} \quad [11']$$

(for $m = a - n$)

In all cases the electrode potential ϵ_h against the standard hydrogen electrode is $\epsilon_h = E_o - 0.059 \cdot \text{pH}$.

Double-phase (heterogeneous) oxides.— During the oxidation of the oxide the upper limit n_1 (point D in Fig. 2 for example) of the phase range may be reached. Then, further oxidation causes a formation of a new phase of the lower limit n_2 (point E in Fig. 2), if the formation of crystal nuclei is fast enough. Then both phases are in equilibrium. When two phases are in equilibrium, the potential will not depend on the ratio of the quantities of the phases. The potential will remain constant during the oxidation until the first phase with the upper limit n_1 is consumed. By analogy the preceding evaluation, the potential is now defined by the quotient of differences instead of the differential quotient

$$\epsilon_h = \frac{1}{2F} \cdot \frac{\Delta G(n_2) - \Delta G(n_1)}{n_2 - n_1} - 0.059 \cdot \text{pH} \quad [13]$$

This equation is used for the two-phase ranges in Fig. 2. If in Fig. 2 the upper and the lower limits of two succeeding single-phase ranges are connected by straight lines, the first equation with the differential quotient can be used in the whole range of degrees of oxidation n . The curve A'F' in Fig. 2 represents the potential ϵ as a function of the degree of oxidation n according to Eq. [8] and [9] or also [13].

Oxide on a Foreign Metal. Metal Ion Equilibrium at the Phase Boundary Oxide/Electrolyte

Contrary to the foregoing discussion on oxide on a foreign metal the equilibrium $\alpha(2,3)$ of the metal ions at the phase boundary oxide/electrolyte $\text{Me}^{z+}(\text{oxide}) \rightleftharpoons \text{Me}^{z+}(\text{electrolyte})$ shall be established. Moreover the equilibrium of the electrons $\beta(1,2)$ and a sufficiently high electronic conductivity shall be assumed again. This means that the reactions

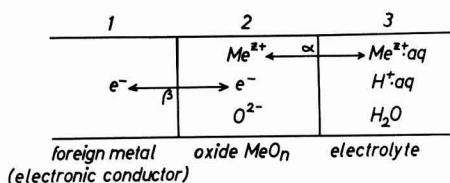
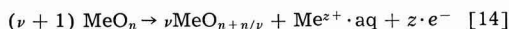


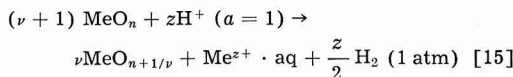
Fig. 3. Phase scheme of an oxide electrode in contact with a foreign metal. Equilibrium of the metal ions.

represented in Fig. 3 are in equilibrium, and all other reactions are essentially inhibited.

The valency z of the metal ion Me^{z+} in the electrolyte must not generally have the same value as the average valency $2n$ of the metal ions in the oxide. By an anodic current metal ions Me^{z+} will be transferred from the oxide into the electrolyte, and the remaining negative charge will be delivered as z electrons to the foreign metal. The total electrode process is a thermodynamically reversible transfer of a metal atom from the oxide and the formation of a metal ion Me^{z+} in the electrolyte. It is assumed that the current is so small that the equilibrium potential differences at the two phase boundaries 1,2 and 2,3 (Fig. 3) are not disturbed to any significant extent. The degree of oxidation n will be increased through this process by a small amount $\Delta n (=n/\nu)$. The quantity of oxygen ions in the oxide remains constant during this process. Therefore the reversible electrode reaction, for zF coulombs and considering a single phase range of sufficient width, is



This reaction involves no hydrogen ions. Therefore the electrode potential will not depend on the pH value, and it will be suitable to choose the standard hydrogen electrode as counter electrode in a reversible galvanic cell. The reversible cell reaction is then



with the electrode reaction valency z . The reversible cell voltage ϵ_h results from the free enthalpy ΔG of reaction [15] according to $\epsilon_h = +\Delta G/zF$. ΔG results by using $\Delta G(n)$ of reaction $\text{Me} + n\text{H}_2\text{O} \rightarrow \text{MeO}_n + n\text{H}_2$ and ΔG_{Me} of reaction $\text{Me} + z\text{H}^+ (a=1) \rightarrow \text{Me}^{z+} \cdot \text{aq} + (z/2)\text{H}_2$ according to the relation

$$\Delta G = \nu [\Delta G(n+n/\nu) - \Delta G(n)] - \Delta G(n) + \Delta G_{\text{Me}} \quad [16]$$

Since

$$\lim_{\nu \rightarrow \infty} \nu \cdot \left[\Delta G \left(n + \frac{n}{\nu} \right) - \Delta G(n) \right] = n \cdot \frac{d\Delta G(n)}{dn}$$

and $\Delta G_{\text{Me}} = zF \cdot \epsilon_{\text{Me}}$ where ϵ_{Me} is the reversible potential of a $\text{Me}/\text{Me}^{z+} \cdot \text{aq}$ -electrode against the standard hydrogen electrode, the potential ϵ_h of the oxide electrode under consideration becomes

$$\epsilon_h = \epsilon_{\text{Me}} + \frac{n}{zF} \cdot \frac{d\Delta G(n)}{dn} - \frac{1}{zF} \cdot \Delta G(n) \quad [17]$$

with

$$\epsilon_{\text{Me}} = E_{o, \text{Me}} + \frac{RT}{zF} \cdot \ln a_{\text{Me}^{z+}}$$

$E_{o, \text{Me}}$ is the standard potential of the metal ions Me^{z+} . ϵ_{Me} is the reversible potential of the electrolyte in contact with the compact metal Me according to the Nernst equation, and the term $[n(d\Delta G(n)/dn) - \Delta G(n)]/zF$ is the deviation of the oxide electrode potential from the reversible potential of the active Me/Me^{z+} electrode.

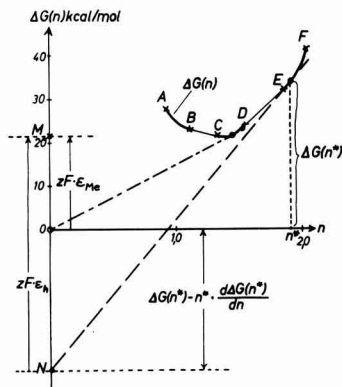
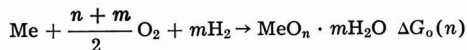


Fig. 4. Free reaction enthalpy $\Delta G(n)$ as function of the degree of oxidation n (arbitrary assumed values). Evaluation of the oxide potential for an equilibrium of the metal ions.

Here instead of $\Delta G(n)$ one can also use the free enthalpy of formation of the oxide $\text{MeO}_n \cdot m\text{H}_2\text{O}$ from the elements $\Delta G_o(n)$ according to the reaction



Then Eq. [10] and [11] are to be taken for $\Delta G(n)$ and $d\Delta G(n)/dn$. However, the formula received in this manner is not very clear.

Equation [17] is graphically interpreted in Fig. 4 and is for the time being only valid for a single-phase, homogeneous oxide with sufficient phase width. For a double-phase heterogeneous oxide $\text{MeO}_{n_1}/\text{MeO}_{n_2}$ instead of the differential quotient $d\Delta G(n)/dn$ the quotient of differences $[\Delta G(n_2) - \Delta G(n_1)]/(n_2 - n_1)$ is to be used. It results that

$$\epsilon_h = \epsilon_{\text{Me}} + \frac{1}{zF} \frac{n_1 \Delta G(n_2) - n_2 \Delta G(n_1)}{n_2 - n_1} \quad [18]$$

The establishment of the equilibrium of the metal ions Me^{z^+} at the phase boundary oxide/electrolyte is only guaranteed if other electrochemical phase boundary reactions are either totally inhibited or in equilibrium. For example it may be possible, that for a nonstoichiometric oxide with $2n \neq z$, ions of the same metal but having another valency z^* can also be dissolved from the oxide in the electrolyte. Only if the electrolyte is saturated with these metal ions Me^{z^*+} with respect to the oxide will the equilibrium of the Me^{z^+} ions not be disturbed.³ Between the Me^{z^+} ions and the Me^{z^*+} ions there exists a redox potential

$$\epsilon_{\text{red}} = E_{z/z^*} + \frac{RT}{(z^* - z)F} \cdot \ln \frac{a^*}{a} \quad [19]$$

Because of the good electronic conductivity and according to Eq. [17] or [18] ϵ_h must be equal to ϵ_{red} (Eq. [19]). This relation defines a ratio a^*/a of the activities of the two dissolved metal ions of different valency. In many cases this ratio will be extremely small. Then the electrolyte can be saturated near the oxide surface through the dissolution of extremely small amounts of z^* valent metal ions. In

³ For example, MnO_2 ($2n = 4$), Mn^{2+} -ions (z), and Mn^{3+} -ions (z^*).

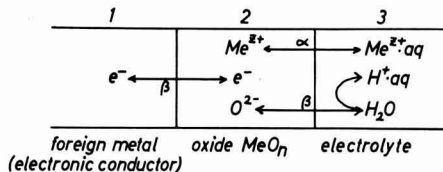


Fig. 5. Phase scheme of an oxide electrode in contact with a foreign metal. Equilibrium of the oxide with the electrolyte.

this manner the conditions will not be appreciably disturbed. However, this circumstance had to be taken into consideration for an application of Eq. [17] or [18].

Oxide on a Foreign Metal in Equilibrium with the Electrolyte (Simultaneous Metal Ion and Oxygen Ion Equilibrium)

If all equilibria, the metal ion equilibrium $\alpha(2,3)$ $\text{Me}^{z^+}(\text{oxide}) \leftrightarrow \text{Me}^{z^+}(\text{electrolyte})$, all other metal ion equilibria $\text{Me}^{z^*+}(\text{oxide}) \leftrightarrow \text{Me}^{z^*+}(\text{electrolyte})$, and the oxygen ion equilibrium $\beta(2,3)$ $\text{O}^{2-}(\text{oxide}) + 2\text{H}^+(\text{electrolyte}) \rightleftharpoons \text{H}_2\text{O}(\text{electrolyte})$ or $\text{O}^{2-}(\text{oxide}) + \text{H}^+(\text{electrolyte}) \rightleftharpoons \text{OH}^-(\text{oxide})$ are established (Fig. 5), the oxide is in a total solubility equilibrium with the electrolyte. This solubility equilibrium differs from the normally discussed equilibrium between a solid stoichiometric substance and a saturated solution only because of the different valency of the metal ions in the electrolyte (z) and in the oxide ($2n$). The normally used solubility product is defined for a solid substance of the same valency as the dissolved ions.

Now we shall discuss the fact that the condition $2n = z$ is not necessary. A solubility equilibrium can also exist when $2n \neq z$. For the evaluation of the equilibrium condition for this case the potentials according to Eq. [8] and [17] must be equal. From Eq. [8] and [17] it results that

$$\epsilon_h = \epsilon_{\text{H}} + \frac{1}{zF} \cdot \frac{d\Delta G(n)}{dn} = \epsilon_{\text{Me}} + \frac{n}{zF} \cdot \frac{d\Delta G(n)}{dn} - \frac{1}{zF} \cdot \Delta G(n) \quad [20]$$

With the potential $\epsilon_{\text{H}} = (RT/F) \cdot \ln a_{\text{H}^+}$ of the hydrogen electrode against the standard hydrogen electrode, and after transformation

$$(n - \frac{z}{2}) \cdot \frac{d\Delta G(n)}{dn} = \Delta G(n) - zF(\epsilon_{\text{Me}} - \epsilon_{\text{H}}) \quad [21]$$

takes place for the equilibrium condition. The terms $zF(\epsilon_{\text{Me}} - \epsilon_{\text{H}})$ and $z/2$ are fixed by the concentrations (activities) of the metal ions and of the hydrogen ions in the electrolyte. According to Eq. [21] the degree of oxidation n of the oxide is defined by the electrolyte. Only one oxide with a definite degree of oxidation n exists in equilibrium with a fixed electrolyte. The value n depends on the electrolyte according to Eq. [21].

Because of a constant value

$$\epsilon_{\text{Me}} - \epsilon_{\text{H}} = E_{\text{o,Me}} + \frac{RT}{zF} \ln a_{\text{Me}^{z^+}} - \frac{RT}{F} \ln a_{\text{H}^+} = \text{constant} \quad [22]$$

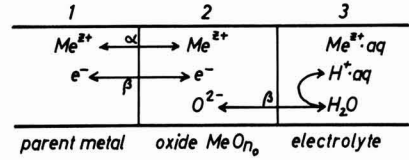
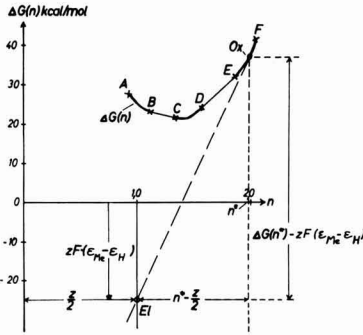


Fig. 7. Phase scheme of an oxide electrode in contact with the parent metal.

On the contrary the parent metal can only be in contact with one oxide, the "equilibrium oxide" MeO_{n_0} (or $MeO_{n_0} \cdot n_0 H_2O$). The composition of this equilibrium oxide generally will depend on the temperature. However at a constant defined temperature only one oxide can exist in a thermodynamic equilibrium with the own metal. In this case, in addition to Fig. 1 the metal ion equilibrium at the phase boundary metal/oxide has also to be established. Figure 7 represents these conditions. In the anodic direction reactions $\alpha(1,2)$ and $\beta(2,3)$ result in the anodic formation of the equilibrium oxide according to



or against the hydrogen electrode in the same electrolyte



The free enthalpy of the reaction is $\Delta G(n_0)$ and therefore the reversible potential of the "equilibrium" oxide electrode is

$$\epsilon_{o,h} = + \frac{\Delta G(n_0)}{2n_0 F} - 0.059 \cdot pH \quad [26]$$

Simultaneously the reaction sequences $\beta(1,2)$ and $\beta(2,3)$ of the case already discussed are in equilibrium so that the potential can also be calculated by using Eq. [8] with the differential quotient of $\Delta G(n)$. Therefore as to be seen in Fig. 2, the tangent of the $\Delta G(n)$ curve at the value n_0 goes through the zero point. The tangent from the zero point to the $\Delta G(n)$ curve results in the value n_0 at the point of contact.

Nonequilibrium Oxide MeO_n on an Intermediate Layer with Electronic Conductivity (Passive Layer)

For all previous considerations of the discussion on potential of oxide electrodes in this paper an electronic equilibrium between the metal and the oxide was supposed. This means that the electrochemical potential $\eta = \mu + zF \cdot \psi^A$ of the electrons from the oxide throughout all the phases up to the metal of the voltmeter wires (mostly copper) is constant. Therefore the potential difference $\psi_1 - \psi_2 = \psi_{1,2}$ results as

$$\psi_{1,2} = \psi_1 - \psi_2 = \frac{1}{F} (\mu_1 - \mu_2) \quad [27]$$

since $\eta = \mu_1 - F \cdot \psi_1 = \mu_2 - F \cdot \psi_2$. If another metal, for example the parent metal (phase 1a) or any electronic conductor, for example the equilibrium

⁴ μ is the chemical potential, μ_e is the chemical potential of the electrons = Fermi potential, ψ is the Galvani potential.

Fig. 6. Free reaction enthalpy $\Delta G(n)$ as function of the degree of oxidation n (arbitrary assumed values). Evaluation of the oxide potential and the degree of oxidation n^* for an equilibrium between oxide and electrolyte.

the degree of oxidation is defined and constant. A "solubility product" $[P(n,z)]$ follows from Eq. [22], thus

$$P(n,z) = a_{Me^{z+}} \cdot a_{OH^-} = P_{H_2O}^z \cdot \exp\left(-\frac{zFE_{o,Me}}{RT}\right) \cdot \exp\left(\frac{\Delta G(n) - (n-z/2) \cdot \Delta G(n)/dn}{RT}\right) \quad [23]$$

with the ionic product $P_{H_2O} = a_{H^+} \cdot a_{OH^-}$ of water. This solubility product depends on the function $\Delta G(n)$ and the valency z of the dissolved metal ions.

Equation [21] can be graphically interpreted in a similar manner as Eq. [8] and [17] in Fig. 2 or 4, respectively. The values of the abscissa and ordinate of point El in Fig. 6 are defined by the electrolyte. The coordinates of point El are $z/2$ (n -scale) and $zF \cdot (\epsilon_{Me} - \epsilon_H)$ in the energy scale ($\Delta G(n)$ -scale). The tangent to the $\Delta G(n)$ curve from the point El results in the degree n^* of oxidation at the point of contact Ox. The slope of the tangent amounts to the reversible electrode potential

$$\epsilon_h = \frac{1}{2F} \cdot \frac{d\Delta G(n^*)}{dn} + \frac{RT}{F} \ln a_H + \quad [8']$$

as calculated from Eq. [8]. For a defined electrolyte ($[Me^{z+}], [H^+]$) only one oxide MeO_{n^*} with a fixed potential ϵ_h (Eq. [8']) exists in the mentioned case of equilibria. Because of the assumed high electronic conductivity of the oxide the condition Eq. [19] $\epsilon_{red} = \epsilon_h$ must be fulfilled for all other possible valencies of the parent metal ions in the electrolyte. In many cases the necessary concentrations of these metal ions will be small or even extremely small. Then this mentioned condition can be easily verified in an experiment.

Oxide on Its Parent Metal (Equilibrium Oxide MeO_{n_0})

At passive metals the oxide layer $MeO_n \cdot mH_2O$ is on its own parent metal of the oxide and not on a foreign metal. Therefore the preceding consideration is to be expanded for a contact between the oxide and its own metal. Here the assumption that the metal is insoluble in the oxide is no longer valid.

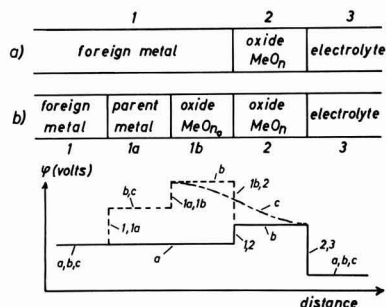


Fig. 8. (a and b). Change of the potential distribution by insertion of other electronic conductors (parent metal, equilibrium oxide MeO_{n_0}) between the foreign metal and the oxide of an oxide electrode; (c) without miscibility gap.

oxide (phase 1b) is inserted between the metal (phase 1) and the oxide (phase 2) as shown in Fig. 8, the cell voltage against the same reference electrode will not be changed. The potential difference $\psi_{1,2} = \psi_1 - \psi_2$ consists of $\psi_{1,2} = \psi_{1,1a} + \psi_{1a,1b} + \psi_{1b,2}$ (Fig. 8). Because of the relations

$$\begin{aligned} \psi_{1,1a} &= \psi_1 - \psi_{1a} = \frac{1}{F} \cdot (\mu_1 - \mu_{1a}) \\ \psi_{1a,1b} &= \psi_{1a} - \psi_{1b} = \frac{1}{F} \cdot (\mu_{1a} - \mu_{1b}) \\ \psi_{1b,2} &= \psi_{1b} - \psi_2 = \frac{1}{F} \cdot (\mu_{1b} - \mu_2) \\ \hline \psi_{1,2} &= \psi_1 - \psi_2 = \frac{1}{F} \cdot (\mu_1 - \mu_2) \end{aligned} \quad [27a]$$

the value $\psi_{1,2}$ remains unchanged in the case when another or even some other electronic conductors are inserted between the metal and the oxide.

The thus inserted electronic conductors can be in the form of the equilibrium oxide MeO_{n_0} in contact with its own metal in phase 1, as represented in Fig. 8b. This is possible if a miscibility gap exists between the two oxides MeO_{n_0} and MeO_n , otherwise a continuous change of the degree of oxidation from n_0 to n will be established (curve c in Fig. 8). In all cases the very important result for all passivity phenomena is the fact that the electrode potential depends only on the thermodynamic properties of the oxide at the phase boundary 2,3 oxide/electrolyte. If the electronic equilibrium through the layer and also the ions equilibrium $\beta(2,3)$ or $\alpha(2,3)$ are established the potential of an oxide electrode cannot depend on the construction of the oxide layer. Therefore the potential of a passive electrode is only defined by the property and the composition of the surface oxide near the electrolyte. The layer thickness and the existence of intermediate layers cannot have any direct influence on the passive potential, may be by an indirect influence of these parameters on the degree of oxidation of the surface oxide. A fixed passive potential signifies a defined surface idea. This statement must be used as the leading idea for all considerations about passivity.

If the pH value is changed, the potential of the passive electrode is

$$e_h = E_o(n) - 0.059 \cdot \text{pH} \quad [28]$$

$E_o(n)$ is a definite function of the degree of oxidation of the surface oxide and is equal to E_o of Eq. [7] or [11], if the reaction $\beta(2,3)$ is potential determining.

Influence of a Corrosion Process on the Potential

The corrosion process of a passive metal covered with a pore-free oxide is represented by the reaction $\alpha(2,3) \text{Me}^{z+}(\text{oxide}) \rightarrow \text{Me}^{z+} \cdot \text{aq}(\text{electrolyte})$. In the previous parts it was assumed that this reaction was either totally inhibited (Section on Oxide on a Foreign Metal. Oxygen Ion Equilibrium Oxide/Electrolyte) or in equilibrium (Section on Oxide on a Foreign Metal. Metal Ion Equilibrium at the Phase Boundary Oxide/Electrolyte). In most cases of passivity the reaction $\beta(2,3) \text{O}^{2-}(\text{oxide}) + 2\text{H}^+(\text{electrolyte}) \rightleftharpoons \text{H}_2\text{O}(\text{electrolyte})$ determines the potential (Section on Oxide on a Foreign Metal. Oxygen Ion Equilibrium Oxide/Electrolyte) although the corrosion reaction $\alpha(2,3)$ is not totally inhibited. Therefore the influence of the rate of this corrosion process on the thermodynamically evaluated electrode potential is discussed here.

Current Equivalent to the Rate of Corrosion

If the corrosion reaction $\alpha(2,3)$ is not completely inhibited, the passive layer will be dissolved by a certain rate in the electrolyte. This loss of oxide can be compensated by an anodic formation of oxide. In the stationary state which is associated with a temporary constant layer thickness, the loss and the anodic formation of oxide must have exactly the same rate. Therefore the anodic current of the stationary state is equivalent to the corrosion rate, it is in fact the corrosion current density i_K . It may be remarked that this result is only valid in the absence of redox processes; therefore no electrons can cross the phase boundary oxide/electrolyte. In spite of the assumed good electronic conductivity no electronic current can then flow through the passive layer. The total current must be an ionic current.

The corrosion process can also be interpreted in another manner, and this may be the better one for regarding the elementary reactions. It was assumed that the electrolyte is not saturated by metal ions. Therefore there exists a thermodynamic tendency for a transfer of the metal ions of the oxide to the electrolyte. The rate of this process is the corrosion rate or the dissolution rate of the oxide. The rate of this metal ion transfer depends on the potential difference oxide/electrolyte and on the composition of the oxide, but it must be essentially independent of other parameters such as layer thickness, construction of the layer, etc. If the electrical field strength in the layer has such a value that the ionic current density is equivalent to the corrosion current density of the metal ions at the oxide/electrolyte boundary, the same amount of metal ions which reach⁵ this boundary by ionic conductance will be transferred to the electrolyte by the corrosion process. A reaction $\text{O}^{2-}(\text{oxide}) + 2\text{H}^+ \cdot \text{aq} \rightleftharpoons \text{H}_2\text{O}(\text{electrolyte})$ does not pass. It is to be recognized by this consideration

⁵ Migrating oxygen ions in the electrical field have the same effect. In this case excess metal ions will remain at the phase boundary and will be transferred to the electrolyte with the corrosion rate. No distinction can be made between metal ion or oxygen ion migration.

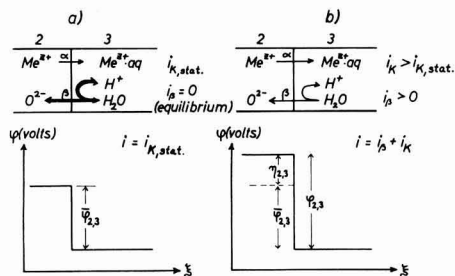


Fig. 9. Phase and potential scheme of the interface oxide/electrolyte. (a) Stationary state $i = i_{K,stat}$ (b) nonstationary state $i \neq i_{K,stat}$. $\eta_{2,3}$ = overvoltage.

that even the oxygen ions equilibrium has to be established if the stationary corrosion current density i_K flows. Therefore all thermodynamically evaluated relations referred to in the section on Potential of an Oxide Electrode assuming equilibrium $\beta(2,3)$ are valid for $i = i_K$. Figure 9a represents these conditions. $\psi_{2,3}$ is the equilibrium potential difference.

No Current

In the currentless case an anodic partial current density i_K of metal ion dissolution $\alpha(2,3)$ continues and must be compensated by an equal cathodic partial current density of oxygen ion recombination with hydrogen ions to form water, reaction $\beta(2,3)$. The equilibrium potential difference $\psi_{2,3}$ of the reaction $\beta(2,3)$ must be cathodically polarized by a current density equal to $i_\alpha \approx i_K$. The electrode potential must differ from the equilibrium potentials Eq. [8], [11], or [13] by the cathodic overvoltage $\eta_{2,3}$ of the reaction $\beta(2,3)$. If the corrosion current density i_K is small compared to the exchange current density i_0 of reaction $\beta(2,3)$ the overvoltage is small according

$$\eta = - \frac{RT}{2F} \cdot \frac{i_K}{i_0} \quad [29]$$

For the nonstationary state the conclusions are also valid if i_K is the nonstationary corrosion current density.

Any Arbitrary Current Density i

If $i \neq i_K$, the layer is not in the stationary state. In absence of a redox process the current must be caused by an ionic migration through the layer in a high electrical field. However, this process is not to be discussed in connection with the problem of potential establishment if the electronic conductivity is good enough that the electrochemical potential $\eta = \mu + zF\psi$ of the electrons can be considered constant throughout the whole layer.

From this point of view the oxide electrode potential assumes a value which differs from the reversible potentials ϵ_h in Eq. [8], [11], or [13] by an overvoltage $\eta_{2,3}$ of the potential difference $\psi_{2,3}$ at the phase boundary oxide/electrolyte (Fig. 9b). This overvoltage is caused by the formation or dissolution of oxygen ions according O^{2-} (oxide) + $2H^+$ (electrolyte) \rightleftharpoons H_2O (electrolyte) with a rate equivalent to the current density $i_\beta = i - i_K$. Primarily a variation of the current can only produce a change

of the electrode potential $\Delta\epsilon = \Delta\eta = \eta_2 - \eta_1 = \eta(i_2 - i_{K,2}) - \eta(i_1 - i_{K,1})$. Very soon a variation of the degree of oxidation n of the surface oxide will follow by the reaction $\beta(2,3)$, and a further change of the potential will ensue. In all these considerations it is important that the corrosion current density i_K does not generally have the stationary value $i_{K,stat}$. The process $\alpha(2,3)$ Me^{z+} (oxide) \rightarrow Me^{z+} (electrolyte) depends on the potential difference $\psi_{2,3}$, which changes with the overvoltage. Therefore $i_K(\eta)$ will be a function of the overvoltage η . Moreover $i_K(\eta)$ is a function of the degree of oxidation n . The thickness or the interior composition and construction of the layer cannot have any primary influence on the passive potential.

Influence of the Inner Layer Construction and Layer Thickness on the Ionic Current

The electrode potential depends only on the surface oxide (n) and the overvoltage $\eta_{2,3}$ of reaction $\beta(2,3)$; however, it does not depend on the construction of the layer. An ionic current can flow only if a gradient of the electrochemical potential of the ions (metal or oxygen ions) exists. Here an electrical field of 10^6 to 10^7 v/cm (4-11) has an important influence. The degree of oxidation n has to increase from the metal boundary to the electrolyte boundary. Only in such a layer can the migration of metal ions from the metal to the electrolyte side and the migration of oxygen ions in the opposite direction lead to an equalization of the different layer compositions at both sides, if this layer would be isolated.

The difference of the electrochemical and chemical potentials $\Delta\eta$ and $\Delta\mu$ of the Me^{zn+} and O^{2-} ions and also the electrical potential difference $\Delta\psi$ inside the layer is fixed by the electrode potential. This is the result of the former discussion. However, the ionic current density depends on the gradient $\partial\eta/\partial\xi$, $\partial\mu/\partial\xi$ and $\partial\psi/\partial\xi$ in the layer. Therefore the ionic current depends at the same potential on the layer thickness. The thicker the layer the smaller is the ionic current. The stationary layer thickness is then reached if at a pretended electrode potential, which defines the value $\Delta\eta = \Delta\mu + zF \cdot \Delta\psi$, the ionic current density is equal to the corrosion current density i_K . This stationary layer thickness δ_0 can be reached from both sides, from $\delta < \delta_0$ by $i > i_K$ and from $\delta > \delta_0$ by $i < i_K$. The variation of the stationary layer thickness by changing the electrode potential depends on the variation of the corrosion current density.

Passive Electrodes with Equal Surface Oxides at Different pH Values

In the stationary case $i = i_K$ the overvoltage $\eta_{2,3}$ of the process $\beta(2,3)$ $O^{2-} + 2H^+ \rightleftharpoons H_2O$ must be zero. Therefore Eq. [8] and [13] must be exactly valid here. Then a stationary passive electrode has the same surface oxide in contact with the electrolyte if the passive potential against the hydrogen electrode in the same electrolyte (same pH value) is equal.

These considerations are necessary to comprehend the dependence of the corrosion current density on the potential and on the pH value. The reaction rate of $\alpha(2,3)$ Me^{z+} (oxide) \rightarrow Me^{z+} (electrolyte) will

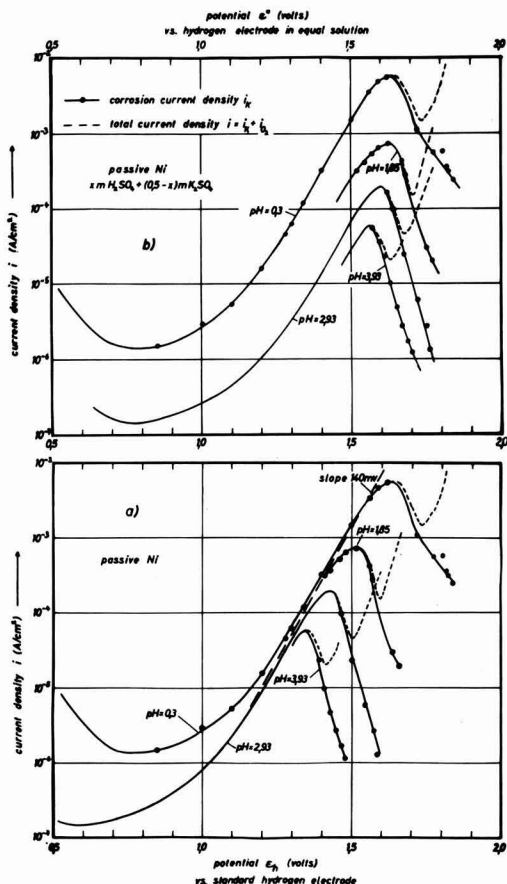


Fig. 10. Corrosion current density i_K of Ni at 25°C in dependence on the potential for different pH values: (a) potential against the standard hydrogen electrode; (b) against the hydrogen electrode of the same pH value.

depend on the potential difference $\psi_{2,3}$ and on the degree of oxidation n of the surface oxide. At the same pH value $\psi_{2,3}$ depends definitely on the value of n . A defined function $i_K(n)$ results. However, at constant n -value $\psi_{2,3}$ depends on the pH value according to

$$\psi_{2,3} = {}_0\psi_{2,3} - 0.059 \cdot \text{pH} \quad [30]$$

At passive Ni, Fe, and Cr this conception may be applied in the following part.

Passive Nickel, pH-Dependence of Corrosion

Figure 10a represents the corrosion current density at passive nickel according to Vetter and Arnold (12). Similar curves were also found by Okamoto (13) and Osterwald, Uhlig, and Feller (14, 15). For all pH values the potential in Fig. 10a is referred to the standard hydrogen electrode. In certain potential range, in which moreover a Tafel line is valid, the corrosion current density seems to be independent of the pH value. It must be understood that this independence is only accidental. Here, two parameters work against each other and compensate almost completely. These two parameters are the change of

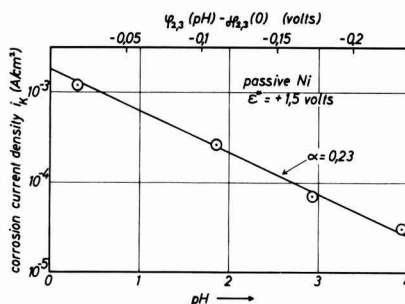


Fig. 11. Dependence of the corrosion current density i_K of Ni on the pH value at a fixed potential (1.5v) against the hydrogen electrode of the same pH value.

the composition of the oxide by the potential and the change of the potential difference at the phase boundary oxide/electrolyte by the pH value of the electrolyte. The states of the oxides which are compared at the same potential ϵ_h for different pH values are not the same ones as mentioned before. The states and compositions of the oxides are always equal for all pH values at the same potential against the hydrogen electrode of the same corresponding pH value. However, the corrosion current densities should be compared advantageously at different pH values with the same oxide of the same degree of oxidation. Therefore for this purpose the corrosion current density has to be drawn against the potential of the hydrogen electrode at the corresponding pH values in Fig. 10b.

In nearly the whole potential range, that is in nearly the whole range of degrees of oxidation, the dependence of the current densities on the pH values is equal in Fig. 10b. For the equivalent state of the oxide the corrosion current density depends on the pH value or on the potential difference oxide/electrolyte, respectively, according to a Tafel relation. This relation is represented in Fig. 11. The straight line corresponds to a transfer reaction of the nickel ion Ni^{2+} with a transfer coefficient $\alpha = 0.23$. The change of the corrosion current density by the potential ϵ is connected with the corresponding change of the degree of oxidation.

Passive Iron, pH Dependence of Corrosion

The corrosion current density of passive iron is in a wide potential range independent of the potential according to Franck and Weil (16, 1). The investigated potential range is above the Flade potential $\epsilon > \epsilon_F$ where a surface oxide of an approximate composition $\gamma\text{Fe}_2\text{O}_3$ is assumed (17-20). The degree of oxidation may change only to a very small extent in spite of the independence of i_K since the potential dependence is very strange and is not yet explained.⁶ The pH dependence of i_K is found by Vetter (21) to be $\log i_K = a - 0.84 \cdot \text{pH}$ and would correspond to a transfer coefficient $\alpha = 0.28$ for trivalent iron ions Fe^{3+} .

Passive Chromium, pH Dependence of Corrosion

The corrosion current density of passive chromium is strongly dependent on the pH value and

⁶ The explanation of Vetter (21) and Schottky (22) must be changed according to the new theory.

also on the potential. According to Heumann (23) and also to our measurements (24) in the range where a Tafel line is valid, the potential for a definite current density depends on the pH value and closely follows the relation $\epsilon_h = \epsilon_o(i) - 0.059 \cdot \text{pH}$. However, at a constant current density, these potentials correspond to a constant surface oxide as could be drawn from the previously presented theory and since the potential change is nearly 59 mv/pH unit. In a representation of the current density against the hydrogen electrode of the same pH value as that of the electrolyte the Tafel lines of different pH values coincide. This means that the corrosion current density, for an oxide of constant composition, is independent of the pH value.

Any discussion of this paper will appear in a Discussion Section to be published in the December 1963 JOURNAL.

REFERENCES

1. K. J. Vetter, *Z. Elektrochem.*, **55**, 274 (1951), special for passive iron.
2. K. J. Vetter, *ibid.*, **66**, 577 (1962).
3. G. S. Bell and R. Huber, *This Journal*, being reviewed.
4. K. J. Vetter, *Z. Elektrochem.*, **58**, 230 (1954).
5. K. J. Vetter, *Z. physik. Chem.*, **202**, 1 (1953).
6. K. J. Vetter, *Z. physik. Chem. N.F.*, **4**, 165 (1955).
7. A. Güntherschulze and H. Betz, *Z. Physik*, **91**, 70 (1934).
8. A. Güntherschulze and H. Betz, *ibid.*, **92**, 367 (1934).
9. D. A. Vermilyea, *Acta Met.*, **1**, 282 (1953).
10. D. A. Vermilyea, *ibid.*, **2**, 476 (1954).
11. D. A. Vermilyea, *This Journal*, **102**, 655 (1955).
12. K. J. Vetter and K. Arnold, *Z. Elektrochem.*, **64**, 244 (1960).
13. G. Okamoto, H. Kobayashi, M. Nagayama, and N. Sato, *ibid.*, **62**, 775 (1958).
14. J. Osterwald and H. H. Uhlig, *This Journal*, **108**, 515 (1961).
15. J. Osterwald and H. G. Feller, *ibid.*, **107**, 473 (1960).
16. U. F. Franck and K. G. Weil, *Z. Elektrochem.*, **56**, 814 (1952).
17. K. J. Vetter, *ibid.*, **62**, 642 (1958).
18. K. G. Weil and K. F. Bonhoeffer, *Z. physik. Chem. N.F.*, **4**, 175 (1955).
19. K. E. Thuesler, K. G. Weil, and K. F. Bonhoeffer, *ibid.*, **15**, 149 (1958).
20. H. Göhr and E. Lange, *Naturwiss*, **43**, 12 (1956).
21. K. J. Vetter, *Z. Elektrochem.*, **59**, 67 (1955).
22. W. Schottky, *Halbleiterprobleme*, **2**, 233 (1955).
23. Th. Heumann and W. Rösener, *Z. Elektrochem.*, **59**, 722 (1955).
24. K. Vetter and W. Phiet, Unpublished paper.

Anodic Passivation of Nickel in Sulfuric Acid Solutions

Norio Sato and Go Okamoto

*Physicochemical and Electrochemical Laboratory, Faculty of Engineering,
Hokkaido University, Sapporo, Japan*

ABSTRACT

The potential decay curve of a passive nickel electrode on open circuit was followed in solutions of pH ranging from 0.4 to 1.4. The three arrest potentials observed in the decay curve correspond to the equilibrium potentials for the NiO/Ni, Ni₃O₄/NiO, and the Ni₂O₃/Ni₃O₄ electrodes, respectively; the second potential is called the Flade potential, and the passivation occurs beyond this potential. A process for formation of the film is proposed that can be represented by the successive reactions, Ni + OH⁻ → NiOH⁺ + 2e, 3NiOH⁺ + OH⁻ → Ni₃O₄ + 4H⁺ + 2e. Then the critical potential beyond which the oxide formation takes place is calculated, under conditions when the solution in the vicinity of the surface becomes saturated with NiOH⁺ corresponding to the solubility product of NiO, and is found to be equal to the Flade potential. The proposed mechanism can also explain the ability of the passive film to protect the metal against active dissolution due to breakdown of the film.

The mechanisms of dissolution of nickel in the passive and overpassive potential regions are discussed from measurements of the Tafel constant [$\tau = RT/F (\partial \ln i/\partial E)$] and the pH dependence of the dissolution rate ($\lambda = \partial \log i/\partial \text{pH}$).

The results are summarized as follows: passive region; Ni²⁺ (oxide) + OH⁻ (aq.) → NiOH⁺ (surface), NiOH⁺ (surface) → NiOH⁺ (aq.): Overpassive region; Ni + H₂O (aq.) → NiOH (ads.) + H⁺ + e, NiOH (ads.) → NiOH⁺ (aq.) + e.

Since the day of Faraday many investigations have been performed on the passivity of metals, but the mechanism of anodic passivation is still to be clarified.

The present authors have made a series of experiments on the passive nickel to find the characteristic behavior on the passivation of this metal (1-12). The purpose of the present investigation is to elucidate the mechanism of anodic passivation of nickel

and dissolution of passive nickel in sulfuric acid solutions.

Experimental

Electroplated (A) and rolled (B) nickel plates were used as specimens. The electroplated specimen was prepared in the following way. A pure nickel plate was welded with a platinum current lead which was sealed by a glass tube. The electroplating was performed in a nickel sulfate bath (NiSO₄·7H₂O

Table I. Composition of specimens

Specimen	Co	Cr	Al	Mg	Mn	Ca	Zn	Ag	Cu	Sn	Pb	Fe	Ni
A	0.88	—	<0.04	<0.015	—	+	—	+	+	—	—	+	Balance
B	0.28	—	<0.04	—	<0.03	+	Trace	—	+	—	—	+	Balance

30g H_2BO_3 3.8g H_2O 100 cc) at a current density of 10 ma/cm² at 40°–50°C, the thickness of the film plated out being about 1 mm. In order to prepare specimen B, an electrolytic nickel plate was melted and cast into an ingot in a vacuum atmosphere; then it was cold rolled into a plate of 5 mm thickness and was annealed at 800°C for 10 min. The specimen of 15 x 10 mm with a small handle was cut out from the plate. After polishing the surface with 4/0 emery paper, a Pt current lead was soldered to the handle of the specimen and was sealed into a glass tube with an epoxy resin. The spectroscopic analysis of these specimens A and B gave the composition as in Table I where the sign (+) referred to detectable elements and (—) the undetectable.

Specimens were degreased by swabbing with benzene, etched with a mixed solution of 50% H_2SO_4 and 50% HNO_3 for about 1 min, followed by washing with a splash of distilled water.

Solutions of various hydrogen-ion concentrations were made from double-distilled water, sulfuric acid, sodium sulfate, and sodium hydroxide of A.R. grade reagents. In all cases the concentration of the sulfate ion was adjusted to a constant value of 0.5m SO_4^{2-}/l . A small amount of phosphate or acetate solution was added to this sulfate solution in order to increase the buffering capacity for hydrogen-ion when necessary.

The glass electrolytic cell, having a capacity of about 500 ml, consists of two compartments that contain the specimen and the auxiliary platinum electrode, respectively. These compartments are connected to each other with a sintered glass filter in order to avoid contamination of the specimen with hydrogen produced on the auxiliary electrode.

Dissolved oxygen and the other impurities in solution were carefully removed by pre-electrolysis with a platinum cathode of 10 cm² for several hours at a current density of about 5 ma/cm² and by bubbling pure nitrogen gas ($O_2 < 0.001\%$) for one day before the experiment. All the experiments were carried out in pure nitrogen gas at temperatures of 25° and 40°C.

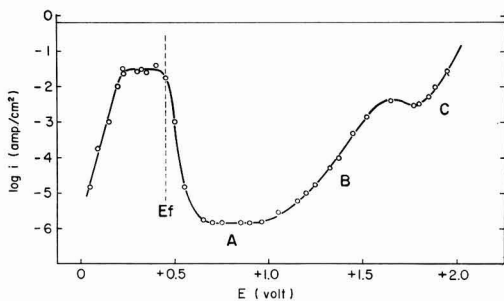


Fig. 1. Steady-state anodic polarization curve of nickel obtained by a potentiostatic method. Electrolyte: 1N H_2SO_4 saturated with pure nitrogen gas; temperature, 25°C.

Potentiostatic and galvanostatic methods were used for polarization measurements. The electronic potentiostat used has a current capacity of 150 ma in both anodic and cathodic directions, and the response-time for potential variation is about 10^{-2} sec/v.

Potential of the specimen was measured with reference to a saturated calomel electrode by a vacuum tube potentiometer and was converted to the standard hydrogen scale.

Results and Discussion

Flade potential.—Figure 1 shows the steady-state anodic polarization curve of nickel obtained by the potentiostatic method in 1N H_2SO_4 solution. The transition from the active to the passive state takes place in the range extending from +0.3 to +0.7v, and hence no clearly defined transition is observed. The dissolution current is almost constant in the passive potential region A, and it increases steeply with rising potential in the over-passive region B. The evolution of oxygen was observed in the potential region C. An oscillation of current is often observed in the transition region between B and C.

The dissolution rate of nickel and the rate of oxygen evolution were measured at various potentials and compared with the anodic current. It is found from the measurement (2, 4) that nickel dissolves into the solution in the form of divalent ion in both regions A and B and that it dissolves as trivalent ion in region C.

In the next experiment, the potential decay of passive nickel was followed after switching the anodic current off. The experiment was started from a fixed potential in region A. Two potential arrests E_2 and E_1 were observed in acid solutions as can be seen in Fig. 2. These potential arrests are longer and more clearly defined the longer is the time of polarization at the fixed potential.

When the potential of nickel was allowed to decay from a steady state in region C, an additional po-

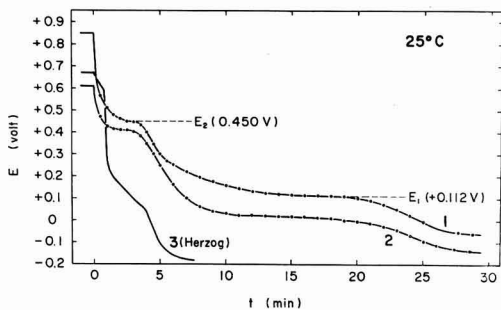


Fig. 2. Potential decay curves of the passive nickel, the initial potential being maintained at a constant potential in the passive region (A region) for about 30 hr: curve 1, 1N H_2SO_4 ; 2, 1M H_3PO_4 , pH = 0.98; 3, 1N H_2SO_4 + 0.1N $NiSO_4$, measured by Herzog (14).

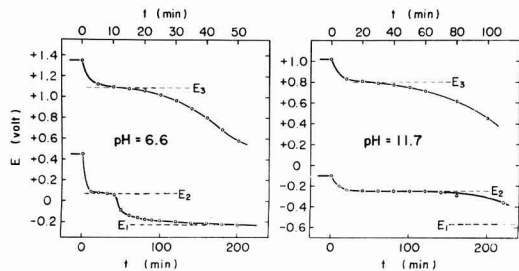


Fig. 3. Potential decay curves of nickel anode in neutral and alkaline solutions at 25°C, in the case of passive state (the curve in the less noble potential region) the initial potential being maintained at a constant potential for about 30 hr. Electrolyte: 0.5M Na₂SO₄ + 0.1M (KH₂PO₄ + K₂HPO₄), pH 6.6; 0.5M Na₂SO₄ + 0.01N NaOH, pH, 11.7.

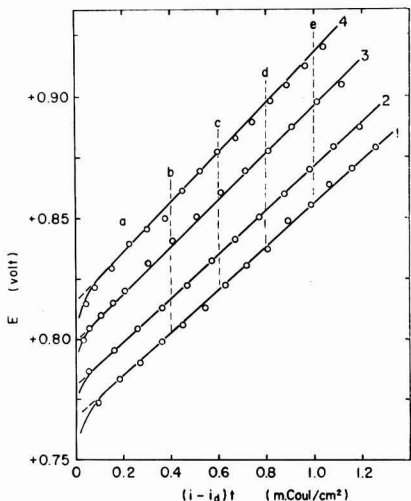


Fig. 4. Relation between potential and quantity of electricity accumulated in the passive oxide film at various anodic current densities. Initial potential, + 0.75v; equivalent dissolution current, $i_d + 6.75 \mu\text{a}/\text{cm}^2$; 40°C; 1N H₂SO₄. Curve 1, i 8.26 amp/cm² K 0.0870 v·cm²/mCoul; curve 2, i 9.36 amp/cm², K 0.0900 v·cm²/mCoul; curve 3, i 11.88 amp/cm², K 0.0950 v·cm²/mCoul; curve 4, i 14.25 amp/cm², K 0.0995 v·cm²/mCoul.

tential arrest appeared around the potential E_3 which was close to the transition potential from region B to region C. These potential arrests, E_1 , E_2 , and E_3 , were also observed in neutral and in alkaline solutions,¹ two examples of which are shown in Fig. 3.

In order to confirm the value of the Flade potential E_f , the time variation of the polarization potential of passive nickel was measured at various anodic current densities in 1N H₂SO₄ (3, 9). The specimen was kept at a fixed potential in region A before the experiment. A linear relation was obtained between the polarization potential and the quantity of electricity accumulated in the passive film as is shown in Fig. 4. From this the spontaneous potential of passive nickel (the Flade potential) was estimated according to the following equation (3, 9, 13).

$$E - E_f = K\delta = K(i - i_d)t + \delta_0 \quad [1]$$

¹ Only the least noble potential E_1 tends to approach the final spontaneous potential with the decrease of hydrogen-ion concentration.

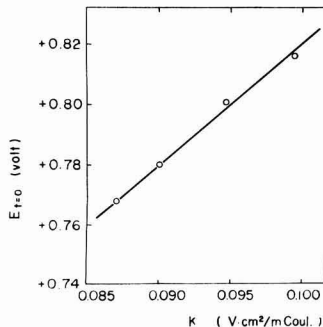


Fig. 5. Relation between estimated potential at $t = 0$ and the slope of the straight line in Fig. 4, which shows that extrapolation of all straight lines in Fig. 4 goes through one point from which the Flade potential E_f and the initial film thickness δ_0 can be estimated. $\delta_0 = 3.85 \text{ mCoul}/\text{cm}^2$.

	$K \text{ v} \cdot \text{cm}^2/\text{mCoul}$	$E_f \text{ v}$
1	0.0870	+0.434
2	0.0800	+0.434
3	0.0948	+0.436
4	0.0995	+0.433

where E is the polarization potential applied at a current density i , E_f the Flade potential, i_d the potential-independent dissolution current in region A, t the time, δ_0 the initial thickness of the passive film, and K a constant. The value of the Flade potential calculated from Eq. [1] which as indicated in Fig. 5 is close to the arrest potential E_2 observed in the decay curve of passive nickel. The arrest potential E_2 is very close to the transition potential for the passivation of nickel that is seen in the anodic polarization curve shown above in Fig. 1.

The arrest potentials E_1 , E_2 , and E_3 and the final spontaneous potential reached after the decay were estimated in sulfate solutions of various pH's extending from acid to alkaline regions. Results are shown in Fig. 6. The pH dependence of these potentials is expressed by

$$E_1 = + 0.13 - 0.060 \text{ pH (V)} \quad [2]$$

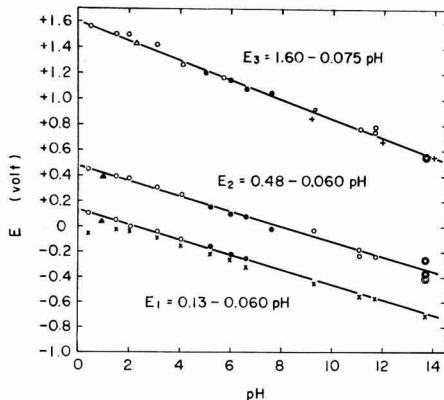
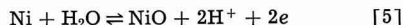


Fig. 6. Effect of pH on E_1 , E_2 , and E_3 at 25°C. x, spontaneous potential; \circ , 0.5M SO₄²⁻; \bullet , 0.5M SO₄²⁻ + 0.1M (KH₂PO₄ + K₂HPO₄); Δ , 0.5M SO₄²⁻ + 0.1M (CH₃COOH + CH₃COOK); \blacktriangle , 1M H₃PO₄; \circ , 1N KOH; +, values measured by Hickling and Spice (15).

$$E_2 = +0.48 - 0.060 \text{ pH (V)} \quad [3]$$

$$E_3 = +1.60 - 0.075 \text{ pH (V)} \quad [4]$$

The arrest potential E_1 seems to agree with the equilibrium potential for the formation of NiO

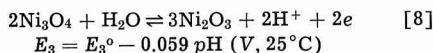
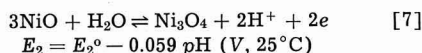


$$E_1(\text{calc}) = +0.108 - 0.059 \text{ pH (V, 25}^\circ\text{C)} \quad [6]$$

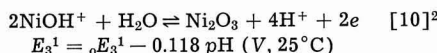
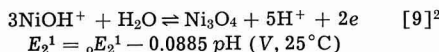
It is therefore a reasonable assumption that E_1 is mainly due to the redox reaction given by Eq. [5].

It is quite natural to presume here that E_2 and E_3 correspond to the potential of the formation of higher oxides. The existence of two types of higher oxide, Ni_3O_4 and Ni_2O_3 have been shown by a number of workers, and the potential of the Ni_2O_3 electrode in an alkaline solution (15) appeared to be very close to the observed potential E_3 .

The present authors assume here that the following reactions are directly related to E_2 (Flade potential) and E_3 , respectively



When the concentration of divalent nickel ion in solution is comparatively large, another possibility of explaining the arrest potentials E_2 and E_3 arises. The reactions are



In the case where the exchange rate of reaction [9] at the equilibrium potential is larger than that of reaction [7], the arrest potential E_2 will be determined by redox reaction (9). This situation could be expected if the concentration of nickel ion in solution is high, since the exchange rate of this reaction increases with nickel ion concentration (17). The discrepancy between the observed pH dependence of E_3 and that expected from reaction [8] may be caused by a side redox reaction involving nickel ion in solution which is produced as the result of the dissolution of nickel. The rate of this side reaction may be relatively large in acid solution.

It is concluded from the above that the Flade potential is not the formation potential of NiO but the transformation potential from NiO to the higher oxide Ni_3O_4 when the concentration of nickel ion in solution is small. The passive oxide film, therefore, will be either the single higher oxide Ni_3O_4 or the duplex oxide of NiO and Ni_3O_4 . The potential of multiple-phase oxide electrode has been discussed in general from the point of view of thermodynamics and electrode kinetics (7).

Mechanism of anodic formation of passive film.—

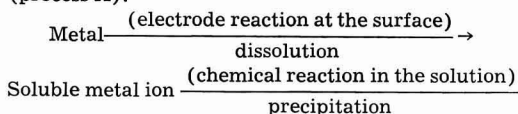
In this section, the authors will explain how the passivation of nickel in acid solution takes place

² The existence of the divalent complex-ion NiOH^+ has been ascertained by several workers (16). The redox reactions involving trivalent nickel ion should also be considered.

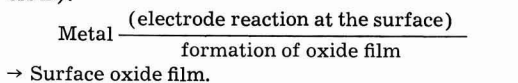
at the Flade potential which is the transformation potential from NiO to Ni_3O_4 .

Two possible processes have been proposed for the anodic formation of passive oxide film on metals (18, 21).

(A) "Precipitation" from supersaturated solution (process A).



(B) Direct reaction of metal with solution (process B).



When the nickel electrode in sulfuric acid solution is polarized anodically in the active region, it dissolves into the solution in accordance with the reaction



the equilibrium potential of which is given by

$$E_\alpha = E_\alpha^\circ + \frac{RT}{2F} \ln [\text{NiOH}^+] [\text{H}^+]$$

$$= +0.0278 - 0.0295 \text{ pH} + 0.0295 \log \text{NiOH}^+, (\text{V, 25}^\circ\text{C}) \quad [12]$$

where E_α° denotes the standard redox potential, $[\text{NiOH}^+]$ and $[\text{H}^+]$ the concentration of NiOH^+ and H^+ ions, respectively.

The rate of anodic dissolution increases with rising potential as schematically shown in Fig. 7. According to electrode kinetics, the rate equation of this reaction could be formulated if the rate of backward reaction is negligible compared to that of the forward reaction. Thus

$$i_\alpha = k_\alpha [\text{OH}^-] \exp \left\{ \frac{\tau_\alpha FE}{RT} \right\} = i_\alpha^\circ \exp \left\{ \frac{\tau_\alpha F (E - E_\alpha)}{RT} \right\} \quad [13]$$

where k_α is the rate constant, i_α° the exchange reaction rate at the equilibrium potential, and τ_α the Tafel constant. As the anodic dissolution proceeds, the concentration of nickel ion in the vicinity of surface will approach an equilibrium value. Thus

$$[\text{NiOH}^+]_{\text{max}} = \frac{1}{[\text{H}^+]} \exp \left\{ \frac{2F (E - E_\alpha^\circ)}{RT} \right\} \quad [14]$$

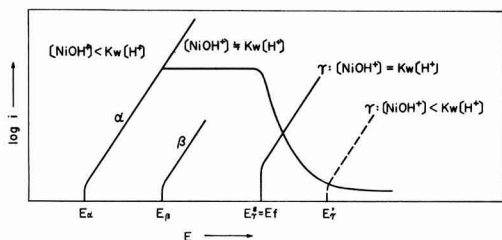


Fig. 7. Schematic potential-current curves of nickel for passivation in acid solution. α , dissolution in active state, $\text{Ni} + \text{OH}^- \rightarrow \text{NiOH}^+ + 2e$; γ , formation in active state, $3\text{NiOH}^+ + \text{OH}^- \rightarrow \text{Ni}_3\text{O}_4 + 4\text{H}^+ + 2e$; E_f , Flade potential; K_w , $[\text{NiOH}^+]/[\text{NiO}][\text{H}^+] = 10^{2.73}$.

When the concentration of NiOH⁺ ion becomes larger than the saturated value which is determined by the solubility product of NiO, the precipitation of NiO occurs in the vicinity of the surface.



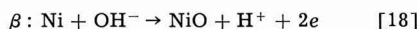
The value of solubility product of NiO has been estimated as

$$K_w = [\text{NiOH}^+]_s / [\text{H}^+] = 10^{2.78} \quad [16]$$

The critical potential above which this precipitation process occurs can be calculated from Eq. [14] and [16]

$$\begin{aligned} E_w &= E_w^0 + \frac{RT}{2F} \ln K_w + \frac{RT}{F} \ln [\text{H}^+] \\ &= +0.108 - 0.059 \text{ pH} \quad (V, 25^\circ\text{C}) \quad [17] \end{aligned}$$

This potential, of course, coincides with the equilibrium potential of the direct formation reaction of oxide on nickel.



$$\begin{aligned} E_\beta &= E_\beta^0 + \frac{RT}{F} \ln [\text{H}^+] \\ &= +0.108 - 0.059 \text{ pH} \quad (V, 25^\circ\text{C}) \quad [19] \end{aligned}$$

Thermodynamically, these two reactions [15] and [18] can occur in the potential region above E_w or E_β .

The oxide film deposited from the solution according to reaction [15] is expected to have a porous character. The limiting current of the active dissolution through pores would be calculated by the following equation if the rate of dissolution is controlled by the diffusion of NiOH⁺ ion from the surface to the bulk of solution. Considering that the surface is saturated

$$i_{\text{limit}} \approx 2F \frac{D}{d} [\text{NiOH}^+]_s \quad [20]$$

where D is the diffusion coefficient and d the thickness of the diffusion layer. The limiting dissolution rate increases with the decrease of pH in accordance

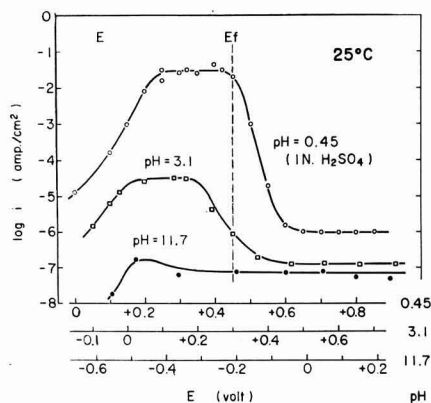


Fig. 8. Steady-state anodic polarization curves of nickel in sulfate solutions of acid and alkali measured by a potentiostatic method. Electrolyte, 0.5M SO₄²⁻/1, saturated with N₂ gas; specimen, electrolytic nickel.

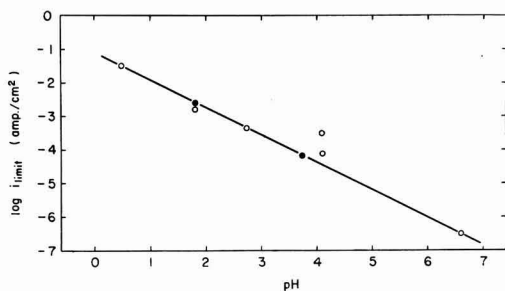


Fig. 9. Relation between pH and the limiting dissolution current of nickel in active state. Log $i_{\text{limit}} = -1.1 - 0.83 \text{ pH}$; 25°C; electrolyte, pH = 0.45 - 4.1, 0.5M SO₄²⁻; pH = 6.6, 0.5M SO₄²⁻ + 0.1M (K₂HPO₄ + KH₂PO₄); ○, electrolytic nickel melted in vacuum; ●, commercial nickel.

with the change in the saturation concentration of NiOH⁺. Thus, in acid solution the dissolution rate is so large that the existence of precipitated oxide NiO does not contribute to the passivation. Figure 8 shows the steady-state anodic polarization curves measured in acid and alkaline solutions. The limiting dissolution current observed in the active state is shown in Fig. 9; the pH dependence of it is close to that expected from Eq. [20].

If the oxide film of NiO is formed by the direct reaction of nickel and water, it would be pore-free and would render the specimen passive. However, it is not clear whether or not such a direct formation of oxide proceeds on the surface where rapid dissolution of nickel is taking place. The rate of the two reactions i_α and i_β is given as follows

$$i_\alpha = i_\alpha^0 \exp \{ \tau_\alpha F (E - E_\alpha) / RT \} \quad [21]$$

$$i_\beta = i_\beta^0 \exp \{ \tau_\beta F (E - E_\beta) / RT \} \quad [22]$$

where i_α^0 and i_β^0 denote the rate of the exchange reactions at equilibrium potentials E_α and E_β , τ_α and τ_β being the Tafel constant for both reactions. In acid solution, the potential current curve for the reaction α is usually in the less noble potential region compared to that for the oxide formation as can be seen in Fig. 7. In order to satisfy the condition $i_\beta > i_\alpha$, the potential of nickel electrode should be kept more noble than the potential E^* .

$$E^* = \frac{\tau_\beta E_\beta - \tau_\alpha E_\alpha}{\tau_\beta - \tau_\alpha} + \frac{RT}{\tau_\beta - \tau_\alpha} \ln \frac{i_\alpha^0}{i_\beta^0} \quad [23]$$

Thus, the passivation of nickel due to the direct formation of oxide is expected to occur above the potential E^* . Accordingly, it is necessary to show that τ_β is unequal to τ_α so that the value of the potential E^* can be realized. However, no value of τ_β has been available, and its exact measurement cannot be made using available electrochemical technique. It seems also to be difficult in the direct formation mechanism to explain the coincidence of the passivation potential observed on the polarization curve with the Flade potential observed on the potential decay.

The present authors, then, proposed a new mechanism that is represented by the electrode reaction

producing a higher oxide film from the metal ion in solution.



$$E_\gamma = E_\gamma^0 - \frac{3RT}{2F} \ln [\text{NiOH}^+] + \frac{5RT}{2F} \ln [\text{H}^+] + 0.725 \\ - 0.1475 \text{pH} - 0.0885 \log \text{NiOH}^+, (V, 25^\circ\text{C}) \quad [25]$$

The concentration of NiOH^+ in the vicinity of the surface will be maintained at about the saturated value of $[\text{NiOH}^+]_s$ in the potential region more noble than E_β , owing to the precipitation of the oxide NiO , so that the critical potential (equilibrium potential) for the formation of this oxide can be derived from Eq. [16] and [25].

$$E_\gamma^s = E_\gamma^0 - \frac{3RT}{2F} \ln K_w + \frac{RT}{F} \ln [\text{H}^+] \\ = +0.480 - 0.059 \text{pH} (V, 25^\circ\text{C}) \quad [26]$$

This is the passivation potential expected from this mechanism. The critical potential E_γ^s is the same as the equilibrium potential of the redox reaction between NiO and Ni_3O_4



$$E_f = E_f^0 + \frac{RT}{F} \ln [\text{H}^+] = +0.480 - 0.059 \text{pH} (V, 25^\circ\text{C}) \\ [28]$$

because the value of $\{E_\gamma^0 - (3RT/2F) \ln K_w\}$ is calculated to be equal to E_f^0 .

Thus, the proposed mechanism interprets without ambiguity the important experimental fact that the passivation occurs beyond the Flade potential, i.e., the transformation potential between NiO and Ni_3O_4 .

According to the electrode kinetics, the rate of oxide formation γ is given by

$$i_\gamma = k_\gamma [\text{NiOH}^+] [\text{OH}^-] \exp \{\tau_\gamma FE/RT\} \\ = i_\gamma^0 \exp \{\tau_\gamma (E - E)/RT\} \quad [29]$$

The current i_γ increases with the rise of potential and also with the increase of the concentration of NiOH^+ which is formed by the dissolution reaction α . Thus, pores in the passive film, if they happen to appear, will be repaired quickly according to the high concentration of NiOH^+ produced at the pores. In other words, the passive film of higher oxide Ni_3O_4 possesses the capacity of self-repairing which brings about more effective protection of the nickel electrode.

The anodic polarization curves of nickel in acid solution (Fig. 1 and 8) show that the specimen must be kept at somewhat more noble potential than the Flade potential in order to obtain the stable passive state. Differences between the Flade potential and the critical potential of the stable passive state have been reported on the anodic passivation of iron in acid and neutral solutions (22-24). According to the proposed mechanism γ , the anodic passivation of nickel in acid solution commences to occur around the Flade potential at which the saturated concentration of NiOH^+ ion and OH^- ion in the vicinity of surface and hence the rate i_γ of

Eq. [29] begins to decrease because of the formation of Ni_3O_4 from these ions and the decrease of the area of bare metal surface. The change of the potential-current curve of reaction γ with the decrease of NiOH^+ concentration is schematically shown in Fig. 7. The decrease in the rate i_γ results in the decrease in the self-repairing capacity of the passive film. Accordingly, in order to obtain the stable passive state it is necessary to polarize the specimen at a somewhat more noble potential than the Flade potential, because the increase of the rate of reaction γ with the rise of potential is also expected.

The standard chemical potentials used are as follows

$$\mu_{\text{NiOH}^+} = -55.41 \text{ kcal/mole} \quad \mu_{\text{NiO}} = -51.7 (25), \quad \mu_{\text{Ni}_3\text{O}_4} \\ = -189.7 (5), \quad \mu_{\text{H}_2\text{O}} = -56.69 (25), \quad \mu_{\text{OH}^-} = -37.595 \\ (25)$$

The value of μ_{NiOH^+} was calculated from the stability constant of the complex ion (16) given by $[\text{NiOH}^+][\text{H}^+]/[\text{Ni}^{2+}] = 10^{-9.4}$, and the value of $\mu_{\text{Ni}_3\text{O}_4}$ was calculated from the Flade potential measurement by the present authors.

Dissolution of passive nickel.—In the passive potential region A, the dissolution rate of passive nickel in sulfuric acid solution is independent of electrode potential as is seen in Fig. 1. The width of region A increases with decreasing pH and in alkaline solutions the active potential region disappears almost completely as can be seen in Fig. 10.

The dissolution current i_A was measured in sulfate solutions of various pH's, the result being shown in Fig. 11. In the acid region, i_A decreases with the increase of pH while in the alkaline region it increases with increasing pH. The relation between i_A and pH in the acid region is expressed by

$$\log i_A = k - 0.46 \text{pH} \quad [30]$$

where k : $1.9 \mu\text{A}/\text{cm}^2$ at 25°C and k : $10.9 \mu\text{A}/\text{cm}^2$ at 40°C . No effect of the concentration of sulfate ion on the dissolution current i_A was observed in acid solutions. The concentration of divalent nickel ion did not affect the dissolution current i_A in acid solution when the concentration was not too large. This means that the rate of the backward reaction is negligibly small compared with that of the forward reaction when the concentration of nickel ion is small.

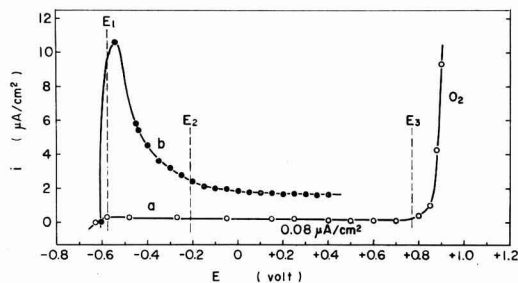


Fig. 10. Potential-current curves of nickel in alkaline solution under the nitrogen atmosphere. pH, 11.7, 25°C . Specimen, electrolytic nickel; electrolyte, $0.5M \text{Na}_2\text{SO}_4 + 0.01N \text{NaOH}$; a, stationary state; b, transient state, the potential being changed with a rate of 0.02 v/min .

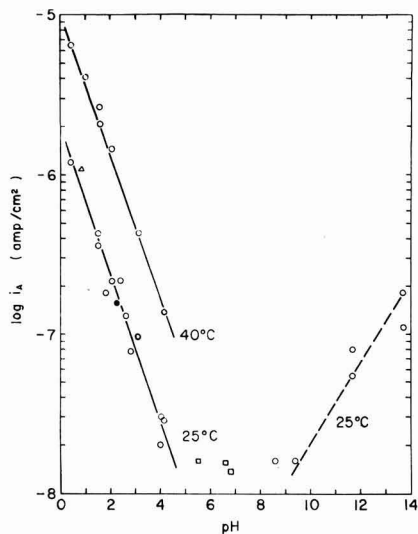
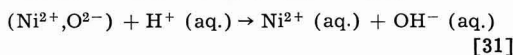


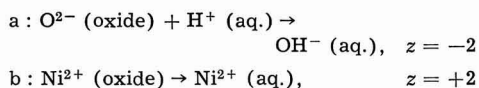
Fig. 11. Effect of pH on the dissolution current of passive nickel. $\log i_A = k - 0.46 \text{ pH}$. Specimen, electrolytic nickel. \circ , $0.5M \text{ SO}_4^{2-}$; \bullet , $1M \text{ CH}_3\text{COOH}$; Δ , $1M \text{ H}_3\text{PO}_4$; \square , $0.5M \text{ SO}_4^{2-} + 0.1M \text{ CH}_3\text{COO}^-$.

When the specimen is in the passive region the formation and the dissolution of passive film proceed simultaneously. The rates of these reactions are exactly the same at the steady state of polarization so as to keep thickness of the film constant. The dissolution reaction may be expressed by



The rate of this reaction is not affected by the electrode potential of nickel, but controlled only by the Galvani-potential difference across the oxide/solution interface.

Reaction [31] is a coupled reaction of the following two processes



where z is the charge of the ion passing across the interphase in the anodic direction. If the nickel ion dissolves as the complex ion NiOH^+ , reaction b could be expressed as follows

Table II. Theoretical pH dependence of the dissolution rate of passive nickel for possible reaction steps

Reaction step	z	$\delta \log i / \delta \text{pH}$
$\text{a}_1: \text{H}^+ (\text{aq}) \rightleftharpoons \text{H}^+ (\text{s})$	-1	
$\text{a}_2: \text{O}^{2-} (\text{oxide}) + \text{H}^+ (\text{s}) \rightleftharpoons \text{OH}^- (\text{s})$	0	
$\text{a}_3: \text{OH}^- (\text{s}) \rightleftharpoons \text{OH}^- (\text{aq})$	-1	
$\text{b}_1: \text{Ni}^{2+} (\text{oxide}) \rightarrow \text{Ni}^{2+} (\text{s})$	0	0
$\text{b}_2: \text{Ni}^{2+} (\text{s}) \rightarrow \text{Ni}^{2+} (\text{aq})$	+2	-2 α
$\text{c}_1: \text{Ni}^{2+} (\text{oxide}) + \text{OH}^- (\text{s}) \rightarrow \text{NiOH}^+ (\text{s})$	0	0
$\text{c}_2: \text{NiOH}^+ (\text{s}) \rightarrow \text{NiOH}^+ (\text{aq})$	+1	- α
$\text{c}_3: \text{NiOH}^+ (\text{aq}) \rightarrow \text{Ni}^{2+} (\text{aq}) + \text{OH}^- (\text{aq})$	0	-1
$\text{d}_1: \text{Ni}^{2+} (\text{oxide}) + 2 \text{OH}^- (\text{s}) \rightarrow \text{NiO}_2\text{H}^- (\text{s}) + \text{H}^+ (\text{s})$	0	0
$\text{d}_2: \text{NiO}_2\text{H}^- (\text{s}) \rightarrow \text{NiO}_2\text{H}^- (\text{aq})$	-1	+ α

(s) designates the surface layer in the passive oxide; z is the number of the elemental charge of ion passing through the phase boundary of oxide/aqueous solution in the anodic direction; α is the symmetry factor of reaction step. In many electrode reactions, it has been known that $\alpha \approx 0.5$.

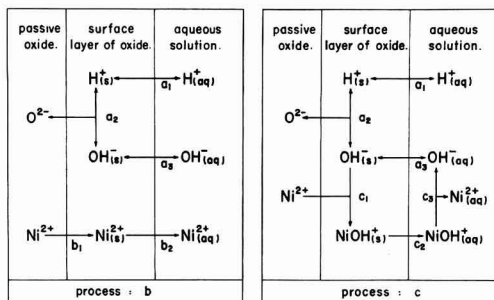
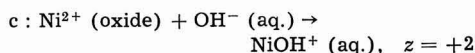
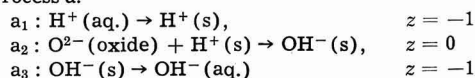


Fig. 12. Possible reaction steps at the phase boundary of oxide/solution in acidic region.

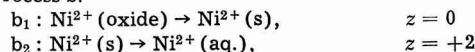


In the same way, the reactions a, b, and c can be divided, respectively, into the following steps.

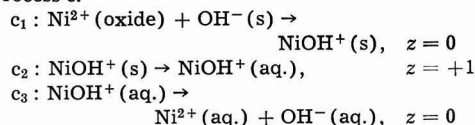
Process a.



Process b.



Process c.



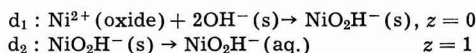
Here, (s) denotes an ion located in the surface layer of the passive oxide. Figure 12 is the schematic representation of these processes.

Since processes a are in equilibrium, the Galvani-potential difference g between the passive oxide and the solution can be expressed as

$$\begin{aligned} g &= g_o + (RT/F) \ln [\text{H}^+ (\text{aq.})] / [\text{H}^+ (\text{s})] \\ &= g_o' + (RT/F) \ln [\text{H}^+ (\text{aq.})] / [\text{H}^+ (\text{s})] \\ &= g_o'' + (RT/F) \ln [\text{O}^{2-} (\text{oxide})] / [\text{OH}^- (\text{aq.})] \end{aligned} \quad [32]$$

where g decreases with the increase of pH. The rate equations can be formulated for process b and process c if the rate-determining step is assumed (26). The pH dependence of dissolution rate was estimated theoretically by assuming the symmetry factor of the rate determining step is 0.5. The results of the calculation shown in Table II were compared with

the pH-dependence of i_A ($\partial \log i_A / \partial \text{pH} = -0.46$) observed for the sulfuric acid solutions, and it was concluded that the dissolution of passive film proceeds through process c in which step c_2 is rate-controlling. The following mechanism may be suggested for the dissolution of passive nickel in alkaline solutions



As can be seen in Table II, the pH-dependence of the dissolution rate is +0.5 for the rate-determining step d_2 . Here, the sign is reversed compared to that for the acidic solution. The experimental results obtained in the alkaline region agreed with this, even though the agreement was not perfect with respect to the number (Fig. 13).

Anodic dissolution in overpassive region.—The steady-state anodic polarization curves of nickel for the sulfuric acid solutions of various pH's were measured in the potential region extending from the passive to the overpassive region. The result is shown in Fig. 14. The anodic current observed in the overpassive region may be regarded as the sum of the dissolution current of passive film i_A and the

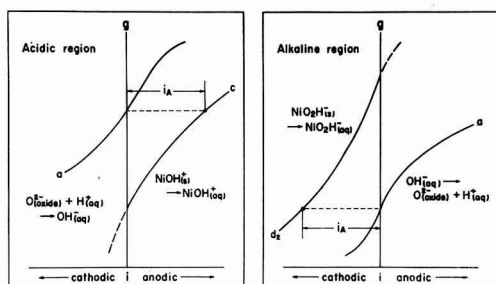


Fig. 13. Postulated Galvani potential-current diagram at the phase boundary of oxide/solution in acidic and alkaline region.

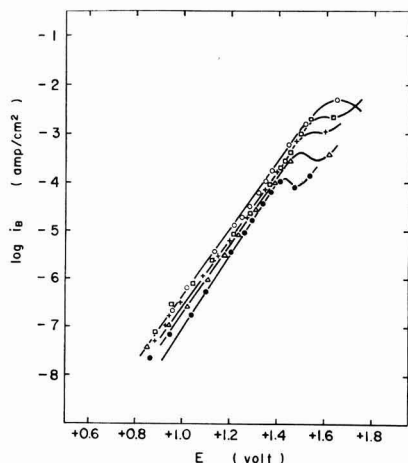


Fig. 14. Effect of pH on the steady-state anodic polarization curve of nickel in the passive and overpassive region. Specimen, electrolytic nickel. 0.5 mole/l SO_4^{2-} , 25°C. \circ , pH 0.45; \square , pH 1.55; $+$, pH 1.80; \triangle , pH 2.08; \bullet , pH 4.01.

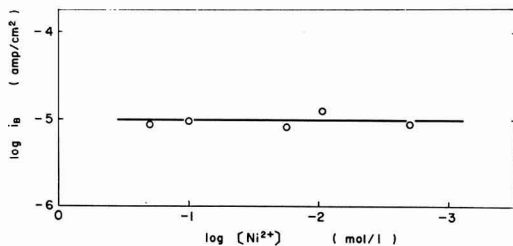


Fig. 15. Effect of pH on the potential-current curve for anodic dissolution of overpassive nickel in sulfate solution. $i_B = i - i_A$. pH, 1.55; 25°C; + 1.25v.

dissolution current of nickel i_B through the active patches in the passive film.

$$i_B = i - i_A \quad [33]$$

It was found that the Tafel relation was observed between the potential and the current i_B and that it was scarcely affected by the hydrogen ion concentration in solution (Fig. 15). The results of the estimation of the Tafel constant are shown in Table III. The mean value amounts to about 0.5 which is close to that observed by Vetter and Arnold (27).

$$\tau = \frac{RT}{F} \left(\frac{\partial \ln i_B}{\partial E} \right) \approx 0.5 \quad [34]$$

The concentration of sulfate ion and nickel ion, as well as that of hydrogen ion, does not affect the dissolution current i_B . However, the maximum value of i_B observed at the potential E_{BC} decreased with the increase of pH according to the equation

$$\log i_B^{\max} = -2.13 - 0.46 \text{ pH}, (\text{amp}/\text{cm}^2), 25^\circ\text{C} \quad [35]$$

The experimental results are shown in Fig. 16 and 17. The relation between the critical potential E_{BC} and pH can be expressed by the equation

$$E_{BC} \approx +1.68 - 0.08 \text{ pH} (\text{volt}) \quad [36]$$

which is not affected by the temperature between 25° and 40°C. The value of this potential and its pH-dependence are in a good agreement with those of the arrest potential E_3 observed in the potential decay curve of anodized nickel electrode (cf. Fig. 6).

In Table IV are shown several possible reaction paths of the potential dependent dissolution of nickel together with the Tafel constant and the pH dependence of reaction rate estimated theoretically by assuming the symmetry factor of each step is 0.5.

Comparison between this and the result of experiment was made in the same way as described above,

Table III. Tafel constant of the dissolution of overpassive nickel measured in 0.5M SO_4^{2-} /l sulfate solutions with various pH values

Solution pH	Slope of Tafel line	Tafel constant $\tau = (RT/F) \partial \ln i_B / \partial E$
0.45	0.123	0.480
1.55	0.129	0.458
1.80	0.122	0.484
2.10	0.125	0.472
2.80	0.131	0.451
3.10	0.131	0.451
4.01	0.125	0.472
4.10	0.121	0.488

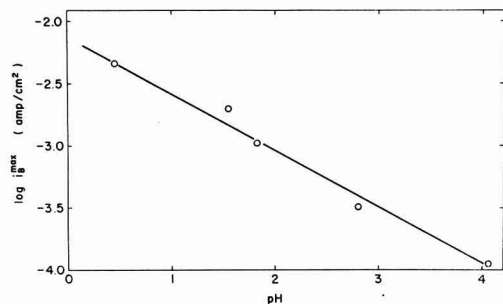


Fig. 16. Effect of pH on the maximum dissolution current of overpassive nickel in sulfate solution. 0.5M SO₄²⁻, 25°C. log $i_{B}^{\max} = -2.13 - 0.46 \text{ pH}$.

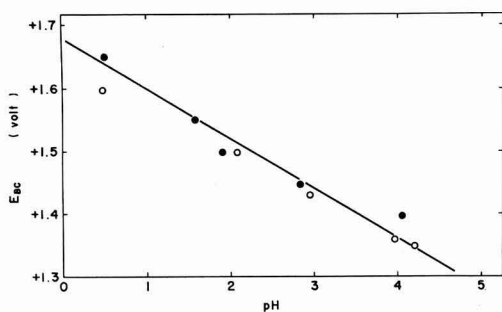


Fig. 17. Effect of pH on the critical potential where the maximum dissolution current i_{B}^{\max} of overpassive nickel were observed. $E_{Bc} = +1.68 - 0.080 \text{ pH}$. 0.5M SO₄²⁻; ●, 25°C; ○, 40°C.

and it is concluded that the rate-determining step is reaction d or possibly reaction b where the whole surface of nickel is covered with NiOH. It has been concluded from a separate series of experiments (12) conducted by the authors that in the active potential region nickel dissolves through the reaction path (a + b) with the rate-determining step a; in other words the rate of step b is larger than that of step a. Therefore, if step b is rate controlling, the dissolution rate observed in the overpassive region should be larger than the dissolution rate of active nickel extrapolated to the same potential region because step a is rate determining in the active region. This is contrary to the experimental result.

Table IV. Tafel constant and pH dependence of reaction rate for various reaction steps

Reaction	Tafel constant $\tau = (RT/F) \cdot \partial \ln i_a / \partial E$	pH dependence $\lambda = \partial \log i_a / \partial \text{pH}$
w: Ni + OH ⁻ (aq) → NiOH ⁺ (aq) + 2e	1	1
c: NiOH ⁺ (aq) → Ni ²⁺ (aq) + OH ⁻ (aq)	2	1
a: Ni + OH ⁻ (aq) → NiOH(ads) + e	0.5	1
b: NiOH(ads) → NiOH ⁺ (aq) + e		
($x_{\text{NiOH}} \rightarrow 0$)	1.5	1
($x_{\text{NiOH}} \rightarrow 1$)	0.5	0
c: NiOH ⁺ (aq) → Ni ²⁺ (aq) + OH ⁻ (aq)	2	1
z: Ni + H ₂ O → NiOH ⁺ (aq) + 2e	1	0
c: NiOH ⁺ (aq) → Ni ²⁺ (aq) + OH ⁻ (aq)	2	0
d: Ni + H ₂ O → NiOH(ads) + H ⁺ + e	0.5	0
b: NiOH(ads) → NiOH ⁺ (aq) + e		
($x_{\text{NiOH}} \rightarrow 0$)	1.5	1
($x_{\text{NiOH}} \rightarrow 1$)	0.5	0
c: NiOH ⁺ (aq) → Ni ²⁺ (aq) + OH ⁻ (aq)	2	0

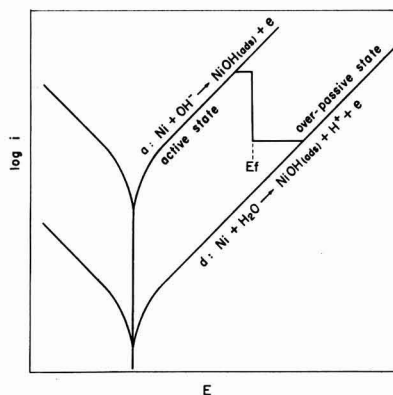


Fig. 18. Postulated potential-current curves of nickel in active and overpassive state.

Thus, step b is discarded. It is then clear that the dissolution reaction in the overpassive region proceeds through the consecutive reaction (d+b) in which step d is rate controlling.

The equilibrium potential of the dissolution reaction (d+b) in the overpassive region is equal to that of the dissolution reaction (a+b) in the active region, even though there is a difference between the rates of these reactions. Figure 18 shows the schematic interpretation for the proposed mechanisms of anodic dissolution in active region and in overpassive region.

Acknowledgment

The authors wish to express their thanks to Dr. M. Nagayama for his helpful discussion.

Any discussion of this paper will appear in a Discussion Section to be published in the December 1963 JOURNAL.

REFERENCES

1. G. Okamoto, H. Kobayashi, N. Sato, and M. Nagayama, *J. Electrochem. Soc. Japan*, **25**, 199 (1957), Overseas Ed., **25**, E45 (1957).
2. G. Okamoto, H. Kobayashi, M. Nagayama, and N. Sato, *Z. Elektrochem.*, **62**, 777 (1958).
3. G. Okamoto and N. Sato, *J. Electrochem. Soc. Japan*, **27**, 321 (1959); Overseas Ed., **27**, E128 (1959).
4. G. Okamoto and N. Sato, *J. Japan Inst. Metals*, **23**, 662 (1959); *Trans. Japan Inst. Metals*, **1**, 16 (1960).

5. G. Okamoto and N. Sato, *J. Japan Inst. Metals*, **23**, 721 (1959).
6. G. Okamoto and N. Sato, *ibid.*, **23**, 725 (1959).
7. G. Okamoto and N. Sato, *ibid.*, **24**, 179, 183 (1960).
8. G. Okamoto and N. Sato, *ibid.*, **24**, 105 (1960).
9. G. Okamoto and N. Sato, *ibid.*, **24**, 130 (1960).
10. N. Sato and G. Okamoto, *ibid.*, **24**, 735 (1960).
11. N. Sato and G. Okamoto, *Trans. Japan Inst. Metals*, **2**, 113 (1961).
12. N. Sato, "Electrochemical Study on the Passive State of Nickel," Dissertation, Hokkaido Univ., Sapporo, Japan (1961).
13. K. G. Weil, *Z. Elektrochem.*, **59**, 711 (1955).
14. N. W. Herzog: Prom. Nr. 2671, Eidgenössischen Techn. Hochschule Zurich (1957).
15. A. Hickling and J. E. Spice, *Trans. Faraday Soc.*, **43**, 762 (1947).
16. K. H. Gayer and L. Woontner, *J. Am. Chem. Soc.*, **74**, 1436 (1952); S. Chaberek, R. C. Courtney, and A. E. Martell, *ibid.*, **74**, 5057 (1952); "Stability Constant of Metal-Ion Complexes, Part II," The Chemical Society, Burlington House, London (1958).
17. J. O'M. Bockris, "Modern Aspect of Electrochemistry," Chap. IV, Academic Press, Inc., New York (1954).
18. W. J. Muller, *Z. Elektrochem.*, **30**, 401 (1924); **36**, 367 (1930); "Die Bedeckungstheorie der Passivität der Metalle," Berlin (1933).
19. E. Müller and K. Schwabe, *Z. Elektrochem.*, **39**, 414, 815 (1933).
20. W. A. Mueller, *This Journal*, **107**, 157 (1960).
21. H. Gerischer, *Agnew. Chem.*, **70**, 285 (1958).
22. U. F. Franck and K. G. Weil, *Z. Elektrochem.*, **56**, 814 (1952).
23. K. G. Weil and K. F. Bonhoeffer, *Z. Physik. Chem. N.F.*, **4**, 175 (1955).
24. K. E. Heusler, K. G. Weil, and K. F. Bonhoeffer, *ibid.*, **15**, 149 (1958).
25. W. M. Latimer, "The Oxidation Potentials," Prentice-Hall, New York (1952).
26. J. O'M. Bockris, "Modern Aspect of Electrochemistry I," Chap. IV, Academic Press Inc., New York (1954).
27. K. J. Vetter and K. Arnold, *Z. Elektrochem.*, **64**, 244 (1960).

The Initiation of Pores in Anodic Oxide Films Formed on Aluminum in Acid Solutions

T. P. Hoar and J. Yahalom

Department of Metallurgy, University of Cambridge, Cambridge, England

ABSTRACT

When pure aluminum is passivated at constant applied voltage in solutions ranging from pH 0-7, the current density representing film growth falls during the first few seconds in a manner that is qualitatively and nearly quantitatively the same for all solutions. The fall of current is succeeded by a rise to a constant value; the rise occurs the earlier, and is the greater, the lower the pH. The fall is interpreted as caused by barrier-layer formation, and the rise as caused by pore initiation when the field across the barrier layer has fallen low enough to allow the entry of protons into the film. Electron micrographs of the film surface show that very few pores are present on specimens that have not been anodized long enough for the initial current fall to halt, and that the pore system is fully established as soon as the succeeding rise is complete. A mechanism for pore formation is proposed.

When aluminum is made the anode in nearly neutral solutions such as those of ammonium borate or tartrate, with a voltage of ca. 4-400v across the cell, it quickly becomes passivated with an oxide film. This continues to thicken, at a decreasing rate, by ion migration under high-field conditions, forming a "barrier" layer; it substantially ceases to thicken when its thickness reaches about 14 Å/v of the cell voltage (1), because at the corresponding field strength, ca. 7×10^9 v/cm, the forming current density has fallen to a very small value. Quantitatively (2, 3)

$$i = A \exp(BE_F/y) \quad [1]$$

where i amp/cm² is the current density, E_F v the p.d. between the metal and the solution, (the "forming voltage") and y cm the film thickness; A and B are constants, found by Charlesby (3) in work on substantial films formed at fairly high voltages to be 10^{-18} amp/cm² and 3.1×10^{-6} cm/v, respectively (3), although the earlier values found by Gunter-schultze and Betz (2) and the more recent values of

Johansen, Adams, and Van Rysselberghe (4) are somewhat different. The exponential current/field relationship arises from the high-field nature of the processes of ion transport either across the metal/film interface or through the film, either or both of which processes may control the over-all current density, according to Verwey (5), Cabrera and Mott (6), and Dewald (7).

When aluminum is made the anode in acid solutions such as 5-20% aqueous sulfuric or phosphoric acid, the current density (at a cell voltage of 10-20v) does not fall to a very small value and the film continues to thicken indefinitely. A barrier layer of thickness some 10 Å/v forms (8), but a very much thicker porous layer forms outside it, and part of the aluminum oxidized appears in the solution. Studies by electron-microscope (9-11), birefringence (12), and a.c.-impedance techniques (13, 14) have shown that the pores are long, nearly cylindrical tubes reaching from the outer surface to the barrier layer, and that they are arranged in a nearly regular hexagonal pattern with a center-to-center spacing of

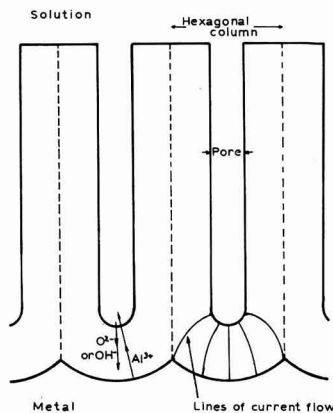


Fig. 1. Porous structure of acid formed anodic film, showing lines of current flow, pore-base structures and hexagonal columns.

about double the thickness of the barrier layer (Fig. 1). The continuing growth of the porous layer has been explained by Hoar and Mott (15) as caused by ion migration of Al^{3+} outward and OH^- inward through the film; oxygen movement inward and sideways from the pore end is necessary to build oxide ions into the hexagonal columns surrounding each pore (see Fig. 1). Migration of O^{2-} is considered (15) less likely than that of OH^- ; this, having migrated through or partly through the growing solid, dissociates to O^{2-} , which stops, and H^+ , which easily migrates back and fetches in more oxygen as OH^- . The total film thickness agrees very closely with that calculated for compact Al_2O_3 from the total charge passed; thus the Al^{3+} found in the solution must have dissolved, not from the surface of the porous film nor from the sides of the nearly cylindrical pores, but solely from the oxide at the base of the pores, and this dissolution is almost certainly field-assisted (15) rather than "thermal."

Franklin (16) from electron microscope studies has suggested that the pores initiate during the formation of the barrier layer, in the nearly hexagonal pattern; he has even suggested that this layer contains pore nuclei from the beginning. Nonetheless, no detailed mechanism for pore initiation, or explanation of the hexagonal pattern, has been given.

We have now studied the early stages of film formation in various acid solutions by measuring current-density transients at constant applied emf, by measuring the a-c impedance of thin formed films, and by electron microscopic examination of the film surface at different stages. The results indicate that the film in its earliest stages is of compact barrier nature, without pore nuclei, in every case. However, when the forming current density has fallen to a particular value, dependent on the anodizing solution and in particular on its pH, it increases considerably and, after passing through a maximum, finally reaches a steady value corresponding to the formation of the porous layer and the dissolution of Al^{3+} at the base of each pore. We interpret the rise in forming current density as

caused by pore initiation, for which we suggest a mechanism. By electron microscopic examination of the film surface at different stages, we have confirmed that pores are indeed initiated during the period when the current density has ceased to decrease according to ideal barrier layer formation, and that the near-hexagonal pore pattern is fully established by the time that the final steady current density is reached.

Experimental Technique

Materials.—Superpure aluminium wire¹ specimens, 0.264 cm in diameter and 22 cm long, were used. They were stopped off at both ends to expose an area of ca. 3 cm² by the method of Hoar and Wood (14). The experimental surface was provided by a final chemical brightening in the following solution, used at 95°–100°C, in which the specimens were immersed with gentle movement for 45–75 sec: phosphoric acid (s.g. 1.75) 78% by volume; nitric acid (s.g. 1.42) 11% by volume; sulfuric acid (s.g. 1.84) 11% by volume; $FeSO_4 \cdot 7H_2O$ 0.8 g/l. Solutions were made from Analar chemicals and water condensed on Pyrex.

Apparatus.—A simple anodizing cell (Fig. 2), held at constant temperature to within $\pm 0.2^\circ C$ by conventional means, was used. Emf was provided from lead/acid batteries with suitable resistors in series, with simple switching. Current was recorded with a Honeywell Recorder (series 153 x 16, 0.25 sec pen speed) or with a Model 1049 Cossor Oscilloscope with a Cossor Camera Model 1428 for the faster transients. The p.d. across the cell (and any compensating resistance, Fig. 2) was measured with an Avometer Model 8 or with a Solartron oscilloscope (CD 513). Impedance measurements were made with the bridge described by Wood, Cole, and Hoar (17), and electron micrographs were obtained on a Siemens Elmiskop I.

Procedure.—Before a particular anodizing, the specimen was degreased in methanol and acetone

¹ 99.99% Al, supplied by the Aluminum Development Association.

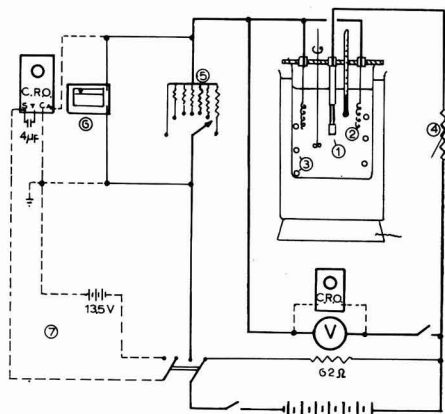


Fig. 2. Anodizing cell and circuit: (1) anode; (2) Pt cathodes; (3) cooling water coil; (4) compensating external resistance; (5) resistors to give a maximum of 10 mv potential drop for various current ranges; (6) pen recorder; (7) external beam-triggering circuit.

and dried. It was then chemically polished, rinsed in tap and distilled water, dipped in distilled water for 1 min, and dipped into the anodizing bath for 1 min before the current was switched on. The emf supply was kept permanently on circuit through a suitable resistor before switching over to the cell, so as to be as stable as possible. Thirty seconds after the current was switched off, the specimen was removed from the bath, rinsed in running distilled water, and dipped for 1 min in distilled water, before it was used for a-c impedance measurements or for producing a carbon replica.

The Honeywell recorder was arranged with shunting resistors to give full scale deflection of 10 mv for various current density ranges, as indicated in Fig. 2. When the current density transients were recorded oscillographically, two alternative methods were employed, the moving-film technique, and the time-base beam-triggering technique with the triggering circuit closed simultaneously with the anodizing circuit. One beam of the oscilloscope was connected across the resistors in the same way as the Honeywell recorder, while the second beam was used as a reference line and as a time control on the oscillogram, with a small 50 cps signal.

Impedance measurements on formed films were carried out at room temperature in a 3% solution of ammonium tartrate, with a cylindrical aluminum counter-electrode as described by Hoar and Wood (14).

Carbon replicas for electron microscopy were prepared on the dried specimens by graphite evaporation *in vacuo*. The carbon film on the specimen was carefully scratched into 2-mm squares, and the specimen was dipped for 2 sec in the chemical polishing solution at room temperature and immediately afterward into distilled water in a Petri dish, in which it was rotated slightly for a few seconds. The replicas then floated on the water surface. This method fulfilled the requirement that no gas, which may break the replica, should be evolved during the oxide dissolution; all the carbon film was stripped off in water, and there was no difficulty in mounting the replica on a 200-mesh electron microscope grid. Rep-

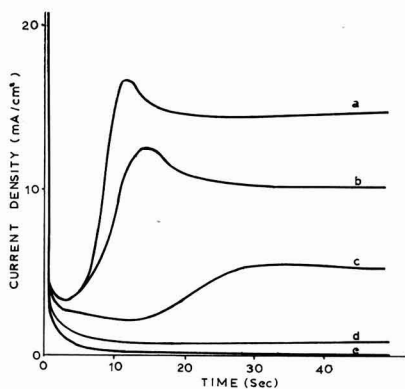


Fig. 3. Current transients for anodizing in various electrolytes at 14.4v, 25°C (pen recorded). a, 15% w/v sulfuric acid, pH 0.02; b, $\text{H}_2\text{SO}_4 + \text{NaHSO}_4$, pH 0.23; c, 183.6 g/l NaHSO_4 , pH 0.36; d, $\text{NaHSO}_4 + \text{Na}_2\text{SO}_4$, pH 1.19; e, 3% ammonium tartrate, pH 7.30.

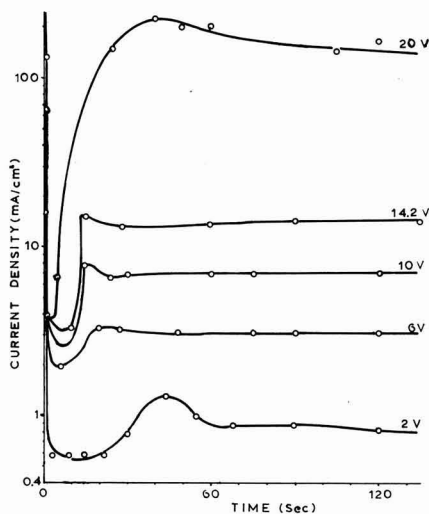


Fig. 4. Influence of cell voltage on current transients 15% w/v sulfuric acid at 25°C.

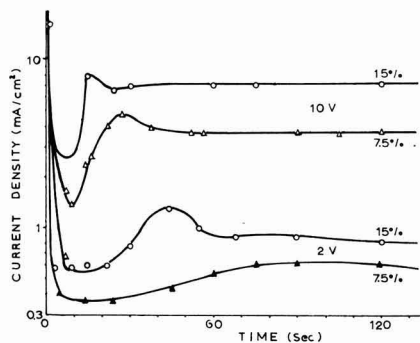


Fig. 5. Influence of sulfuric acid concentration on current transients at applied emf of 2v and 10v.

licas were shadowed with gold-palladium alloy to improve contrast, and electron micrographs were taken at a magnification of 60,000X.

Results and Interpretation

Current-density/time relation.—Typical continuously recorded current density transients, for anodizing at 25° and 14.4v applied emf in several solutions, are shown in Fig. 3. It is evident that the initial parts of all the curves are very nearly identical. Also, the minimum c.d. and the final steady c.d. are higher and occur earlier, the lower the pH of the solution. The fall of c.d. to a minimum, and its subsequent rise to a final steady value, are well-known features of sulfuric acid anodizing giving porous films (18).

Influence of cell voltage.—Figure 4 shows some manually recorded current density transients for anodizing in 15% w/v sulfuric acid at 25°C at applied emf from 2 to 20v. The shape of all the curves is similar and the final steady c.d. is dependent on the applied voltage.

Influence of acid concentration.—Figure 5 shows the effect of diluting sulfuric acid from 15% to

Table I. Thickness of pore-base layer, shortly after the start of steady-state anodizing, and in later stages, showing influence of forming voltage

Solution	Temp, °C	Run	Steady state current density, i_s , ma/cm ²	Forming voltage, E_F , v	Total charge passed, c/cm ²	Balancing capacitance at 30 cps, $\mu F/cm^2$	Thickness of pore-base layer, y , Å	$\frac{E_F}{y}$, v/cm $\times 10^7$
H ₂ SO ₄ (15% w/v)	17	1	1.53	7.4	2.7	1.13	66	1.13
		2	3.93	11.2	2.8	0.707	105	1.07
		3	7.73	15.3	2.8	0.525	142	1.08
		4	7.33	15.3	20.0	0.541	137	1.12
		5	43.3	21.4	19.9	0.421	177	1.21
H ₂ SO ₄ (7.5% w/v)	25	6	0.55	3.5	2.8	2.77	27	1.30
		7	1.03	7.4	2.8	0.887	84	0.88
		8	3.70	11.3	2.8	0.707	105	1.08
		9	3.67	11.3	19.7	0.729	102	1.11
		10	6.47	15.3	19.7	0.537	138	1.11
		11	17.8	21.2	19.7	0.533	139	1.53
H ₂ SO ₄ (15% w/v), pH 0.02	25	12	0.83	3.4	2.8	2.96	25	1.36
		13	1.77	5.3	2.8	1.63	46	1.15
		14	3.17	7.3	2.8	1.23	60	1.22
		15	—	ca 11.2	2.8	0.750	99	—
		16	7.0	11.2	19.7	0.752	99	1.13
		17	13.7	15.2	19.7	0.550	135	1.13
		18	127	21.1	19.7	0.450	165	1.28
		19	9.43	15.7	5.7	0.517	144	1.09
H ₂ SO ₄ + NaHSO ₄ ,* pH 0.23	25	19	9.43	15.7	5.7	0.517	144	1.09
NaHSO ₄ (18.36% w/v),* pH 0.36	25	20	4.65	15.8	2.8	0.509	146	1.08
NaHSO ₄ + Na ₂ SO ₄ ,* pH 1.19	25	21	1.43	15.8	0.9	0.467	159	0.99

* SO₄²⁻ concentration as in H₂SO₄ (15% w/v).

7.5%; it is similar to that obtained by changing to sulfate solutions of higher pH (Fig. 3).

Influence of temperature.—Reducing the bath temperature from 25° to 17°C had a marked influence on the final anodizing current density, Table I, but not on the general shape of the curves. These results are discussed later.

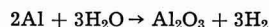
Initial part of the transients.—The initial parts of some of the transients were examined in more detail by photographically recording oscillograph traces. Figure 6a shows a typical trace for anodizing in 3% ammonium borate solution, Fig. 6b one for 15% sulfuric acid solution. These are not strictly comparable because of the much higher electrolytic resistance of the ammonium borate solution, which produced a considerable ohmic drop; Fig. 6c shows a typical trace for the 15% sulfuric acid solution with a 16.8

ohm compensating resistor in series, and the close qualitative resemblance of this trace to Fig. 6a is evident. Figure 6d is a typical trace for the 18.36% sodium dihydrogen sulfate solution, pH 0.36, also with a series resistor; it is almost identical with the trace of Fig. 6c. It is evident that the early part of the film formation is substantially the same for all solutions, and it seems very probable that the process is the formation of a barrier layer of Al₂O₃ (γ or amorphous) in every case.

We shall assume that an Al₂O₃ layer grows according to Eq. [1] with $A = 10^{-18}$ amp/cm², $B = 3.1 \times 10^{-6}$ cm/v. E_F , the forming voltage across the film between the metal and the solution, is given by

$$E_F = E_{app} + E_{int} - \eta_c - i\sigma(R_{sol} + R_{ext}) \quad [2]$$

Here E_{app} v is the applied emf (Fig. 2). E_{int} v is the emf of the cell having as over-all reaction



As pointed out by Vermilyea (19), such an "internal" emf must be included as part of the driving force in the anodizing circuit; from the free energy of formation data in the literature (20) we take it as 1.50v. η_c v is the overpotential at the cathode, measured in separate experiments. i amp/cm² is the current density at the anode and σ cm² its surface area, R_{sol} Ω is the resistance of the cell solution (measured with a bright platinum anode of the same geometry as the aluminum anodes at 10 kc/sec on an a-c bridge) and R_{ext} Ω is the external series resistance as shown in Fig. 2. Thus, substituting the value of E_F given by Eq. [2] in Eq. [1], we can estimate the

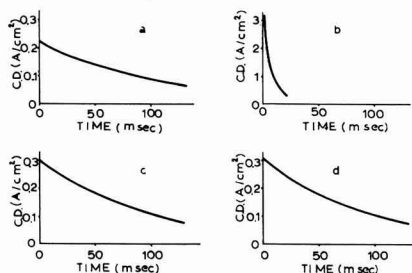


Fig. 6. Current transients for anodizing at 14.4v and 25°C in various solutions oscillographically recorded (a) 3% ammonium borate; (b) 15% w/v sulfuric acid; (c) 15% w/v sulfuric acid with 16.8 ohm in series; (d) NaHSO₄ (183.6 g/l) with 16.8 ohm in series.

Table II. Anodic film thickness at earliest stages, estimated from charge passed (X) and from Eq. [1] (Y)

Applied emf: 14.4v. Temp, 25°C												
Solution	Solution resistance, R_{sol} , ohm	Series resistance, R_{ext} , ohm	Area of specimen, σ , cm ²	Time of anodizing, t , msec	Current density, i , ma/cm ²	Cathode over-potential, η_c , v	Forming voltage, E_F	Charge passed, $\int_0^t i dt$, mc/cm ²	Anodic film thickness from $\int_0^t i dt$, X, A	Total film thickness from i and Eq. [1], A	Anodic film thickness from i and Eq. [1], Y, A	$\frac{X}{Y}$
H ₂ SO ₄ (15% w/v)	0.3	16.8	2.59	0	300	0.8	1.8	0	0	13	0	—
				50	181	0.7	7.2	12.0	62	56	43	1.44
				100	108	0.6	10.5	19.2	99	83	70	1.41
NaHSO ₄ (18.36% w/v)	0.5	16.8	2.56	0	313	0.5	1.5	0	0	11	0	—
				50	184	0.3	7.5	12.2	63	58	47	1.34
				100	107	0.3	10.9	19.4	100	86	75	1.33
Ammonium borate (3% w/v)	17.9	0	2.69	0	225	0.8	4.3	0	0	33	0	—
				50	140	0.8	8.4	8.8	46	66	33	1.39
				100	90	0.7	10.9	14.6	75	87	54	1.39
Ammonium tartrate (3% w/v)	5.5	6.0	2.68	0	330	0.9	4.8	0	0	37	0	—
				50	190	0.8	9.2	13.4	69	71	34	2.03
				100	119	0.7	11.5	21.6	111	91	54	2.05

film thickness y cm for any current density i . We can also estimate the thickness of film formed by anodizing from the charge passed at time t , $\int_0^t i dt$, and the density of Al₂O₃, taken as 3.42, assuming a roughness factor of unity and no film dissolution. Film thicknesses estimated by the two separate methods, for $t = 0, 50$, and 100 msec, for several solutions, are given in Table II, of which the salient features are:

(A) The initial film thickness, before the application of the anodizing emf, is small but significant: from the value in the borate (pH 8) solution, it is about what would be expected for the film left after chemical polishing. The smaller values found in the acid solutions may indicate some dissolution of the initial film, occurring before the anodizing emf was applied. These estimates assume, of course, that the film left after chemical polishing obeys Eq. [1] with the same values of A and B as those appropriate to Charlesby's anodic films.

(B) The agreement between the film thickness as obtained from the i/E_F relationship and from $\int_0^t i dt$ might be thought as good as could be expected, in view of the thinness of the films. However, the differences found are almost certainly significant. It is notable that the ratio

Anodic film thickness estimated from charge passed

Anodic film thickness estimated from Eq. [1]

is always in the range 1.33-2.05. It is probable that the small ratio arises mainly because the "roughness factor" is somewhat larger for our surfaces with very thin films than it was for the much thicker films from which A and B in Eq. [1] were determined by Charlesby (3); it is evident that the estimate of film thickness from charge passed diminishes in inverse proportion to the roughness factor, and it is easily shown that the estimate from Eq. [1] increases slightly with increase of roughness factor. The use of values for A and B given in the early work of Gunterschultz and Betz (2), 3.62×10^{-23} amp/cm² and 4.25×10^{-6} cm/v, respectively, merely alters the

range of the above ratio to 1.2-1.9, without affecting the argument.

These quantitative results, experimentally scarcely distinguishable for the various solutions, are good confirmation that the initial process is the formation of a barrier layer almost independent of the solution.

The current density at which the i/t relationship for the film-forming begins to deviate from that for the nearly neutral solutions, i_p , the minimum current density, i_m , and the final steady current density, i_s , (Fig. 3, 4, 5, 7) depend on the solution, in particular on its pH and temperature. Decrease of pH and/or increase of temperature leads to larger values of i_p , i_m , and i_s ; i_p is, of course, difficult to determine quantitatively. i_m , evidently governed by the overlap of transients representing different processes, Fig. 7, has qualitative relevance in that it occurs earlier, showing that the second process leading to the increase of i with time begins sooner, at lower pH values and higher temperatures.

These results are most easily interpreted by supposing that at i_p pores begin to form, and that by the time i_s is reached, the pore distribution is complete; the growing porous film subsequently offers very little resistance to its own growth, its resistance being almost completely provided by the steady-state pore-base layer. We note here particularly that

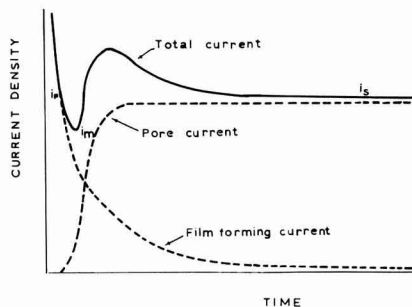


Fig. 7. Schematic illustration of "overlapping" processes leading to minimum in current transient.

the process leading to deviation from the initial barrier growth does not begin until i , and thus the field between the metal and the solution (Eq. [1]), is small enough. Since this process begins at higher values of E_F when the solution pH is lower and/or the temperature higher, we conclude that it is the thermal entry of protons from the solution into the barrier film against the field. We consider later a mechanism by which such a process may be expected to initiate pores.

Electron microscopic examination.—Figures 8a and b are electron micrographs of shadowed carbon replicas of the surface of anodic films formed at 25°C 14.4v respectively for 0.5 sec and 10 min in 3% ammonium tartrate solution. In Fig. 8a no pores are

visible; the few singularities of irregular distribution are defects in the original pre-anodizing film or in the replica. In Fig. 8b there are distinct indications of a few pores, which may be supposed to have become initiated just as in the acid-formed films, but after the much longer time lapse. Figures 9a and b show similar replicas of the surface of anodic films formed in sulfuric acid at 14.4v, 25°C respectively for 0.25 sec and 5 sec. In Fig. 9a a substantial pore-free area is visible, although some pore initiation has already occurred; it was impossible to anodize for a short enough time and to remove the specimen before i_p was reached. In Fig. 9b the pore system may be seen to be fully established.

These results are in harmony with the interpretation of the current density transients, that pores are

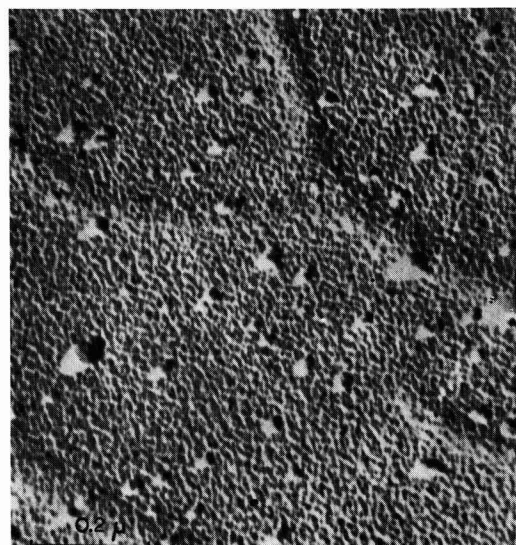
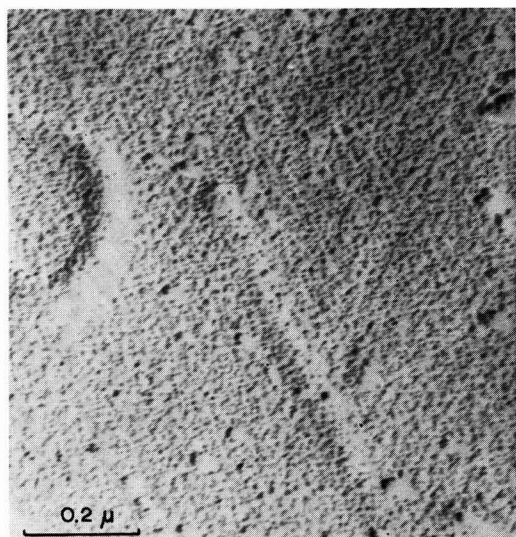


Fig. 8. Electron micrographs of oxide surface of specimens anodized in 3% ammonium tartrate at 14.4v 25°C (carbon replica, Au-Pd shadowed). (a) (top) anodizing for 0.5 sec; (b) (bottom) anodizing for 10 min.

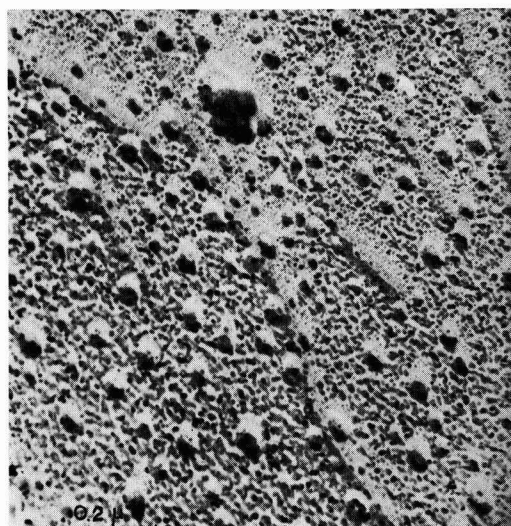
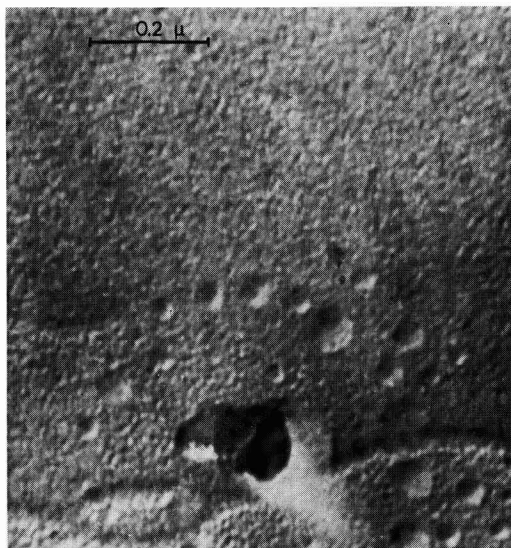


Fig. 9. Electron micrographs of oxide surface of specimens anodized in 15% H_2SO_4 at 14.4v, 25°C (carbon replica Au-Pd shadowed). (a) (top) anodizing for 0.26 sec; (b) (bottom) anodizing for 10 sec.

not initiated until the field across a first-formed barrier layer falls low enough, to a value that is lower for higher solution pH and lower temperature. It is significant that these are well-known conditions for the formation of less porous and nearly non-porous films.

Franklin's conclusion (16) that formed barrier-layer films may contain pores is also confirmed, but his suggestion that these pores originate in the earliest stages of formation formed is not supported by our results.

Later part of the transients.—Impedance measurements.—To confirm that the pore distribution is complete and a steady-state pore-base layer established by the time i_s is reached, the specific impedance of the electrode surface was measured with specimens anodized as far as i_s and after. The bridge method of Hoar and Wood (14) with an input of ca. 3 mv at 30 cps was used; as shown by Hoar and Wood, a balancing capacitance with series resistance gives the pore-base-layer capacitance very closely under these conditions, since the impedance is almost solely that of the pore-base-layer capacitance in series with the pore resistance of any porous layer. The pore-base-layer capacitance per unit area, together with the density 3.42 and dielectric constant 8.4 of Al_2O_3 , then gives directly the pore-base-layer thickness, and even if wrong values of the parameters are used,² the results are comparable. That the outer conductor of the assumed "parallel plate" pore-base-layer capacitor consists of an hexagonal pattern of small pore-bases rather than a complete plate scarcely matters, as shown by Dekker and Urquhart (22).

Some results for sulfuric acid and sulfate solutions are given in Table I. It may be seen that barrier layers of thickness some 10 Å/v of forming voltage E_F are indeed present when i_s has been reached, and that they change very little with the total amount of film formation (runs 3,4; 8,9; 15,16). The slightly thicker pore-base layers found with the less acid solutions (runs 17, 19, 20, 21) are qualitatively in line with the smaller values of i_s .

Figure 10 is a plot of $\log i_s$ vs. E_F/y , the "mean" field across the pore-base layer of thickness y . There is no obvious correlation, even among groups of points representing different pore-base layers in the same solution. However, all the points lie fairly close to lines

$$\log i_s = \log A + \frac{BE_F}{2.303y}$$

the logarithmic form of Eq. [1], whether we take $A = 10^{-18}$ amp/cm², $B = 3.1 \times 10^{-6}$ cm/v following Charlesby (3) or $A = 3.62 \times 10^{-23}$ amp/cm², $B = 4.25 \times 10^{-6}$ cm/v from the earlier results of Gunterschultz and Betz (2), both obtained from relatively thick barrier layers formed at high forming voltages in various ammonium borate solutions. This is further evidence that the thin pore-base layer under-

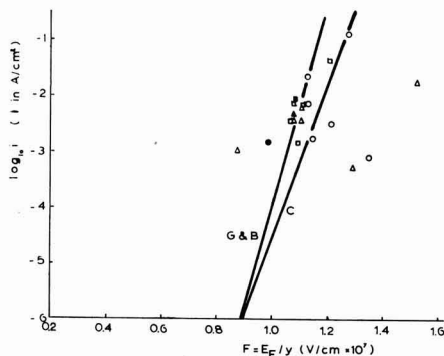


Fig. 10. Logarithm of current density vs. electric field across the pore base. □, H_2SO_4 (15% w/v), 17°C; △, H_2SO_4 (7.5% w/v), 25°C; ○, H_2SO_4 (15% w/v), 25°C; ■, $H_2SO_4 + NaHSO_4$ pH 0.23, 25°C; ▲, $NaHSO_4$ (183.6 g/l) pH 0.36, 25°C; ●, $NaHSO_4 + Na_2SO_4$ pH 1.19 25°C; G & B, line given by $\log i = \log A + BF/2.303$ using $A = 3.62 \times 10^{-23}$ amp/cm²; $B = 4.25 \times 10^{-6}$ cm/v according to Gunterschulze and Betz (2); C, similar line using $A = 10^{-18}$ amp/cm²; $B = 3.1 \times 10^{-6}$ cm/v, according to Charlesby (3).

lying the porous layer in sulfuric acid or sulfate solutions has electrical properties that are nearly quantitatively the same as those of the thick barrier layers formed in borate solutions.

Discussion

During the early stages of barrier-layer thickening, the cell voltage comprises potential drops across the metal/film interface, through the film, across the film/solution interface, through the solution, and at the cathode. As the (nonohmic) film resistance increases and the current density decreases, the potential drop through the film increases and all the other potential drops, including that across the film/solution interface, decrease. Thus pore initiation at the film/solution interface, so far from being field-assisted, appears to be field-inhibited; it occurs only when the field across the film/solution interface is sufficiently low. The only processes that could operate against the anodic field are the "thermal" passage of O^{2-} anions outward or that of H^+ cations inward. Either process would clearly be favored by an acid solution as compared with the nearly neutral solutions in which pores are not nearly so readily initiated. We think that proton passage into the film is much the more probable, because it leads to no loss of anions from the barrier layer, which becomes only very slightly thinner during the subsequent porous film formation.

If protons enter the barrier layer against the field, either statistically at random or at already welcoming positions such as a grain boundary, a vital consequence ensues. It is known that the hydrated oxides of aluminum have lower specific electrical resistance than the anhydrous oxides. It is thus very likely that quite a small degree of protonation gives an appreciable drop of specific resistance. Thus at a favorable protonated spot, the current density increases. Local Joule heating in the adjacent solution and in the film itself then still further favors the rate of proton uptake, and that of Al^{3+} dissolu-

²Hoar and Wood (14) used 10.0 for the dielectric constant; others have used 8.4. It is unlikely that the barrier layer material is in fact stoichiometric Al_2O_3 ; it may well contain protons and SO_4^{2-} ions in amounts depending on the conditions. Furthermore the dielectric "constant" ϵ no doubt increases at high frequencies (21). Within the range of our conditions, however, ϵ is probably very nearly constant.

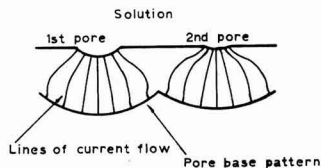


Fig. 11. Schematic picture demonstrating the spreading of pore nuclei on the surface of the initial barrier film.

tion. Thus a pore begins to form in depth, (any thinning caused by any O^{2-} dissolution further reducing the film resistance), and also to spread radially.

If the heating effect were the sole consequence of proton entry followed by pore initiation, the pore would spread radially until general film dissolution occurred, as indeed happens at forming voltages greater than 25v in 15% sulfuric acid. Otherwise put, the probability of initiation of a second pore is greatest at the edge of the first, where the heating effect is largest. We have to explain why the pore spreads to only a small degree (radius ca. 50-100Å) and why subsequent pores in fact nucleate at a distance from the first.

The possible charge carriers within the barrier layer are Al^{3+} , O^{2-} , OH^- , and H^+ ions, moving under high-field conditions. Considerably more Al^{3+} than the equivalent of O^{2-} or OH^- must be transported through the barrier layer, because some of the Al^{3+} dissolves into the solution in the pore. It is unlikely that the values of the various cation and anion mobilities are close to each other. If the Al^{3+} mobility is greater than that of O^{2-} and OH^- , in the steady state there will be a positive ionic space charge in the barrier layer in the neighborhood of the nucleated pore. Such a charge distribution will tend to inhibit further H^+ uptake from the solution into the barrier layer, the inhibiting effect being greatest nearest to the growing nucleus, and to discourage the further concentration of current near to the pore; thus the probability of initiation of a second pore will increase with the distance from the first.

The opposing effects set out above will lead to a maximum probability of further H^+ uptake at a particular distance from the center of the first nucleus; owing to the geometrical form of current distribution spreading in the barrier layer from the first nucleus (Fig. 11) this distance will be approximately twice the barrier layer thickness. As soon as a second nucleus has so developed on the circumference of such a circle around the first, a third nucleus may be expected at the intersection of the similar circles around the first and second; repetition of the process will, of course, produce the hexagonal pattern. This may be expected to spread over the surface from a relatively small number of primary nuclei, in the short period during which the mean total current density over the whole surface increases to the value characteristics of porous-film formation.

The electrical properties of the initial barrier layer and the steady-state pore-base layer that form in sulfuric acid and sulfate solutions are evidently closely similar to those of thin or thick barrier layers formed in nearly neutral borate or tartrate solutions. It is clear that all these films are, basically, nearly anhydrous, nearly amorphous alumina: the well-known incorporation of substantial amounts of sulfate, borate, etc., anions into the "lattice" has no very great effect on the electrical or mechanical properties, probably because one SO_4^{2-} replaces four O^{2-} , one BO_3^{3-} , three O^{2-} etc., a matter we shall discuss elsewhere. The entry of protons, however, gives the very marked effect that we suggest perhaps because of the great modification of the anion lattice consequent upon the production of OH^- and of hydrogen bonding.

Acknowledgments

The authors are grateful to the Aluminum Development Association for a maintenance allowance to one of them (J.Y.) for the period during which this work was carried out, and to Messrs. J. C. Bailey and F. C. Porter of the Association for very useful discussions and for arranging supplies of aluminum.

Any discussion of this paper will appear in a Discussion Section to be published in the December 1963 JOURNAL.

REFERENCES

- G. Hass, *J. Am. Opt. Soc.*, **39**, 532 (1949).
- A. Guntherschultze and H. Betz, *A. Physik*, **92**, 367 (1934).
- A. Charlesby, *Proc. Phys. Soc.*, **66B**, 317 (1953).
- H. A. Johansen, G. B. Adams, and P. Van Rysselberghe, *This Journal*, **104**, 339 (1957).
- E. J. W. Verwey, *Physica*, **2**, 1059 (1935); *J. Chem. Phys.*, **3**, 592 (1935); *Z. Krist.*, **91**, 65, 317 (1935).
- N. Cabrera and N. F. Mott, *Rep. Prog. Phys.*, **12**, 163 (1948).
- J. F. Dewald, *This Journal*, **102**, 1 (1955).
- M. S. Hunter and P. Fowle, *ibid.*, **101**, 481, 514 (1954).
- F. Keller and A. H. Geisler, *Trans. AIME*, **156**, 82 (1944).
- F. Keller, M. S. Hunter, and D. L. Robinson, *This Journal*, **100**, 411 (1953).
- C. J. L. Booker, J. L. Wood, and A. Walsh, *Brit. J. Appl. Phys.*, **8**, 347 (1957).
- K. Huber, *Z. Elektrochem.*, **62**, 675 (1958); *J. Colloid Sci.*, **3**, 197 (1948).
- A. C. Jason and J. L. Wood, *Proc. Phys. Soc.*, **68B**, 1105 (1955).
- T. P. Hoar and G. C. Wood, *Electrochim. Acta*, **7**, 333 (1962).
- T. P. Hoar and N. F. Mott, *J. Phys. Chem. Solids*, **9**, 97 (1959).
- R. W. Franklin, *Nature*, **180**, 1470 (1957).
- G. C. Wood, M. Cole, and T. P. Hoar, *Electrochim. Acta*, **3**, 179 (1960).
- R. B. Mason, *This Journal*, **102**, 671 (1955).
- D. Vermilyea, *ibid.*, **101**, 389 (1954).
- W. L. Latimer, "Oxidation Potentials," 2nd Ed., Prentice-Hall, (1959).
- J. J. McMullen and M. J. Pryor, 1st Int. Congr. Met. Corrosion, Butterworths, London, p. 52 (1962).
- A. J. Dekker and H. Urquhart, *Can. J. Res.*, **B28**, 541 (1950).

The Corrosion of 1100 Aluminum in Oxygen-Saturated Water at 70°C

J. E. Draley, Shiro Mori, and R. E. Loess

Argonne National Laboratory, Argonne, Illinois

ABSTRACT

In oxygen-saturated distilled water at 70°, the rate and amount of corrosion during short exposure are influenced by experimental conditions. One noteworthy effect is that contamination of the water by the reaction increases the corrosion rate. Subsequent to the first several days, the amount of corrosion varies with the logarithm of the exposure time. This behavior holds for at least 180 days; it is believed to hold for as long as tests have provided reasonable data, the longest being about 650 days. These results are interpreted in terms of local film rupture and growth. A method of averaging the over-all corrosion rate on the basis of cyclical local reactions is derived.

The corrosion of aluminum in nearly pure water has been under study in this laboratory for a number of years. Originally 1100 aluminum (then 2S) was chosen for study at temperatures below 100° because it was under consideration for use in water-cooled nuclear reactors. Subsequently, when the research objective became simply the determination of corrosion mechanisms, the same alloy was continued under study. Although this alloy contains a number of impurities, the major ones being iron, silicon, and copper, its behavior is reproducible, and the backlog of information previously obtained is helpful in interpreting more recent results and in testing hypothesized mechanisms.

A certain amount of research has also been done with pure aluminum in water. From the point of view of kinetic studies this material does not lend itself to relatively simple treatment because of the local penetrating attack which takes place at grain boundaries, and because of a sensitivity to the amount of impurities present.

In a previous publication (1), many of the features of the corrosion of 1100 aluminum in oxygen-saturated distilled water at 70° have been described. Of particular interest to the present investigation are: (A) No gross pitting occurs, although micropits of the order of 20 μ in diameter form. These do not grow in size, but their number increases. Localized, self-stiffing reaction is indicated. (B) After sufficiently extended exposure, bits of the corrosion product slough or flake off, leaving a metallic sheen. The corrosion product does not again grow thick in those places, and there is no observable increase in corrosion of the specimens. It is apparent that, at least at long exposure times, the protective oxide is thin and the bulk of the corrosion product coating is not significantly protective.

Also in the same publication, some aspects of the kinetics of the reaction were given. For the first several hours of exposure of wet-ground specimens the amount of corrosion varied as the logarithm of time; subsequently, an increase in rate occurred, followed by a period of diminishing corrosion rate. The shape of this part of the curve was not established.

In the present publication, some of the features of the initial period of corrosion are explored, the kinetics of the reaction during long exposure is de-

termined, and for the latter there is derived a rate expression which seems to fit the known facts.

Experimental

Water.—High quality water was provided for all tests by passing laboratory steam condensate through ion exchange resins and then distilling. Occasional spectrographic analyses showed only a few metallic elements present above the limit of detection. Sodium, potassium, and magnesium contents varied from a few ppb (grams per 10⁹g H₂O) up to 50 ppb.

This water was vigorously boiled in Pyrex carboys at room temperature (by pumping with a steam ejector) for degassing, and oxygen was bubbled through it for a period of time. Periodic measurement showed the water to have a pH of 6.5 \pm 0.2 and specific resistance 1.4 \pm 0.2 \times 10⁶ ohm-cm. No noticeable change in pH was caused by passage over the specimens; there was sometimes a slight increase in resistivity, indicating that the oxide-covered specimens had somewhat purified the water.

Method of exposure.—Eight (or fewer) specimens were suspended on Pyrex glass in the chamber shown in Fig. 1 (thermostatted to 70° \pm 1°C). Fresh water from the carboy was added continuously through a regulating section of Pyrex capillary, and the excess water was discharged to the drain.

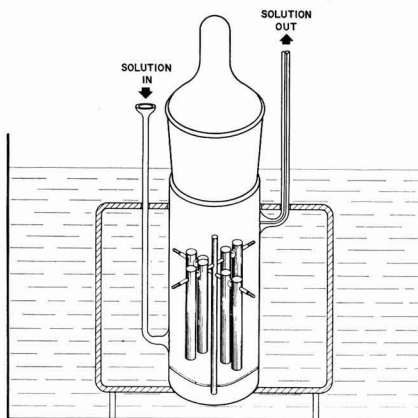


Fig. 1. Corrosion test chamber

The difference between the temperature and pressure in the test chamber and those in the storage carboy (2-4 psig O₂) caused continuous slow evolution of oxygen gas during the corrosion exposure. For the test of long duration, two chambers were used in series, with the refreshing water passing through each in turn; the rate was about 15 cc/min for the first 5 days and 7 cc/min thereafter.

Material and sample preparation.—The material source was one batch of commercially extruded 1100 aluminum rod. Analyses showed impurities to consist of: 0.54% Fe, 0.12% Cu, 0.07% Si, 0.017% Zn, 100-200 ppm Ti, 25-50 ppm Zr, 5 ppm Mo. Samples were prepared by careful machining to a size just slightly too large for use in the eddy current thickness gauge. They were then degreased and etched (10 cc conc. HNO₃, 1 cc 48% HF, 89 cc H₂O; about 60°C) until approximately 50μ had been removed. Specimens were rinsed and annealed (15 min at 360°C, slow cooled) before being weighed, measured in the thickness gauge, and corroded.

Determination of amount of corrosion.—Since the predominant corrosion product is an adherent oxide, specimen weight gain provides an approximate measure of the amount of corrosion. However, some of the oxide is lost to the water (dissolution, spallation, etc.), and the composition of the product changes with time as well as with exposure conditions. These features are illustrated in Fig. 2 where, for a single specimen, the gain in weight (G), the amount of metal corroded (L), determined by the eddy current gauge to be described, and the amount of aluminum lost from the specimen (ξ) during exposure to O₂-saturated water at 70°C are shown. The amount of metal lost was determined by chemical analyses of the effluent solution from the test chamber, after it had been concentrated by evaporation. It was necessary to correct these values for the amount of aluminum initially present in the water.

Using the approximation that the composition of the corrosion product is Al(OH)_x, the value of x is

readily shown to be equal to $\frac{G + \xi}{L - \xi} \cdot \frac{27}{17}$. This ratio

is observed to decrease with exposure time for the present experiment, although other types of change have sometimes been observed. It is typically not equal to 3.0, the stoichiometric composition of the

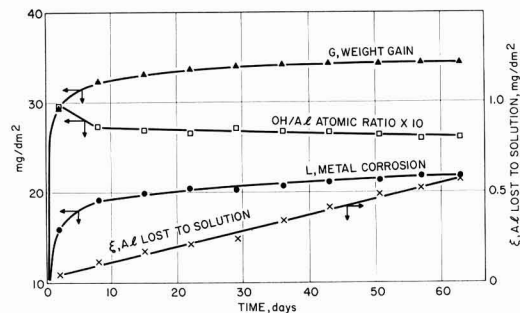


Fig. 2. Corrosion product composition and loss to water

oxide (bayerite) indicated by x-ray diffraction to comprise the bulk of the corrosion product.

There are two chemical methods available for determining directly the amount of unreacted metal at the end of an exposure. The metal can be dissolved in a solution of iodine in methanol (2), or the oxide can be dissolved from the surface (1). Both of these methods have been considered unsatisfactory for the present research. The errors for the specimens used range from about 0.1 mg (for the film removal method) to something several times this magnitude for the metal dissolution method. These errors are objectionably high and would make impossible a satisfactory determination of the kinetics of the reaction of 1100 aluminum with water after the first few months of exposure.

In addition to the inaccuracy of these two methods there is another problem. Different specimens characteristically corrode to a different extent, even though the corrosion rates in an individual test are generally identical, as well as can be measured, after extended exposure. Any method of determining the amount of corrosion which destroys the sample for subsequent exposure adds a kind of statistical scatter in the data which has made it impossible to determine curve shapes with reasonable confidence.

A specially developed eddy current thickness gauge is insensitive to the amount of oxide coating. For a few years it has been used in obtaining data which are believed reliable and of acceptable precision ($\pm 25\text{\AA}$ penetration). The change in the inductive properties of a coil are measured as a function of the thickness of metal placed within it. Details of this gauge are yet to be reported, although a first model (3) and a usable but less sensitive version have been described (4). The calibration curve, as used in the present investigation, is given in Fig. 3. The straight line drawn through the points for samples which were etched in HNO₃-HF solution continued linearly, beyond this figure, up through 200 mg of metal removed per sample. Since all specimens had the same surface area ($29.19 \pm 0.01 \text{ cm}^2$), this calibration curve could readily be used to determine the amount of corrosion in mg/dm².

The solid points are for specimens which had been corroded in water; most of those showing more cor-

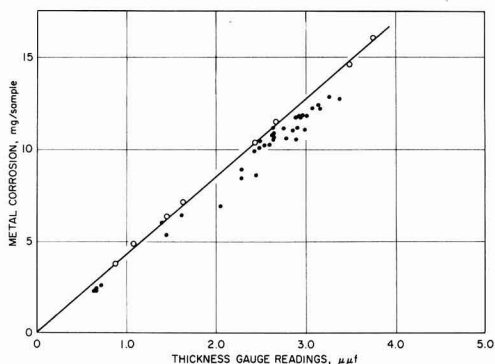


Fig. 3. Thickness gauge calibration curve; ○, etched HNO₃-HF; ●, corroded in H₂O.

rosion than 10 mg/sample were the ones used in determining the kinetics for extended exposure. In all such cases, the weight of metal corroded was obtained after removal of the corrosion product coating following exposure. It is noted that these points generally fall below the line. This is apparently a consequence of uneven corrosion of the specimens. During the early part of the exposure the specimens had less corrosion product near the ends than in the center, suggesting that less corrosion had taken place at the ends. As a consequence it is believed that data reported at present can be expected to apply to the central portion of the specimens only. The phenomenon is believed related to a water contamination effect during the initial stages of the corrosion reaction (see next section). For the longest exposure times, there is also another factor contributing to deviation of the points from the line. This will be described later.

Data and Results

Short time behavior.—In ref. (1) it was indicated that the amount of corrosion in water at 70° is proportional to the logarithm of time through about the first 7 hr of exposure. The characteristics of the corrosion kinetics in this stage have been investigated somewhat further. It is not considered suitable to discuss here all of the experimental parameters which influence the rate and amount of corrosion during early exposures. However, it is considered desirable to point out a few of the important observations for the purpose of adding perspective in the consideration of the longer time corrosion.

Effect of exposure interruption.—If it is desired to make a series of measurements of the amount of corrosion on the same sample, with further corrosion exposure between measurements, it is important to know whether the amount of corrosion has been influenced by removal from the test water and drying. Subsequent to the first several days of exposure, when reaction rates have become low, it has been demonstrated that there is no discernible effect of this interruption of the exposure.

For short exposures the situation is different. A series of 10 specimens was placed in one chamber and corroded together. These specimens were removed one at a time for exposures up through 48 hr, dried, and the amount of metal corroded determined

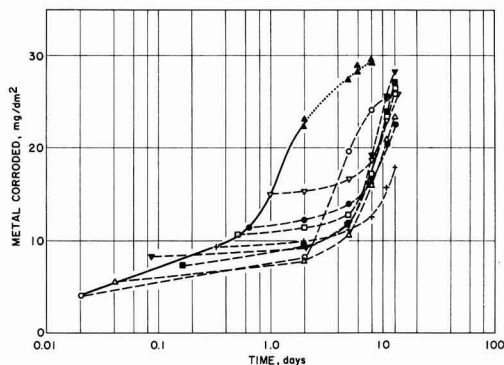


Fig. 4. Effect of exposure interruption

with the eddy current thickness gauge. Each of these specimens was subsequently reinserted in the test for further exposure, up to a total of about 13 days. The points representing continuous exposure are connected by a solid line in Fig. 4. This line is quite similar in character to data previously reported (1). There is apparently a logarithmic corrosion behavior up to something less than half a day, followed by an increase in slope of the line on semilog coordinates.

Note that after initial exposures through 1 day all specimens corroded at much lower rates on re-exposure to the water. The dependence of the rate on further exposure is not well determined, but there is a common break upward in the curves after a time of the order of 5 days. It is thus evident that removing the specimens and drying them causes a substantial reduction in subsequent corrosion rate and a delay of the upward break in the semilog plot.

Number of specimens.—There are a number of indications that during the initial stages, a product of the corrosion reaction contaminates the water and increases the amount of corrosion occurring. One of the indications of this is illustrated in Fig. 5. Two tests were run identically except that one chamber contained eight specimens and the other contained only one. It is characteristic that substantially more corrosion occurred per specimen in the chamber containing the greater area of corroding metal.

A number of other such comparative experiments have shown that the time of onset of the upward break in the semi-log plot and its magnitude are the most sensitive aspects of the corrosion reaction to this variable.

Refreshment rate.—When the number of specimens in the chamber was made the same but the rate of addition of refreshing water was changed from 5 to 16 ml/min similar results were obtained. Apparently the higher flow rate diluted the contaminant and reduced the magnitude of its corrosion-inducing effect.

Further illustration of this effect is shown in Fig. 6. Here the gain in weight of specimens corroded in identical fashion for 16 hr is plotted as a function of the rate of refreshment. It is indicated that for these particular conditions, something above 20 ml/min refreshment rate minimizes the effect of the

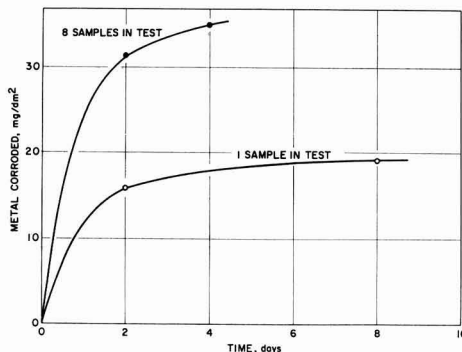


Fig. 5. Influence of number of specimens in test, refreshment rate 6 ml/min.

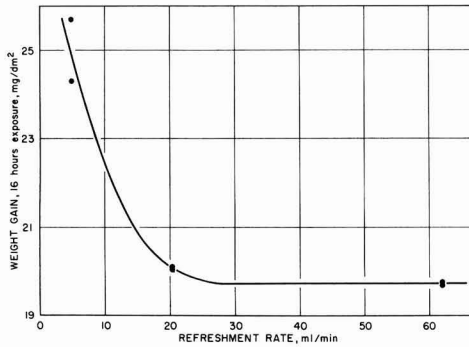


Fig. 6. Effect of rate of refreshment on amount of corrosion

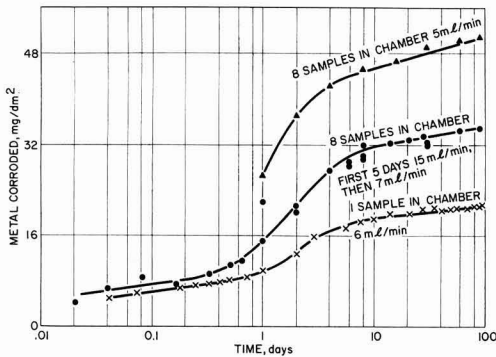


Fig. 7. Various effects of water contamination

contaminant, and that further increase in the refreshment has no further effect. The specimens in this series of experiments were wet-ground before exposure, but the results are believed to be indicative of the behavior of initially etched surfaces. The weight gain provides only an approximation of the amount of metal corroded, but the trend is evident.

In Fig. 7 are shown curves which seem to illustrate all of the three effects so far discussed: interruption, number of specimens, and refreshment rate. Comparison of the top two curves indicates that a high refreshment rate provides a smaller amount of corrosion (abetted by early interruption). Comparison of the middle and bottom curves shows that the effect of the number of specimens was greater than that of the refreshment rate. The middle curve was run at conditions which have now been taken as standard. For the earliest part of the exposure the flow rate was maintained high to minimize the effect of contamination; subsequently the refreshment rate was decreased for ease in performing the long time experiment.

Reproducibility.—For longer tests it is characteristically observed that different specimens in the same test show amounts of corrosion which differ by perhaps 10% although the rates of corrosion seem to be identical. This effect is a consequence of variable behavior of specimens during early exposure. The slopes of the logarithmic curves generally have been equal prior to the upward break: however the time at which the break occurs has varied over a

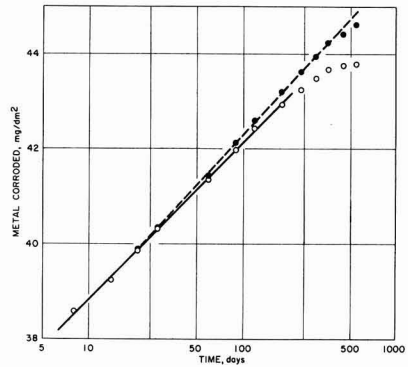


Fig. 8. Long term kinetic behavior; ○, uncorrected; ●, corrected

fairly wide range, and this has influenced the height of the final plateau.

Long Time Behavior

The results of one long test will be described here. As a precaution against possible metallurgical changes in the specimens which would influence the readings taken on the eddy current thickness gauge, three specimens were maintained in a helium environment. These were kept in the same constant temperature bath which was used for the corrosion exposure, and they were removed and replaced at the same times as the corroding specimens. Their apparent thicknesses, as determined by the gauge, were recorded periodically.

The changes in thickness gauge readings were significant, but very erratic. The general trend and all total changes were in the direction opposite to the change caused by corrosion, although there were irregular reversals, sometimes quite large. It was concluded that some metallurgical changes, influencing thickness gauge readings, were occurring at corrosion temperature. Aging was suspected as the primary change; its rate and even the rate law were not satisfactorily determined. It was clear that the change was minor for about the first 180 days of test.

For corroding specimens, plots of thickness gauge readings from 8 days onward showed that corrosion was logarithmic for 180 days exposure. Such data for one specimen (No. VI) are shown as the open circles in Fig. 8. A good straight line is formed, with relatively little scatter. Subsequent to 180 days, consistent deviation of the points from a straight line is observed. Only one reading, at one day, was taken for each specimen at times less than 8 days. This point was consistently far below the extrapolated long-time line. It is indicated that at that time the amount of corrosion had not yet reached the plateau following the upward short time break in the corrosion curve.

At 180 days, there remained six specimens in each chamber; two from each had been removed earlier to provide data for calibrating the thickness gauge. Data from these twelve were plotted (uncorrected) as in Fig. 9, and the basic constants of the logarithmic curves were determined for all except No. XV

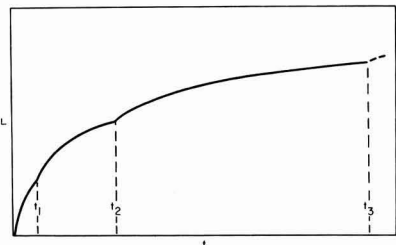


Fig. 9. Suggested corrosion at one point

(which unexplainably showed too much scatter to be used). The slopes and the extrapolated amounts of corrosion at one day (logarithmic "intercepts") are shown in Table I. The intercept values perhaps reflect the fact that the exposure was interrupted at 1 day and thus must be considered representative only of the particular experimental conditions employed.

Specimens II through VII were in the second chamber; their refreshing water was the effluent from the first chamber. The chamber containing specimens X through XIV received refreshing water directly from the storage carboy. Both the slopes and intercepts of the second chamber specimens were greater than those of the specimens in the first chamber (by about 17%).

It was clear that the available information was not sufficient to determine whether corrosion continued logarithmically to the end of the test at 547 days. In an effort to provide a reasonable estimate, corrections were calculated from the thickness gauge readings of the standard samples which had been aged in helium. It was assumed that the aging (or other metallurgical change) had occurred at a constant rate throughout the time they were kept at 70°, and that the average for the three standard specimens could legitimately be applied to each corrosion specimen. Accordingly the "least squares" slope of all of the thickness gauge changes of the standards (as a function of time) was determined and used to calculate "corrections" to be added to the basic data for the corrosion specimens. As illus-

Table I. Constants for logarithmic corrosion
1100 Aluminum, distilled water, 70°C, O₂-saturated

Specimen No.	Slope,* mg/dm ² -cycle	L at 1 day,* mg/dm ² (extrapolated)
II	3.15	35.36
III	3.22	36.70
IV	3.28	33.47
V	3.16	36.98
VI	3.26	35.61
VII	3.29	34.20
Average	3.23	35.59
X	2.62	30.20
XI	2.83	30.37
XII	2.91	30.15
XIII	2.77	30.95
XIV	2.78	29.32
Average	2.78	30.20

* Determined from uncorrected data.

trated in Fig. 8, the "corrected" points formed reasonably good straight lines on the semilog plots for the full test duration. There was also a slight increase in slope in going to corrected values, but in view of the uncertainties in the corrections it is not considered desirable to report the corrected slopes and intercepts.

Some years ago, before the thickness gauge had been perfected, a corrosion test was run, at the same nominal conditions as those for the present report, for a total exposure time of 940 days. The average gain in weight of all the specimens varied linearly with the logarithm of time from 18 through 650 days. Beyond that time, the weight gain showed some decrease and some erratic behavior, probably because of the sporadic sloughing of some of the corrosion product. Although the weight gain is not considered to be a truly reliable indication of the amount of corrosion, these observations tend to support the opinion that long-term corrosion remains logarithmic.

Discussion

The dependence of short time corrosion on many experimental parameters indicates the need of extensive investigation to understand the reactions. In particular, the nature of the water contamination by the corrosion reactions and how this influences corrosion rate should be studied. Some efforts to do this are being made in this laboratory. The variation of the pH of the water is being measured as a function of time and position, both along the surface and normal to it. Substantial pH changes do occur, particularly close to the corroding surface (0.1 mm).

It has seemed to be true that initial corrosion is logarithmic and is followed in turn by an increase in rate and by a subsequent extended period of logarithmic reaction. It has not been determined for how long this extended period endures. The rate law seems clearly to hold for at least 180 days; subsequently, it can only be guessed that to a total observation time of 650 days no change in kinetics occurs.

It is interesting to speculate as to the mechanism which is responsible for the long time, reproducible, logarithmic corrosion behavior. Previous observations, as pointed out in the introduction, have indicated that at any one time much of the corrosion reaction occurs at a small number of localized points, and that most of the corrosion product coating is not influential in determining corrosion rate. These observations suggest that previous derivations (5) are not sufficient to explain the corrosion behavior. The following development of a rate expression is based on the periodic logarithmic growth and breakdown of protective oxide.

It is assumed that at any point on the specimen surface corrosion follows logarithmic curves of the type indicated in Fig. 9. Subsequent to each time that breakdown of the protective film occurs the initial rate of reaction is less than at the preceding break. The total amount of corrosion occurring in each cycle is the same; consequently the duration of succeeding cycles is longer.

It is also assumed that at any time the various points on the corroding specimen are behaving as

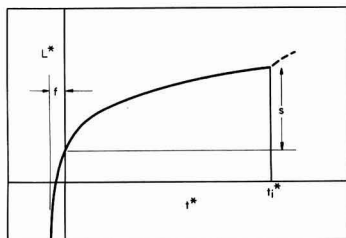


Fig. 10. Hypothetical rate curve for one time

though at random points along a characteristic logarithmic growth curve. Thus, corrosion rates of points on the specimen are equal to slopes of various portions of the following general equation from 0 to t_i^* (illustrated in Fig. 10)

$$L^* = a + b \ln (t^* + f) \quad [1]$$

The value of f determines the initial slope. t_i^* is the end of the curve segment, and s is the (constant) amount of corrosion occurring in the cycle.

The average corrosion rate will be the average slope of this line from 0 to t_i^* . The value of this is

$$\frac{dL^*}{dt^*} = \frac{s}{t_i^*} \quad [2]$$

Now, realizing that s is equal to $L_{t_i^*}^* - L_0^*$, an expression for it can readily be obtained from Eq. [1]. Rearranging, by solving for t_i^* , gives Eq. [3]

$$t_i^* = f (e^{s/b} - 1) \quad [3]$$

Substituting this into Eq. [2] gives Eq. [4], which is the average (over the surface) rate of corrosion for the specimen at any one time.

$$\frac{dL^*}{dt^*} = \frac{s}{f (e^{s/b} - 1)} \quad [4]$$

In order to decrease (with respect to time) the corrosion rate immediately following the various breaks in the local corrosion curve, it is now assumed that $f = ct$. Substituting this into Eq. [4] and dropping the $*$, since we are dealing with actual corrosion rather than a hypothetical curve for some particular time, the over-all rate expression in Eq. [5] is obtained.

$$\frac{dL}{dt} = \frac{s}{ct (e^{s/b} - 1)} \quad [5]$$

Integrating, and using the boundary condition that $L = a$ when $t + ct = 1$, the expression given in Eq. [6] is obtained.

$$L = a + \frac{s}{c(e^{s/b} - 1)} \ln [t(c + 1)] \quad [6]$$

This is observed to be a simple logarithmic equation of the form $L = K_1 + K_2 \ln t$.

It has not been possible to demonstrate that this derivation correctly explains the logarithmic dependence of the amount of corrosion on time. It does seem to fit the known observations. It is an attractive hypothesis in that the amount of corrosion for each cycle at any particular point on the specimen surface is constant. This suggests that the cause of the break is some direct effect of the total amount of corrosion which occurred during this cycle. At this time the part of the corrosion process which is preferred to explain this is the liberation of gaseous hydrogen beneath the protective oxide film. It is assumed that a fixed percentage of the corrosion product hydrogen is produced beneath the oxide film (6); that when the gas at any point reaches the amount required to generate pressure sufficient to rupture the oxide, the film is broken and the next cycle of the logarithmic growth is ready to begin. This analysis suggests that a given area is alternately cathodic and anodic (in accordance with surface appearance), and that the cathodic activity is largely responsible for activation and the change to active anodic corrosion.

There is nothing in the present research which offers an explanation for the apparent fact that local oxide growth is logarithmic. Evans (5) has derived such a rate expression in which it is assumed that there is healing or filling of internal cracks and voids in the (protective part of the) oxide film. On the basis of a number of observations, this explanation seems tenable, although the actual pore-filling mechanisms seem likely to be different from the simple one used by Evans.

It is believed that the present method of deriving an over-all rate expression for nonuniform corrosion is potentially applicable to many corrosion systems. A limitation to the value at the present time is that it appears to be quite difficult to determine experimentally the constants basic to the mechanism.

The work on this paper was performed under the auspices of the U. S. Atomic Energy Commission.

Any discussion of this paper will appear in a Discussion Section to be published in the December 1963 JOURNAL.

REFERENCES

1. J. E. Draley, "Aqueous Corrosion of 1100 Aluminum and of Aluminum-Nickel Alloys," Proceedings of AEC-Euratom Conference on Aqueous Corrosion of Reactor Materials, Brussels, Oct. 14-17, 1959; TID-7587 (U.S. Atomic Energy Commission), pp. 165-187.
2. M. J. Pryor and D. S. Keir, *This Journal*, **102**, 370 (1955).
3. W. B. Doe, "Eddy Current Type Diameter Gauge for Corrosion Measurements," ANL-5001 (Feb. 1, 1953) Argonne National Lab.
4. W. E. Ruther, *Corrosion*, **14**, 387t (1958).
5. U. R. Evans, "The Corrosion and Oxidation of Metals," pp. 829-30, 834-35, 837, Edward Arnold, Ltd., London (1960).
6. J. E. Draley and W. E. Ruther, *This Journal*, **104**, 329 (1957).

Contribution to the Electrochemical Behavior of Chromium and Iron-Chromium Alloys in the Transpassive Region

Th. Heumann and H. S. Panesar

Institut für Metallforschung der Universität Münster/Westf., West Germany

ABSTRACT

The polarization curves of Cr in electrolytic solutions containing different anions showed that these anions did not have any influence on the mechanism of dissolution of Cr in the transpassive region and that only OH^- ions take part. The current/potential curves of CrOOH and Cr_2O_3 demonstrated the possibility of the former compound being present in the passive layer. Measurements of the roughness factor of Cr after polarization in the active or the passive state indicated that the roughness of the surface remains constant within the accuracy of this method. The average roughness factor was 1.7. Further surface measurements were carried out on a Fe-Cr alloy (containing 27% Cr) which demonstrated an increase in the roughness of the surface after polarization of the alloy in the primary transpassive region.

During the past few years many investigations (1-9) of the electrochemical behavior of chromium and iron-chromium alloys have been carried out, which demonstrate their great tendency toward passivation. These experiments still do not give sufficient data to explain clearly the mechanisms of: 1, passivation; 2, dissolution in the transpassive region; and 3, activation and cathodic deposition. Almost all the investigations were carried out in sulfuric acid.

In order to discuss the most important mechanisms of passivation and dissolution in the transpassive state, we will consider current/potential curves which have been measured using the potentiostatic method. Figure 1 shows the current/potential curves of chromium in H_2SO_4 of different nor-

malities. An anodic current density of 10^{-3} amp/cm² in 0.2N H_2SO_4 , applied to a chromium specimen in the active state causes passivation. The passivation is complete at a potential value of -300 mv. As the potential is further increased, the sign of the current is reversed. Evolution of hydrogen takes place on the passive surface of the chromium. The next change in the current sign takes place at a potential which can vary over a wide range. The variations in this equilibrium rest potential are due to a small exchange current density. The smaller the amount of adsorbed hydrogen on the surface of the chromium, the greater is the value of the equilibrium rest potential.

In the passive region, chromium dissolves as trivalent Cr^{3+} , and when the potential is raised to 1050 mv and above it goes into solution as chromate. The polarization curves for the dissolution of Cr as chromate, which are reproducible, are displaced toward higher potentials as the pH of the electrolytic solution decreases and are parallel to each other (1). It was assumed from these observations that the dissolution of Cr as chromate in the transpassive region required 2 OH^- ions.

In the case of Fe-Cr alloys (Cr above 11%) a double passivation is observed (4). In the primary transpassive region the polarization curves of Fe-Cr alloys coincide with that of pure Cr and in the secondary transpassive region with that of pure iron.

The further investigations described in this report were designed to test or measure: (i) the influence of anions on the mechanism of dissolution of pure Cr in the transpassive region; (ii) the behavior of the compounds CrOOH and Cr_2O_3 on anodic polarization, because the passive layer on chromium could be composed of one of these compounds; and (iii) the true surface area of the Cr and Fe-Cr specimens after different preliminary treatments.

The electrolytic chromium was reduced in a hydrogen atmosphere at about 1300°C. Microscopic examination showed afterwards an absence of oxide

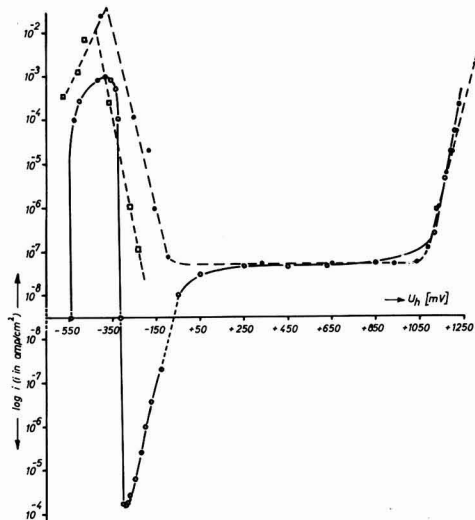


Fig. 1. Current density/potential curves of Cr in H_2SO_4 with different normalities measured potentiostatically; \circ — \circ , 0.2N H_2SO_4 (3); \square — \square , 0.1N H_2SO_4 (Kolotyrkin) and \bullet — \bullet , 1N H_2SO_4 (Kolotyrkin) (7), analytically determined.

inclusions. The material which had a larger grain size (1-2 mm) in comparison to the original one, was used for all further investigations.

The iron-chromium alloys were prepared by melting carbonyl iron and the purified chromium and annealed to homogenize before use.

Experimental details are given in the literature (1,2). All the investigations were carried out at 20°C.

Dissolution of Chromium in the Transpassive Region in the Presence of Different Electrolytes

The current/potential curves were measured in solutions of chromic, sulfuric, hydrochloric, nitric, and acetic acids. These acids contained the corresponding potassium salts to increase the conductivity and buffer action.

Figure 2 shows the results for hydrochloric acid. All the curves are parallel to each other and show the same potential/pH dependence as was observed in the previous investigations (1). The current/potential measurements in the remaining solutions gave identical results. When the potentials for a

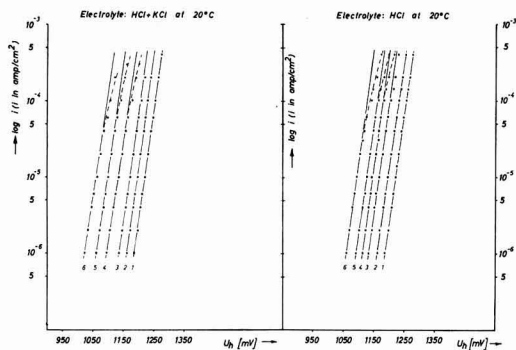


Fig. 2. Polarization curves of Cr with and without addition of KCl; left, pH, 1, 0.15; 2, 0.60; 3, 0.91; 4, 1.70; 5, 2.20; 6, 2.65; right pH, 1, 0.10; 2, 0.60; 3, 1.10; 4, 1.27; 5, 1.70; 6, 2.40.

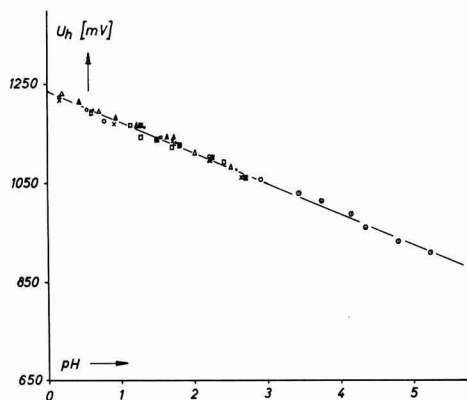


Fig. 3. Potential of Cr in different electrolytes in relation to the pH value with an anodic current density of 10^{-5} amp cm^{-2} . Solid circle, HNO_3 ; open triangle, 0.1M KNO_3 + HNO_3 ; open square with an x, H_2SO_4 ; open circle, 0.1M K_2SO_4 + H_2SO_4 ; x, HCl; open square, 0.1M KCl + HCl; open dotted triangle, chromic acid; open dotted circle, K-acetate + acetic acid.

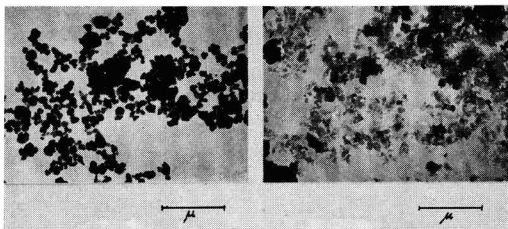


Fig. 4. Electron microscope photographs of CrOOH (right) and Cr_2O_3 (left) powder.

particular current density are taken from the curves for the different solutions and plotted against the corresponding pH a straight line with an inclination 65 mv/pH is obtained, as shown in Fig. 3. This shows clearly that the presence of different anions in the solution does not have any influence on the dissolution of chromium as chromate in the transpassive region and that only the OH^- ions are responsible. The transfer coefficients had the same value for the different electrolytes in the studied pH range. The Fe-Cr alloys show the same behavior as far as the primary transpassive region is concerned.

Polarization Curves of CrOOH and Cr_2O_3

These substances, in a very fine powder form,¹ were first examined with the aid of an electron microscope. Electron micrographs, in Fig. 4, show that their grains have almost the same size but different shapes.

Because of the low electrical conductivity of these materials it was not easy to study them electrochemically. The following treatment was successful, however.

The material, in a fine grained powder form, was suspended in a solution containing previously precipitated platinum. After stirring the solution for about 30 min it was possible to obtain a good homogeneous mixture. It was then filtered, washed with distilled water many times to get rid of Na^+ and Cl^- ions, and then dried. This mixture, containing an excess of platinum, was pressed into tablet form using a pressure of 150 kg/cm². The specimen so prepared possessed high conductivity and hardness. After imbedding in a special plastic material, they were abraded on 6/0 emery paper. These specimens then showed metallic luster. The ratio of the surface areas, oxide to Pt was 1:1.5 with corresponding weight ratios of 0.15:1.2g. The equilibrium rest potential values of the oxide electrodes in 0.1N H_2SO_4 were identical with those of Pt.

Before measuring current/potential curves on these electrodes by the galvanostatic method, they were cathodically polarized with a current density of 1 ma/cm², resulting in hydrogen evolution on the surface.

In order to investigate the influence of the Pt black in the electrode, a specimen consisting of a Pt-ring and a chromium disk was prepared. Figure 5 shows the Pt ring-Cr specimen. The polarization curves of this specimen are shown in Fig. 6. It is observed that the potential remains constant as the

¹ The authors are grateful to Dr. Hundt for supplying the pure compound CrOOH .

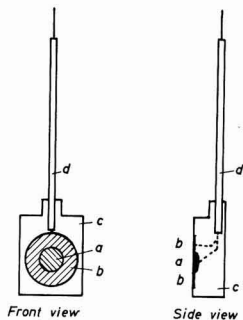


Fig. 5. Electrode composed of Pt ring and Cr disk; a, Cr; b, Pt ring; c, plastic material; d, isolated Cu wire.

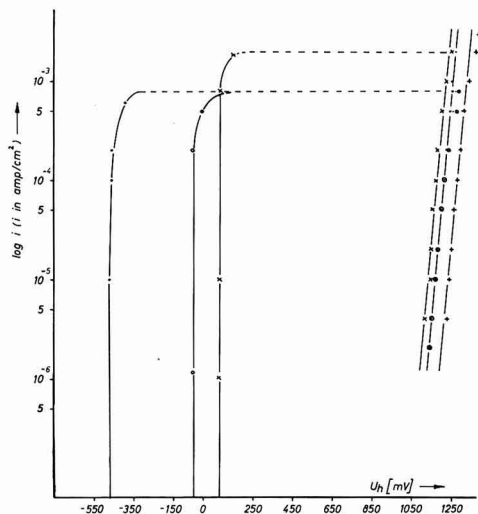


Fig. 6. Current density/potential curves of Cr, CrOOH, Cr₂O₃, and Cr-Pt ring electrodes. Electrolyte, 0.1N H₂SO₄ at 20°C; ○, Pt ring + Cr; ●, Cr; ×, Pt black + CrOOH; +, Pt black + Cr₂O₃.

current density increases. When the current density reaches a value of 1 ma/cm², there is a sudden increase in potential, and simultaneously the yellow color due to the formation of chromate is seen.

This fact is observed not only on the platinum ring-chromium electrode, but also on CrOOH and Cr₂O₃ electrodes. For the sake of verification, the polarization curve of pure chromium is plotted in the same figure. It is seen that in the transpassive region the Pt-ring-Cr curve completely coincides with the current/potential curve of the pure chromium electrode. It is therefore assumed that the presence of platinum does not in any way influence the dissolution of CrOOH and Cr₂O₃ as chromate, but increases only their conductivity.

Further, Fig. 7 shows that the current/potential curves of CrOOH and Cr₂O₃ and passive Cr are parallel to each other. With reference to the Cr curve, the CrOOH curve is displaced by 35 mv to a lower potential, and the Cr₂O₃ curve is shifted by 80 mv to a higher potential.

The parallel displacement of the CrOOH curve is due to the greater surface area of fine powdered

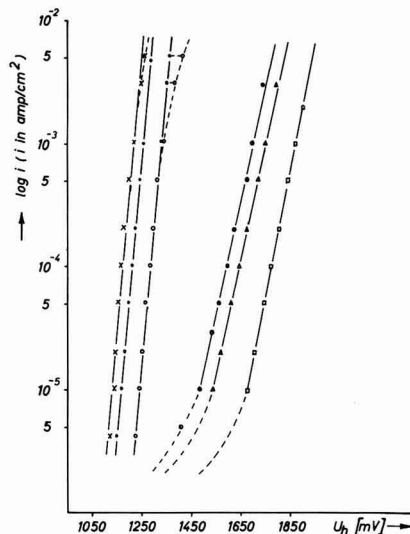


Fig. 7. Current density/potential curves on different electrodes in 0.1N H₂SO₄ at 20°C. ×, CrOOH; ●, Cr; ○, Cr₂O₃; □, Pt; △, Pt black pressed; ◇, Pt black deposited on Pt electrode.

CrOOH in comparison to that of chromium. The displacement of the curves to a lower potential, due to the increase in the surface area, can be explained by the results of the following investigation carried out on platinum.

Figure 7 shows the current/potential curve on platinum, platinum black in pressed form and platinum black deposited on a platinum electrode. They all run parallel to each other and are displaced in order of their surface areas to the lower potential values (surface areas: Pt black deposited > Pt black pressed > Pt). In the same figure the current/potential curves of oxide electrodes which were measured in a separate experiment, are plotted. Now because both the oxide materials have almost the same grain size (see Fig. 4) and therefore possibly the same areas and the same porosity when mixed and pressed with Pt black in the same proportion, the displacement of the Cr₂O₃ curve to the higher potential is not due to the smaller surface area but due to a higher overvoltage which is needed for the oxidation of trivalent Cr to hexavalent Cr. It can also be seen that if the Cr and the CrOOH specimen had the same surface areas, their current/potential curves would coincide.

It can therefore be said that the passive layer on Cr is possibly composed of CrOOH and not of the less probable Cr₂O₃. It is difficult, however, to come to unequivocal conclusion about the nature of the passive layer on the basis of these experiments. The question of how far the electrochemical properties of the thin oxide films differ from those of the compact materials must first be thoroughly studied before a specific decision is made.

Determination of the Roughness Factor (R.F.)

The quantitative evaluation of electrochemical investigations fail mostly because the true surface area of the specimen is not known. In calculations

of such results, one generally assumes a roughness factor of 2-3. In previous investigations using this R.F., the thickness of the passive layer on electrolytic chromium was found to be 1-2 atoms thick. It is important therefore to find a method for determining the true surface area, as far as possible. Furthermore, as most of the electrodes used possessed surface areas of about 1 cm², methods like B.E.T. or dye adsorption were excluded.

The method of Erbacher (10) for determining R.F. was found to be the most suitable for this purpose. By this electrochemical method, cations of a metal, more noble in potential than the substrate, are deposited by direct atom exchange from their solution, without using any external current on the surface of the metal electrode. According to Erbacher (10), the layer so deposited is only one atom thick. The amount of the element deposited, being very small, could only be determined with the help of a radioactive tracer. In our case, Bi²¹² isotope, occurring as a decay product in the radioactive thorium series, was used as tracer. For the accuracy of this method, it may be said that the results obtained are not completely exact, but enable us to draw valuable conclusions when used in the electrochemical calculations. This method, verification of its assumptions, and the obtained results are described below.

In the preliminary experiments, a passive chromium electrode was placed into BiCl₃ solution which contained an excess of 0.1N HCl. The change in equilibrium rest potential was noted with time. After about 2 hr, the equilibrium rest potential of chromium reached a constant value. This value corresponds to the one observed for a Bi electrode in the same solution, under similar conditions. Figure 8 shows the noted potential/time dependence.

The Bi²¹² isotope used as tracer was separated from the natural radioactive thorium in the following way. The emitted radon gas (Rn²²⁰) was collected on a platinum foil. Rn²²⁰ isotope decays further into other isotopes, but the one with the longest half life, 10.6 hr, is Pb²¹². The Pb²¹² isotope further decays into Bi²¹², which subsequently decomposes into radioactive products with very short half life, finally producing inactive Pb²⁰⁸. On the platinum foil were mainly Pb²¹² and Bi²¹² in equilibrium with each other.

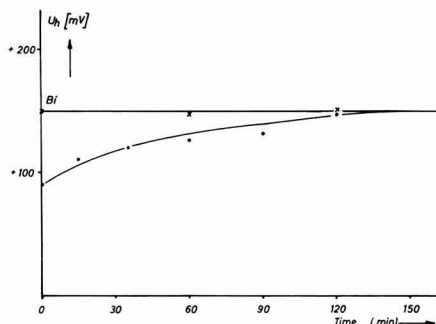


Fig. 8. Potential/time curves on Bi and Cr electrodes in BiCl₃ solution; conc., 1 mg Bi/l; electrolyte, BiCl₃ at 20°C; ×, Bi; ●, Cr.

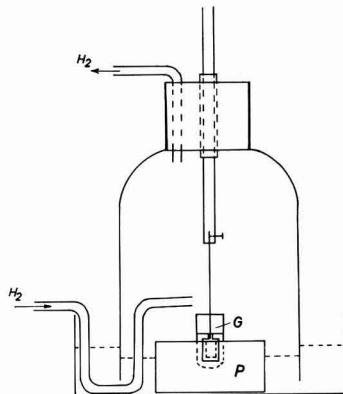


Fig. 9. Experimental arrangement for depositing Bi. G, small test tube; P, plastic material.

The platinum foil was kept in radioactive atmosphere of natural thorium for about 36 hr in order to get a large quantity of Pb²¹² isotope.

For the separation of Bi²¹² from the Pb²¹² isotope, the radioactive deposit was dissolved electrolytically from the platinum foil in 0.1N HCl. The hydrochloric acid used was air free and saturated with hydrogen. This solution was placed under the vessel shown in Fig. 9. The glass test tube G, containing about 40 ml of the solution, was fixed in a bored plastic material P, which was itself fitted in a glass base containing distilled water. Hydrogen was passed through the glass vessel during the whole experiment to prevent the entrance of oxygen from the atmosphere into the glass vessel. Oxygen or air redissolves the deposited bismuth in hydrochloric acid. A platinum foil, 1 cm² in area, was dipped in the radioactive solution and rotated in it. After about 90 min Bi isotope deposition was complete. In order to prevent the adsorption of even a small amount of lead isotope on the platinum foil, 1 mg of solid PbCl₂ was added to the original solution. The particles of inactive lead adsorbed on their surface the active Pb isotope. The deposition of Bi²¹² isotope on platinum foil under these conditions takes place preferentially because of its nobler potential against that of lead.

This separated Bi²¹² was electrolytically dissolved in 0.1N HCl, and by using a "Bohrloch crystal" its half life was determined. Figure 10 shows the intensity/time curve. The half life period determined in this way was in good agreement with the one stated in the literature.

For depositing bismuth on the surface of the chromium electrode, the same experimental apparatus was used as shown in Fig. 9.

To 1 ml of the active solution, 0.5 ml of inactive bismuth solution (conc. 1 mg Bi/liter) was added. This concentration is sufficient to cover the surface of the chromium with a bismuth layer of only one atom thickness.

The difference in the measured radioactive intensity before and after deposition enabled the determination of the absolute amount of bismuth deposited. The intensity measurements were carried out by means of a scintillation counter. In separate

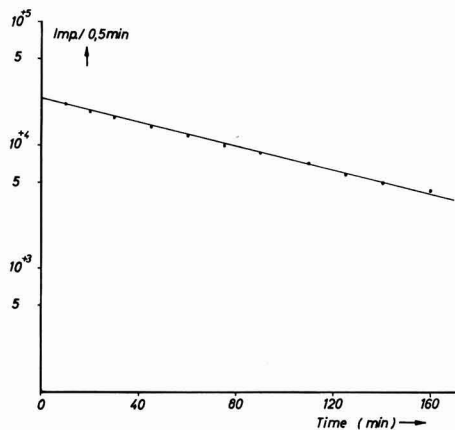


Fig. 10. Radioactive decay of experimentally separated Bi isotope. τ , 62.0 min; in literature, τ , 60.5 min.

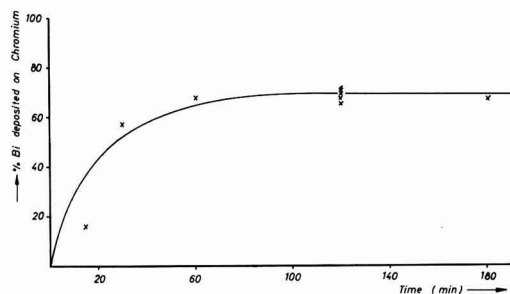


Fig. 11. Amount (%) of Bi, deposited on Cr, plotted against time. Geometrical surface area of Cr, 0.625 cm²; concentration of Bi in solution before deposition, 1 mg/l.

experiments, the amount of bismuth adsorbed on the plastic material, in which the Cr and Fe-Cr electrodes were imbedded, was determined. It was found to be about 5% of the quantity of bismuth in solution. It was therefore always subtracted from the observed values of the bismuth deposition. In a close-packed layer of bismuth atoms the surface area occupied by a single bismuth atom according to Erbacher (10) is $6r^2 \tan 30^\circ$, where r is the radius of the bismuth atom. Figure 11 shows the amount in per cent of bismuth deposited, plotted against time. As seen from this figure, after about 100 min the whole surface of the electrode seems to be covered with bismuth atoms.

Varying the concentration of bismuth in solution between 3×10^{-6} g and 5×10^{-7} g bismuth per liter did not affect, within the accuracy of this method, the quantity of bismuth finally deposited on the electrode. It is therefore assumed that the amount of bismuth deposited is independent of the original bismuth concentration. This justified further the basis of this method.

All the specimens were abraded on 6/0 emery paper and given different preliminary treatments.

Table I presents the data from a series of measurements, and Table II gives all the results for the different roughness factor determinations.

Table I. Data from a series of measurements

No.	g Bi in solution	% Bi deposited	g Bi deposited	Surface area found, cm ²	Geometrical surface area, cm ²	R.F.
1	5×10^{-7}	71.10	3.55×10^{-7}			
2	5×10^{-7}	68.21	3.41×10^{-7}			
3	5×10^{-7}	71.13	3.55×10^{-7}	1.12	0.625	1.81
4	5×10^{-7}	68.04	3.40×10^{-7}			
5	5×10^{-7}	65.48	3.27×10^{-7}			
			3.43×10^{-7}			

Table II. Results for different roughness factor determinations

Specimen	Preliminary treatment	R.F.
Cr	Abraded on 6/0 emery paper	1.8
Cr	Abraded on (6/0) and polarized in the active state	1.6
Cr	Abraded on (6/0) and polarized in the passive state	1.7
Fe-Cr (27%)	Abraded on (6/0)	2.0
Fe-Cr (27%)	Abraded on (6/0) and polarized in the primary transpassive region	2.7

The values found for the R. F. seem to agree in order of magnitude with the one generally assumed in electrochemical calculations.

It is worth noting that the true surface area of the chromium remains practically constant after anodic dissolution in the transpassive region with an anodic current density of 5×10^{-4} amp/cm² or after polarization with a cathodic current density of -10^{-5} amp/cm² in the active state. This agrees with the fact that the polarization curves can be reproduced so well, pointing to an even dissolution of the chromium surface.

Using the quantity of current 1.4 millicoulombs/cm² required for passivation (3), and the average R.F. of 1.7, the thickness of the passive layer on chromium is found to be about 1.5 atoms thick.

In earlier investigations (2) for untreated electrolytic chromium the quantity of current necessary for passivation was found to be 2.3 millicoulombs/cm². It can therefore be concluded that the R.F. for this material is about 1.6 greater than the one found for hydrogen-treated chromium.

The R.F. for an Fe-Cr alloy (27% Cr) is increased after polarization in the primary transpassive region. This agrees with our supposition that the passive layer, on this alloy in the primary transpassive region, is almost identical with the passive layer on pure chromium. The mechanism of dissolution gives rise to a greater surface roughness, which remains constant on further polarization of the alloy.

Current investigations have shown that this "chromium passivity" is observed not only in case of Fe-Cr alloys but also for Ni/Cr, Co/Cr, and Mn/Cr alloys containing Cr in solid solution. They all show similar mechanisms of dissolution in the primary transpassive region. It can therefore be said that chromium, because of its outstanding property of passivity, confers it on all alloys containing at least 10% Cr.

It was not possible to strip off the passive layer from the Fe-Cr alloys by the known bromine-methanol technique (11), after passivating them in the primary transpassive region. The reason is obviously that the primary passive layer is only about 1-2 atoms thick. In contrast, the passive layer from the Fe-Cr alloy after passivating in the secondary transpassive region could be removed.

Absolute analytical results are hard to produce because a selective dissolution and a back adsorption, during the process of stripping, cannot be excluded. It is possible *e.g.*, to show that Cr was adsorbed by the passive layer from the bromine-methanol solution, which can simulate a higher concentration. Satisfactory results can only be obtained if a technique is found which can be used to analyze the passive layer while it remains on the surface of the alloy.

One of the authors wishes to thank the Deutscher Akad Emischer Austauschdienst, Bad Godesberg, West Germany for their financial support of this research.

Any discussion of this paper will appear in a Discussion Section to be published in the December 1963 JOURNAL.

REFERENCES

1. Th. Heumann and W. Rösener, *Z. Elektrochem.*, **59**, 722 (1955).
2. Th. Heumann and W. Diekötter, *ibid.*, **62**, 745 (1958).
3. Th. Heumann and W. Diekötter, To be published in *Z. Elektrochem.*
4. Th. Heumann and R. Schürmann, *Werkstoff und Korrosion*, **9**, 560 (1961).
5. M. Prazak and V. Prazak, *Z. Elektrochem.*, **62**, 739 (1958).
6. R. Olivier, *Passivität von Fe und Fe-Cr Leg.* Diss. Leiden, 58 ff (1955).
7. Y. M. Kolotyrykin, *Z. Elektrochem.*, **62**, 664 (1958).
8. H. Gerischer and M. Käppel, *Z. Phys. Chem. N.F.*, **8**, 258 (1956).
9. R. H. Roberts and Shutt, *Trans. Faraday Soc.*, **34**, 1455 (1938).
10. O. Erbacher, *Z. Phys. Chem.*, **A163**, 215 (1933); O. Erbacher, W. Herr, H. Babo, and M. Ebert, *Arch. Metallk.*, **12**, 409 (1949).
11. N. A. Nielsen, E. M. Mahla, and T. N. Rhodin, *Trans. Electrochem. Soc.*, **89**, 167 (1946).

The Passivity of Iron-Chromium Alloys

Gerald Aronowitz¹ and Norman Hackerman

Department of Chemistry, The University of Texas, Austin, Texas

ABSTRACT

Chronopotentiometry and differential capacity measurements were used to study the passive films formed by anodic polarization of a series of Fe-Cr alloys in dilute H₂SO₄. Steady-state conditions were established by electronic control of the electrode potential prior to making measurements.

Cathodic reduction studies indicated the presence of at least three types of surface materials. One is nonprotective in the case of Fe and several of the lower Cr alloys, but achieves considerable stability to reduction or dissolution at an alloy composition approaching 12% Cr. Another material is essential for passivity of Fe and the alloys with Cr content less than 12% and plays an important role in the electrical properties of the films on these alloys. A third type of surface material appears as a by-product of processes occurring in the transpassive region.

In the composition range 2.70-9.02% Cr, capacity-potential curves are quite similar and capacities follow a reciprocal relation with electrode potential over a range of potentials. Extrapolation of these data was used to obtain a relation between film thickness, dielectric constant, and charge equivalents involved in film reduction. Film dielectric constant values, calculated assuming the reduction of normal Fe₂O₃, varied from 29.1 to 87.5, depending on the reduction reaction assumed. At an alloy composition approaching 12% Cr, the passive film assumes optimum protective properties. Correspondingly, humps develop in the capacity-potential curves, and the curves shift in the direction of higher capacity values with increasing Cr content.

At present, two major points of view exist as to the cause of passivity: the adsorbed film theory and the bulk oxide theory. While the ultimate formation of an oxide having bulk properties on passive Fe, Ni, Cr, etc., is generally recognized, the problem is centered on the exact nature of these films in their early stages and on whether or not adsorption plays a role in passivity.

In this connection, a theory was put forth recently which attempts to reconcile these views by postulating a sequence consisting of adsorption, electron transfer to the adsorbate, and ultimate formation of bulk amorphous oxide *via* cation migration into the adsorbed array (1).

Iron which demonstrates the main features of the active-passive transition, has been studied probably more than any other metal. In recent years, however, considerable interest has been shown in the passivity of stainless steel and the iron-chromium alloys because of the wide range of corrosion resistance shown by these metals. In addition, the attainment of optimum corrosion resistance and ease of passivation at a critical alloy composition in the neighborhood of 12% Cr has raised further questions.

Chronopotentiometry was employed in this work to determine passive film charge equivalents. Anodic film formation techniques very often do not satisfy the requirement of known or 100% current efficiency because of simultaneous anodic dissolution. Cathodic film reduction studies can suffer from these

¹ Present address: American Oil Company, Research & Development Department, P. O. Box 431, Whiting, Indiana.

disadvantages if the film breaks down spontaneously during the reduction, if solution components are simultaneously reduced, or if electrode roughening occurs. By suitable choice of experimental variables these difficulties may be avoided. In principle, the method should also differentiate between separate reduction steps and thus indicate the existence of more than one type of passive film component.

Differential capacity measurements have been used with some success in recent years in determining the thickness of anodic films formed on metals such as tantalum and aluminum (2). Recent studies on passive iron (3, 4) have shown that reciprocal capacity-potential relations exist to a degree of approximation, but that the electrical properties of the system are more complicated than for anodized tantalum or aluminum. Differential capacity studies were included to provide comparisons with the behavior of metals like anodized tantalum and clean surface metals such as platinum and mercury, and to see if electrical property changes in the passive film parallel property changes such as corrosion resistance and ease of passivation at some critical alloy composition.

Experimental Materials and Procedures

A series of Fe-Cr alloys ranging from 2.70 to 19.1 wt % Cr was obtained from the laboratories of Professor H. H. Uhlig. Their preparation is discussed elsewhere (5, 6). The iron used came from a stock of zone-refined iron, supplied by the Battelle Memorial Institute. Their analysis shows: carbon, 10 ppm; oxygen, 23 to 28 ppm; nitrogen, 2 ppm; hydrogen, 0.1 ppm. Cylindrical electrodes, approximately 2 cm long and 0.2 cm in diameter, were abraded with 4/0 emery paper, electropolished according to the method of Sewell *et al.* (7), and mounted in a Pyrex holder with polyethylene. Immediately before use, electrodes were electropolished briefly and then rinsed in conductivity water. Electrodes pretreated by mechanical abrasion only gave poor reproducibility.

The cell and pre-electrolysis vessel were constructed of Pyrex. The use of stopcock grease was avoided entirely. All solutions were 0.1M in Na_2SO_4 and were prepared from 3x recrystallized Na_2SO_4 and conductivity water of specific resistance $> 3 \times 10^6$ ohm cm. The range of solution pH used was from 0.6 to 13.6 and was adjusted with H_2SO_4 or NaOH. Freshly prepared solutions were subjected to pre-electrolysis for periods up to 120 hr at a c.d. of ~ 8 ma/cm². It was found that a 24-hr pre-electrolysis was sufficient to insure that difficulties due to solution impurities would be avoided. Bureau of Mines Grade A helium was bubbled through the test solution for 12 hr prior to beginning an experiment, and also during the experiment. All runs were made at $4.5^\circ \pm 0.2^\circ\text{C}$.

Chronopotentiometric studies were made in the usual way by recording the potential decay during constant current polarization and measuring the lengths of arrest regions in the traces. Capacities were measured as a function of anodization potential, using the constant current pulse method of Riney *et al.* (8) modified for square wave charging.

A description of the electrical apparatus and circuit is available elsewhere (3). Electrode potentials were measured with respect to a $\text{Hg}/\text{Hg}_2\text{SO}_4(\text{s})/\text{Hg}_2\text{SO}_4 + \text{K}_2\text{SO}_4$ (sat'd) half cell, which was allowed to assume the temperature of the laboratory atmosphere ($25^\circ \pm 3.0^\circ\text{C}$). Connection was made to the cell through a salt bridge filled with test solution. Because of small but unknown thermal and concentration junction potentials and potential variations induced by the square wave signal, electrode potentials are reported only to the nearest 0.01v. All electrode potentials given were corrected to the normal hydrogen electrode (NHE).

Experimental Results

Preliminary studies were performed to determine the potential regions in which measurements could be made with a minimum of metal dissolution occurring, as significant changes in surface roughness and in the Cr content of the surface layers of the alloy were undesirable. For similar reasons cold 0.1M Na_2SO_4 , adjusted to pH 2.2, was employed in most of this work. For the present purposes, this was sufficiently well buffered and assured relatively low coulomb and c.d. requirements for passivation of the alloys, and for maintenance of the passive state.

Anodic current densities.—The anodic c.d. in the passive potential region varied from 10^{-6} amp/cm² for the 2.70% Cr alloy to 10^{-7} amp/cm² for the 12.2% Cr alloy. For alloys with Cr content $\geq 9.02\%$, and at anodization potentials more noble than 1.05v, the anodic c.d. increased above these steady values to a peak at about 1.35v. This was followed by a decline just prior to reaching the O_2 evolution region. The peak values varied from $3.5 \mu\text{a}/\text{cm}^2$ for the 9.02% Cr alloy to $22 \mu\text{a}/\text{cm}^2$ for the 19% Cr alloy. Shifting the electrode potential in the opposite direction, from O_2 evolution to 1.05v, resulted in lower values of the anodic c.d. throughout this region. While these data are not too reproducible, the behavior noted has been observed previously and agrees qualitatively with observations made by other investigators, e.g. ref. (9).

At potentials more noble than 1.65v, the anodic c.d. for O_2 evolution followed a Tafel relation with electrode potential. Table I lists the *b* values of the potentiostatically obtained electrode potential-log c.d. plots for several of the alloys, corrected for resistance overvoltage.

Cathodic chronopotentiometry.—Examples of the time-potential behavior of a passive alloy under constant current cathodic polarization are shown in Fig. 1. Curve 1 is for 2.70% Cr and shows a potential arrest (B) at a more active potential than the Flade

Table I. *b* values of electrode potential-log c.d. plots for several alloys

Alloy	<i>b</i> , (pH 2.2)	<i>b</i> , (pH 13.6)
7.14% Cr	0.043	
9.02% Cr	0.042	
12.2% Cr		0.050
18.6% Cr	0.052	

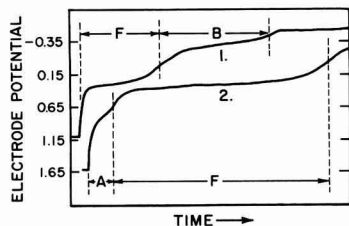


Fig. 1. Time-potential curves taken during constant current cathodic polarization of a pre-anodized electrode in 0.1M Na_2SO_4 , pH 2.2, 5.0°C. Curve 1, 2.70% Cr alloy, c.d. $1173 \mu\text{a}/\text{cm}^2$; curve 2, 12.2% Cr alloy, c.d. $17.5 \mu\text{a}/\text{cm}^2$.

arrest (F). Curve 2 for 12.2% Cr shows still another arrest (A) at a more noble potential than the Flade arrest. These arrests were studied with respect to occurrence and growth as a function of anodization potential, E , chromium content, and pH. In addition, the effect of cathodic c.d., chromium content, and pH on the arrest potentials, V , was examined. Arrest lengths were estimated to be between points of inflection in the arrest break off regions of the traces. With these, specific charge values in units of $\mu\text{coul}/\text{cm}^2$ (Q) were obtained from the traces. Time independent values of Q for a given E were usually attained within several minutes, but anodizations of 5-min duration were uniformly used. The experimental points in the Q - E curves for A and F were in most cases averaged over three separate runs with freshly prepared electrodes and fresh solution each time. Average deviations did not exceed 10% for more than 95% of the points. Q - E curves for B were plotted from the data of individual runs, but that for the 2.70% Cr alloy represents an average of three separate runs with average deviations not exceeding 6.0%.

For the alloys with Cr content $\geq 4.98\%$, A makes its initial appearance at 1.05v. Figure 2 shows the

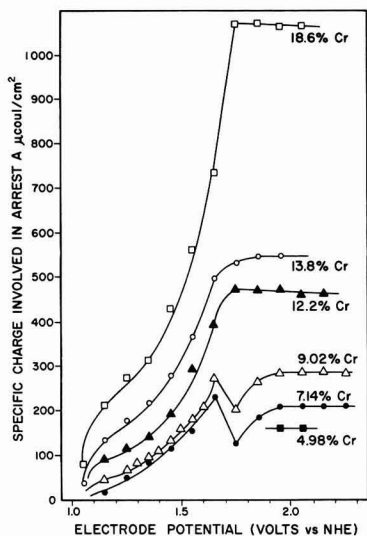


Fig. 2. $Q(A)$ - E curves for alloys from 4.98 to 18.6% Cr in 0.1M Na_2SO_4 , pH 2.2, 5.0°C.

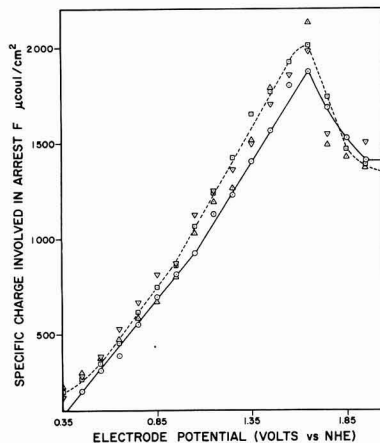


Fig. 3. $Q(F)$ - E curves for the "lower" range alloys in 0.1M Na_2SO_4 , pH 2.2, 5.0°C. Open dotted circle, 2.70% Cr; open dotted square, 4.98% Cr; inverted dotted triangle, 7.14% Cr; open dotted triangle, 9.02% Cr.

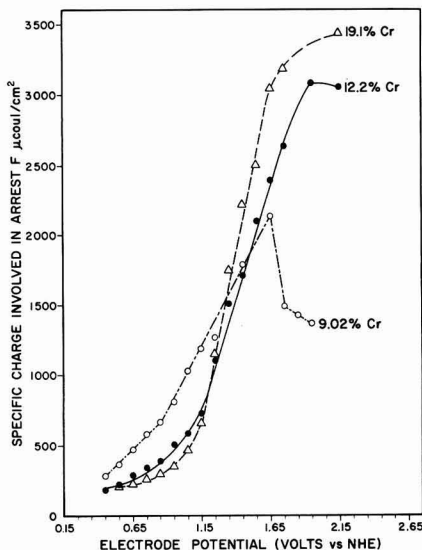


Fig. 4. $Q(F)$ - E curves for alloys from 9.02 to 19.1% Cr in 0.1M Na_2SO_4 , pH 2.2, 5.0°C. The curve for the 9.02% Cr alloy is presented for comparison and was replotted from Fig. 3.

variation in specific charge, $Q(A)$, involved in A, with anodization potential. A shift to higher $Q(A)$ values is found with increasing Cr content. In the O_2 evolution region, $Q(A)$ is independent of E . If the latter $Q(A)$ values are plotted as a function of the mole % Cr, the plot is nearly linear, at least up to 14.8 mole %.

Arrest F, which was observed here before (10, 11) on either open-circuit decay or forced decay of passive iron electrodes in acid solutions, can be seen for all the alloys investigated. The arrest region is not well defined for $E < 0.55\text{v}$, but the arrest potential, $V(F)$, does not vary with E for E noble to 0.55v. The $Q(F)$ - E curves shown in Fig. 3 and 4 indicate a change in form between the "lower" alloys (2.70

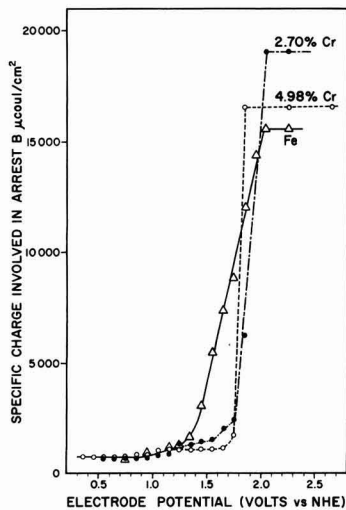


Fig. 5. $Q(B)$ - E curves for Fe, a 2.70% Cr alloy, and a 4.98% Cr alloy in 0.1M Na_2SO_4 , pH 2.2, 5.0°C.

to 9.02% Cr) and the "higher" alloys (12.2 to 19.1% Cr).

$Q(B)$ - E curves are shown in Fig. 5 for Fe, 2.70% Cr and 4.98% Cr alloys. $V(B)$ shifted to more negative values with increasing Cr in the "lower" range, resulting in a poorly defined arrest for alloys with Cr content >4.98%. If cathodic polarization charging was interrupted after passing F, $Q(B)$ decreased on subsequent cathodic treatment with time of open-circuit treatment. While 5-10 sec was sufficient to reduce $Q(B)$ to zero for Fe, or a 2.70% alloy, arrest B could not be removed for alloys with Cr content $\geq 12.2\%$ without a vigorous cathodization or repolishing of the electrode.

The potentials of the various arrests were taken to be at the point of minimum slope in the arrest region. These values varied linearly with solution pH from pH 0.6 to 13.6. The following relations were obtained from extrapolation of the V -pH plots

$$V(A) = 0.89 - 0.066 \text{ pH} \quad [1]$$

$$V(F) = 0.45 - 0.066 \text{ pH} \quad [2]$$

While $V(A)$ did not vary with Cr content over the range studied, $V(F)$ (calculated for pH = 0) varied from 0.55v for Fe to 0.45v for a 19.1% Cr alloy. $V(B)$ -pH studies were not done here, but from data reported for Fe in a previous work (3), e.g.

$$V(B) = 0.30 - 0.063 \text{ pH} \quad [3]$$

For a given value of E , $Q(A)$ and $Q(B)$ did not vary with cathodic c.d. for values $>100 \mu\text{a}/\text{cm}^2$. $Q(F)$ was independent of c.d. between $4.0 \mu\text{a}/\text{cm}^2$ and $10 \text{ ma}/\text{cm}^2$ for alloys in the "lower" range. In these cases c.d.'s from $\sim 0.5 \text{ ma}/\text{cm}^2$ to $\sim 1.5 \text{ ma}/\text{cm}^2$ were employed. For the "higher" alloy range, c.d.'s $<50 \mu\text{a}/\text{cm}^2$ were used as otherwise $Q(F)$ decreased with increasing c.d. In addition, neither Q nor V was affected by solution stirring or replenishment.

If, after a normal anodization, E was changed and held at a more negative value, Q values normally

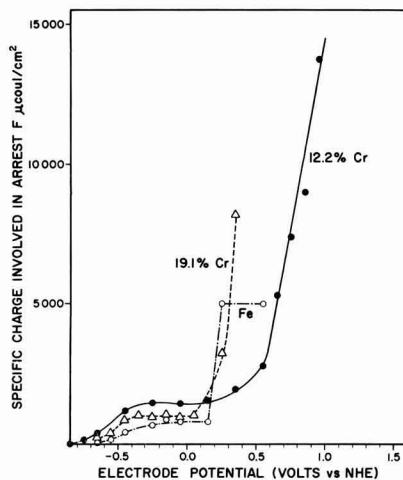


Fig. 6. $Q(F)$ - E curves for Fe, a 12.2% Cr alloy, and a 19.1% Cr alloy in a 0.1M $\text{NaOH} + 0.1\text{M} \text{Na}_2\text{SO}_4$ at 5.0°C.

found at E persisted for several hours upon cathodic polarization from the more negative potential. This hysteresis was not apparent from potentials within 0.1-0.2v noble of the arrest potentials. In summary, Q was metastable with respect to E , except for E values approaching V .

At pH values <2.2 , the traces retained their form but Q values were lower. In alkaline solutions $Q(A)$ decreased sharply with increasing pH, and A could not be observed in 1.0M NaOH . Figure 6 shows $Q(F)$ - E curves for several alloys in 0.1M NaOH along with one for Fe taken from a previous work (3).

Anodic chronopotentiometry.—Figure 7 is a time-potential trace for constant current anodic polarization of an initially active 19.1% Cr alloy. The trace can be divided into three regions; 1, 2, and 3. The specific charge involved in region 1 was difficult to reproduce, but that for regions 2 and 3 could be reproduced to better than 10% if the electrode were briefly etched in warm 50% H_2SO_4 after electroplating. In this case specific charge values for regions 2 and 3 were independent of anodic c.d. over the range of c.d. studied ($\sim 200 \mu\text{a}/\text{cm}^2$ to $\sim 5 \text{ ma}/\text{cm}^2$). Region 3 appeared only for alloys with Cr content $\geq 9.02\%$. The charge involved in region 3 increased with increasing Cr content. Figure 8 shows

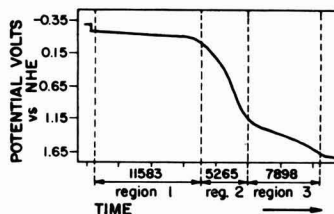


Fig. 7. Time-potential trace for anodic polarization of an initially active 19.1% Cr alloy. Anodic c.d. $1755 \mu\text{a}/\text{cm}^2$, 2.0 sec/div. Specific charge values in $\mu\text{coul}/\text{cm}^2$ involved in the various regions are noted below the trace.

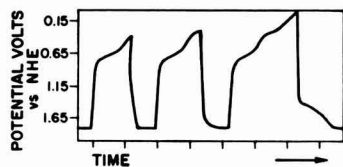


Fig. 8. Time-potential traces for alternate cathodic and anodic polarization of a 19.1% Cr alloy initially at an O_2 evolution potential. Anodic c.d. $3510 \mu\text{a}/\text{cm}^2$, cathodic c.d. $567 \mu\text{a}/\text{cm}^2$ 2.0 sec/div.

the results of alternate cathodic and anodic charging on a 19.1% Cr alloy initially at an O_2 evolution potential. Specific charge values involved in the anodizing and cathodizing portions respectively, agreed if only arrest A was passed as in the first two traces. In the third trace, F is passed as well and region 3 of Fig. 7 appears in the anodizing portion.

Differential capacity measurements.— Throughout the potential region studied, time independent values of the capacity, C , could usually be obtained in the order of seconds, although at least two readings, 5–10 min apart, at a given electrode potential, and agreeing to within 1.0%, were used for all of the plotted data. As the C - E curves showed hysteresis in terms of the direction of potential change, runs were begun by setting E at the extreme negative end of the passive potential region. It was then altered in the direction of more noble values in increments of 0.01v. At 1.75v, E was then changed in the opposite direction until the lower limits of stable passivity had been reached, or on to the approach of the H_2 evolution region. Capacities were not studied in the regions of H_2 or O_2 evolution. In the former, measurements drifted with time, while in the latter, the time-cell voltage trace showed considerable curvature and slopes were difficult to measure accurately.

Capacity values for an electrode on open circuit were measured immediately after immersion in the solution. Open-circuit potentials were -0.39 to -0.40 v. Capacity measurements for a given alloy could be reproduced to better than 3.0% and values of $16.9 \mu\text{f}/\text{cm}^2$ and $18.1 \mu\text{f}/\text{cm}^2$ were obtained for a 2.70% Cr alloy and a 13.8% Cr alloy, respectively. These values averaged to $17.5 \mu\text{f}/\text{cm}^2$.

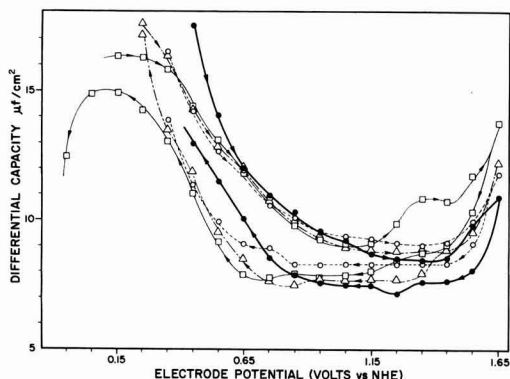


Fig. 9. C - E curves for the "lower" range alloys in 0.1M Na_2SO_4 pH 2.2, 5.0°C . ●—●, 2.70% Cr; ○—○, 4.98% Cr; △—△, 7.14% Cr; □—□, 9.02% Cr.

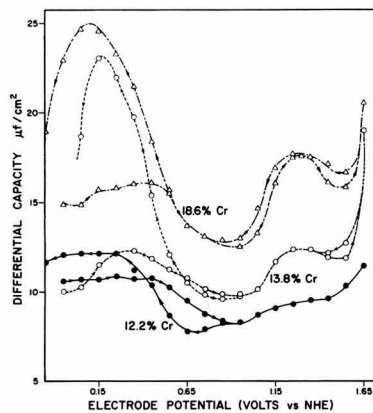


Fig. 10. C - E curves for the "higher" range alloys in 0.1M Na_2SO_4 , pH 2.2, 5.0°C . ●—●, 12.2% Cr; ○—○, 13.8% Cr; △—△, 18.6% Cr.

Figures 9 and 10 show C - E plots for the alloys in pH 2.2 solution. The points on these plots represent values averaged from between two and four runs made with fresh solution and with freshly prepared electrodes each time. Average deviations were less than 6.0%.

Except for the small hump in the vicinity of 1.35v for the 9.02% Cr alloy, and several slightly high values for the 2.70% Cr alloy at the left of the curves, the curves for the alloys in the "lower" range (Fig. 9) are quite similar. Figure 11 is a plot of $1/C$ vs. E for the points of the curves in Fig. 9 taken in the direction of increasingly noble values, i.e., the upper branches. Except for the two most negative potentials for the 2.70% Cr alloy, C appears to follow a reciprocal relation with E up to ~ 1.05 v, i.e.

$$E = 13.4/C - 0.475$$

Figure 10 shows that important changes occur in going to the "higher" range alloys. The hysteresis is opposite to that found with the "lower" alloys (note arrowheads on curves).

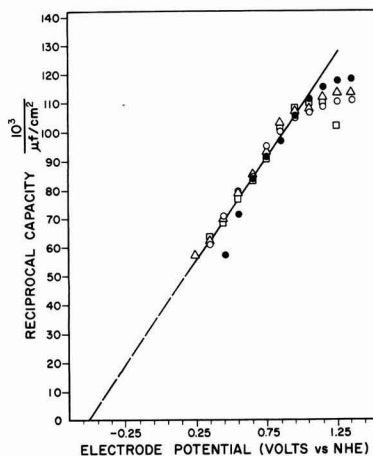


Fig. 11. $1/C$ vs. E plots of the upper branches of the curves in Fig. 7. ●, 2.70% Cr; ○, 4.98% Cr; △, 7.14% Cr; □, 9.02% Cr.

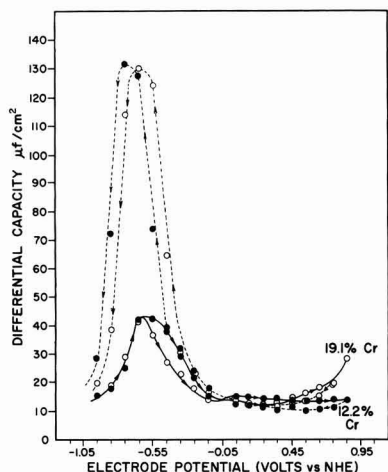


Fig. 12. C-E curves for a 12.2% Cr alloy and a 19.1% Cr alloy in 0.1M NaOH + 0.1M Na₂SO₄ at 5.0°C.

At the left of the curves a broad peak is found for the 13.8 and 18.6% Cr alloys with maximum values of C increasing, and shifting to more negative E with increasing Cr content. This region was examined further. Beginning with a freshly prepared specimen, E was adjusted to some value noble to the peak region. The potential was then altered in the negative direction and capacities were measured. Peak heights were found to increase as more noble potentials were reached. With vigorous cathodization after anodization at 1.65v, peak heights decreased with time of cathodic treatment. However, it was necessary to repolish the electrode to reproduce the original capacity values in the peak region (-0.05 to 0.45 v).

Figure 12 shows C-E plots for the 12.2 and 19.1% Cr alloys in 0.1M NaOH + 0.1M Na₂SO₄. Although the plotted points represent individual runs, an additional run on the 19.1% Cr alloy indicated that reproducibility of better than 6.0% could be expected for all but a few of the points. The plots are characterized by a small hump in the negative potential region of the plots on going to more noble potentials and a general decrease in C in this direction. In the opposite direction, capacities increase gradually and then rise to a peak value in excess of $130 \mu\text{coul}/\text{cm}^2$ at the more negative potentials. The hysteresis behavior observed in this region is qualitatively similar to the results obtained for the higher alloys in acid solutions. The curves seen in Fig. 9 compare favorably to C-E curves reported for Fe in alkaline solution (3).

Discussion

A number of observations provided evidence that the potential arrests correspond to a pH dependent reduction of surface compounds. Q was independent of solution stirring rate, solution replenishment, or cathodic c.d. but not of E . Added to these were the pH dependences of the arrest potentials, the hysteresis behavior of the Q-E curves, and the Q values themselves. The latter were too great to be ac-

counted for by such processes as reduction of solution impurities or buildup of concentration over-voltage for hydrogen evolution.

A comparison of the Q-E curves for arrests A, B, and F showing an absence of any obvious correlations, indicates that the form of the cathodic time-potential curves does not result from a sequence of reduction steps originating from a single reactant but involves the reduction of three individual surface materials; "A," "B," and "F."

Material "B" becomes increasingly stable with respect to both reduction and dissolution in the "higher" alloy range. Reduction of "A" and "F" fails to activate a 12.2% Cr alloy. That "B" can sustain passivity for alloys $\geq 12.2\%$ Cr without the presence of "F," is also indicated by the discrepancy of several hundred millivolts between $V(F)$ and the passivation potential of these alloys. Both the rapid growth of "B" with E in the O₂ evolution region and the strong time dependence of this growth at a given O₂ evolution potential suggests that material "B" grows in this region by diffusion of O₂ or some intermediate of O₂ evolution through the film.

While lower $Q(F)$ values have been reported for Fe (11, 12), $V(F)$ and the passivation potential do not change in going to a 2.70% Cr alloy. The observed pH variation of $0.066 \text{ mv}/\text{pH}$ unit can be compared to the value $0.059 \text{ mv}/\text{pH}$ unit reported for Fe (13). Since the "lower" range alloys behave almost identically with respect to both $Q(F)$ and capacity, it seems reasonable to conclude that material "F" changes little in structure or composition between Fe and an alloy composition of 9.02% to 12.2% Cr.

Arrest A makes its appearance for alloys $\geq 4.98\%$ Cr at $E > 1.05$ v, i.e., the potential of the onset of a region of secondary activity characteristic of the Fe-Cr alloys and Cr. It is attributable to chromate production on comparing the polarization curves of the alloys with that for chromium (14). The material reduced during the arrest may well be hexavalent chromium. This is suggested by the general increase in $Q(A)$ with increasing Cr content of the alloy, and by the noble value of $V(A)$. A Cr⁺³ containing species should be reduced at a more negative potential. While correlation between $V(A)$, its pH coefficient, and the thermodynamic CrO₃/Cr₂O₃ or H₂CrO₄/Cr⁺³ potentials was not found, a comparison can be made with the thermodynamic potential of 0.90v at pH = 0 for the reaction $\text{HCrO}_4^- + 3\text{H}^+ + 3e^- = \text{CrO}_2^- + 2\text{H}_2\text{O}$. This was calculated using the reported standard potentials (15, 16) for the reactions: $2\text{H}_2\text{O} + \text{Cr} = \text{CrO}_2^- + 4\text{H}^+ + 3e^-$ and $\text{HCrO}_4^- + 7\text{H}^+ + 6e^- = 4\text{H}_2\text{O} + \text{Cr}$. The drop in $Q(A)$ with increasing pH fits a previously reported observation that decreases in solution chromate uptake on a Cr surface occurs with increasing pH (17). This was explained as due to competitive adsorption by OH⁻.

Region 3 of the anodic time-potential curve (Fig. 7) is a potential arrest occurring at ~ 1.35 v i.e., at the potential of the peak c.d. in the transpassive region. In addition, the range of alloy composition in which region 3 appears, i.e., $\geq 9.02\%$ Cr, parallels

the range in which the secondary activity is observed. Region 3 must then be connected with the production of the secondary passivity. Both the traces of Fig. 8 and the simultaneous appearance of arrest A with the onset of the secondary activity suggest that material "A" does not produce the secondary passivity but is probably a by-product of processes occurring in the transpassive region. Changes in "F," which prevent the continuous passage of chromium through the passive film, must be looked to.

Both the $Q(F)-E$ and $1/C$ vs. E plots are linear between ~ 0.35 and $1.05v$ for the "lower" alloys. In addition, both show hysteresis. It seems reasonable to connect these data. If material "F" were the dielectric of a parallel plate capacitor in this potential range, an equation relating thickness of F, d , $Q(F)$, and dielectric constant, k , can be obtained assuming a passive film-solution interfacial capacity, $C_{\text{film-sol-n}}$ in series with a film capacity, C_{film} , and that "B" makes no contribution to the measured capacity, C . From the linear portion of the curve of Fig. 11, the branch of the lower curve in Fig. 3 which lies at potentials less than about $1.05v$, and the parallel plate capacitor formula:

$$E = 13.4 (1/C_{\text{film}} + 1/C_{\text{film-sol-n}}) - 0.475 \quad [4]$$

$$E = 8.43 \times 10^{-4} Q(F) + 0.254 \quad [5]$$

$$C_{\text{film}} = k/0.113 d \quad [6]$$

If [4] and [5] are combined with the condition that $1/C_{\text{film}} = 0$ when $Q(F) = 0$, a value for $C_{\text{film-sol-n}}$ can be obtained

$$C_{\text{film-sol-n}} = \frac{13.4}{0.475 + 0.254} = 18.4 \mu\text{f}/\text{cm}^2$$

This value is comparable to the value of $17.5 \mu\text{f}/\text{cm}^2$ obtained experimentally for an active electrode at $\sim -0.40v$. Combining Eq. [4], [5], and [6] with the value obtained for $C_{\text{film-sol-n}}$

$$Q(F) = 1.80 \times 10^3 d/k \quad [7]$$

or

$$k = 1.80 \times 10^3 d/Q(F)$$

If the reduction reaction, the density, and the molecular weight of "F" are known, a relation between $Q(F)$ and d can be obtained. Assuming the reaction is



then

$$d/Q(F) = \frac{159.7 \times 10^8 \times 10^{-6}}{5.12 \times 2/3 \times 96,500} = 4.85 \times 10^{-2}$$

Combining this result with Eq. [7], a value for the apparent dielectric constant of "F" can be obtained

$$k = 1.80 \times 10^3 \times 4.85 \times 10^{-2} = 87.5$$

If the reaction of $\text{Fe}_2\text{O}_3 + 2\text{H}^+ + 2e^- = 2\text{FeO} + \text{H}_2\text{O}$ is assumed, a value of 29.2 obtains for k . Reduction to Fe can be ruled out since d less than the $\text{O}^=$ diameter would obtain for some values of E . Values reported for the dielectric constants of normal oxides of iron range from 7 to 20 (18-20).

For E more noble than $1.05v$, $1/C$ vs. E relations fail, and a hump develops in the $C-E$ curves for the "higher" range alloys. This can be contrasted with the behavior of Fe in dilute H_2SO_4 , in which case C continues to decrease hyperbolically with increasing E (3,4). While for iron, small anodic current flow extends to the beginning of oxygen evolution, a potential of $1.05v$ marks the onset of the secondary activity region for the alloys in the pH 2.2 solution used. A connection can thus be established between the secondary activity and the observed change in electrical properties. Electrical changes in "F," perhaps caused by the continuous passage of chromium through the film, may be involved. Significant structural changes seem unlikely since $V(F)$ is independent of E .

The shift of the curves to higher C values between 12.2 and 18.6% Cr could be accounted for if either the dielectric constant or the electronic conductivity of the film increased. At 18.6% Cr, the $C-E$ curve (except for the hump in the transpassive region) compares quite favorably with $C-E$ data obtained for "clean" Pt in neutral Na_2SO_4 solutions (21).

Conclusion

While the alloys studied show some of the behavior found on phase oxide covered metals like Ta and Al, the fact that a $1/C$ vs. E relation holds only for the "lower" range alloys over a restricted range of anodization potential and only in acid solutions indicates that a classification with the latter group of metals is not appropriate. At the same time, a film consisting of monolayer quantities or less of a single type of adsorbate, i.e., O, OH, O_2 , cannot be reconciled with the results either. Indeed $Q(F)$ attains values too high for this to occur.

The results might be accounted for better by a model consisting of a monolayer of oxygen atoms adsorbed on the metal over which an amorphous mixture of metal ions and oxygen ions might form by metal ion movement through the adsorbed array. Some evidence can be presented to support this view. $Q(B)$ remains at ~ 0.7 mcoul/cm² over a range of E , i.e., close to the value of 0.6 mcoul/cm² calculated for reduction of a monolayer of adsorbed oxygen atoms in 1:1 correspondence with the surface metal atoms. That "B" is nonprotective for Fe but achieves optimum protective properties at $\sim 12\%$ Cr fits an electron configuration theory of passivity which relates this critical composition to d -electron vacancies in the alloy components and the resulting ability of the alloy to chemisorb oxygen (22). Indeed, that "F" fails to grow as rapidly with E , at $E < 1.05v$ for the "higher" range alloys as for the "lower" range suggests that strong adsorption forces inhibit the movement of metal ions through the adsorbed array for the former metals. The hysteresis behavior in the $C-E$ curves for these alloys seems more reasonable on the basis of such a model.

The change in the form of the $C-E$ curves for the "higher" range alloys parallels the attainment of optimum passive film stability with respect to both "F" and "B." Other investigators have observed this composition to mark the attainment of either optimum ease of passivation or maximum corrosion re-

sistance (5). The validity of the capacity data in studies like these is thus supported.

Acknowledgment

The authors are pleased to acknowledge the Robert A. Welch Foundation and the Office of Naval Research for Financial support. Appreciation is extended to the Battelle Memorial Institute for their gift of zone-refined iron and to Professor Herbert H. Uhlig for kindly providing the alloys used.

Any discussion of this paper will appear in a Discussion Section to be published in the December 1963 JOURNAL.

REFERENCES

1. Norman Hackerman, *Z. Elektrochem.*, **62**, 632 (1958).
2. L. Young, *Anodic Oxide Films*, Academic Press, Inc., New York (1961).
3. N. E. Wisdom and Norman Hackerman, To be published.
4. W. J. Engell and B. Illschner, *Z. Elektrochem.*, **59**, 716 (1955).
5. P. F. King and H. H. Uhlig, *J. Phys. Chem.*, **63**, 2026 (1959).
6. H. H. Uhlig and G. E. Woodside, *ibid.*, **57**, 280 (1953).
7. P. D. Sewell, C. D. Stockbridge, and M. Cohen, *Can. J. Chem.*, **37**, 1813 (1959).
8. J. S. Riney, G. M. Schmid, and Norman Hackerman, *Rev. Sci. Inst.*, **32**, 588 (1961).
9. M. Prazak *et al.*, *Z. Elektrochem.*, **62**, 739 (1958).
10. E. S. Snavey and N. Hackerman, *Can. J. Chem.*, **37**, 268 (1959).
11. W. H. Wade and Norman Hackerman, *Trans. Faraday Soc.*, **53**, 1 (1957).
12. G. M. Schmid and Norman Hackerman, To be published.
13. K. J. Vetter, *Z. Elektrochem.*, **62**, 642 (1958).
14. W. A. Mueller, *Corrosion*, **18**, 73t (1962).
15. W. M. Latimer, "Oxidation Potentials," p. 248, Prentice Hall, Inc., New York (1952).
16. M. S. Udy, "Chromium," Vol. I, p. 134, Reinhold Publishing Corp., New York (1956).
17. N. Hackerman and R. A. Powers, *J. Phys. Chem.*, **57**, 139 (1953).
18. T. Takei, *J. Inst. Elec. Engrs. Japan*, **66**, 121 (1946).
19. F. Wagenknecht, *Kolloid-Z.*, **112**, 35 (1948).
20. A. W. Kohlschutter, *Z. Anorg. u. allgem. Chem.*, **278**, 270 (1951).
21. P. V. Popat and Norman Hackerman, *J. Phys. Chem.*, **62**, 1198 (1958).
22. H. H. Uhlig, *Z. Elektrochem.*, **61**, 700 (1958).

The Influence of Film Thickness on the Thermodynamic Properties of Thin Oxide Layers on Iron

K. G. Weil

Eduard Zintl Institut der Technischen Hochschule Darmstadt, Lehrstuhl für Physikalische Chemie, Darmstadt, West Germany

The properties of a passive metal are, in general, determined by the properties of the oxide films which cover the metal surface. Recently Vetter (1) showed how to calculate the equilibrium potential of such an oxide-covered electrode from the free energy of formation of the oxide. To use his formulae the free energy of formation of the oxide must be known as a function of the degree of oxidation. This information, however, can only be acquired by experiments which are usually done on bulk oxides. In this paper it will be shown that it may be risky to use results obtained for such bulk materials to calculate equilibrium properties of thin films.

In the first stage the free surface energy will be taken into account. In a system metal/oxide/solution there may be three interfaces, and therefore the free energy change of such a system at constant volume and temperature may be written as

$$dF = \sum_i \mu_i dn_i + \sum_j \left(\frac{\partial F}{\partial O_j} \right)_{v,T} dO_j \quad [1]$$

where the integer i denotes the different species involved in the oxide forming reaction and the integer $j = 1, 2, 3$ denotes the three different interfaces O_j . Introducing the extent of reaction λ according to de Donder we obtain

$$dn_i = \nu_i d\lambda$$

and

$$dO_j = \frac{dO_j}{d\lambda} d\lambda$$

and finally

$$dF = \left\{ \sum_i \mu_i \nu_i + \sum_j \left(\frac{\partial F}{\partial O_j} \right)_{v,T} \frac{dO_j}{d\lambda} \right\} d\lambda \quad [2]$$

When equilibrium is obtained the term in brackets must vanish, i.e.,

$$\sum_i \mu_i \nu_i + \sum_j \left(\frac{\partial F}{\partial O_j} \right)_{v,T} \frac{dO_j}{d\lambda} = 0 \quad [3]$$

Comparing Eq. [3] with the equilibrium condition for chemical reactions in bulk phases: $\sum_i \mu_i \nu_i = 0$, we find, that an influence of the free surface energy is to be expected in all cases in which $dO_j/d\lambda \neq 0$. This is the case when the metal surface is not completely covered by the oxide, and the fraction of the surface covered varies during the reaction. It may also be the case when the oxide does not form a smooth film, but forms whiskers the height of which, and therefore also the oxide surface, varies during the reaction. In this case a change in the roughness factor will be related to the term $dO_j/d\lambda$.

Under certain conditions another effect may be responsible for deviations in the free energy of formation of an oxide film from the value obtained by experiments done on bulk phases. Thermodynamically an oxide is defined by its chemical composition as well as by its crystallographic state, especially by the concentration and distribution of lattice defects and interstitials. These properties are very likely to be different in oxide layers grown on solid surfaces from those in bulk oxide phases. Especially when

the film thickness is of the same order of magnitude as the lattice constant of the oxide crystals forming the film, considerable deviations are to be expected.

In these cases a term depending on the film thickness is to be introduced into the equation for the free energy change

$$dF = \sum_i \mu_i dn_i + \left(\frac{\partial F}{\partial \xi} \right)_{v,T} d\xi \quad [4]$$

(ξ is the film thickness). Assuming the growth of a smooth film with uniform density and chemical composition we have the following relation between $d\xi$ and the extent of reaction

$$d\xi = \frac{M}{\rho O} \nu_{\text{oxide}} d\lambda$$

(M is the molecular weight of the oxide, ρ its density, ν_{oxide} the stoichiometric number of the oxide in the oxide forming reaction, O the amount of surface.)

The equilibrium condition in this case reads

$$\sum_i \mu_i \nu_i + \left(\frac{\partial F}{\partial \xi} \right)_{v,T} \frac{M}{\rho O} \nu_{\text{oxide}} = 0 \quad [5]$$

Evaluating the first term of Eq. [5] we get

$$\sum_i \mu_i \nu_i = \sum_i \mu_i^0 \nu_i + \sum_i RT \ln p_i^{\nu_i} = -RT \ln K_p^\infty + RT \sum_i \ln p_i^{\nu_i} \quad [6]$$

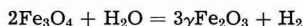
with $K_p^\infty =$ equilibrium constant of the oxide forming reaction for $\xi \rightarrow \infty$. Introducing Eq. [6] into [5] we obtain finally

$$\sum_i \ln p_i^{\nu_i} = \ln K_p^\infty - \left(\frac{\partial F}{\partial \xi} \right)_{v,T} \frac{M}{\rho O RT} \nu_{\text{oxide}} \quad [7]$$

In cases in which the p_i can be measured as a function of ξ , $\left(\frac{\partial F}{\partial \xi} \right)_{v,T}$ can be obtained as a function of ξ , as will be shown for one typical case in the section on thin FeO films at high temperatures.

Application to the Theory of the Flade Potential

In the case of passive iron the Flade potential corresponds to the free energy of the reaction (2, 3)



According to the considerations in the preceding section it should depend on the thickness of the film formed during the reaction. Unfortunately it seems impossible to find experimental conditions under which the film is formed with definite known thicknesses. On the other hand, the film thickness does not decrease uniformly over the whole surface during the activation process so that one cannot associate with certainty the observed activation potentials to different film thicknesses.

Nevertheless, it can be shown that the properties of the passive film depend on its thickness, provided the film thickness is of the same order of magnitude as the lattice constant of its constituents. In a previous paper (4) it could be proved that the film thickness in the stationary state in acid solutions is over a wide range of potentials proportional to the potential-difference $U - U_f$ (U is the potential of

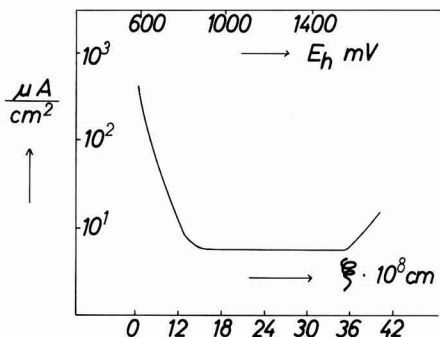


Fig. 1. Steady-state current vs. layer thickness. Iron in 1N H_2SO_4 . Upper abscissa, potential against normal hydrogen electrode.

the passive electrode, U_f the Flade potential measured against the same reference electrode). Using the figures given in that paper it is possible to plot the steady-state current of a passive iron electrode against the film thickness. Such a plot is shown in Fig. 1, using data reported by Herbsleb and Engell (5). [Similar data are reported by Bartlett and Ord (6) and by Osterwald (7).] It is very obvious from the figure that the properties of the passive iron are dependent on the film thickness between 0 and about 12 Å and are completely independent at higher thicknesses. [The increase at ~ 1500 mv is caused by oxygen evolution.]

Herbsleb and Engell also showed that in the region between 600 and 850 mv, where the steady-state current is thickness-dependent, Fe^{++} ions are formed as corrosion product besides Fe^{+++} ions which are found in the whole range of passivity (8). They related the occurrence of the ferrous ions to the existence of fluctuating pores in the passive film within this potential range.

These findings fit very well the assumption that the properties of an extremely thin film differ from those of a thicker one. Generally the film thickness will not be uniform over a macroscopic region of a surface. This spatial fluctuation does not matter in cases when the film thickness is high enough to provide a free energy independent of film thickness ($\partial F/\partial \xi = 0$). If, however, ξ is so small that $\partial F/\partial \xi > 0$ then fluctuations in ξ will give rise to fluctuations in the free energy, and therefore a reaction is possible. As can be seen from Fig. 2 places with lower ξ are less stable with respect to those with higher ξ ,

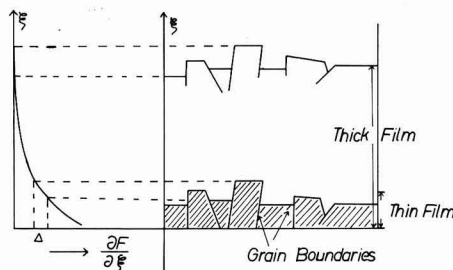
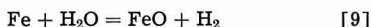


Fig. 2. Influence of fluctuations in thickness on free energy fluctuations for normal and extremely thin films.

and so the reaction leads to the formation of pores at those positions where spots of lower film thickness were situated originally. Whether the pores formed by this process will grow and cause total activation of the passive metal, or whether they will be closed by tangential growth of the film is merely a question of the capacity of the potentiostat used in the experiment.

Thin FeO Films at High Temperatures

The fact that it was possible to describe some properties of the passive film using the concept of a thickness-dependent free energy encouraged us to carry out some experiments to show the influence of film thickness on equilibrium properties in a more quantitative manner. The system Fe/H₂O_{vapor} was chosen, for the equilibrium constant of the reaction



can easily be determined by simple measurements of the pressure if the partial pressure of the steam is kept constant during the experiments.

Experimental Design

The iron specimen consisted of "Magnetreineisen" of the Vakuumschmelze Hanau. Ten sheets with a total geometric surface of 100 cm² were mounted in a glass vessel which was fixed in the center of the coil of a high-frequency furnace. The glass vessel was cooled by running water supplied by a thermostat kept at a temperature of 18°C. The iron specimen was kept in its position by two thin wires of Pt and Pt/10 Rh which at the same time served as a thermocouple. The vessel could be connected with a container filled with a saturated CaCl₂ solution carefully thermostatted at 15°C to maintain the partial pressure of the steam at 5.1 Torr. The total pressure in the system was measured by a mercury manometer, the readings being taken by means of a cathetometer.

It is essential to keep the total volume of the reacting system as small as possible. This may be shown by the following considerations. In the initial state the iron surface is free of oxide ($\lambda = 0$) and the atmosphere consists only of steam at a given partial pressure. When reaction [9] occurs the hydrogen pressure increases in proportion to the extent of reaction

$$p_{\text{H}_2} = \frac{RT}{V} \lambda \quad [10]$$

As the partial pressure of the steam is kept constant during the reaction, the pressure ratio also increases proportionally

$$p_{\text{H}_2}/p_{\text{H}_2\text{O}} = \frac{RT}{p_{\text{H}_2\text{O}} \cdot V} \lambda \quad [11]$$

The reaction comes to an end when this pressure ratio equals the equilibrium constant of reaction [9]. This is illustrated schematically in Fig. 3. The unbroken curve represents the equilibrium constant as a function of λ as expected according to the considerations in the preceding sections. The two dotted lines show the increase of the pressure ratio with λ for two different values of the product $p_{\text{H}_2\text{O}} \cdot V$. It

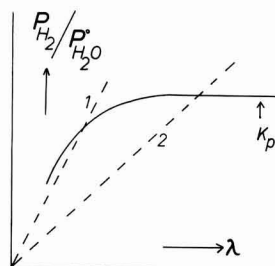


Fig. 3. K_p and $p_{\text{H}_2}/p_{\text{H}_2\text{O}}$ vs. extent of reaction for two different apparatus.

is obvious from Fig. 3 that an apparatus in which $p_{\text{H}_2\text{O}} \cdot V$ has the value used for the construction of curve 2 is useless for measurements of the dependence of K_p on λ . The apparatus used in the investigations reported here corresponded to curve 1 with $p_{\text{H}_2\text{O}} \cdot V \cong 10^3$ Torr cm³ ($p_{\text{H}_2\text{O}} = 5.1$ Torr, $V = 187$ cm³).

The necessity of working in such a small volume makes it impossible to use an apparatus according to the advice of Emmett (9). The measured equilibrium constants therefore may be erroneous due to any effect of thermal diffusion. But as is seen from Table I only the quotients $K_p \infty / K_p$ are needed for the purposes of this paper, and therefore the error will be reduced remarkably. On the other hand, as long as there is no information about the true surface, the uncertainty which arises from the estimation of the roughness factor will be much larger than that arising from the thermal diffusion effect.

Experimental Procedure

All experiments were carried out with the temperature of the metal at 815°C. At the beginning of each experiment the iron specimen was annealed in a hydrogen atmosphere of 200 Torr for 2 hr. This was followed by a second annealing *in vacuo* for 2 hr. Finally, the specimen was annealed in a hydrogen atmosphere of 10 Torr to saturate the metal with hydrogen at about the same pressure as would be established in the oxidation reaction following.

The hydrogen in the gas phase was then removed very rapidly before opening the stopcock between the reaction vessel and the container with the CaCl₂ solution. From then on pressure readings were taken every minute until equilibrium was established.

Table I

$n_{\text{FeO}}/\text{cm}^2, 10^3$	K_p	$K_p \infty / K_p$	$\xi, \text{\AA}$	$\left(\frac{\partial F}{\partial \xi}\right)_{v, T}, \text{kcal/cm}^2$
16.0	1.38	1.00	67.2	0
14.1	1.38	1.00	59.2	0
11.9	1.35	1.02	50.0	0.33
10.2	1.31	1.05	42.8	0.85
8.9	1.27	1.09	37.3	1.49
8.0	1.25	1.103	33.7	1.70
6.4	1.10	1.255	26.9	3.95
6.0	1.10	1.255	25.2	3.95
5.5	1.04	1.33	23.1	4.82
4.8	0.95	1.46	20.2	6.55
4.1	0.85	1.625	17.2	8.37

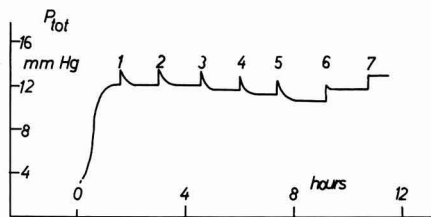


Fig. 4. Pressure readings in one set of experiments, showing the decrease in total pressure with decreasing amount of oxide.

The next steps of the process are easily described with help of Fig. 4. At various times, denoted with 1, 2, . . . , small amounts of hydrogen were added to the equilibrium mixture. (The amount of hydrogen added in each step was about 1/5 to 1/10 of the amount formed in the oxidation reaction at the beginning of the experiment.) This caused a sudden rise in the total pressure, followed by a slow decrease until the new equilibrium was established. Each equilibrium state corresponds to a different amount of oxide present on the iron surface. It can be seen from Fig. 4 that a remarkable decrease in equilibrium pressure is observed in the steps 3, 4, and 5 as the amount of oxide diminishes more and more. After the 6th addition of hydrogen all the oxide is reduced, and equilibrium is no longer reached.

To calculate the amount of oxide present at the various stages of the process it is necessary to know the amount of hydrogen formed or consumed at these stages. As the temperature is not uniform in the system the gas laws cannot be applied directly. We determined the average temperature in the following way. The whole system was kept at room temperature and hydrogen added up to a pressure $p(T_1)$. Then the iron specimen was heated to 815°C , and the pressure $p(T_2)$ was measured. During this experiment the CaCl_2 solution was covered with a film of silicon oil to prevent the formation of water vapor in the system. The average temperature can then be calculated

$$p(T_1)/p(T_2) = T_1/T_{\text{average}} \quad [12]$$

This ratio proved to be pressure-independent in the range of pressures used in the experiments. The average temperature was calculated to be $T_{\text{average}} = 383^\circ\text{K}$. All the experiments were repeated several times and showed a fairly good reproducibility.

Results

The results of the experiments are given in Table I. The figures in the first two columns are calculated directly from the experimental data without introducing any assumptions. To calculate the values of ξ from those obtained for n_{FeO} assumptions must be made for the density of the oxide and for the roughness factor. The density was taken as 5.7 g cm^{-3} , being the value for the bulk material at room temperature. The roughness factor was estimated to be 3, as the metal recrystallized during the annealing procedure, and showed a considerably rough surface after the experiments. To calculate the value of $(\partial F/\partial \xi)$ Eq. [7] was used. The density again was

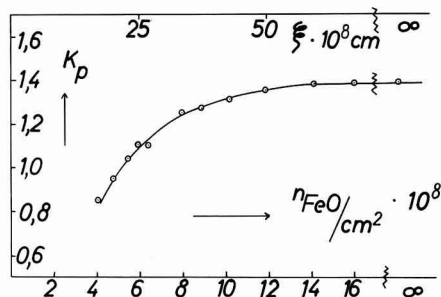


Fig. 5. K_p as a function of the amount of oxide on the metal. Upper abscissa, estimated film thickness (ξ).

assumed to be 5.7 g cm^{-3} , for O the geometrical surface was taken. Figure 5 shows graphically the results for K_p as a function of the amount of oxide on the surface.

It is striking to see from Fig. 5 that deviations from normal behavior become obvious at film thickness as high as $\sim 50\text{\AA}$. It is very unlikely that a film of 50\AA which consists of at least 15 atomic layers would show an abnormal equilibrium behavior. But these values of ξ are, of course, average values, and it is possible that a reasonable part of the surface is covered by a thinner film even if the average film thickness equals 50\AA .

Conclusions

The experiments reported above gave evidence for the existence of thickness-dependent equilibrium properties of solid layers on solid materials. The experimental data, however, are not sufficient to suggest any detailed mechanism. The only conjecture that can be made is that it is very likely that mechanical stresses caused by the difference in lattice parameters of the base metal and the layer are responsible for this behavior. These stresses act on each atom in the interface in a different direction so that no yield processes are possible and the total energy of strain is stored in the interface and its surroundings.

It is to be noticed that thermodynamically this concept differs from that of a surface energy. The existence of a surface energy can only influence equilibria the establishing of which is connected with a change in surface. Nevertheless, the physical causes for the existence of a surface energy between two solids will be the same as those responsible for the existence of a thickness-dependent free energy in thin films.

Acknowledgments

The author wishes to thank Dr. H. Witte for his valuable advice as well as for his help and encouragement during the investigation.

Any discussion of this paper will appear in a Discussion Section to be published in the December 1963 JOURNAL.

REFERENCES

1. K. J. Vetter, *Z. Elektrochem.*, **66**, 577 (1962).
2. H. Göhr and E. Lange, *Naturwissenschaften*, **43**, 12 (1956).
3. K. J. Vetter, *Z. Elektrochem.*, **62**, 642 (1958).

4. K. G. Weil, *ibid.*, **59**, 711 (1955).
5. G. Herbsleb and H. J. Engell, *ibid.*, **65**, 881 (1961).
6. J. L. Ord and J. H. Bartlett, Technical Report No. 7, (1962).
7. J. Osterwald, *Z. Elektrochem.*, **66**, 401 (1962).
8. U. F. Franck and K. G. Weil, *ibid.*, **56**, 814 (1952).
9. P. H. Emmett and J. F. Shultz, *J. Am. Chem. Soc.*, **55**, 1376 (1933).

Ion-Exchange Properties of the Film on Passive Iron and Steel

G. H. Cartledge and Dieter H. Spahrbiel¹

Chemistry Division, Oak Ridge National Laboratory,² Oak Ridge, Tennessee

ABSTRACT

Measurements of ion exchange between the film on passive ferrous metals and aqueous ions have been made as a means of studying the chemical and electrochemical interactions of the film *in situ*. It is shown that the chromate ion, in particular, is held exchangeably in amounts approaching a monolayer. This exchanged slowly with alkaline or weakly acidic sulfate solutions, and the kinetics of the exchange has been studied. It was found that the rate equation contains both a linear depletion term and a term exponential in the extent of the replacement reaction. This is interpreted mathematically by an activation energy which increases linearly with the quantity exchanged. The similarity to the kinetics of adsorption of gases on metals in certain cases is pointed out.

The chemical state and electrochemical properties of the surface of a passive metal have been regarded in a variety of ways since Faraday ascribed its peculiar behavior to a film of oxygen fixed in some undetermined form. In recent years, the film on passive iron has been examined by a number of experimental techniques, but almost all the procedures used required the drying of the film or even its removal from the metallic substrate. Hence, the results do not necessarily disclose the nature of the film as it exists in contact with its aqueous environment. For the understanding of the relation of the properties of the film to electrochemical processes occurring at or through it, one needs to study the appropriate phenomena with the film *in situ*, and only a few experiments of this kind have been described.

Thus, it has been shown that the passive film on iron in nitric acid has a low electronic resistivity (1), and the capacity of passive metal surfaces has been measured in a few instances, although the results are not easily understood. It has been shown also (2, 3) that the film produced when iron is passivated in oxygenated inhibitor solutions exhibits the Flade potential when activated by added anions and hence has an electrochemical character similar to that of the film produced by anodic polarization in a strongly acidic solution. Cathodic reduction processes at passive surfaces on zirconium (4), stainless steel (5), and iron (6-9) have been reported recently from this laboratory. These measurements have shed some light on the behavior of the surface films with respect to transport of charge across the interface. They also disclosed marked acceleration of cathodic processes when Os(OH)₄ or Tc(OH)₄ was deposited over the passive iron film.

Although the film on iron is generally described as an oxide and electron diffraction of dry film reveals the structure of magnetite or γ -Fe₂O₃, there is

some reason to believe that the material *in situ* is at least partially hydroxylated, perhaps as γ -FeOOH. Such data as exist show that this compound (or the α -form) has considerable stability under passivating conditions (10). Whatever the mechanistic source of the Flade potential may be, its dependence on the hydrogen-ion concentration and the rapid response of the potential of a passivated electrode to changes in acidity demonstrate that some kind of proton interaction is involved at the interface. In several instances, it has been shown (11-14) that partial oxidation of a solid M(OH)₂ consists of the mere loss of a proton and an electron without change of structure. These facts make it probable that protons need to be considered as essential components of the passive film and as participants in any electrochemical processes at the surface.

That anions, as well as protons, may interact with the passive surface is indicated by numerous studies in this laboratory (9, 15) as well as elsewhere. Further, measurements of effects related to zeta potentials have demonstrated definite and specific interactions between an "oxide" surface and dissolved ions (16). These effects are most readily understood as a kind of acid-base interaction.

Finally, it has been demonstrated by Kraus *et al.* (17) that several precipitated oxides or insoluble hydrous salts possess highly specific ion-exchange properties. Thus, it was shown that the chromate ion is firmly bound on certain of them but may be exchanged by anions such as the hydroxide ion. The same substrate failed to adsorb pertechnetate ions (TcO₄⁻) in the same medium, in the experiments of these authors. They observed, further, that the exchange capacity diminished when the precipitates were sintered at only moderately elevated temperatures.

All these lines of investigation suggest a need for a more intimate knowledge of the chemistry of the passive film in its unique state while intervening between a metal and an aqueous environment. If it also

¹ Present address: Varta AG, Zentral Laboratorium, Frankfurt, Germany.

² Operated for the United States Atomic Energy Commission by the Union Carbide Corporation, Oak Ridge, Tennessee.

enters into specific exchange processes with neighboring ions, it can be treated no longer merely as an inert barrier to transport of charge (electrons, ions, or defects), because its composition, structure, and the gradient of potential through it will be dependent on the composition of the solution with which it is in contact. For these reasons, we have studied ion-exchange processes at the surface of passivated iron, steel, and stainless steel, in the hope that a comprehensive knowledge of the behavior of ions of different types may lead to a clearer understanding of the thin outer surface of the film, where the kinetics of corrosion and other electrochemical processes is so largely determined. The present paper describes the orienting experiments with several systems and gives an analysis of the kinetics of exchange for one particular system.

Experimental

In preliminary experiments, the metals used were carbonyl iron powder and carbon steel (0.1% C). The powder consisted of spheres without porosity; after brief treatment with 1f HClO₄, its surface area was determined by the B.E.T. method to be 0.4 m²g⁻¹.³ Sufficient powder (3-10g) was rinsed in 1f HClO₄ and then passivated for 3-5 da in aerated chromate or molybdate solutions adjusted to pH values as low as 3.5. Samples of this size provided a sufficiently large surface for spectrophotometric procedures to be used in analyzing the extracts subsequently made. In this way, it was possible not only to determine the amount of chromium or molybdenum recovered from the film, but also, in the case of chromium, to demonstrate that it was removed as the anion containing Cr(VI), rather than as some reduction product. Chromate ions were determined by use of diphenylcarbazide, which is not sensitive to Cr(III). Molybdenum was determined by the thiocyanate procedure.

The passivated powder was washed repeatedly on a suction filter with distilled water having the pH value of the passivating solution and then was extracted with successive portions of 3f NH₄OH at 24°. It was found that the seventh water wash contained a barely detectable amount of Cr(VI), whereas the first subsequent ammonia extract was sometimes visibly yellow. Thus, in a typical experiment, the total amount removed in four 10-min extractions with 3f NH₄OH at 24° was 1 x 10⁻⁸g (Cr)cm⁻², and additional extractions with a more alkaline solution showed that all the Cr(VI) had not been removed. The results of several such experiments indicated that the total exchangeable Cr(VI) approached monolayer coverage, if the chromate ion is taken to cover 25A² [3.47 x 10⁻⁸g(Cr)cm⁻²]. Similar experiments with iron powder passivated in aerated molybdate solutions showed that molybdenum also is removed by ammonia.

Preliminary experiments were conducted also with the pertechnetate ion as passivating agent. The metal was either No. 36 iron wire ("for standardization") or 1 x 2 cm pieces of low-carbon steel. The passivating solutions were 1.5-5x10⁻⁴ fKTCO₄ at pH ca 6. No exchangeable TcO₄⁻ exceeding possibly a

percent or so of a monolayer was detected by measuring the beta activity both of the extracts (after suitable treatment) and of the metal itself. This negative result would agree with the observations of Kraus *et al.* (17), but in view of subsequent experiments does not exclude the possibility that some exchange might be found if passivation could be effected at a lower pH and with a more highly concentrated pertechnetate solution. Further efforts in this direction will be made.

In a test for cation exchange, tracer Zn⁶⁵ was used with steel sheet which was first passivated in oxygenated 10⁻²f phthalate inhibitor at pH 5.87. In a typical experiment, subsequent exposure to Zn⁶⁵ in the passivating medium for 15 hr gave a zinc content of 2.31 x 10⁻⁸g(Zn)cm⁻² on the rinsed specimen. The metal was then extracted with 10⁻²f Mg(NO₃)₂ in 10⁻²f phthalate at pH 6.88. In 5 extractions over a period of 3 hr, 1.18 x 10⁻⁸g(Zn)cm⁻² was removed. The total amount on the metal would correspond to only a few per cent of a monolayer of zinc ions if it were all confined to the surface.

Rate measurements.—Since the existence of anion exchange was demonstrated and shown to be a slow process, a study of the rate of exchange was undertaken. For this purpose, the chromate-sulfate-hydroxide system was selected, in view of the convenience and sensitivity of radiometric measurements with Cr⁵¹ of 27.8-day half-life.

For the preparation of the radioactive inhibitor solution, 4-6 mc of Cr⁵¹ as CrCl₃ was freed of chloride by precipitation of Cr(OH)₃ and converted to Cr₂O₇⁼ in 10⁻²f K₂Cr₂O₇ adjusted to pH 2.35. The freshly prepared passivating solutions had such specific activities as to give 1 count/min for about 2 x 10⁻¹¹g Cr, when using enough channels of a multi-channel analyzer to cover the 0.32 mev peak of Cr⁵¹. By measuring the loss due to absorption when thick metallic electrodes were used, it was possible to check the material balance at the end of an experiment.

Because of the slowness of the exchange, the first experiments were conducted at 40° with a concentrated solution as extractant, namely, 1f (NH₄)₂SO₄ in 6f NH₄OH. In later experiments, 0.5f K₂SO₄ buffered to pH 9.22 by a 0.1f carbonate mixture was used. For the quantitative rate measurements, type 347 stainless steel specimens were used in order that passivity might be maintained by air throughout the experiment. The specimens were either pieces of 3-4 cm² sheet or cylinders 1 cm in diameter by 2 cm long (ca. 7 cm² area, counting only one exposed circular section). They were prepared with surfaces of differing roughness by electropolishing, alternate activation in H₂SO₄ and passivation in HNO₃, etching in 6N HCl + H₂O₂, or abrading with 2/0 emery. In some instances, the specimens were re-passivated in 0.1N H₂SO₄ in air or by addition of a small amount of H₂O₂ to the acid. They were then passivated in the 10⁻²f dichromate solution for periods of 16 hr to several days at 24°. Before extraction, the specimens were rinsed 30 sec under running distilled water, since it was known from work with the pertechnetate ion that this treatment effectively removes adhering solution.

³ The authors are indebted to the Analytical Chemistry Division for this measurement.

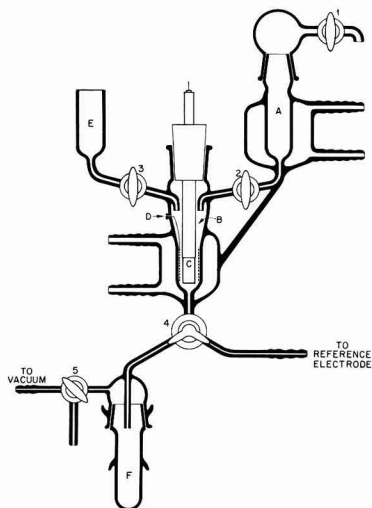


Fig. 1. Apparatus for ion exchange. A, Water-jacketed reservoir; B, jacketed extraction cell; C, specimen, held by a Teflon support having an axial stainless steel rod for electrical connection; D, contact for platinum gauze counter electrode; E, reservoir for rinsing; F, holder for counting tubes.

The extractions were conducted by exposing the specimens to successive 2 or 3 ml portions of solution for measured times, either in tubes which fitted into the well of the detector of the analyzer or in the apparatus shown in Fig. 1. In both instances, the extraction vessel was held at 40° by water circulating through a constant-temperature bath. To determine whether the kinetics was affected by agitation, a comparison was made in two experiments under identical conditions except that, in one, the solution was continuously agitated by a stream of oxygen, whereas there was no deliberate stirring in the other. The results were alike.

Figure 1 shows the details of the apparatus used when it was desired to follow or control the potential of the specimen during the extraction.

Two types of experiments were made in order to establish the correctness of the presumption that only surface chromium was being exchanged with significant rapidity. In the first type, two specimens were prepared with as nearly similar surface treatments as possible. One specimen was passivated in 10⁻²f, K₂Cr₂⁵²O₇ (at pH 2.35), while the other was passivated in a similar solution containing Cr⁵¹. The two specimens were then extracted by successive portions of 1f (NH₄)₂SO₄ in 6f NH₄OH at 40° over a period of 22 hr. Then, without intervening treatments, both specimens were soaked for 1 hr at 24° in the Cr⁵¹ passivating solution and again carried through the extractions. Thus, one specimen contained Cr⁵¹ throughout its film, whereas the other could have contained it only so far as it might have penetrated into the pre-existing film in the 1 hr exposure. In the parallel extractions in two sets of experiments of this type, the two rate curves almost coincided during the first 5 hr, when depletion began to be indicated for the specimen having only superficial Cr⁵¹. In the subsequent kinetic analysis of the

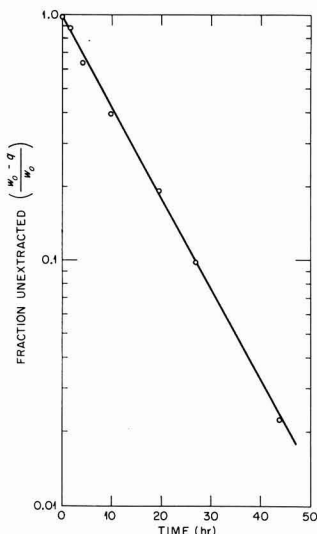


Fig. 2. First-order exchange of Cr⁵¹ on surface by aqueous Cr₂⁵²O₇; w₀ is the initial exchangeable chromate and q the amount exchanged at time t. The curve represents the slow exchange following a rapid initial removal of some Cr⁵¹.

data, it was found that they followed the same kinetics. The significance of a very slow residual extraction of Cr⁵¹ from the specimen initially passivated in K₂Cr₂⁵¹O₇ will be considered at a later point.

In the second type of experiment, the kinetics of ion exchange of film Cr⁵¹ by aqueous Cr⁵² was determined. Having the aqueous Cr₂⁵²O₇ in large excess, one would expect the rate of exchange to be first order with respect to Cr⁵¹ remaining on the surface at time t if only a surface-exchange process were rate determining. This should not be true if diffusion from the interior of the film were the limiting factor. In each of three experiments, first-order kinetics was demonstrated, following a fast initial process which will be treated more fully in a subsequent paper. Figure 2 illustrates one of the series of measurements which was carried to about 98% completion in 43 hr. The excellent agreement with first-order kinetics thus demonstrates that the measurements are not significantly complicated by either diffusion or a reverse process.

Results

Since the measurements extended from 1 min to several days, as a rule, it was found convenient not to count the first extraction of 1 min duration in the kinetic analysis because of irregularities involved in the adjustment of temperature, wetting of the specimen, and response of the surface to the considerable difference in pH between passivating medium and the solution for extraction. From the type of kinetics followed by the system, it will become apparent that the mathematical analysis may be started at any point early in the experiment, the only difference being in the values of the constants. The amount of chromium found in the first extract has been counted, however, in the total quantity of chromium exchanged, W.

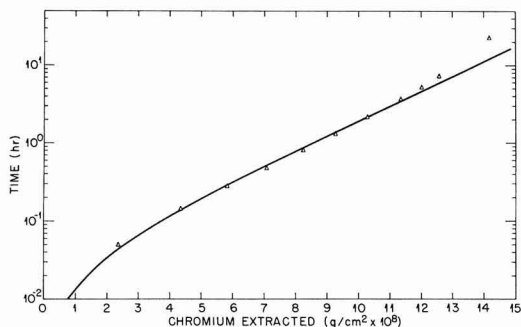


Fig. 3. Typical exchange-log time curve. Passivation in $10^{-2}f$ $K_2Cr_2O_7$ at pH 2.35; extraction at 40° by $1f$ $(NH_4)_2SO_4$ in $6f$ NH_4OH . Specimen etched and abraded. (Point 11 in Fig. 7.)

The points of Fig. 3 are from a typical measurement. One might have expected a first-order dependence of rate on chromium activity remaining on the surface, in view of the enormous excess of the extracting ion. The rate diminished initially much too rapidly for such a relationship, however, and it was found that a plot of q , the amount exchanged per square centimeter of projected area at time t against $\log t$ became almost linear after some minutes. The curve in Fig. 3 is a least-squares fit of the data to an equation of the form

$$q = m \log(nt + 1) \quad [1]$$

the derivation of which will be given below. The q - $\log t$ relation held for several hours in measurements at 40° , until the rate became slower, evidently by depletion of the exchangeable chromium on the surface.

The $\log t$ relationship suggests an analogy to the Elovich equation, which applies to the rate of adsorption or desorption of a gas on a metal. As shown experimentally by Scholten and Zwietering (18), this type of kinetics arose in their system

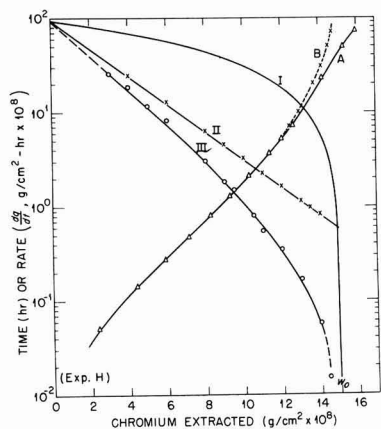


Fig. 4. Curve A, data of Fig. 3; Curve B, corrected by an "end-effect" factor. Analysis of experimental rate- q curve (III) into a first-order term (I) and a term exponential in q (II). Circles on III are taken from tangents to a linear plot of q (corrected) vs. t .

because of a linear variation of the activation energy with the extent of coverage, θ . A rate equation for the ion-exchange process was therefore developed from the Eyring absolute rate theory, under the provisional assumption that the activation energy increases linearly with the extent of exchange, as measured by q , that is

$$\Delta H_q^\ddagger = \Delta H_o^\ddagger + \frac{rq}{f} \quad [2]$$

In order that the constant r may be referred to the true area available for ion exchange, the factor f was introduced to represent the ratio of this area to the projected area on which q is based. The factor r thus has the dimensions $\text{cal mole}^{-1} \text{cm}^2 \text{g}^{-1}$ based on the available area, when q is in g (Cr) cm^{-2} (projected). (Unlike a conventional roughness factor, f may readily be less than unity, since it refers only to sites that are both chemically and geometrically accessible to the exchange process.)

The complete rate equation then contains a linear depletion factor, $w_o - q$, where w_o is the amount of chromium exchanged from time zero to the limit, and an exponential term in q

$$\frac{dq}{dt} = S_o' [w_o - q] \exp \left[-\frac{rq}{fRT} \right] \quad [3]$$

Here S_o' includes the usual kinetic factors, the constant concentration of the extracting species, $\exp[-\Delta H_o^\ddagger/RT]$, and the entropy term, variation of which is assumed to be of minor importance. This equation may be explicitly integrated only over such a time as the exponential term is dominant. For this case, we obtain for a particular experiment

$$q = 2.3 \frac{fRT}{r} \log \left[\frac{rS_o}{fRT} \cdot t + 1 \right] \\ \equiv 2.3 m \log \left[\frac{S_o}{m} \cdot t + 1 \right] \quad [4]$$

S_o being the initial rate, $S_o'w_o$, ($q = 0$). This is seen to be equivalent to Eq. [1], which closely describes the course of the exchange process for some hours at 40° (Fig. 3). All of the series of measurements followed this relationship for periods of time which varied according to the treatment given the specimens before exposure to the Cr^{6+} passivating solution.

The applicability of Eq. [3] for longer times was tested in the following way. If the right side of the equation is multiplied by w_o/w_o , we may obtain Eq. [5]

$$\log \frac{dq}{dt} = \log S_o + \log \frac{w_o - q}{w_o} - \frac{rq}{2.3 fRT} \quad [5]$$

or

$$\log \left[\frac{dq}{dt} \cdot \frac{w_o}{w_o - q} \right] = \log S_o - \frac{rq}{2.3 fRT} \quad [6]$$

Rates were taken as tangents to linear plots of q vs. t . $\log dq/dt$ was then plotted vs. q , as shown by curve III in Fig. 4. If Eq. [6] is valid, it should be possible

to find a value of w_0 , consistent with the value approximately indicated by the experimental curve III, such that a graph of the left side of Eq. [6] against q is linear and extrapolates to a value of S_0 at $q = 0$ that also is consistent with the experimental rate curve. Curve II in Fig. 4 is such a result, curve I being the rate that would have been observed for the first-order depletion process with constant activation energy. This type of analysis was made for 15 experiments in 10^{-2} to 1f sulfate at 40° , the solution being alkaline with NH_4OH in 11 cases, buffered at pH 9.22 with a 0.1f carbonate mixture in 2 cases, and at pH 4.82 in 2 cases.

In addition, one experiment was conducted at 0° . Even after 70 hr, the extraction was still following the simplified Eq. [4] so closely that an accurate estimate of w_0 was not possible. In another experiment at 40° , the rate of extraction of chromium by distilled water was measured. This followed the same type of equation, but substitution of 0.5f $\text{K}_2\text{SO}_4 + 0.1\text{f}[\text{Na}, \text{H}]_2\text{CO}_3$ at pH 9.22 for water toward the end of the experiment showed the rate (for a 15-min extraction) to be about 25 times faster in the salt solution than it was in water.

When experiments were extended for some days at 40° , a complication appeared after the rate had diminished by something like 3 to 4 orders of magnitude from the initial value. It was apparent that the rate now decreased more slowly than was required by the depletion term. As was pointed out previously, depletion was approached closely when only the surface of the passive film contained Cr^{51} , whereas, after several hours, Cr^{51} in appreciable amounts continued to pass into the extracts when the entire film contained Cr^{51} . In the long-continued experiments (25-200 hr), it was therefore necessary to take this end effect into account as a minor correction, if it was desired to deduce values of w_0 . The corrections became significant, however, only when the exchange rate had fallen to a few tenths of a percent of the initial rate, as seen in Fig. 6, for one example. Here Curve III-A gives the experimental rates and III-B the rates corrected for a constant "end effect" of $7 \times 10^{-11} \text{g}(\text{Cr})\text{cm}^{-2} \text{hr}^{-1}$. It is seen that the experimental rate curve showed signs of

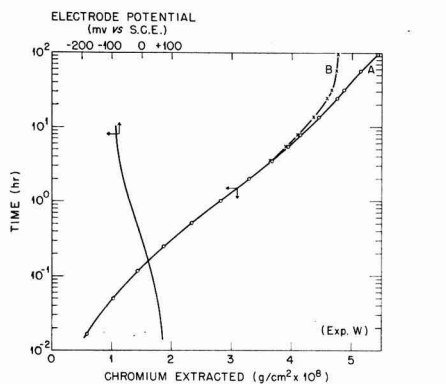


Fig. 5. Curve of q vs. $\log t$ showing variation in potential during exchange. Passivation in $10^{-2}\text{f} \text{K}_2\text{Cr}_2\text{O}_7$ at pH 2.35. Extraction at 40° by 0.5f $\text{K}_2\text{SO}_4 + 0.1\text{f} [\text{Na}, \text{H}]_2\text{CO}_3$ at pH 9.22.

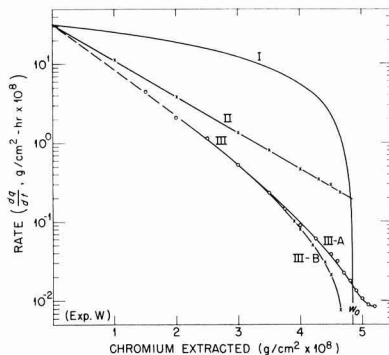


Fig. 6. Analysis of the data of Fig. 5

leveling off at some such value, the extractions having been continued for 95.5 hr.

It is not clear whether the end effect arises from a continuing corrosion process, a simple dissolution of film, diffusion of $\text{Cr}(\text{VI})$ from the interior of the film, or, possibly, a slow isotopic exchange whereby $\text{Cr}^{51}(\text{III})$ in the film passes into $\text{Cr}^{51}(\text{VI})$ and then into solution. The rate is probably of the right order of magnitude for the corrosion rate in the alkaline medium, but, in any case, is so low as not to disturb the conclusions regarding the kinetics over by far the greater part of the process. The correction was observed to be greater when a sulfate solution at pH 4.2 was used for the exchange.

Discussion

It appears that Eq. [3], containing the assumption of varying activation energy, applies to the exchange process under a variety of conditions and over a range of rates extending over something like four orders of magnitude. By treating the surface in a variety of ways before exposing it to $\text{Cr}^{51}(\text{VI})$, it was possible to begin the experiments with amounts of exchangeable chromium ranging between 2.3 and $20.3 \times 10^{-8} \text{g}(\text{Cr})\text{cm}^{-2}$ (projected). (These numbers are W_0 and include the amounts remaining on the specimen after the 30-sec rinse with distilled water, even though w_0 , used in the calculation of rates, excludes the amount removed during the first minute.) To gain some information as to r , the rate at which the activation energy increases during exchange, the data were treated in the following way.

The values of W_0 increased with the roughness of the surface, which was known qualitatively from the pretreatment given the specimens. Hence, the values of f/r given by curves like II in Fig. 4 and 6 were plotted against W_0 . The points for the 15 experiments roughly indicated a linear relation $f/r = a + bW_0$. A least-squares line computed for this equation had an intercept on the f/r axis at -0.14 , with $b = 2.44 \times 10^{-4}$. Within the statistical precision of the data, this intercept equals zero, which it should do for physical reasons, since the factor f is a measure of the relative surface area available for exchange and $W_0 = 0$ when $f = 0$. Hence, a second least-squares line was computed with $a = 0$ in the equation above. This gave $b = 2.32 \times 10^{-4}$; the resulting curve is drawn in Fig. 7. It is seen that 10 of

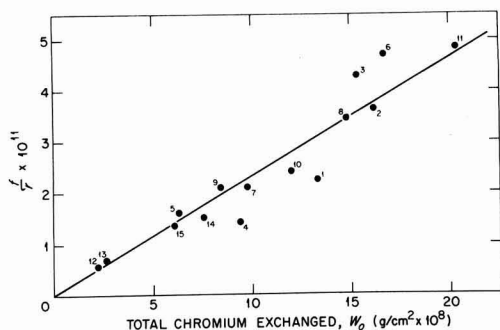


Fig. 7. Graph of f/r vs. W_0 . The numerals merely identify the experiments in chronological sequence.

the points fall very close to the curve, with some scatter for the others.⁴

The least-squares value of $W_0 r/f$ given by Fig. 7 is 4.31×10^3 cal mole⁻¹, and this represents the amount by which the activation energy of the process increases upon exchange of the amount of chromium corresponding to a complete layer of ions. To evaluate r , it is necessary to determine W_0/f , which may be derived at least approximately by the following considerations.

The close approach to linearity in the relation between f/r and W_0 is strong evidence both for the constancy of r in these experiments and for the assumption that the total initial amount of exchangeable chromium is simply proportional to the available surface area, for the given conditions of passivation. If both of these conditions were not satisfied, it would then be necessary to assume that simultaneous variations in r and W_0 were just such as to give the observed linearity by compensating each other. This seems unlikely. It follows also that, in all the experiments, the initial fractional coverages must have been very approximately equal.

That the chromium is not initially derived in significant amounts from underlying parts of the film was demonstrated in the experiments described previously (see above, page 646). Hence, we can consider the sites for exchange to be on the more or less flat surface of the passive film. From the dimensions of the chromate ion in crystals, one may calculate that a tetrahedral face of the ion has an area of 25\AA^2 . If such ions were closely packed on a plane surface, complete ionic coverage would require 3.47×10^{-8} g (Cr) cm⁻² (true area). The actual areas of the specimens are, of course, not known accurately. Specimens for experiments 12 and 13 were heavily electropolished, however, to a very bright finish; they also had the lowest values of f/r . Specimen 12 was polished somewhat more heavily than 13. No great error can therefore be introduced by assuming that the surface factor for chromate ions is essentially equal to unity for specimen 12, so far as geometry alone is concerned. (The value might be larger for smaller adsorbable entities.) On this assumption, the minimum value for complete

coverage would be the observed W_0 for specimen 12, or 2.26×10^{-8} g cm⁻². This is 0.65 of the maximum value calculated from the dimensions of the ion. It is certainly a reasonable result, especially since close packing of anions without some means of diminishing the repulsive forces is hardly to be expected.⁵ If we then take $f = 1$ and $W_0 = 2.26 \times 10^{-8}$ g cm⁻² for experiment 12, we obtain $r = 1.91 \times 10^{11}$ cal mole⁻¹ g⁻¹ cm².

The magnitude of r accounts for the relative effects of the depletion factor $(w_0 - q)/w_0$ and the activation-energy term, $\exp(-rq/fRT)$, in causing the rate dq/dt to decrease during the exchange process. For a typical experiment, 8, for example, the depletion factor alone reduces the rate by one order of magnitude at $q = 0.9 w_0$, the exponential term alone by two orders, for an over-all reduction of the rate by three orders. This large effect of the exponential term accounts for the fact that the q vs. $\log t$ graphs become linear after a short time and remain so over a large portion of the extraction process.

The experiments thus give additional evidence for the chemical activity of the passive film towards the solution which bathes it. It is seen also that the ion-exchange process at the passive interface of a metallic substrate differs radically from a simple reversible chemical process. Until other systems have been examined quantitatively, it would be premature to draw conclusions as to the details of the electrochemical reasons for this difference. It is suggested, however, that the results emphasize the necessity to consider the passive film as a region in which energy levels or potential gradients are markedly influenced by the population of ions on its surface, in quite the same manner as Boudart has treated the adsorption of gaseous molecules on a metallic substrate (19). Otherwise, it would be difficult to understand why the kinetics of the exchange process should be so different when the radioactive film interacts with Cr⁵² chromate ions, in one case, and with sulfate or hydroxide ions, in the other.

The experiments are being continued with other systems and under other conditions.

Any discussion of this paper will appear in a Discussion Section to be published in the December 1963 JOURNAL.

REFERENCES

1. K. J. Vetter, *Z. Elektrochem.*, **55**, 274 (1951).
2. G. H. Cartledge and R. F. Sympton, *J. Phys. Chem.*, **61**, 973 (1957).
3. H. H. Uhlig and P. F. King, *This Journal*, **106**, 1 (1959); see *ibid.*, p. 1074 for discussion of this paper.
4. R. E. Meyer, *ibid.*, **107**, 847 (1960).
5. Franz A. Posey, G. H. Cartledge, and R. P. Yaffe, *ibid.*, **106**, 582 (1959).
6. G. H. Cartledge, *J. Phys. Chem.*, **64**, 1877 (1960).
7. G. H. Cartledge, *ibid.*, **64**, 1882 (1960).
8. G. H. Cartledge, *ibid.*, **65**, 1009 (1961).
9. G. H. Cartledge, *ibid.*, **65**, 1361 (1961).

⁴ Figure 7 includes experiments done early in the study, before the conditions for attaining highest accuracy in the values of W_0 had been established. The linear relationship is confirmed by measurements in other systems which will be published elsewhere.

⁵ Also, it is not yet determined experimentally whether all the area geometrically available is also chemically suitable for exchange. There is some evidence that this depends somewhat on the acidity of the passivating solution. This point is being investigated further.

10. R. Fricke and W. Zerrweck, *Z. Elektrochem.*, **43**, 52 (1937); cf. J. D. Bernal, D. R. Dasgupta, and A. L. Mackay, *Nature*, **180**, 645 (1957).
11. W. Feitknecht and G. Keller, *Z. anorg. Chem.*, **262**, 61 (1950).
12. W. Feitknecht, H. R. Christen, and H. Studer, *ibid.*, **283**, 88 (1956).
13. G. W. D. Briggs and W. F. K. Wynne-Jones, *Trans. Faraday Soc.*, **52**, 1272 (1956).
14. W. Feitknecht and W. Marti, *Helv. Chim. Acta*, **28**, 129 (1945).
15. F. A. Posey and R. F. Sympson, *This Journal*, **109**, 716 (1962).
16. See, for example, P. J. Anderson, "Proceedings of the Second International Congress on Surface Activity," p. 67, Butterworth's Scientific Publications, London (1957); and *Trans. Faraday Soc.*, **54**, 130 (1958).
17. K. A. Kraus, H. O. Phillips, T. A. Carlson, and J. S. Johnson, "Second United Nations Conference on the Peaceful Uses of Atomic Energy," vol. 28, p. 3, (1958).
18. J. J. F. Scholten and P. Zwietering, *Trans. Faraday Soc.*, **53**, 1363 (1957).
19. M. Boudart, *J. Am. Chem. Soc.*, **74**, 1531, 3556 (1952).

Corrosion and Passivity of Molybdenum-Nickel Alloys in Hydrochloric Acid

H. H. Uhlig, P. Bond,¹ and H. Feller²

Corrosion Laboratory, Massachusetts Institute of Technology, Cambridge, Massachusetts

ABSTRACT

Data are presented on corrosion rates of 3-25% Mo-Ni alloys in 10% HCl at 25°, 70°C, and the boiling point. Data also include measurements of corrosion potentials, critical current densities for passivity, anodic polarization in the active potential region, and hydrogen overvoltage. Molybdenum-nickel alloys, like other passive metals, corrode under anodic control, but their corrosion potentials, unlike values for the passive chromium alloys, are more active than the corresponding Flade potentials at which a passive film is established. Corrosion resistance derives apparently from a sluggish anodic dissolution reaction, such as a low rate of ion hydration. Chemical properties of Mo are imparted to Ni or to Ni plus Fe alloys at critical ratios related to electron configuration of the component metals.

Chromium is outstandingly passive, and it confers this property on alloys of iron at a minimum concentration of about 12% Cr. The latter alloys make up the stainless steels. Chromium also confers passivity on other alloys, e.g., of nickel, the minimum composition coming at about 14% Cr, and of cobalt, the minimum composition coming at about 8% Cr as measured by critical current densities for passivity in H₂SO₄ (1). Nearest to chromium in atomic electron configuration is molybdenum, which except for an extra closed shell of electrons, has the same outer configuration. It might be expected, therefore, that molybdenum similar to chromium would also impart passivity to its alloys, and, in fact, several commercially important corrosion resistant nickel-base alloys are produced.

But there are outstanding differences in chemical properties between Mo and Cr alloys. For example, the Mo alloys react readily with nitric acid and with many other oxidizing agents contrary to Cr and the passive chromium alloys. On the other hand, Mo and Mo alloys tend to be corrosion resistant to hydrochloric acid in which Cr alloys corrode at high rates. Also, Mo tarnishes in the atmosphere, whereas Cr is free of visible surface films and remains bright for a long time. These differences suggest that the electron configuration of Mo and Cr despite similarities

of the atoms are not alike in the metallic state. It is of interest nevertheless to compare the passive properties of the two metals, and to compare the atomic percentages at which either metal confers optimum corrosion resistance and passivity on its alloys.

Experimental Procedure

Measurements were made of the potentials, polarization behavior, and corrosion rates of molybdenum-nickel alloys. These alloys exist in solid solution up to 20 wt % Mo. Passivity in the molybdenum-iron alloys is not as easy to study because a two-phase structure begins at 7 wt % Mo, limiting any possible interpretation of results within the passive composition range.

Relatively pure alloys were made up in a vacuum furnace using alumina crucibles. The melts were drawn into 7 mm quartz tubes in an atmosphere of helium purified by passing the gas over Ti sponge at 800°C, and the ingots were quenched in water. Carbonyl nickel and commercially pure molybdenum were used; a few alloys (3.1 and 5.6% Mo) were melted using spectroscopically pure Mo and hydrogen-decarburized carbonyl Ni (0.001% C, < 0.002% S) in order to check the effect of impurities. No essential differences in properties were found for the two sets of alloys. Ingots were homogenized at 1100°C for 12 hr. They were then rolled to 0.10 in.

¹ Present address: Ford Scientific Laboratory, Dearborn, Michigan.
² Present address: Institut für Metallkunde der Technischen Universität, Berlin, West Germany.

(0.25 cm) strip, heated for 15 min at 1000°C in He or A, and water quenched. Composition was determined by chemical analysis. Specimens measuring 0.5 to 1 cm wide, 3 cm long and 0.2 cm thick were cut from the strip. A hole was drilled at one end of each specimen from which it was suspended by a glass hook. Surface preparation was by abrasion, ending with No. 600 silicon carbide paper applied wet. Specimens were washed in water, degreased with boiling benzene, and pickled in warm 6N HNO₃.

Corrosion rate determinations in hydrochloric acid at 25°C were conducted in separate 2-liter glass vessels for each specimen. The vessels were placed in an air thermostat maintained at 25° ± 0.5°C. At 70°C, 1-liter glass vessels were located in a water thermostat, each vessel being fitted with an air-cooled reflux condenser. Air or nitrogen at 40 ml/min entered the acid through gas dispersion tubes, the acid being saturated with either gas several hours before each run. Nitrogen was purified by passing the gas over copper turnings at 450°C. Purified hydrogen was used to deaerate the acid at 25°C. Corrosion rates were determined both by weight loss of the specimen and by analysis of the acid for Ni⁺⁺ using a standard colorimetric method employing dimethylglyoxime as indicator (2). Reported corrosion rates are steady-state values determined from slopes of metal loss *vs.* time (4-8 day tests at 25°C, 1-3 days at 70°C). From a few weight loss-time curves carried out at 70°C for alloys containing between 3 and 9% Mo, it was found that the initial rate is higher than the final rate and that the steady-state rate is achieved after about 1 hr. For boiling acid, only weight loss values were determined; these results, therefore, represent average corrosion rates including an induction time (1-2 day tests). Gases were not bubbled through the boiling acid, contrary to the lower temperature runs.

Polarization measurements were conducted at 25°C in an air thermostat using Ag-AgCl, 0.1N KCl as reference electrode. A constant current was supplied by 30 dry cells in series with a variable resistance. Critical current densities were determined by the method of Uhlig and Woodside (3) using de-aerated acid. This method consisted of applying increasing increments of current and observing the steady-state potential. The lowest current which brought the specimen to the passive potential was taken as the critical value. To make certain that the applied current was or was not below the critical, polarization was continued in each instance until the potential changed less than 2 mv/min.

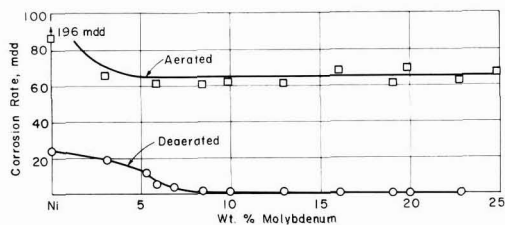


Fig. 1. Corrosion rates of nickel-molybdenum alloys in aerated and deaerated 10% HCl at 25°C (4-8 day exposure).

Results

Corrosion rates in aerated and deaerated 10% HCl at 25°, 70°, and 102°C (boiling) are shown in Fig. 1-4. At 25°C in aerated acid, the average corrosion rate of alloys at and above 3% Mo is 65 mdd; in deaerated acid the rates are lower becoming extremely small above 10% Mo, and zero within the experimental accuracy of the measurements at 19.1% Mo and above. At 70°C, rates in deaerated acid are also substantially lower than in aerated acid. In deaerated acid, a minimum rate is reached

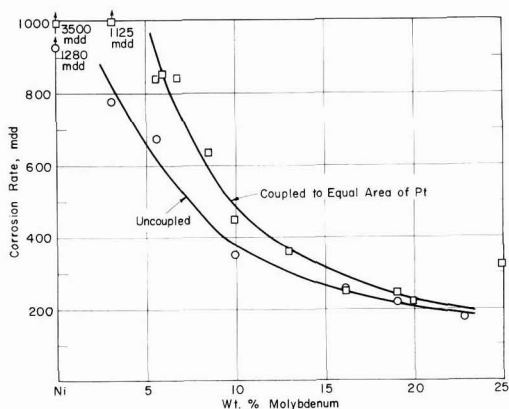


Fig. 2. Corrosion rates of nickel-molybdenum alloys in aerated 10% HCl at 70°C (1-3 day exposure).

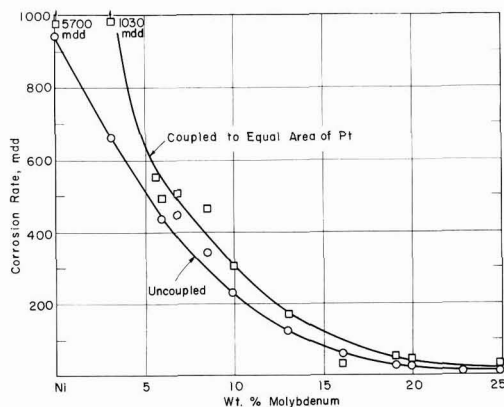


Fig. 3. Corrosion rates of nickel-molybdenum alloys in deaerated 10% HCl at 70°C (1-3 day exposure).

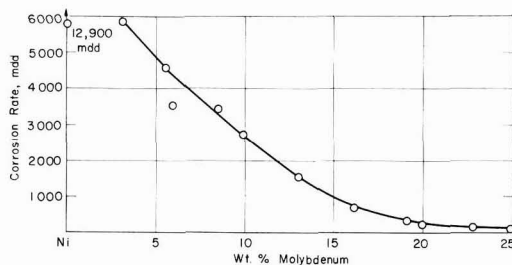


Fig. 4. Corrosion rates of nickel-molybdenum alloys in boiling 10% HCl (1-2 day exposure).

at or above 20% Mo; a similar minimum is also observed in boiling 10% HCl. The present results do not agree with earlier results of Field (4) who reported much higher corrosion rates in 10% HCl at 70°C for 5 and 10% Mo compositions. On the other hand, the present results are in reasonable accord with those of Grube and Schlecht (5) who obtained data in 4.3N HCl (15%) at 60°C. Their alloys were slowly cooled from 1280°C, and the specimens for corrosion tests were rotated at 500 rpm.

The present data show reproducible slight discontinuities in corrosion rate at about 7% Mo (Fig. 2 and 3). Although sufficient points are not available to reach a definite conclusion, it may be significant that the Curie temperature for these alloys also occurs at the same approximate composition, and hence a change in magnetic properties may account for the observed fluctuation in corrosion rate.

In order to determine the possible effect of cathodic impurities, and also whether the rate is anodically or cathodically controlled, parallel runs were conducted in 10% HCl at 70°C for alloys galvanically coupled to an equal area of platinum. Rates with Pt are somewhat higher in aerated acid, with the difference diminishing as Mo content of the alloys increases. In deaerated acid, the rates with or without Pt are not greatly different except for Ni and the 3% Mo-Ni alloy. Alloying, on the other hand, has an appreciable effect on the rate. In boiling 10% HCl, for example, the rate for 20% Mo-Ni alloy is only 1/50 the rate for Ni. The lowering of the corrosion rate which results from alloying additions of Mo is more pronounced in deaerated than in aerated acids. There was a tendency toward intergranular attack in a few of the low-Mo alloys for which the corrosion rate was highest. This tendency persisted even in the pure alloys prepared from spectroscopically pure Mo and decarburized Ni.

Corrosion potentials of all the alloys in H₂-saturated 5% H₂SO₄ at 25°C were within 2 mv of a hydrogen electrode in the same solution. Similar values for H₂-saturated 10% HCl are given in Table I.

Critical current densities for passivity in 0.01N H₂SO₄ at 25°C, deaerated with purified N₂, showed no definite trend with composition. The values ranged from 0.3 to 0.83 ma/cm². On the other hand, alloyed molybdenum had an appreciable effect on anodic polarization in the active potential region in contrast to the passive region. Values of potential at an anodic current density of 0.3 ma/cm² in deaerated 0.01N H₂SO₄ and in deaerated 0.01N HClO₄ are shown in Fig. 5. Polarization in each acid reaches a maximum beginning at about 15 wt % Mo (9.8 at. % Mo).

Hydrogen overvoltage measurements showed no trend with alloy composition. The overvoltage at 1 ma/cm² at 25°C in pre-electrolyzed 5% H₂SO₄ saturated with purified hydrogen was the same for

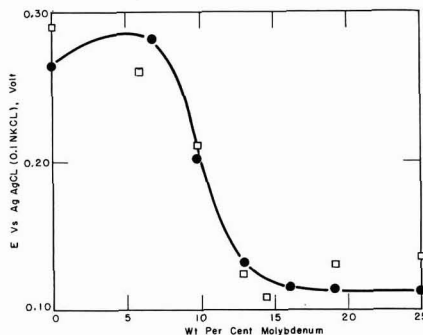


Fig. 5. Anodic polarization of nickel-molybdenum alloys at 0.3 ma/cm² in N₂-saturated H₂SO₄ or HClO₄ at 25°C. □, 0.01N HClO₄; ●, 0.01N H₂SO₄.

all alloys including pure nickel, averaging 0.30 ± 0.08v. At 10 ma/cm², the value was 0.43 ± 0.05v. Lack of an effect may be real or may be caused by a similar composition surface for all alloys, brought about by selective etching. The latter possibility would not enter anodic polarization measurements to the same extent because of continuous removal of the alloy surface by anodic dissolution.

Discussion

It is apparent that the Mo-Ni alloys in 10% HCl, despite a low corrosion rate, are not passive in the same sense as are the stainless steels in dilute sulfuric acid. The Mo-Ni alloys, for example, corrode more rapidly in aerated than in deaerated acid, contrary to the behavior of passive chromium alloys. Also, the corrosion potentials in deaerated acid are not noble but are close to or equal to the potential of the hydrogen electrode (Table I). This behavior indicates marked polarization of anodic areas on the alloy surface and, furthermore, that the alloys corrode under anodic control. Although anodic control is typical of passive metals, corrosion potentials of the present alloys are more active than the corresponding Flade potentials, contrary to passive Cr alloys the corrosion potentials of which are more noble than their Flade potentials. Although hydrogen overvoltage values show no significant change with alloy composition, anodic polarization data, on the other hand, show an appreciable change, the maximum beginning at about 15% Mo in either 0.01N H₂SO₄ or HClO₄. Maximum polarization beginning at about 15% Mo was also reported by Masling and Roth (6) for alloys polarized as anode in 2N deaerated HCl. Similar anodic behavior in three different acids suggests that the critical alloy composition, although possibly resulting from an invisible reaction-product film which differs from the passive film forming at the Flade potential, more likely results from a high activation energy for dissolution of metal ions. The latter may be caused, for example, by a slow rate of ion hydration. Along these lines, the rate of dissolution of pure Mo in HCl and in H₂SO₄ is appreciably below that of Ni. A difference in activation energies can also account for the relative ease of electrodepositing Ni from solutions of its salts, compared to the difficulty or

Table I. Corrosion potentials of Mo-Ni alloys (anode) in H₂-saturated 10% HCl, 25°C vs. H₂ electrode (cathode) in same solution

Wt % Mo	0.0	3.0	6.8	9.9	13.0	22.8
Potential, v	0.099	0.017	0.005	0.000	0.000	0.000

impossibility of electrodepositing Mo. The electron configuration theory in agreement with results of anodic polarization predicts that the critical alloy content for imparting chemical properties of Mo to Ni lies at about 9.1 at. % or 14 wt % Mo (7).

The minimum corrosion rate in deaerated acid begins at the somewhat higher alloy composition of about 20% Mo rather than at 15% Mo. This is true of values at 70° and 102°C, and even at 25°C in deaerated acid, the rate decreases from 0.9 mdd at 9.9% Mo to 0.0 mdd at 19.1% Mo and higher Mo compositions. One possible reason for the difference is that the presence of hydrogen generated by corrosion tends to shift the critical composition to a higher molybdenum value. A similar effect of interstitial hydrogen has been observed in the Cr-Fe alloy system (8).

Aeration increases the corrosion rate by increasing the potential difference between anodic and cathodic areas, the potential of cathodic areas approaching but not attaining the potential of the oxygen electrode. Mixed control of the corrosion rate predominates in aerated acids except at 25°C, where it appears that the rate of oxygen reduction on the alloy surface is controlling. On pure Ni, for example, oxygen reduction proceeds at a higher rate and the corresponding corrosion rate is higher than for the alloys, all of which corrode at the same rate despite change in anodic polarization. Oxygen reduction, therefore, may be an activation-controlled reaction rather than diffusion controlled. The rate for all the Mo-Ni alloys (65 mdd) falls below the maximum rate of about 100 mdd calculated from the limiting diffusion current for oxygen reduction in air-saturated water at room temperature [0.039 ma/cm² (9)]. The calculated value should be reduced about 20% because of reduced solubility of O₂ in 10% HCl, but the corrected value is still larger than 65 mdd.

Corrosion resistance of commercial Mo-Ni-Fe alloys of about 30% Mo, 60% Ni, and 10% Fe composition probably also follow a mechanism paralleling that described above for the Mo-Ni alloys, and similarly their corrosion potentials lie at values more active than the corresponding Flade potentials at which a passive film forms. These alloys are used in practice to withstand relatively concentrated nonoxidizing acids such as HCl or H₂SO₄. Since they are active in potential and cannot set up passive-active cells as do the passive Cr alloys, they are not subject to pitting in the chemical media to which

they are usually exposed. The maximum amount of Fe which can be tolerated in such solid solution alloys for optimum corrosion resistance corresponds in accord with the electron configuration theory to an atomic ratio Mo/Fe equal to or greater than 0.2 (10). Results of Schmidt and Wetteknick (11) for corrosion of various Mo-Ni-Fe alloys in boiling 29.8% H₂SO₄ confirm that a ratio of this order is observed. This is similar to the ratio accounting for passivity beginning at about 12 wt % Cr (atomic ratio Cr/Fe = 0.15) in the Cr-Fe alloys. This ratio, it was found (12), is preserved in the solid solution ternary Cr-Fe-Ni alloys, being most pronounced in alloys below 50% Ni.

Hence, although passivity in the Mo alloys apparently derives from a sluggish anodic reaction in contrast to the Cr alloys which form a metastable passive film accompanied by a noble potential, the alloying proportions leading to optimum corrosion resistance are similar for both metals and can be related to their similar atomic configuration.

Acknowledgment

The authors are pleased to express appreciation for support of this investigation both to The Shell Oil Companies in the U.S. and to The Office of Naval Research on Contract No. Nonr 1841(09) NR 036-007. They are also indebted to N. Stolica for obtaining the anodic polarization data in perchloric acid.

Any discussion of this paper will appear in a Discussion Section to be published in the December 1963 JOURNAL.

REFERENCES

1. P. Bond and H. Uhlig, *This Journal*, **107**, 488 (1960).
2. E. B. Sandell, "Colorimetric Determinations of Traces of Metals," Interscience Publishers, Inc., New York (1944).
3. H. Uhlig and G. Woodside, *J. Phys. Chem.*, **57**, 280 (1953).
4. B. Field, *Trans. AIME*, **83**, 149 (1929).
5. G. Grube and H. Schlecht, *Z. Elektrochem.*, **44**, 413 (1938).
6. G. Masing and G. Roth, *Werkstoffe u. Korrosion*, **3**, 176, 253 (1952).
7. H. H. Uhlig, *Z. Elektrochem.*, **62**, 700 (1958).
8. H. Uhlig, N. Carr, and P. Schneider, *Trans. Electrochem. Soc.*, **79**, 111 (1941).
9. H. H. Uhlig, *This Journal*, **108**, 327 (1961).
10. "Corrosion Handbook," Fig. 4, p. 29, H. H. Uhlig, Editor, John Wiley & Sons, Inc., New York (1948).
11. M. Schmidt and L. Wetteknick, *Korrosion u. Metallschutz*, **13**, 184 (1937).
12. H. Feller and H. Uhlig, *This Journal*, **107**, 864 (1960).

Optical Studies of the Formation and Breakdown of Passive Films Formed on Iron Single Crystal Surfaces in Inorganic Inhibitor Solutions

Jerome Kruger

National Bureau of Standards, Washington, D. C.

ABSTRACT

Polarized light was used to measure the thickness and optical properties of passive films as they were forming while simultaneous electrochemical measurements were being made. The film formation studies showed that a change in film thickness of 15-20Å was associated with the onset of a passive potential. A direct, logarithmic-type law governed the growth of a semiconductor film with crystallographic orientation of the substrate having little effect.

When iron surfaces prepared in an ultrahigh vacuum (a vacuum of the 10^{-9} Torr order of magnitude), were passivated a 20Å film formed instantaneously on the introduction of an air-saturated 0.1N NaNO_2 . This film then dissolved and a new film commenced to grow. A passive potential coincided with a film 15Å thick. No such initial dissolution occurred when the solution contained only dissolved oxygen, the instantaneously formed film continuing to grow and a passive potential occurring after the growth of around 40Å. When the solution contained no dissolved gases, the instantaneous film did not form.

Film breakdown studies revealed that only the 20-30Å film next to the metal was responsible for passivity even if thicker films were initially present. Studies of the sites of film breakdown showed that the number of sites was highest for films on {110} iron surfaces and that these sites were not related to points where dislocations intersected the surface. These studies support the oxide film theory of passivity.

One of the great experimental obstacles to resolving the controversy that exists between the various schools of thought on the nature of the passivity of iron, which Faraday (1) referred to as "this very beautiful and important case of voltaic condition presented to us by the metal iron," is the great difficulty in being able to distinguish between an adsorbed film and a thin compound film. Even if this difficulty did not exist, there would still remain the problem, common to all surface studies, of how to be sure that there does not exist already on the surface a precursor to the passive film or a chemical species that drastically modifies the passivation process, giving rise to a false picture of the passivation process. Primarily because of these two experimental difficulties and because of theoretical ones, the controversy continues between those who favor an adsorbed oxygen film (2-4) and those who favor a three-dimensional oxide film (5-7). An intermediate group in the controversy (8, 9) says that the first step in the passivation process is the adsorption of an oxygen film which confers temporary passivity; this then becomes an oxide film by incorporation of a metal ion into the adsorbed oxygen.

This work describes experimental approaches that attempt to attack these difficulties by a technique that enables one to learn something about the nature of the passive film and the passivation processes while they are actually going on. This

technique uses elliptically polarized light to measure the thickness of a film formed and to determine some of its optical properties. An advantage of this technique is that film thicknesses as low as 3-5Å can be measured simultaneously with the electrochemical potential to give an indication of the onset of passivity. This technique was pioneered over thirty years ago by Tronstad (10, 11).

This work differs from that of Tronstad in that greater attention has been paid to starting with clean, well-characterized surfaces. This has been made possible by the use of modern ultrahigh vacuum techniques (12) and single crystal surfaces. The use of ultrahigh vacuum techniques is especially important in such a study since one of the sources of contention is the existence of a monolayer film that is supposed to be responsible for passivity. Unless ultrahigh vacuum techniques are used such monolayer films can form on a surface at pressures of 10^{-6} Torr in times less than 1 sec (13). Hence, only by the use of such ultrahigh vacuum techniques can one start to cope with the question of the importance of a monolayer film of oxygen in conferring passivity to an iron surface.

In the studies described here, elliptically polarized light is used to follow both the formation and the breakdown of passive films produced in inorganic inhibitor solutions.

Because a complete description of passivation involves, in addition to a knowledge of the nature of

the passive film, an understanding of the role played by the atomistic structure of the metal surface, the influence of surface structure on formation kinetics and on the sites where breakdown of a passive film occurs was studied. The breakdown studies used optical and thin foil electron microscopy to examine surfaces treated by a technique which decorated the sites of breakdown of passive films. The crystallographic orientation of the metal surface and the presence of defects in it were related to breakdown sites using this approach.

Passive Film Formation

In all of the present studies concerned with following the formation of passive film with time, ellipsometry was used. A description of the ellipsometer and the method used to evaluate the results is given elsewhere (14). This technique was used to measure both the thickness of the films that existed on a surface at a given time and the optical properties of the film. A very comprehensive description of the theoretical and experimental aspects of the use of elliptically polarized light to study surfaces is given by Winterbottom (15).

To compare this ellipsometric method for studying passive film formation directly with another entirely different technique, the kinetics of passive film growth on iron in K_2CrO_4 solution was first studied. This system had been studied with a radio-tracer technique by Brasher and Kingsbury (16). The iron specimen [240 ppm impurities and described by Moore (17)] was mechanically polished using a $\frac{1}{4}\mu$ diamond abrasive as the final polish and then chemically polished in a chemical polishing solution.¹ After rinsing the specimen in distilled water and spectrographic grade methanol, and taking a reading on the dried surface, the specimen was placed in a vessel containing 0.0025M K_2CrO_4 solution. Readings were then taken periodically by the ellipsometer on the surface so immersed in the inhibitor solution. The film thicknesses² measured on a {100} iron surface in 0.0025M K_2CrO_4 solution are plotted against $\log(t + 1)$ in Fig. 1. The thicknesses plotted in this figure are not absolute values, but increments of thickness over that of the initially present air-formed film. Other grains on the specimen used gave essentially the same readings as the {100} grain. A rate constant of 1.43Å was obtained, treating this data in the manner described by Kubaschewski and Brasher (18). This ellipsometric value compares reasonably well with that of 1.5Å obtained by the entirely different radiotracer technique (18).

Similar preliminary experiments were carried out using concentrated HNO_3 as the passivating solution. It was rather difficult to make precise enough measurements in this case to determine what sort of rate law governed the passivation process for a number of reasons. First, the refractive

¹ MiroFe, a chemical polishing solution for iron manufactured by MacDermi Corporation, containing an alcohol and phosphoric acid. Three parts of this were then mixed with 1 part of 30% H_2O_2 to produce the proper polishing bath.

² These were based on the approximation, used by Tronstad and Borgmann (11), for films less than 100Å that the mean thickness is proportional to the difference in the phase retardation values of the "film-free" and film-covered surface ($\Delta - \Delta_0$), 1° corresponding approximately to 5Å.

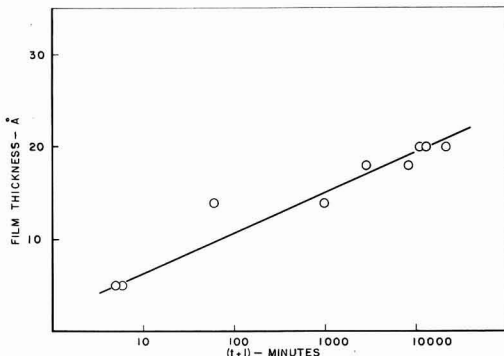


Fig. 1. Growth of a passive film on a {100} iron surface in an air-saturated 0.0025M K_2CrO_4 solution. Logarithmic plot.

index of the solution changed with time because of the slight decomposition of nitric acid that occurred. Second, the surface was somewhat roughened on introduction of the specimen into the acid during the short time interval before it became passive. Finally, thick films formed in a not too reproducible manner.

Usually a film approximately 60Å thick formed on the iron in a period of 1 hr. When the specimen was allowed to remain in the concentrated HNO_3 overnight, a film with a thickness greater than 100Å formed, and the specimen exhibited passivity to a copper sulfate solution. The thickness of the films formed on the large-grained iron specimen varied with the crystallographic orientation of the grains. This could be seen with the unaided eye, for different grains exhibited different colors.

For more controlled studies of passive film growth in inorganic inhibitor solutions, sodium nitrite solutions were selected because the complication of the introduction of other metallic elements into the film, such as chromium when chromates are used, is absent.

The apparatus used in this study is shown in Fig. 2. It was similar to the apparatus described elsewhere (19) in that no greased joints were used, the

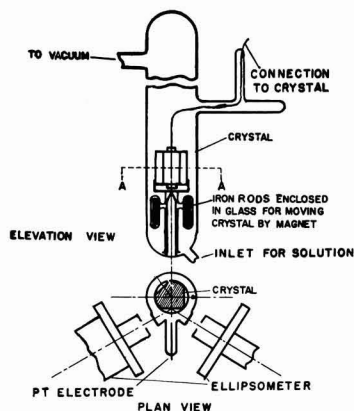


Fig. 2. Apparatus for studying the optical properties and the electrochemical potentials of an iron surface immersed in a passivating solution.

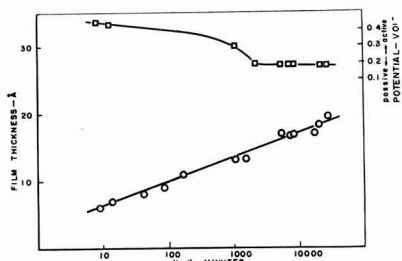


Fig. 3. Growth of a passive film on a {110} iron surface in an air-saturated 0.1N NaNO₂ solution. Logarithmic plot.

specimen being sealed in for each run and the solution introduced after the specimen had been annealed in purified hydrogen at 500°C. After this anneal and evacuation, readings were made on the "bare" surface, and solution was introduced. This apparatus differed from the previously described apparatus in that a platinum wire was sealed into the apparatus to permit measurement of the potential of the iron specimen with respect to the solution in which it was immersed.³ The iron specimen used was of the same purity and had the same surface pretreatment described for the chromate experiments just given. It had two large grains having {110} and {211} orientations, and ellipsometric measurements could be made on each of these two grains. Runs were carried out in an atmosphere of pure oxygen or air.

Figure 3 shows the results obtained for a {110} surface in a 0.1N NaNO₂ solution saturated with air. The potential was measured at the same time as the film thickness and is shown on this curve. In this figure and in all the other figures to follow where potential is plotted, the initial rapidly changing values are not shown. It should be mentioned, however, that a change of around 0.8v occurred in the transition from an active to a passive iron surface. No great differences in behavior between the two different orientations, {110} and {211}, studied in this manner were observed, a difference of less than 4Å being observed after 40 days of exposure. The rate of growth appears to obey a direct logarithmic law. The fact that the line obtained does not extrapolate to zero thickness indicates either that there already existed a film at the beginning of the process or that the formation of the initial monolayers was nonlogarithmic.

Because a direct linear logarithmic relationship was observed for the growth of passive films on iron in both nitrite and chromate solutions, the theory of Hauffe and Ilshner (20) may be applicable. This theory suggests that for extremely thin films a direct logarithmic rate law is obeyed because electron movement rather than ion transport through the film is the rate-determining step. The growth

³Platinum was used rather than a more suitable reference electrode in order to avoid the introduction of anions other than those of the passivating salt and to enable the construction of a cell which could be heated to high temperatures. The potential measurements were thus made to determine the onset of passivity rather than to determine thermodynamically meaningful values. That the values of potential obtained by using a platinum electrode do correspond to the onset of passivity was verified in another cell where both a saturated calomel reference electrode and a platinum electrode were used to measure the potential of iron in an air-saturated 0.1N NaNO₂ solution. If oxygen were excluded from the solution, however, the platinum could not be reliably used to determine the onset of passivity.

Table I. Constants obtained from Hauffe-Ilshner theory

Passivating solution	Rate constant, l_0 , Å	Height of potential barrier, Φ , ev
0.0025M K ₂ CrO ₄	1.43	0.46
0.1M NaNO ₂	1.00	0.95

law based on this theory was formulated by Kuba-schewski and Brasher (18) as follows

$$l = l_0 \ln(t + 1)$$

where l is the film thickness, t time and $l_0 = h/4\pi \sqrt{2M\Phi}$ where h is Planck's constant, M mass of electron, and Φ the height of the potential barrier across the film. In Table I are listed the values of l_0 , the rate constant, and Φ for the films formed in the solutions studied. The values of Φ are of the order of magnitude consistent with those found for semiconductors (21).

Since there was undoubtedly present on the iron surface at least a monolayer film under the conditions prevailing in the experiments just described it was necessary to go to the now well-known techniques (12) for working *in vacua* of the 10⁻⁸ Torr or better. By taking readings on surfaces prepared under such ultrahigh vacuum conditions one could be better assured that the starting point of the passivating process, before the introduction of an inhibiting solution, approached a "bare" surface. Such considerations are, of course, extremely pertinent in view of the importance ascribed to a monolayer film by the adsorption theory of passivity.

The final version of a number of different modifications of the apparatus used in these ultrahigh vacuum studies is shown in Fig. 4. In this version the specimen was screwed into place by opening the bottom of the cell and then sealing the glass bottom with a torch. Thick quartz windows (3 mm) were used to minimize thermal and mechanical strains which would affect the optical measurements.

The iron specimen,⁴ mechanically polished using ¼μ diamond abrasive for the final polish, was

⁴In these experiments polycrystalline vacuum melted iron (Ferro-Vac) was used rather than the iron previously described because it was easier to outgas.

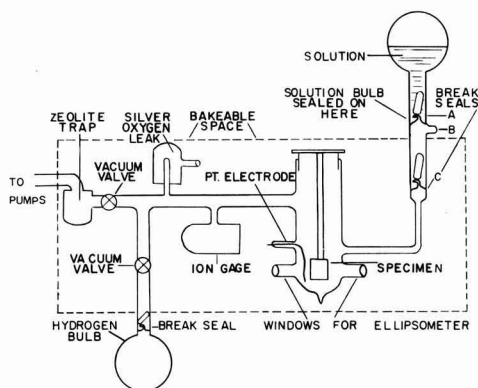


Fig. 4. Ultrahigh-vacuum apparatus for studying the optical properties of and the electrochemical potential of an iron surface immersed in a passivating solution.

etched for a second in dilute nitric acid and immediately rinsed in spectrographic grade methanol.

It was then out-gassed by vacuum annealing it in another vacuum apparatus at 900°C until the pressure in this system went down to approximately 10^{-6} Torr with the specimen still at temperature. After this outgassing, the specimen was sealed into the ultrahigh-vacuum system and annealed in hydrogen to remove the oxide film formed during the sealing-in procedure. The system was then baked at 430°C for 5-6 hr and a pressure of 10^{-9} Torr obtained. The specimen was heated to redness using an induction coil in assayed reagent grade hydrogen⁵ admitted to a pressure of 1-2 μ . At this pressure a glow discharge occurs in the field of the high-frequency induction coil so that the iron surface was thus bombarded by hydrogen atoms and ions. Readings were made with the ellipsometer after each step in the surface treatment, the values of the optical parameters, Δ , the relative phase retardation, and ψ , the amplitude reduction, changing in a direction indicating that the surface was becoming cleaner. This procedure was continued until no changes in Δ and ψ were observed with further hydrogen annealing. The specimen was then vacuum annealed and the system baked out again. No changes in Δ and ψ were again noted, and the values measured at this point were used as those for a clean surface.

In some experiments a solution open to the air and saturated with air was used to approximate the majority of passivity experiments in the literature.

In other experiments the solutions were prepared so that their dissolved gas content could be controlled. The solution in the bulb shown above break-seal C in Fig. 4 was degassed in another vacuum system by alternate freezing and thawing five times in vacuum and then introducing either assayed reagent grade oxygen or argon⁶ (for experiments where oxygen was to be excluded). This bulb, in which the solution was in equilibrium with 0.5 atm of gas, was then sealed off from the solution preparation system and sealed onto the ultrahigh-vacuum system above break-seal C. The space between A and C was then pumped out by a zeolite sorption pump at B, the pump then being removed by sealing off at B. A run was started by breaking break-seal A and then C, the solution covering the specimen in less than 15 sec. Readings could then be made with the ellipsometer and potential measurements made of the iron surface *vs.* the platinum electrode.

The results obtained, using such an approach, differed from those obtained under less rigorous conditions (Fig. 1 and 3) in that at the beginning of the passivation process the relative phase retardation, Δ , increased rather than decreased with time. Such initial increases in Δ were found occasionally by Tronstad and Borgmann (11) for films formed in concentrated HNO₃. This is shown in Fig. 5, along with a simultaneous plot of the potential of the iron

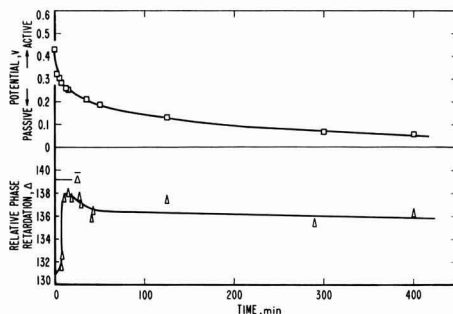


Fig. 5. Change in phase retardation with time for an iron surface immersed in air-saturated 0.1N NaNO₂ solution.

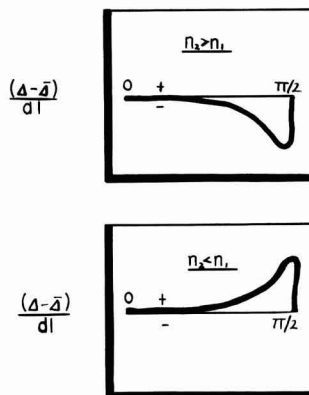


Fig. 6. Influence of the optical constants of the film and the medium on the variation of the phase retardation with thickness for different angles of incidence. [After Winterbottom (15) p. 46.]

surface *vs.* platinum for an air saturated 0.1N NaNO₂ solution.

Because the growth of oxide films is accompanied by a decrease in Δ (11), the increase found indicates that at the beginning of the passivation process something else was occurring. Figure 6 which is taken from Winterbottom (15) points to one possible reason for the increases. The curves show that for a metal surface such as iron the change in Δ with thickness $(\Delta - \bar{\Delta})/dl$ is negative if the refractive index of the film n_2 is less than that of the surrounding medium n_1 and is positive if $n_2 > n_1$. This implies that a rise in Δ could indicate that a film is forming with a refractive index less than 1.3349, the refractive index of 0.1N NaNO₂ solution for the wavelength of the light used in all of the studies reported here, 5461Å. None of the oxides of iron whose refractive indices are known or indeed any of the possible solids whose values are known which could constitute the film have a refractive index lower than that of the nitrite solution. On the other hand, an oxygen film (14) or an adsorbed nitrite film would probably have a refractive index lower than the solution.

This interpretation does not apply in this case, however, because although a rise in Δ -values was initially observed, Δ was always less than $\bar{\Delta}$, the value of the phase retardation for the film-free surface. This quantity (shown in Fig. 5) was obtained from a calculation of its value in nitrite solution

⁵ This was specified to have no impurities as found by mass spectrographic analysis.

⁶ Impurities in the oxygen were in mole per cents 0.0040 A, 0.02 H, 0.019 N, 0.0063 CO₂, and 0.00018 total hydrocarbons, and in the argon were none as indicated by mass spectrographic analysis.

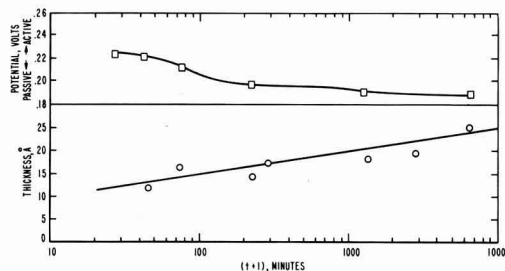


Fig. 7. Growth of a passive film on an iron surface in an air-saturated 0.1N NaNO_2 solution. Logarithmic plot.

based on the all-important measurements made in ultrahigh-vacuum. During the time when the solution was introduced into the cell containing the specimen, and a reading was made (in some cases less than 0.5 min), Δ had decreased 4° . This corresponds to the formation of a 20Å film, whose refractive index was higher than that of the solution, during the time of solution introduction. Thus the rise of Δ -values was due either to the adsorption of a low index film ($n_2 < n_1$) on top of the film formed almost instantaneously at the beginning of the process, or the dissolution of this initial film, where decreasing film thickness values cause an increase in Δ -values. The fact that Δ max. always approached $\bar{\Delta}$ closely, but never exceeded it argues for the film dissolution interpretation. If the instantaneously formed film was Fe_3O_4 , as is quite likely (7) in the atmosphere of air and water vapor that existed between the time the system was opened to the solution and the solution covered the specimen, its dissolution in the air saturated nitrite solution (pH 5.8), based on Pourbaix's diagram for iron and water (22), is thermodynamically reasonable. In Fig. 7 the thickness and potential data obtained for an air-saturated solution are plotted logarithmically for times after the initial adsorption or dissolution processes had stopped (after about 45 min).

In order to see if initial film dissolution was occurring because of the low pH of the air-saturated solution due to the CO_2 present in it, outgassed solutions, prepared as described earlier, in equilibrium with 0.5 atm of high-purity oxygen were used. As can be seen from Fig. 8 the initial rise in Δ is completely absent, the instantaneously formed film instead continuing to increase (Δ decreasing) with

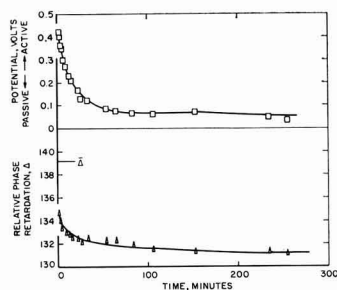


Fig. 8. Change in phase retardation with time for an iron surface immersed in 0.1N NaNO_2 solution in equilibrium with 0.5 atm of pure oxygen.

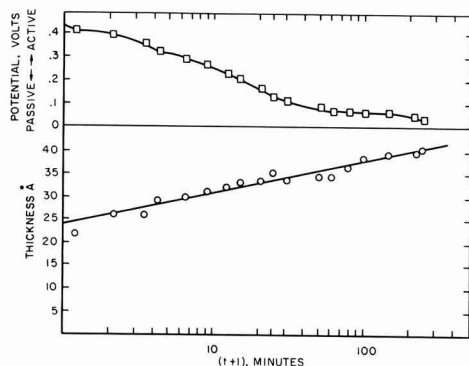


Fig. 9. Growth of a passive film on an iron surface in 0.1N NaNO_2 solution in equilibrium with 0.5 atm of pure oxygen. Logarithmic plot.

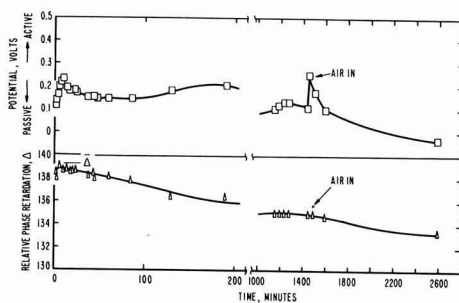


Fig. 10. Change in phase retardation with time for an iron surface immersed in a deaerated 0.1N NaNO_2 solution.

time. Thus it appears that the initial rise in Δ for air-saturated solutions was due to film dissolution rather than to the adsorption of a low index film on top of instantaneously formed film, for the condition for the latter possibility still existed when oxygen was the only gas present. Figure 9 shows a logarithmic plot of the thickness and potential data for the solution in equilibrium with pure oxygen.

To ascertain whether the instantaneously formed film was produced during the solution introduction interval by interaction with oxygen and water vapor, experiments were carried out using deaerated solutions and high-purity argon as the gas for pushing the solution in rapidly. As Fig. 10 shows, an extremely thin film ($< 5\text{\AA}$) formed in the almost completely deoxygenated solution. An initial adsorption on top of or dissolution⁷ of this film appeared to take place; it then started to grow. As mentioned before, the potential measurements using a platinum electrode in the absence of oxygen do not give a meaningful indication of the onset of passivity. After 1400 min air was introduced and, as Fig. 10 shows, the rate of film formation increased. The changes in potential that occurred after air was introduced probably suggest that the 20Å film that was present before the introduction of air was not yet a passive film. No dissolution occurred upon introducing air indicating that the film formed

⁷ On the basis of Pourbaix's diagram for iron, low oxygen concentration would tend to have the same effect on the dissolution of Fe_3O_4 as low pH. Thus dissolution seems to be the more likely alternative here as it was for the air-saturated solution.

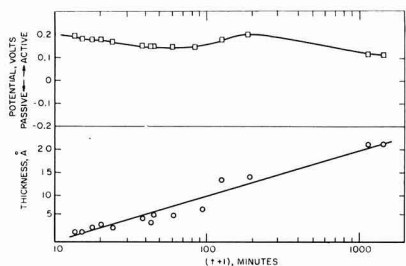


Fig. 11. Growth of a film on an iron surface in a deaerated 0.1N NaNO₂ solution. Logarithmic plot.

in the presence of the inhibitor differs from the film formed instantaneously during the solution introduction interval. Figure 11 is a logarithmic plot of the potential and thickness data for the deaerated solution. The fluctuations in film thickness probably mean nonuniform film formation not really amenable to analysis by the Hauffe-Ilschner theory. However, the constants calculated using this theory are compared in Table II for the deaerated solution along with the other solutions studied.

Passive Film Breakdown

These studies, qualitative in nature, were concerned with the changes in film thickness that occur when a passive film passes through the Flade potential.

In one set of experiments an iron specimen was rinsed in distilled water and then placed in a solution that would cause a decay in passivity in the same manner as described by Uhlig and King (23). Film thickness changes were measured with the ellipsometer during decay through the Flade potential. Activation was carried out in the acid, neutral, and alkaline regions of the pH scale.

Acid.—Here distilled water with a pH of approximately 3.5 (adjusted by the addition of HNO₃) was used to cause a decay in the passivity. For iron passivated in concentrated HNO₃ a change in film thickness of over 100Å was observed after passage through the Flade region. The time to go from - 0.22v to + 0.62v (vs. saturated calomel electrode) was less than 1 min. Measurements indicated that the iron surface was essentially bare after activation. Similar behavior was observed with iron passivated in 0.0025M NaNO₂, the film thickness change again indicating the dissolution of the entire passive film, 30Å thick in this case. The time to go from the passive to the active state was approximately 5 min.

Neutral.—0.2M Na₂SO₄ solution was used as the activating solution. Iron passivated in concentrated

HNO₃ overnight took 35 min to pass through the Flade region. The change in film thickness accompanying the change from the passive to the active potential was 40Å. A film of greater than 100Å thickness remained on the iron surface after an active potential was reached.

Alkaline.—It was difficult to activate passivated surfaces in the alkaline region. KOH solutions having a pH of 9 and 0.2M Na₂SO₄ solutions whose pH was adjusted to 9 with KOH were used. For surfaces passivated in either concentrated HNO₃ or NaNO₂ activation was very slow and erratic. In those cases where the surfaces were rendered active in the alkaline solution, the change in film thickness observed was 10Å or less.

The behavior observed in the neutral and alkaline solutions would seem to bear out a suggestion of Pryor's (24) that erratic breakdown that occurs at high pH is due to exchange between oxide and hydroxyl ions which decreases ionic resistance so that an active potential may be measured without much dissolution of the film.

Besides the method of causing a decay of passive films just described, another method was employed for iron passivated in concentrated HNO₃. In these studies the decay of the passive film was brought about by the slow addition of water to the HNO₃. When the concentrated HNO₃, in which was immersed an iron surface bearing a film of greater than 100Å thickness, was diluted to less than 20 parts of acid to 1 part of water by the addition of water, the thickness of the film on the iron remained the same. If, however, the HNO₃ was diluted still further to, e.g., 10 to 1, the film on the iron decreased to a thickness of 20-30Å, although the potential exhibited by the iron surface to the HNO₃ solution was still a passive one. Further additions of water caused periodic breakdowns of this 20-30Å film. These breakdowns coincided with the exhibition of momentarily active potentials as determined by the use of a recorder. Such a recorder trace is shown in Fig. 12. This breakdown and repair of the passive film continued at more frequent intervals as more water was added until complete breakdown occurred. This phenomenon could be followed by making ellipsometer and potential measurements simultaneously.

This sort of experiment shows that the thick films that form on iron in concentrated HNO₃ may be made up of two components, the outer layer not being responsible for passivity; for, when this was

Table II. Hauffe-Ilschner constants for 0.1N NaNO₂ solutions containing different gases

Passivating solution	Rate constant, <i>t₀</i> , A	Height of potential barrier, ϕ , ev
Air-saturated solution	2.13	0.21
Oxygenated solution	3.00	0.11
Deaerated solution	4.17	0.01

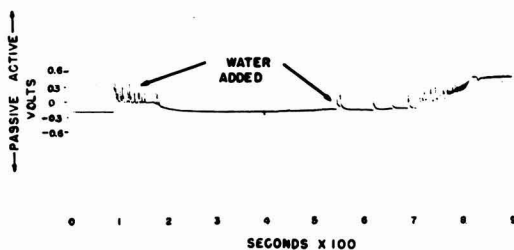


Fig. 12. Breakdown of a > 100Å passive film formed in concentrated HNO₃ by the addition of water. Film is 20-30Å thick after first addition of water shown on curve.

removed, the thin film remaining still rendered the surface passive. This thicker outer film was also responsible for the differences in film thicknesses observed on surfaces of different crystal orientations as mentioned above for iron passivated in concentrated HNO_3 . No large orientation effect was observed when the thin passive film was present.

Sites of Film Breakdown

Other than electron diffraction studies [some of the most recent by Cohen (15)] little work has been done on the influence of the structure of the iron surface on the nature and properties of the passive film. This is so because the passive film is too thin to be observed even by using the electron microscope. Thus, an indirect approach was used which investigated the influence of the surface structure on the breakdown of the film, or actually the sites of breakdown, rather than the properties of the film itself.

A technique was used for decorating the sites where the passive film breakdown occurs. It involved placing the passivated iron surface in a solution containing copper ions and allowing it to remain there until the potential exhibited by iron started slowly to become active. The specimen was then quickly removed and rinsed before the whole surface became coated with copper. Examination by the optical microscope and by the electron microscope revealed the formation of discrete (some having definite geometric shapes) crystallites at many sites on the surface. The copper apparently precipitated at sites in the passive film where film breakdown had taken place first. An example of the results obtained with a polycrystalline specimen using a 0.01M solution of copper sulfate is shown in Fig. 13. This shows the difference in density of decorated sites on different orientations. There also appears to be a piling up of sites at one of the grain boundaries. The density of sites is seen to vary between the grains, and there also appears to be two distinct types of sites where decoration occurs.

In order to learn about the nature of the materials making up the sites and the influence any imperfections in the iron may play in initiating them, thin foil electron microscopy studies were carried out.

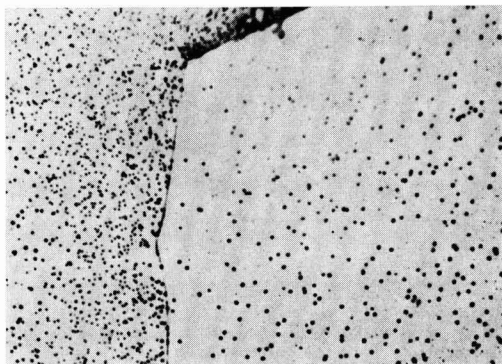


Fig. 13. Polycrystalline iron surface passivated in 0.1N NaNO_2 solution with sites of film breakdown decorated using 0.01M CuSO_4 as decorating solution. Magnification approximately 700X.

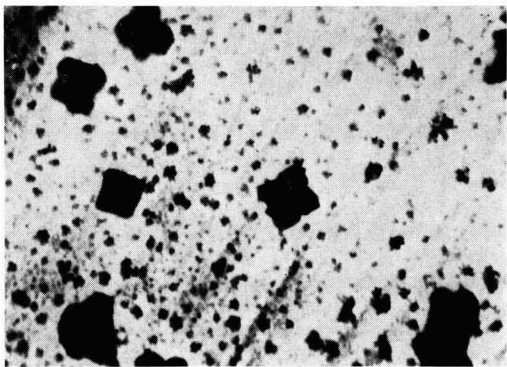


Fig. 14. Transmission electron micrograph of a thin foil treated as in Fig. 13. Magnification approximately 7000X.

A 0.05 mm thick foil of Armco iron 99.9% annealed in hydrogen at 950°C for 18 hr was placed in the chemical polishing solution mentioned earlier for 2 min. It was then placed in fresh polishing solution and allowed to remain there until the foil had thinned sufficiently so that it started to float on top of the solution. Usually portions of the foil had been dissolved away. At this point in the procedure the thinned foil was rapidly removed, rinsed in distilled water for one minute and then placed immediately in a passivating solution. After passivation and breakdown-decoration the foil was rinsed in spectrographic grade methanol. A small portion near the edge of a dissolved-away part of the foil was then cut out and mounted for study with the electron microscope. Such pieces were less than 1000\AA in thickness.

The decorated sites were studied by looking at them in transmission with the electron microscope. Selected area diffraction patterns were made of the various decorated sites. Figure 14 shows an electron micrograph made from one of these foils. The diffraction patterns showed that the cubes were, as thought, copper, and the other material was

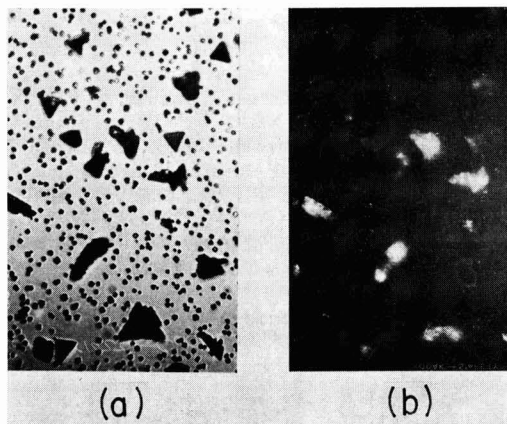


Fig. 15. Polycrystalline iron surface passivated in 0.1N NaNO_2 solution with the sites of film breakdown decorated by 0.015M CuCl_2 as decorating solution. Note two types of breakdown sites. (A) Bright field illumination; (B) polarized light illumination. Magnification approximately 700X.

Table III. Breakdown sites $\times 10^{-7}/\text{cm}^2$

Orientation of surfaces	{110}	{100}	{210}	{211}	{111}
Cathodic sites	6.4	3.7	2.5	4.7	3.8
Anodic sites	0.28	0.16	—	—	—

γFeOOH . This agrees with the work of Mellors, Cohen, and Beck (26) who showed that in the breakdown of passive films γFeOOH forms as blisters at discrete spots.

Thus using the decoration technique one could decorate the cathodic sites where reduction takes place on the metal surface with copper and the anodic sites where Fe^{++} ions enter the solution with γFeOOH . Since γFeOOH is birefringent it could be picked out with polarized light. Figure 15 shows this for the case where 0.015M CuCl_2 was used as the decorating solution.

The effect of crystallographic orientation is shown in Table III where a comparison of the numbers of cathodic and anodic sites (determined from a large number of photographs) for different crystal orientations is presented.

With regard to these experiments the question arises as to whether the decorations are characteristic of the passive films or the metal substrate. To answer this, unpassivated surfaces were decorated. They gave a much higher concentration of anodic sites per unit area, and there was no one-to-one correspondence with the cathodic sites found when the same area was passivated and decorated. Thus, it appears that the phenomena observed on passivated surfaces depended on the properties of the film, this being affected, in turn, by the metal substrate, since surface orientation had an influence on the number of breakdown sites.

The fact that the closest packed plane for the body-centered-cubic structure, the {110}, exhibited the largest number of breakdown sites coincided with earlier studies on the pitting of iron in water (27) which found that this plane also exhibited the largest number of pits. The reason for the greater reactivity of the closest packed plane may be connected with the observation made by Germer, Mac-

Rae, and Hartman (28), using low energy electron diffraction, that in the face-centered-cubic system the less densely packed planes form a firmer bond with foreign atoms such as oxygen than the more densely packed planes. Perhaps this is also the case for the body-centered-cubic iron.

The question then arises as to the nature of breakdown sites. A brief study was carried out to determine whether they were related to sites where dislocation lines emerge from the iron surface. An etchant ($\text{HCl}:\text{HNO}_3:\text{HF} = 10:5:1$) was developed that produced etch pits at sites that looked as if they were related to dislocations when compared with similar phenomena in the literature (see Fig. 16). At any rate, these etch pits could be obtained repeatedly at the same sites each time they were removed by repolishing. When this same surface was polished mechanically, chemically polished, passivated, and decorated, there was no relationship between the decorated sites and these etch pits. Thus it appears that the breakdown sites in the passive film were not related to dislocations (or the sites where the etch pits formed). Likewise, no connection between breakdown sites and dislocations was noted in the thin foil electron experiments.

This may indicate that the surface free energy change for breakdown is considerably higher than the differences that may exist between perfect and imperfect surface sites.

Discussion

The most significant results reported in this study are those obtained in the ultrahigh vacuum experiments. These experiments were aimed at fulfilling the need, so far unsatisfied (29), for a positive way for distinguishing between the adsorption and solid film theories of passivation. By using ellipsometry it is possible to determine whether the passivation process involves the adsorption of an oxygen film, the growth of a three dimensional oxide, or a combination of both, a transformation of an adsorbed film into an oxide. The theoretically derived variation of Δ with thickness for each of these three models is shown in Fig. 17.

The optical and potential measurements made on an iron surface passivated in nitrite solution containing only pure oxygen clearly indicated that oxide growth was present even before a passive potential was observed. Thus it should be emphasized that this film, formed almost instantaneously

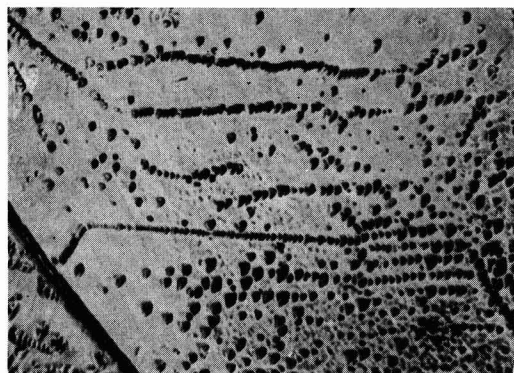


Fig. 16. Etch pits formed on iron using an etchant containing 10 parts HCl, 5 parts HNO_3 , and 1 part HF. Magnification approximately 350X.

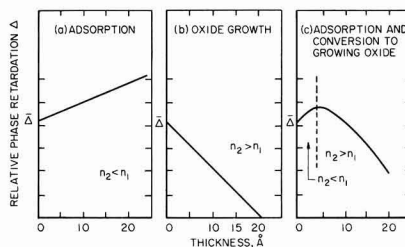


Fig. 17. Theoretically derived curves for the variation of the phase retardation with film thickness for: (A) a film whose refractive index is less than the solution ($n_2 < n_1$); (B) a film whose refractive index is greater than the solution ($n_2 > n_1$); (C) a film where initially $n_2 < n_1$, but later n_2 becomes greater than n_1 .

while solution was being introduced, was not yet the passive film. Indeed, it took still further growth and/or alteration of this film before a passive potential was observed. However, when a passive potential was finally observed, a three dimensional film of $> 30\text{\AA}$ thickness was present on the iron surface. On the basis of the work of Vetter (6), Cohen (7), and others this oxide film which formed instantaneously by reacting with the moist oxygen atmosphere was Fe_3O_4 , and during the passivation process the outer layer, at least, of the Fe_3O_4 was converted into $\gamma\text{Fe}_2\text{O}_3$. It is not possible by ellipsometry to establish positively this composition of the passive film. The optical studies do, however, indicate the formation of a film with a refractive index greater than that of the solution. In fact, calculations indicate that it is approximately the complex number, $2.5-0.3i$, a value close to that found for the oxide film formed by oxidizing iron in air (30). The rate studies also indicate, if the Hauffe-Ilschner theory is correct, the formation of a film with a potential barrier reasonable for a semiconductor. Hence all indications point to the presence of a growing oxide film from the very moment that the oxygenated nitrite solution contacts the iron surface.

The possibility that the film observed in this case is an adsorbed oxygen film is completely ruled out for two reasons. First, the refractive index of an adsorbed oxygen film would probably be lower than 1.25, the value found for solid oxygen films on gold (14) and the variation in Δ with thickness would be as Fig. 17a rather than 17b. Second, even if the refractive index of the oxygen film were higher than that of the solution, the values of Δ would indicate adsorbed oxygen films around 40\AA when the surface had become passive as judged by the potential measurements. Such a thick adsorbed oxygen film (10-15 monolayers) is very unlikely.

When the iron was passivated in air-saturated nitrite solution, the variation of Δ with time (or thickness) (see Fig. 5) appears to follow the model illustrated by Fig. 17c, the initial adsorption of an oxygen film followed by its conversion to an oxide. Were it not for the readings made on the iron surface in the ultrahigh-vacuum system, this conclusion would be reasonable. However, because these measurements were made on the essentially bare iron surface prior to the introduction of the solution, it could be seen that the Δ -values measured were always less than Δ . This means that there was always present on the surface an $n_2 > n_1$ film. As mentioned earlier the increase in Δ values initially observed could be either the adsorption of oxygen or nitrite ions on top of the instantaneously formed Fe_3O_4 film, or, more likely, the initial dissolution of this Fe_3O_4 and the subsequent formation of $\gamma\text{Fe}_2\text{O}_3$. The results obtained on the less rigorously prepared iron surface tend to bolster the latter interpretation. No initial increase in Δ values were observed for passivation in air-saturated nitrite solution here. Since the iron surfaces in these experiments were prepared in a system where the pressure was never lower than 10^{-6} Torr an oxide film undoubtedly existed on this surface, and according to Sewell, Stockbridge, and Cohen (31) this oxide formed in

the dry conditions existing in the vacuum, was probably $\gamma\text{Fe}_2\text{O}_3$ at the oxide-gas interface. Apparently when this oxide is present in the beginning rather than Fe_3O_4 the initial dissolution process does not occur.

It therefore can be concluded that the experimental observations described for passive film formation strongly support the oxide film model. The film breakdown experiments, however, point to an area which still needs a great deal of study, the special properties of this oxide film. For instance the breakdown experiments in nitric acid showed that the special properties of the 20-30 \AA film next to the metal were responsible for passivity and not the rest of the thick film observed. Nielsen and Rhodin found essentially the same situation for oxidized stainless steels (34). The fact that no great differences in passive film thickness on substrates of different crystallographic orientation were observed also points to the special properties of the three-dimensional film, indicating an absence of the factors that affect rate differences between different crystallographic planes such as strain and the presence of grain boundaries. It is planned to go into the breakdown process in greater detail in future experiments where the optical properties of iron surfaces whose potentials will be fixed at various active, passive, and transpassive values with a potentiostat will be studied.

Acknowledgments

The author wishes to express his sincere thanks to J. P. Calvert and H. T. Yolken for their aid in carrying out some of the experiments. Grateful acknowledgment is also made to the Corrosion Research Council which partially supported this work.

Any discussion of this paper will appear in a Discussion Section to be published in the December 1963 JOURNAL.

REFERENCES

1. M. Faraday, "Experimental Researches in Electricity," Vol. 2, p. 250, London (1844).
2. B. W. Erschler, *Doklady Acad. Nauk*, **37**, 258, 262 (1942).
3. Y. M. Kolotyrlin, *Z. Elektrochem.*, **62**, 664 (1958).
4. H. H. Uhlig, *ibid.*, **62**, 626 (1958).
5. U. R. Evans, *ibid.*, **62**, 619 (1958).
6. K. J. Vetter, *ibid.*, **62**, 642 (1958).
7. M. Cohen, *Can. J. Chem.*, **37**, 286 (1959).
8. N. Hackerman, *Z. Elektrochem.*, **62**, 632 (1958).
9. L. V. Wanyukowa and B. N. Kabanov, *Zhur. Fiz. Khim.*, **28**, 1025 (1954).
10. L. Tronstad, "Optische Untersuchungen Zur Frage der Passivitat des Eisens und Stahls," Det Kgl Norske Videnskabers Selskabs Skrifter 1931, I F. Bruns Bokhandel, Trondheim (1931).
11. L. Tronstad and C. W. Borgmann, *Trans. Faraday Soc.*, **30**, 349 (1934).
12. D. Alpert, *J. Appl. Phys.*, **24**, 860 (1953).
13. T. A. Vanderslice, *Chem. and Eng. News*, **39**, [51], 86 (1961).
14. J. Kruger and W. J. Ambs, *J. Opt. Soc. Amer.*, **49**, 1195 (1959).
15. A. B. Winterbottom, "Optical Studies of Metal Surfaces," Det Kgl Norske Videnskabers Selskabs Skrifter 1955, I, F. Bruns Bokhandel, Trondheim (1955).
16. D. M. Brasher and A. H. Kingsbury, *Trans. Faraday Soc.*, **54**, 1214 (1958).
17. G. A. Moore, *J. Metals*, **5**, 1443 (1953).

18. O. Kubaschewski and D. M. Brasher, *Trans. Faraday Soc.*, **55**, 1200 (1959).
19. J. Kruger, *This Journal*, **108**, 504 (1961).
20. K. Haufler and B. Ilchner, *Z. Elektrochem.*, **58**, 382 (1954).
21. A. J. Cornish, *This Journal*, **106**, 685 (1959).
22. M. Pourbaix, *Z. Elektrochem.*, **62**, 670 (1958).
23. H. H. Uhlig and P. F. King, *This Journal*, **106**, 1 (1959).
24. M. J. Pryor, *ibid.*, **106**, 557 (1959).
25. M. Cohen, *J. Phys. Chem.*, **56**, 451 (1952).
26. G. W. Mellors, M. Cohen and A. F. Beck, *This Journal*, **105**, 322 (1958).
27. J. Kruger, *ibid.*, **106**, 736 (1959).
28. L. H. Germer, A. V. MacRae, and C. D. Hartman, *J. Appl. Phys.*, **32**, 2432 (1961).
29. T. P. Hoar in "Modern Aspects of Electrochemistry," J. O'M. Bockris, Editor, Vol. 2, p. 280, Butterworths Scientific Publications, London (1959).
30. A. B. Winterbottom, *J. Iron Steel Inst.*, **165**, 9 (1950).
31. P. B. Sewell, C. D. Stockbridge, and M. Cohen, *This Journal*, **108**, 933 (1961).

Investigation into the Nature of Anodic Passive and Barrier Coatings

K. Schwabe¹

Technische Hochschule, Dresden, East Germany

I. Effect of Cl^- on the Anodic Behavior of Iron in Alkaline Solutions

The rendering passive of many metals, especially nickel, is possible according to our investigations and in conformity with the ideas of Uhlig (1) and Kolytyrkin (2) by means of a chemisorbed oxygen film. Even if a given metal is coated with a bulk oxide, nevertheless the decisive effect on its passive behavior is exerted by the phase boundary between the metal and the oxide, which can also be regarded as an oxygen chemisorption layer. The removal of this layer can be achieved by having very adsorptive anions, e.g., Cl^- , displace the chemisorbed oxygen, thus making the metal active. From the anodic behavior of nickel in alkaline solutions in the presence of Cl^- or Br^- it has been shown that the displacement of oxygen from the chemisorption layer by the halogen ions determines the potential curve up to the active region if a constant anodic current density is applied to the metal.

The frequently investigated effect of chloride ions on the anodic behavior of iron in alkaline solution was now assumed in principle to be based on the displacement of the oxygen by the Cl^- . In this case, however, we do not expect to find the same quantitative relationships because iron differs considerably from nickel in its exchange current density. Therefore its passivation current density under comparable conditions is about 1,000 times greater than that of nickel. Moreover the over-voltages of the electrode process and the adsorption behavior of anions on both metals is very different. At least the anodic products (nickel or ferric hydroxide) have different solubilities. This latter point was important inasmuch as no reproducible voltage-time curve at constant current density could be obtained for nickel at first on account of the precipitation of nickel hydroxide at the anode; only when the precipitation of the hydroxide was prevented by the addition of ammonia could the curves be reproduced reliably and interpreted quantitatively. In the case of iron it was not possible to avoid the precipitation of ferric hydroxide. The addition of complex forming anions was to be avoided because otherwise no

clear statement could be made concerning the effect of the Cl^- . Consequently the anodic voltage time curves for iron at constant anodic current density have a less regular shape than those for nickel in the presence of ammonia. By intensive movement of the electrolyte in front of the electrode surface it was indeed possible to eliminate to a large extent the effect of the ferric hydroxide separating out; on the other hand the conditions with respect to the electrolyte composition at the anode were considerably altered compared with the investigations of nickel, a point which will have to be examined in greater detail.

Test Set-up and Procedure

As in the amperostatic investigations with nickel the rod-shaped anode of soft steel with traces of Cr, Cu, and As was situated in a ground section on the bottom of the electrolytic cell. However, the reference electrode was not situated in a capillary probe near the surface of the electrode; instead a

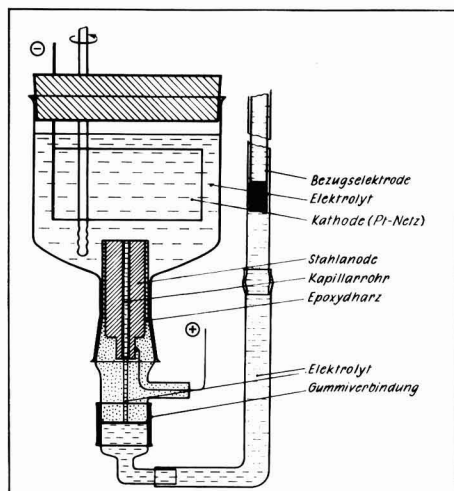


Fig. 1. Cell for measuring with Müller-Soller probe. The inserts top to bottom are: reference electrode; electrolyte; cathode (Pt gauze); steel anode; capillary tube; epoxy resin; electrolyte; rubber connection.

¹ Experiments of Chr. Voigt, Q. Nguyen, and M. Paul.

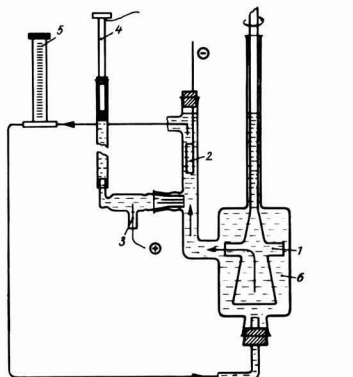


Fig. 2. Cell for flow experiments

- | | |
|-----------------------|----------------------|
| 1. Circulating pump | 4. Calomel electrode |
| 2. Pt cathode | 5. Flow meter |
| 3. Anode (cf. Fig. 1) | 6. Electrolyte |

Müller-Soller probe was used in which the steel cylinder was pierced and the capillary tube inserted into the hole projected into the lower part of the ground section which was filled with the electrolyte and which provided the liquid connection with the reference electrode (saturated calomel electrode) through a U tube (Fig. 1). A lead wire insulated from the electrolyte solutions and brought laterally from the ground section was soldered to the steel cylinder and connected to the positive terminal of the polarizing current source. The steel anode was coated up to its front face with an insulating compound (epoxy resin) so that the effective electrode surface was 0.6 cm^2 . In order to remove rapidly the ferric hydroxide formed at the surface of the anode, a plastic wiper was rotated against the anode in some of the tests; in other tests the steel anode with Müller-Soller probe was inserted temporarily in a glass tube through which the electrolyte was pumped at high variable speed by means of a glass circulating pump (Fig. 2). The arrangement for producing a constant direct current and for measuring or recording the anode voltage with reference to the saturated calomel electrode was the same as that described previously (5).

Before each test the anode was ground [with graded sand paper (180 to 700)] and degreased. After insertion in the test cell and filling with electrolyte a certain time, generally 15 min, was allowed before switching on the polarizing current. Generally speaking the electrolytic solutions were not deaerated so that the effect of oxygen on the voltage behavior could be studied; however, tests were also carried out under nitrogen with solutions from which O_2 had been eliminated carefully. The KOH concentrations were varied from 10^{-3} to 2 moles/l, those of the KCl from 10^{-4} to 2.5 moles/l. Tests carried out in 3-4M KOH solutions showed no activation of the iron even at KCl saturation. Current densities were varied in a range from 0.1 to 35 ma/cm^2 (7).

Test Results

When the current is switched on the potential jumps to a positive value and then falls to negative

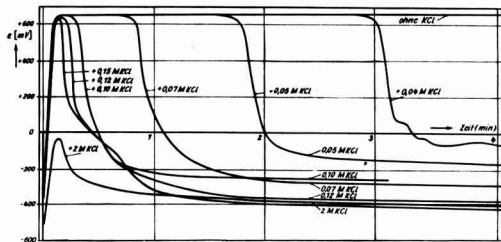


Fig. 3. Effect of KCl concentration at constant (0.1M) KOH and anode current density ($j = 1 \text{ ma/cm}^2$). Air-saturated solutions. Waiting-time 15 min.

values (in the active region) the faster the higher the KCl concentration, but the voltage decrease does not occur so regularly as in the case of nickel (Fig. 3).

We must therefore distinguish between the following potential regions:

1. The potential region of rest before the current is switched on is always in the active region [-300 to -500 mv (SCE)].
2. The passive region after the current is switched on [approximately $+650 \text{ mv (SCE)}$].
3. The potential drop to the active potential.
4. The active region accompanied by anodic formation of ferric hydroxide.

The time that it stays in the passive region (t_p) is determined by the composition of the electrolyte, by the time spent in the solution before switching on the current, and the oxygen content. In accordance with the considerations presented earlier and confirmed on nickel, the anode potential should vary exponentially with time according to the function

$$\epsilon_t = \epsilon_p - K \cdot (1 - e^{-Kt}) \quad [1]$$

where ϵ_p is the potential of the passivation. For very brief times therefore the potential is at the passive value. The value of the constant is determined by the ratio of the KCl and KOH concentrations at the surface of the electrodes. At constant KOH concentrations (0.1M) t_p decreases exponentially with the concentration of KCl (c mole/l) according to Eq. [2]

$$t_p = 687 \cdot e^{-35.7 \cdot c} \quad [2]$$

at 25°C in the concentration range 0.03-0.12 moles/l (Fig. 4). For every KOH concentration there is a minimum KCl concentration (c_{\min}), which just barely suffices to bring about a decreasing potential in the active region. Generally speaking we may write

$$1/t_p = K_2 (c - c_{\min}) \quad [3]$$

where the constant K_2 depends on the KOH concentration, agitation or flow conditions, and all the time prior to polarization (Fig. 5). The time t_p in air or O_2 saturated solutions increases approximately proportionally to the waiting time; in oxygen free solutions it is almost independent of the waiting time. With increasing current densities the time remaining in the passive region, t_p , decreases approximately proportionally (in the range 0.1-20 ma/cm^2).

$$t_p = a \cdot j + b \quad [4]$$

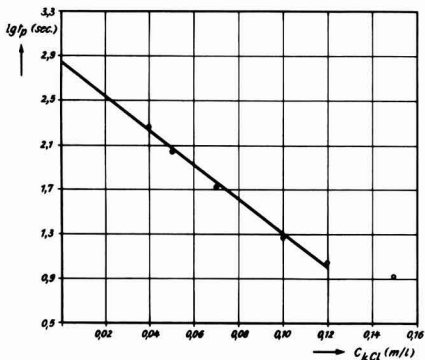


Fig. 4. Time in passive region (t_p) as function of KCl concentration.

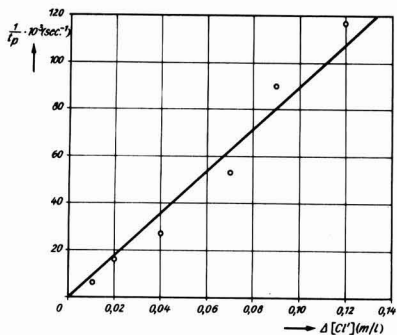


Fig. 5. t_p as function of KCl concentration. $1/t_p = K(C_{KCl} - C_{KCl,min})$.

where j is the current density in ma/cm^2 , and a and b are constants depending on the composition of the electrolyte.

When the electrolyte flows past the anode, then where the KCl concentration is small in relation to the KOH concentration and the flow velocity is sufficiently high so that the electrode can be kept passive for an arbitrarily long time ($t_p \rightarrow \infty$); when the flow is stopped, a drop to the active region takes place and when the circulation pump is turned on again the anode gradually becomes passive once more (Fig. 6). At high KCl concentrations, however, t_p is decreased by the flow of the electrolyte.

When the variation of the potential (ϵ_m) after the time t_p is analyzed as a function of t , we find in the first seconds a relationship of the form

$$\epsilon_m = \epsilon_p - (t - t_p)^3 \cdot K_3 \quad [5]$$

furthermore, K_3 increases approximately in proportion to the ratio c_{Cl^-}/c_{OH^-} (see Fig. 7a and b). Over

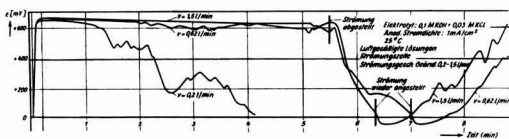


Fig. 6. Effect of electrolyte flow velocity (0.1 M KOH + 0.03 M KCl; $j = (ma/cm^2)$).

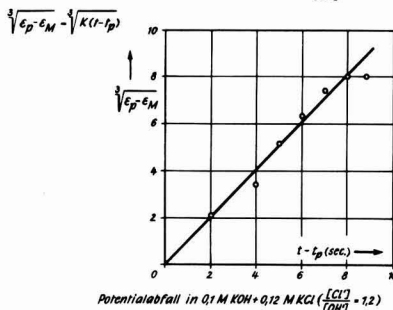
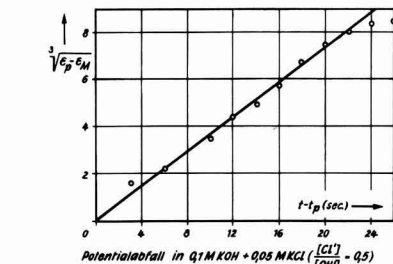


Fig. 7a, b. Potential fall after the time t_p

longer periods of time irregularities in the potential decrease appear (see Fig. 3 and 6) which do not permit the calculation of a function, but it can be assumed that in principle the potential follows an exponential function from the beginning of the flow of current to the active region, as we found earlier for the case of nickel.

In the active region the measured potentials correspond approximately with the process $Fe \rightarrow Fe^{+2} + 2e$.

Discussion

The results can be interpreted if we again assume, as in the case of nickel, that the iron is at first covered by chemisorbed oxygen, which is displaced by the Cl^- , and that this displacement leads to the activation of the iron. As already stated for nickel a greater ratio c_{Cl^-}/c_{OH^-} will prevail at the anode than in the solution owing to the current which accounts for discharge of OH^- in the passive state and the transference of Cl^- . Also for activation, therefore, the important consideration is not the ratio in solution but that at the electrode surface. Hence, a high concentration of KCl without polarization does not suffice to bring about for instance activation in 0.1M KOH; only at a ratio of more than twenty in the solution does the electrode become active practically immediately. The necessity of increasing the ratio c_{Cl^-}/c_{OH^-} as a condition for the activation also explains the decrease in the time t_p with the current density in accordance with Eq. [4]. During the time in the passive region the increase in the Cl^- concentration at the anode is proportional to the current density and according to [3] inversely proportional to the time t_p . If the electrode rests in the solution in the presence of oxygen, a small amount of corrosion occurs as the potential situation indicates and leads to a porous non-

Table I. Minimum KCl concentration with activating effect for $j = 1 \text{ ma/cm}^2$ on iron as a function of the KOH content at 25°C

KOH (m/l):	10^{-3}	10^{-2}	0.05	0.10	0.15	0.20	0.50	1	2
KCl (m/l):	10^{-4}	10^{-3}	10^{-2}	0.03	0.07	0.1	0.33	0.75	2.5
				On nickel					
			KOH (m/l):	0.035	0.070	0.14			
			KCl (m/l):	0.05	0.080	0.20			

passivating coating. However, this coating prevents the arrival of the Cl^- partly in a mechanical way and partly perhaps by forming basic chlorides and thus delaying the concentration of Cl^- at the electrode surface; this expresses itself in prolonging the time spent in the passive region. When the electrolyte flows past the anode at high velocity, the required enrichment cannot occur at not too great concentrations, and thus the electrode remains passive, but when the flow is interrupted the required concentration takes place. The higher the current density, the more rapid will be the enrichment process. The increased rapidity of the transition to the active state at high Cl^- concentrations is perhaps due to the fact that, on account of the high Cl^- concentrations, corrosion even in the passive region is still so considerable that inhibiting coatings are formed which are removed by the flow. To interpret the change of potential after passage through the passive region it must first be noted that the attack on the iron, when occurring, always takes the form of pitting; thus the active part of the surface, f , is very small in relation to the total surface and even to the passive part (1-3% compared with 1-f). When it is assumed therefore that the potential ϵ_m at a given time t can be calculated from the passive potential and the reversible potential of the iron dissolution ϵ_{Fe} according to

$$\epsilon_m = (1-f) \cdot \phi_p \epsilon_p + \phi_{\text{Fe}f} \cdot \epsilon_{\text{Fe}} \quad [6]$$

and if at the same time the proportionality factors ϕ_p and ϕ_{Fe} are regarded as constant, the first term can be put approximately equal to $\phi_p \cdot \epsilon_p = \text{constant}$.²

According to Engell and Stolica (8) the radius of pitting increases proportionally with the time, i.e., $r = c_1 t$ ($c_1 = \text{constant}$) and so does the number of pits $z = c_2 \cdot t$ ($c_2 = \text{constant}$), from which follows that the fraction of the active surface by integration of $F = \int_0^z F_i \cdot dz$, where F_i is the area of a pit and O is the total electrode surface and the form $f = \frac{2\pi c_1^2 \cdot c_2 \cdot t^3}{3 \cdot O}$ or with $\frac{2\pi c_1^2 \cdot c_2}{3 \cdot O} = G$ then $F = G \cdot t^3$.

For ϵ_m we then have

$$\epsilon_m = \phi_p \cdot \epsilon_p + \phi_{\text{Fe}} \cdot G \cdot \epsilon_{\text{Fe}} t^3$$

If we count the time from the beginning of the decreasing potential, ϕ_p is approximately 1 and take into account ϵ_{Fe} is negative, we obtain in conformity with the experiments in the formula

$$\epsilon_m = \epsilon_p - K_3 (t - t_p)^3$$

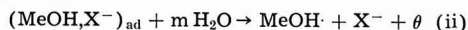
²In reality these factors will be a function of the ratio of exchange current density and partial current density of the process involved. In each case it can be assumed that $\phi_p \ll \phi_{\text{Fe}}$. Cf. K. Bonhoeffer and W. Renneberg, *Z. phys. Chem.*, 118, 389 (1941), who introduce a "critical threshold area."

Of course, since $(1-f) = 1$ was implied we can expect to find this curve only at the beginning of activation. As the process continues we must expect an exponential drop according to Eq. [1] derived earlier. It must be borne in mind of course that K and K_1 contain, in addition to the concentration of Cl^- and OH^- , also their adsorptivities on the metal in question as well as the rate constants of adsorption, and that consequently these constants could assume quite different values. Moreover, in derivation [5] of this equation the coefficients ϕ_p and ϕ_{Me} are not taken into account, but actually it must be assumed that $\phi_{\text{Fe}} > \phi_{\text{Ni}}$ because with iron the reaction $\text{Me} \rightarrow \text{Me} \cdot + 2\theta$ is much less inhibited than in the case of Ni. Because of this also the activation by Cl^- can follow a different course with the two metals; however, we can actually find no differences in principle between the behavior of nickel and that of iron in alkaline solutions in the presence of halogen ions. The time remaining in the passive region is considerably shorter for nickel than for iron which, as already stated, can be attributed to the differing adsorptivities of the anions or to different exchange current densities, and also perhaps to the fact that in the case of nickel the phase oxide form has been kept in solution by the addition of NH_3 . With nickel the potential decrease is slower than with iron, but it is much more strongly affected by Cl^- concentration, and the minimum Cl^- concentration required for activation is greater (Table I).

It can be concluded from the results that for iron and nickel (probably also for cobalt) the active anodic dissolution of metal in alkaline solutions containing halide does not take place until the halogen ions have displaced chemisorbed oxygen or adsorbed OH^- ; in the course of this, intermediate products may occur in accordance with



and



as Frumkin (9) for example has assumed. If we suppose at the same time that the activating adsorption of halogen ions and the passivating adsorption of OH^- occur as competing simultaneous reactions (4), it

Table II. Change in dissolution potential for 2N KCl = constant and $j = 1 \text{ ma/cm}^2$ with the KOH content (measured in each case after 3.5 min) at 25°C

KOH (m/l):	10^{-3}	10^{-2}	10^{-1}	1
(mv SCE):	-505	-450	-385	-265

Table III. Change of dissolution potential at 0.1N KOH = constant and $j = 1 \text{ ma/cm}^2$ with the KCl — content (measured after 3.5 min in each case) at 25°C

KCl (m/l):	0.04	0.05	0.07	0.12	0.15
ϵ (mv, SCE):	-40	-150	-280	-390	-425

also becomes understandable that for constant Cl^- concentration with increasing OH^- concentration the

potential becomes more positive $\frac{\partial \epsilon}{\partial \ln c_{\text{OH}^-}} > 0$

(Table II), whereas for the process



a negative coefficient $\frac{\partial \epsilon}{\partial \ln c_{\text{OH}^-}} = -\frac{RT}{F} 2.303$

would have to occur.

We have found, of course, similar to observations of Popowa and Kabanow (10) that at very small current densities ($< 0.5 \text{ ma/cm}^2$) the gradient actually does become negative. Possibly the reaction always occurs to a slight extent and at small current densities where reactions (i) and (ii) are not required for the penetration of the charge, becomes the determining factor for the potential. The gradi-

ent $\frac{\partial \epsilon}{\partial \ln c_{\text{Cl}^-}}$ as expected is negative ($\sim -73 \text{ mv}$)

(Table III).

On the other hand Heusler and Cartledge (11) have found that in acids containing halide for iron

$\frac{\partial \epsilon}{\partial \ln c_{\text{OH}^-}} = -59 \text{ mv}$ and $\frac{\partial \epsilon}{\partial \ln c_{\text{Cl}^-}} = +53 \text{ mv}$. Thus,

for the anodic dissolution in acids containing halide still other factors must be decisive. For example the strong adsorptivities of the halogen ions after removal of the passive film could prevent dissolution, just as it can of course, inhibit the H^- -dis-

charge. The negative gradient $\frac{\partial \epsilon}{\partial \ln c_{\text{OH}^-}} = -59 \text{ mv}$,

which is attributive of course to the catalytic effect of the OH^- on the dissolution of the iron (12), is at first difficult to interpret (13). Theoretical investigations and experiments with tracer ions are at present in progress with regard to this question. It must not be overlooked that reliable quantitative statements are made much more difficult by the fact

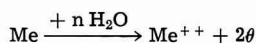
that the corrosion current densities and the form of the attack on the electrode surfaces depend very strongly on the prehistory and pretreatment of this surface, on the purity of the electrode metal (14), and on the voltage situation. As proof we may cite three micrographs of nickel electrodes from which, under completely similar conditions at different potentials, approximately the same quantity of nickel was brought anodically into solution in 5N H_2SO_4 , whereas in the active range [$\sim +50 \text{ mv}$ (SCE) and at $+1400 \text{ mv}$ (SCE)] a completely uniform surface attack takes place. At $+1700 \text{ mv}$ a definite grain boundary corrosion occurs. These results are confirmed by many determinations (15).

REFERENCES

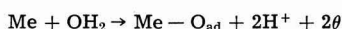
1. Compare H. H. Uhlig and P. F. King, *This Journal*, **106**, 1 (1959).
2. Y. M. Kolotyrkin and W. M. Knjashewa, *J. Phys. Chem., U.S.S.R.*, **30**, 9 (1956).
3. K. Schwabe and G. Dietz, *Z. Elektrochem.*, **62**, 751 (1958); K. Schwabe, *Wiss. Z. TH Dresden*, **8**, 240 (1958/59); *Z. physik. Chem., Leipzig*, **214**, 343 (1960).
4. Compare K. Schwabe, *Electrochim. Acta*, **3**, 186 (1960).
5. K. Schwabe and R. Radeaglia, *Werkstoffe u. Korrosion*, **13**, 281 (1962).
6. Haber and Goldschmidt, *Z. Elektrochem.*, **12**, 62 (1906); B. Kabanow and D. Leikis, *Acta Physic. UdSSR*, **21**, 769 (1946); B. Kabanow and D. Leikis, *Ber. Akad. Wiss. UdSSR*, **58**, 1685 (1947); L. Wanjukowa and B. Kabanow, *Ber. Akad. Wiss. UdSSR*, **59**, 917 (1948); L. Wanjukowa and B. Kabanow, *J. Phys. Chem., U.S.S.R.*, **28**, 1025 (1954); I. Rosenfeldt and Maximtschuk, *ibid.*, **35**, 1832 (1961); I. Rosenfeldt and Maximtschuk, *Z. Phys. Chem.*, **215**, 25 (1961); T. Popowa and B. Kabanow, *J. Phys. Chem., U.S.S.R.*, **35**, 1295 (1961); B. Kabanow, R. Burstein, and A. Frumkin, *Discussion Faraday Soc.*, **1**, 259 (1947); G. Schmidt and N. Hackerman, *This Journal*, **108**, 741 (1961).
7. For closer values see Dipl.-Arbeit Chr. Voigt, TU Dresden 1962, Institut für Electrochemie und phys. Chemie.
8. *Z. physik. Chem. N.F., Frankfurt*, **20**, 113 (1959).
9. B. Kabanow, R. Ch. Burstein, and A. Frumkin, *Discussions Faraday Soc.*, **1**, 259 (1947).
10. *J. Phys. Chem., U.S.S.R.*, **35**, 1295 (1961).
11. K. E. Heusler and G. H. Cartledge, *This Journal*, **108**, 732 (1961).
12. K. Heusler, *Z. Elektrochem.*, **62**, 582 (1958).
13. C.f., J. O'M. Bockris, D. Drazic, and A. R. Despic, *Electrochim. Acta*, **4**, 325 (1961).
14. J. O'M. Bockris and D. Drazic, *ibid.*, **7**, 293 (1962); G. Trumpler and W. Saxer, *Helv. Chim. Acta*, **36**, 1630 (1953).
15. Dissertation E. Kunze, T. U. Dresden, in preparation.

II. Investigations of Ion Conducting Barrier Layers with Anodic Polarization

Whereas in the case of metals with restricted passage reaction



e.g., for nickel, iron, and cobalt we regard a chemisorbed oxygen film formed by the competing reaction



(see Part I), as sufficient for their passivation, for metals with unrestricted passage reaction such as Ag, Zn, Cd, and Al ion conducting barrier layers of salts or oxides can produce high anodic polarization.

On zinc salt barrier layers were investigated which in many respects show a behavior similar to the aluminum barrier layer (1), in saturated solutions of zinc sulfate and other salts. In particular very high positive potentials (up to greater than

10v) were measured even with the interrupted method. These were interpreted as condenser charges.

On mercury in chloride solutions using oscillographic switch off curves, we have found that the high anode potentials we were able to measure during polarization were made up of three components, an ohmic voltage drop (resistance polarization), a type of condenser charge, and the relatively slight chemical polarization which can be attributed primarily to the fact that after exceeding saturation, i.e., at a certain supersaturation, solid salt must be formed from the metal directly on the surface of the electrode. If the voltage drop is plotted semi-logarithmically against the time, three rectilinear curve segments are obtained which correspond to the three polarization effects. We now apply this method to zinc in a saturated sulfuric acid zinc sulfate solution. We shall not discuss here the details of the experimental procedure, especially the verification of the fact that this does involve a zinc sulfate layer which brings about the polarization. In any case it was again found that, after a steep drop which takes place in less than 10^{-3} sec and which in relation to the total polarization decreases with increasing anode potential during the flow of current, a potential drop occurs which goes according to a function $U = K \cdot e^{-t/\tau}$ and increases with increasing total polarization, and finally a relatively slow drop which is more or less independent of the total polarization (Fig. 1). Here, too, we interpret the first steep drop as a resistance polarization, the second as a condenser discharge, and the slow drop at the end as chemical polarization; of course, these three processes overlap to some extent.

When we compare the rate of the potential drop on zinc in NaOH with that in saturated zinc sulfate solution (3), we find that it takes place more slowly by several orders of magnitude with zinc oxide in NaOH than in sulfate. The rapid drop in sulfate and other salt solutions was long ago (4) attributed to the fact that the salt layer is dehydrated electro-osmotically by the high potential gradient, and hence its insulation resistance is considerably increased. This would also explain the rectifying effect of such layers because with cathodic charging of electrodes with such layers the water is returned, and hence the barrier effect is practically eliminated. Several years ago Müller (5) expressed the view that the rectifier effect in the case of oxide coated

aluminum is due essentially to such dehydration, to which it was subjected; however, (6) aluminum shows a rectifier effect even in nonaqueous sulfuric acid. We have now demonstrated that in the case of zinc in a saturated sulfate solution water is forced out of the barrier layer by an anodic field. For this purpose we connected a zinc electrode in saturated zinc solution, in which the water had been tagged with tritium, to the anode and polarized it until there was a drop in current density, i.e., until the barrier layer had been formed; the current was then turned off and the electrode was removed from the radioactive solution, washed with dioxane to conserve the salt layer, and immersed in an inactive saturated $ZnSO_4$ solution. From this point on, by taking samples, the activity of this continuously stirred solution was measured with a liquid scintillator counter and a coincidence measuring position (7). After a certain time when isotope exchange equilibrium had become established at the surface, and thus the activity was constant, the electrode was connected to the anode, whereupon after a high initial value the current immediately decreased sharply. At the same time the activity of the solu-

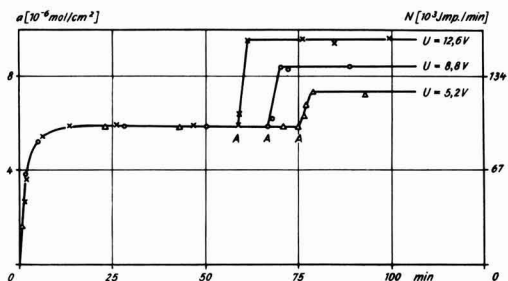


Fig. 2. Dehydration of barrier layer as function of time at various field strengths. (Zn in saturated $ZnSO_4$ solution). Anodic potential applied at A.

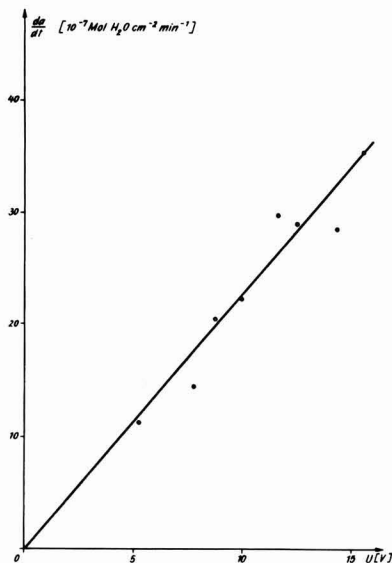


Fig. 3. The rate of water emergence as a function of anodic voltage (Zn in saturated $ZnSO_4$ solution).

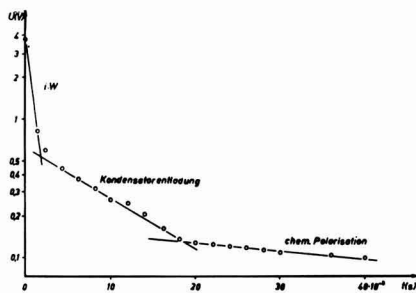


Fig. 1. The three polarization effects on Zn

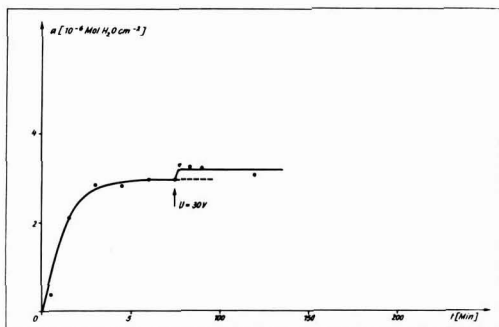


Fig. 4. Dehydration of Zn anode in 90% H_2SO_4 saturated with ZnSO_4 .

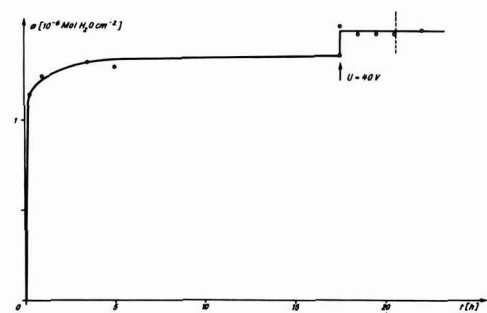


Fig. 5. Dehydration of Al anode in ammonium borate solution

tion was measured; it immediately showed a steep increase and then remained constant (Fig. 2). The rate of water emergence measured by the increase in the pulse rate is proportional to the applied voltage, as was to be expected in an electroosmotic dehydration process (Fig. 3). In 90% sulfuric acid saturated with zinc sulfate, the much smaller effect is just barely measurable at 30v applied voltage (Fig. 4). For aluminum we were also able to demonstrate such a dehydration effect in a similar way with T_2O tagged ammonium borate solution. The increase of pulse rate per cm^2 of course was very much smaller, probably because of the smaller coating thicknesses. For the electrode, therefore, we used a hollow aluminum cylinder with an inside surface area of about 250 cm^2 and placed it about 3 mm away from a solid aluminum cylinder as the cathode; the electrolyte volume was therefore very small (7). Otherwise the same procedure was followed as for zinc in zinc sulfate; however, the anode voltages were considerably larger. Figure 5 shows that when 40v are applied there is a sudden increase in the tritium activity which corresponds approximately to a water emergence of 1 to $1.5 \cdot 10^{-7}$ mole $\text{H}_2\text{O}/\text{cm}^2$. Because of the much smaller effect here we could not establish a clear relationship between the water emergence rate and the applied voltage. Nevertheless for aluminum also Mueller's assumption that the rectifier effect is brought about or at least promoted by an electroosmotic dehydration is thereby given considerable support. The rectifier effect in nonaque-

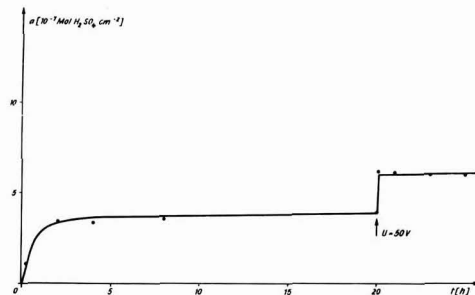


Fig. 6. H_2SO_4 emergence at an Al anode

ous sulfuric acid could then be explained by an electroosmotic ejection of H_2SO_4 from the barrier layer, especially when it is considered that the dielectric constant of H_2SO_4 (84) is decidedly greater than that of the Al_2O_3 barrier layer (7.5 for Al_2O_3). In order to clarify this question we carried out measurements in fuming sulfuric acid which had been tagged with S^{35} , after first establishing that a dehydration of the barrier layer by fairly long pretreatment in this acid does not influence the rectifier effect, the quotient; $J_{\text{Cl}}/J_{\text{eff}}$ both before and after the treatment was 0.40-0.45.

After the aluminum electrode had been connected for a fairly long time to the anode in sulfuric acid tagged with $\text{H}_2\text{S}^{35}\text{O}_4$ the current was switched off and the cylinder was removed, washed, and put in inactive sulfuric acid. After the isotope equilibrium had been established various anode voltages were again applied. In all cases a rapid increase in the pulse rate in the inactive sulfuric acid took place; after a short time the activity became constant. Figure 6 shows the effect for an applied voltage of 50v; the establishment of isotope exchange equilibrium in the case of aluminum always requires a considerably longer time than for zinc even in aqueous solutions. As a result of the applied voltage about $2 \cdot 10^{-7}$ mole $\text{H}_2\text{SO}_4/\text{cm}^2$ are given off. This is of the same order of magnitude as that for water.

This seems to us to prove that the barrier forming effect of aluminum oxide layers is determined to a large extent by electroosmotic effects, and thus a previous assumption, which was proposed by Fischer (8) is confirmed. Of course the cathodic electrode process also plays a part in saturated zinc sulfate solution. We do not observe any queer rectifier effect ($J_{\text{Cl}}/J_{\text{eff}} \approx 0.01$). In 90% H_2SO_4 saturated with ZnSO_4 an effect is present ($J_{\text{Cl}}/J_{\text{eff}} \approx 0.15$). In the first case there is deposition of zinc during the cathodic impulses, as is evident under the microscope, but the saturation at the anode is thereby eliminated, and thus passage for the current of the anodic impulse is made possible. In 90% H_2SO_4 because of the slight solubility of ZnSO_4 at the high hydrogen ion concentration no appreciable Zn deposition takes place, and therefore we observe a rectifying effect here. Our view is further supported by the fact that silver in chloride solution has no rectifier effect (9), whereas magnesium in magnesium sulfate does show such an effect, if only a slight one (10). In each case

of course it depends on the structure of the layer, and this is determined not only by the composition of the electrolyte but also by the method of its formation.

Any discussion of this paper will appear in a Discussion Section to be published in the December 1963 JOURNAL.

REFERENCES

1. K. Schwabe, Habilitationsschrift, TH Dresden, 1933; K. Schwabe and F. Lohmann, *Z. physik. Chem.*, **215**, 158 (1960).
2. *Electrochim. Acta*, **7**, 1 (1962).
3. B. K. Schwabe, *ibid.*, **3**, 47 (1960).
4. K. Schwabe, *Ber. Verhndl. sächs. Akad. Wiss. Leipzig*, **101**, 1 (1954).
5. W. J. Müller and K. Konopicky, *Z. physik. Chem.*, **A141**, 343 (1929).
6. A. Günther-Schulze, *ibid.*, **A143**, 62 (1929).
7. V. K. Schwabe, *Naturwiss.* **49**, 56 (1962). Einzelheiten der Versuchs- und Messtechnik werden in Kurze an anderer Stelle mitgeteilt.
8. *Z. physik. Chem.*, **48**, 211 (1904); *Z. Elektrochem.*, **10**, 877 (1904).
9. A. Günther-Schulze, *Ann. Physik*, **26**, 373 (1908).
10. A. Günther-Schulze, *ibid.*, **24**, 43 (1907).

The Anodic Oxidation of Iron in a Neutral Solution

II. Effect of Ferrous Ion and pH on the Behavior of Passive Iron

Masaichi Nagayama¹ and Morris Cohen

Division of Applied Chemistry, National Research Council, Ottawa, Canada*

ABSTRACT

The anodic polarization curve, the static passive potential, and the behavior of the decay of the polarized passive potential of iron were examined in neutral boric acid/borate solutions with and without Fe^{++} ion addition. It was found that the passivation potential is a function of the $[\text{Fe}^{++}]$ and pH and corresponds to the equilibrium potential of the reaction of $\gamma\text{-Fe}_2\text{O}_3 + 6\text{H}^+ + 2e \rightleftharpoons 2\text{Fe}^{++} + 3\text{H}_2\text{O}$. The polarized passive potential in the steady state is related to a pseudoequilibrium potential that corresponds to a higher defect concentration in the oxide surface and to a lower $[\text{Fe}^{++}]$ at the oxide/solution interface. The potential gradient across the film appears to be very small. The decay of the polarized passive potential on open circuit is explained as due mainly to the change in the defect-concentration and consequently of the film composition at the oxide/solution interface either by the outward migration of iron through the film or by the reaction with Fe^{++} ion in solution when the latter had been added or supplied by a small amount of self-corrosion.

It was shown in the previous paper (1) that anodically passivated iron in a boric acid/borate buffer solution at a pH of 8.41 is covered with an oxide film (10–30Å) consisting of an inner Fe_3O_4 and an outer $\gamma\text{-Fe}_2\text{O}_3$ layer of which the outermost portion is a cation-deficient structure such as $\text{Fe}_x^{6+} \cdot \text{Fe}_{2-2x}^{3+} \cdot \square_x \cdot \text{O}_3$. The thickness of the layers and the concentration of defects were estimated as functions of the applied passive potential. The slope of the film-thickness/potential curve becomes smaller beyond the potential E_a^2 which is found between the passivation potential E_a^1 and the oxygen evolution potential E_a^3 , whereas the concentration of defects begins to increase appreciably above this potential. It was also found in the previous investigation that the $\gamma\text{-Fe}_2\text{O}_3$ layer begins to be produced or to be reduced above and below the passivation potential E_a^1 . The reduction occurs as the dissolution of Fe^{++} ion in the solution with almost 100% current efficiency.

The main purpose of this investigation is to interpret the significance of the characteristic potentials E_a^1 (the passivation potential) and E_a^2 , and the role of defects in the mechanism of passivity.

¹ Postdoctorate Fellow; present address: Faculty of Engineering, Hokkaido University, Sapporo, Japan.
* N.R.C. No. 7436.

Experimental

Materials and their preparations were the same as those used in the previous investigation (1). Specimens were electropolished Ferrovac iron sheets. Electrolytes were a mixture of 0.15N boric acid and 0.15N sodium borate solution, saturated with purified nitrogen. Electrolytes of various pH's between 5 and 9 were prepared by changing the ratio of these solutions; the buffering capacity was fairly small below pH 7. An equivalent mixture at a pH of 8.41 was mainly used as a standard solution, and it was kept in the first storage vessel. The second storage vessel was filled with the standard solution or with a solution of different pH. Fe^{++} ion could be added by the anodic dissolution of an iron wire inserted into the vessel.

The electrolytic cell and the electrical circuits were the same as employed in the previous investigation. Anodic passivation of the specimen was always done in the standard solution by the potentiostatic method, by starting with a fresh iron surface from which all previous oxide film had been removed by cathodic treatment. In the experiments in which the effect of Fe^{++} ion and pH were examined, the solution was changed from the standard

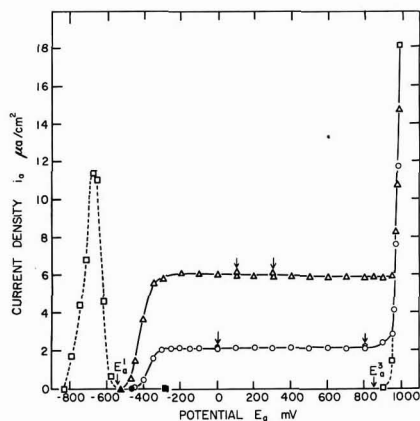


Fig. 1. Effect of ferrous ion concentration on the anodic polarization curve of passive iron; pH = 8.41. Δ , $\text{Fe}^{2+} = 5.81 \times 10^{-4}$ mole/l; \circ , $\text{Fe}^{2+} = 2.06 \times 10^{-4}$ mole/l; \square , no ferrous ion addition. Fe^{2+} in the passive potential region is of the order of 10^{-7} mole/l; \blacktriangle , \bullet , \blacksquare , static passive potentials for above solutions, \downarrow current was checked after renewal of the solution.

solution to the solution of different pH and Fe^{2+} ion content, without interrupting the anodic polarization. The cathodic reduction of the passive specimen was conducted only in the fresh standard solution by a galvanostatic method with a constant c.d. of $10 \mu\text{A}/\text{cm}^2$. The amount of ferrous ion in solution was analyzed by the o-phenantroline method.

Experimental Results

Effect of ferrous ion on the polarization curve.—

The steady-state potential/current relationship for the passive iron was measured in solutions (pH 8.41) to which Fe^{2+} ion had been added at various concentrations. The result is shown in Fig. 1, together with the polarization curve obtained in a solution without Fe^{2+} ion addition (the standard solution). The limiting current is observed to increase with the ferrous ion concentration in the passive potential region above -200 mv. The current gradually drops to zero as the potential is lowered to the region of the passivation potential, E_a^1 . The results were the same when measured in the direction of either increasing or decreasing potential. It was determined by chemical analysis of the solution that the current observed roughly corresponds to the rate of oxidation of Fe^{2+} ion to ferric oxide at the oxide/solution interface (Table I). Because of the gradual decrease of Fe^{2+} ion concentration with time, the solution had to be

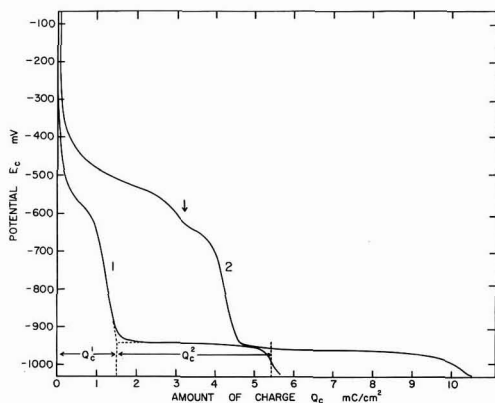


Fig. 2. Comparison of the cathodic reduction curves obtained for thin and thick passive films; standard solution, c.d. = $\mu\text{A}/\text{cm}^2$; Expt. 1, cathodically pretreated iron was passivated at $+850$ mv for 1 hr in the standard solution. The amount of charge passed during anodic polarization is about $Q_a = 6.80 \text{ mc}/\text{cm}^2$, $Q_c^1 = 1.54 \text{ mc}/\text{cm}^2$, $Q_c^2 = 3.92 \text{ mc}/\text{cm}^2$. Expt. 2, After repetition of Expt. 1, solution was changed for one containing about 1.8×10^{-4} mole/l Fe^{2+} ion, and passivation was continued for half an hour. The amount of charge accumulated on the surface after the change of solution was $Q_a = 3.82 \text{ mc}/\text{cm}^2$, [$Q_c^1 = 4.55 \text{ mc}/\text{cm}^2$, $Q_c^2 = 5.64 \text{ mc}/\text{cm}^2$] Inflection of Curve 2 indicated by arrow is explained by the noncontinuous change between the primary and the secondary oxide films which are obtained before and after the change of solution.

changed twice during the measurement of the polarization curve. The value of the limiting current was finally checked by the renewal of the solution at the end of the measurement as is indicated by arrows in Fig. 1. Thus, if the anodic polarization is continued for a long period of time in the presence of Fe^{2+} ion in solution, an oxide film of any thickness can be obtained in contrast to the maximum film thickness of about 30\AA obtained in a solution originally free from Fe^{2+} ion (cf. Fig. 9). The behavior on cathodic reduction of the thicker film, however, was quite similar to that of the thin passive film, even though the number of coulombs required to reduce the thick film is of course much greater (Fig. 2). This indicates that the oxide formed by the oxidation of Fe^{2+} ion in solution is essentially the same as that formed by anodic oxidation of iron.

A straight line passing through the origin is obtained when the limiting current measured at $+600$ mv is plotted against the Fe^{2+} ion concentration as is seen in Fig. 3. The pH of the solution seems to have no effect on the results. The limiting current

Table I. Comparison between the amount of charge passed and the amount of oxidation of Fe^{2+} ion during anodic polarization in solutions with Fe^{2+} ion addition (pH = 8.41)

No.	Pre-polarization E_a^1 , mv	t_a^1 , min	Polarization E_a , mv	t_a , min	Amount of charge passed Q_a^{obs} , mc	Initial amount of Fe^{2+} ion W_1 , μg	Final amount of Fe^{2+} ion W_2 , μg	$W_1 - W_2$, μg	*Calculated amount of charge Q_a^{cal} , mc	$Q_a^{\text{cal}}/Q_a^{\text{obs}}$
1	+590	40	+590	60	46.5	223.5	196.1	27.4	47.4	1.02
2	+400	80	+400	48	37.7	246.2	225.1	20.7	35.8	0.95
3	+600	120	-200	78	42.5	153.7	127.9	25.8	44.6	1.05
4	After Expt. No. 3		+100	60	15.6	76.2	65.6	10.6	18.3	1.17

* Calculated by assuming the reaction $\text{Fe}^{2+} \rightarrow \text{Fe}^{3+} + e$.

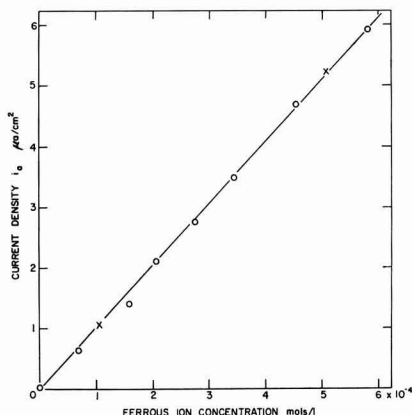


Fig. 3. Relation between ferrous ion concentration and the anodic current. $D_{Fe^{++}} = 5.3 \times 10^{-6} \text{ cm}^2 \text{ sec}^{-1}$. \circ , + 600 mv, pH, 8.41; \times , + 850 mv, pH, 7.31.

was markedly increased by stirring the solution. It is clear from these experimental facts that, in the potential region where the limiting current is observed, the reaction is controlled entirely by the rate of diffusion of ferrous ion from the bulk of solution to the oxide/solution interface where the ferrous ion concentration is considered to be very small. The diffusion coefficient of ferrous ion was estimated as $D = 5 \times 10^{-6} \text{ cm}^2 \text{ sec}^{-1}$ by using the simple diffusion equation

$$i_a = nFDC/d \quad (n = 1)$$

where i_a (amp/cm²) is the limiting current at a ferrous ion concentration of C (mole/cm³), F is the Faraday, and the effective thickness of the diffusion layer d in a stagnant solution is assumed to be 5×10^{-2} cm. The value obtained seems to be reasonable.

Effect of $[Fe^{++}]$ and pH on the static passive potential.—When the circuit is interrupted after applying anodic polarization the potential decays until a static passive potential is reached. The final steady potential, which is in the region of the passivation potential, is often called the Flade potential (2). The effect of ferrous ion concentration and pH of the solution on the static passive potential was examined in a series of experiments. The results obtained are summarized in Table II.²

The relation between the potential and the logarithm of the ferrous ion concentration at constant pH is a straight line having a slope of 60 mv per logarithmic unit (Fig. 4). A linear relationship is also found between the potential and pH at a constant ferrous ion concentration, the slope being 163 mv per pH unit (Fig. 5). It should be emphasized that the value of the measured static potential is not dependent on the previous history of the specimen, such as the applied anodic potential, the time of polarization or the film thickness, but is determined only by the existing Fe^{++} ion concentration

² During the experiment it was noticed that the static potential was normally maintained steadily for an indefinite time, although at high concentration of ferrous ion ($C = 3 \times 10^{-4}$ mole/l) the value sometimes fell off again after showing a plateau. In the latter case plateaus were not perfectly level but had a slight downwards slope; in such cases the potential values shown in Fig. 4 were taken just before the sharp drop at the end of the plateau.

Table II. Effect of pH and $[Fe^{++}]$ on the static potential of passive iron (boric acid-sodium borate buffer solutions)

E_a , mv	t_a , hr	pH	$[Fe^{++}]$, mole/l	E_{stat} , mv
+850	2.5	9.21	3.63×10^{-6}	-444
	2.6	9.21	9.88×10^{-6}	-472
	11.0	9.21	4.23×10^{-5}	-513
	3.0	9.21	5.37×10^{-5}	-512
	5.0	9.21	1.04×10^{-4}	-538
+850	3.0	8.41	4.7×10^{-7}	-285
	—	8.41	2.15×10^{-6}	-328
	3.0	8.41	7.25×10^{-6}	-347
	3.0	8.41	9.52×10^{-6}	-352
	4.5	8.41	1.02×10^{-5}	-360
	2.5	8.41	1.85×10^{-5}	-370
	4.3	8.41	4.95×10^{-5}	-404
	3.0	8.41	5.80×10^{-5}	-410
	2.5	8.41	7.86×10^{-5}	-410
	5.0	8.41	1.66×10^{-4}	-430
-100	3.0	8.41	2.39×10^{-4}	-430
	2.7	8.41	5.75×10^{-4}	-460
	16.5	8.41	5.54×10^{-6}	-338
	2.0	8.41	1.93×10^{-5}	-381
	2.0	8.41	1.36×10^{-4}	-425
+850	16.0	8.41	2.72×10^{-4}	-432
	1.0	7.31	3.01×10^{-6}	-156
	1.0	7.31	7.85×10^{-6}	-189
	1.0	7.31	1.70×10^{-5}	-208
	3.0	7.31	9.78×10^{-5}	-255
	1.0	7.31	1.05×10^{-4}	-254
	3.0	7.33 (7.31)	5.09×10^{-4}	-295 (-293)†
	1.0	6.31	1.61×10^{-6}	+22
	3.0	6.31	4.90×10^{-6}	+1
	4.0	6.31	1.02×10^{-5}	-22
+850	5.5	6.34 (6.31)	3.21×10^{-5}	-62 (-57)†
	6.0	6.35 (6.31)	7.31×10^{-5}	-83 (-77)†
	12.5	6.38 (6.31)	1.09×10^{-4}	-102 (-91)†
	4.0	6.36 (6.31)	1.73×10^{-4}	-108 (-100)†
	5.5	6.44 (6.31)	3.62×10^{-4}	-144 (-123)†
	3.0	6.54 (6.31)	1.01×10^{-3}	-189 (-152)†
+850	3.4	5.78	9.14×10^{-5}	+34
+850	17.0	5.58	3.34×10^{-5}	+98
+850*	1.25	4.02	3.42×10^{-5}	+232
	6.0	4.02	9.39×10^{-4}	+151

* 0.15N sodium borate-acetic acid solutions.

† . . . Value of potential was corrected with the aid of the equation shown in section on Effect of $[Fe^{++}]$ and pH on the static passive potential.

and pH. The measured points indicated in Fig. 4 as circles are obtained for the specimen prepolarized at +850 mv for various periods of time ranging from 1 to 15 hr. The points indicated by triangles correspond to prepolarization at -100 mv, the times ranging from 2 to 16 hr. On the basis of this experiment, the static passive potential can be expressed as $E_{stat.} = 958 - 163 \text{ pH} - 60 \log [Fe^{++}]$ mv (vs. N.H.E.).

Decay of the polarized potential and the effect of Fe^{++} ion on it.—The static potentials mentioned above were obtained after the decay of the polarized passive potential on open circuit. The characteristics of the decay of potential will now be described in this section. Curves 1, 2, and 3 in Fig. 6 were obtained in standard solution (pH 8.41) without the addition of ferrous ion. The specimens were prepolarized at +850 mv for various periods of

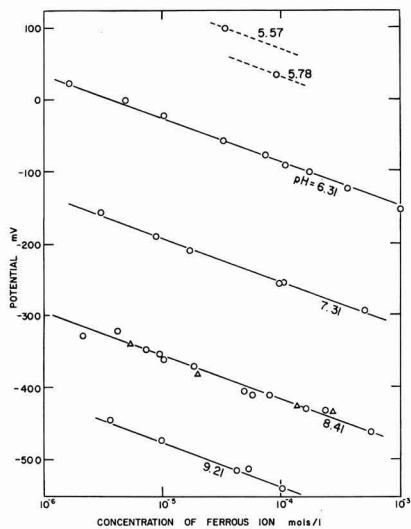


Fig. 4. Effect of ferrous ion concentration on the static potential of passive iron; \circ , $E_a = +850$ mv; Δ , $E_a = -100$ mv; 0.15N boric acid-borate solutions.

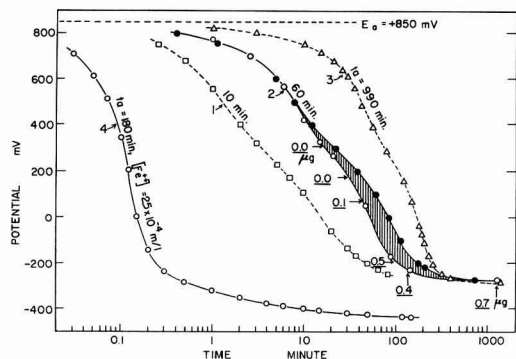


Fig. 6. Effect of time of anodic polarization and ferrous ion addition on the decay of the polarized potential. Numbers attached to curve 2 indicate the amount of Fe^{++} ion found in solution during the decay of potential.

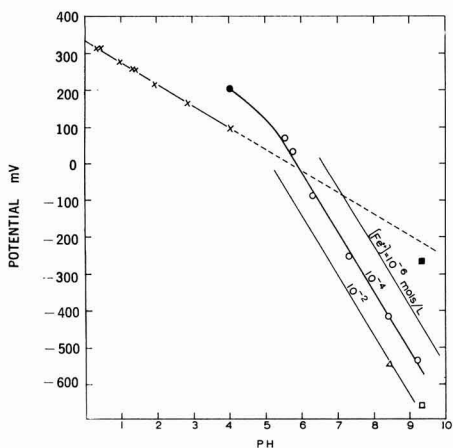


Fig. 5. Effect of pH on the static potential of passive iron. \circ , 0.15N boric acid-borate solutions (pH, 5-9); \bullet , 0.15N acetic acid-borate solutions (pH, -4); X, results obtained by Franck for acid solutions; Δ , passivation potential E_a^1 appeared in the anodic polarization curve (standard solution at pH, 8.41); \square , passivation potential E_a^1 and activation potential E_a^2 which appeared in the anodic polarization curve and in the cathodic reduction curve, respectively, of Heusler, Weil, and Bonhoeffer for borate solution at a pH of 9.3.

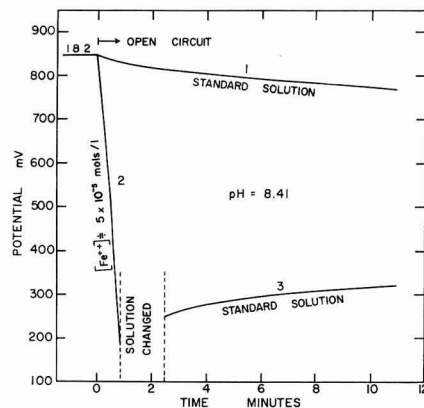


Fig. 7. Effect of the change of solution on the behavior of decay of potential. Expt. 1, the decay of potential was followed in the standard solution for a specimen prepolarized at +850 mv for 960 min in the same solution; Expt. 2, after Expt. 1, the specimen was polarized again at +850 mv for 60 min in the standard solution and the decay of potential was followed in another solution containing about 5×10^{-5} mole/l ferrous ion; Expt. 3, after Expt. 2, cell and specimen were both quickly rinsed twice with standard solution and the change of potential with time was followed on open circuit in the standard solution.

time. It is seen that there is no sharp drop of potential on cutting the current and that the rate of decay is fairly slow and decreases with the time of prepolarization; the reproducibility of the curves becomes worse below about +300 mv. The amount of Fe^{++} ion dissolution during the decay was then followed by separate experiments. From the results indicated by the numbers on curve 2, it seems that Fe^{++} ion dissolution begins to occur below about the characteristic potential E_a^2 (0 mv) even though the amount detected was very small. No effect of

stirring of the solution was observed in these experiments.

It was found that the addition of large amounts of Fe^{++} ion to the solution accelerated the decay quite remarkably. In this case the rate of decay was observed to increase sharply by stirring. Curve 4 in Fig. 6 was obtained for a Fe^{++} ion concentration of 2.5×10^{-4} mole/l after 3-hr prepolarization in a solution without Fe^{++} ion addition. The final static potential obtained in this case is, of course, much lower compared to that shown in curves 1, 2, and 3, as would be expected from the much higher concentration of Fe^{++} ion in solution.

In the next experiment, after following the decay of potential for a short time in a solution containing a large amount of Fe^{++} ion, the cell and specimen were both quickly rinsed with the standard solution, and the change of potential with time was traced on open circuit in the standard solution (Fig.

7). As can be seen, a slow rise of potential was obtained instead of the continuation of the decay. The same sort of potential change was observed after interruption of a cathodic current which had been applied to the passive specimen for a short period of time.

Change of cathodic reduction curve during decay.

—In order to obtain further knowledge of the mechanism of the decay of the polarization potential, two kinds of experiments were conducted in the standard solutions for specimens prepolarized at +850 mv for 1 hr: expt. 1, cathodic reduction curves were observed at different times during the decay without the addition of Fe^{++} ion to the solution; expt. 2, after draining the solution after passivation, dried specimens were exposed to a nitrogen atmosphere for different periods of time, and cathodic reduction curves were then measured.

The cathodic reduction curve obtained is always of a typical shape having three arrests or two waves as can be seen in Fig. 2. In general, the transition from the first to the second wave becomes sharper with the time of decay or of nitrogen exposure. The change in the number of coulombs Q_c^1 and Q_c^2 associated with the first and the second waves was followed in expt. 1 and 2; the results are shown in Tables III and IV, respectively. In the preceding investigation (1), the first and the second waves were shown to correspond to the reduction of the outer " $\gamma-Fe_2O_3$ " layer to Fe^{++} ion in solution and to the reduction of the inner Fe_3O_4 layer to metallic iron, the current efficiency of these reactions being almost 100% and 40%, respectively. If it is assumed here that the over-all current efficiency of these reduction reactions does not change with the time of decay or of exposure, the change in the values of Q_c^1 and Q_c^2 would give a rough idea of the change of composition of the passive film with time.

Table III. Effect of the time of decay on the cathodic reduction curve

No.	Time of decay, min	Static potential after decay, mv	Q_c^1 , mc/cm ²	ΔQ_c^1 , mc/cm ²	Q_c^2 , mc/cm ²	ΔQ_c^2 , mc/cm ²
0	0	+850	1.540	1.54	3.92	—
0'	0	+850	1.541			
0''	0	+850	1.534			
1	18	+380	1.53	-0.07	3.91	-0.01
2	27	+330	1.51	-0.03	3.88	-0.04
3	58	+188	1.50	-0.04	4.01	+0.09
4	125	+20	1.48	-0.06	3.94	+0.02
5	289	-190	1.42	-0.12	4.16	+0.24
6	295	-233	1.40	-0.14	4.22	+0.30
7	1260	-270	1.36	-0.18	—	—
7'	1260	—	1.38	-0.18	4.32	+0.40

Table IV. Effect of the time of exposure to a nitrogen atmosphere on the cathodic reduction curve

No.	Time of exposure, min	Static potential after exposure, mv	Q_c^1 , mc/cm ²	ΔQ_c^1 , mc/cm ²	Q_c^2 , mc/cm ²	ΔQ_c^2 , mc/cm ²
0	0	+850	1.54	—	3.92	—
1	90	+250	1.48 ₅	-0.05 ₅	4.05	+0.13
2	960	+92	1.43	-0.11	4.25	+0.33
3	5280	-63	1.39	-0.15	4.83	+0.91

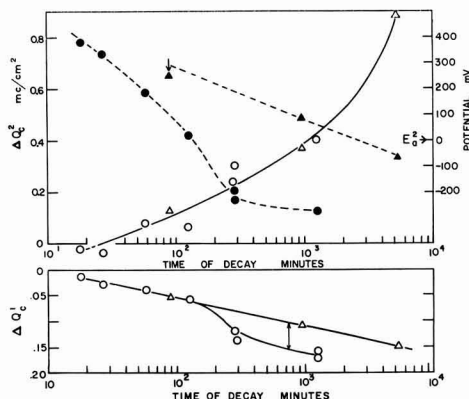


Fig. 8. Change in the amount of charge associated with the first and the second waves of the cathodic reduction curve during the decay of polarized potential. \circ , Q_c^1 or Q_c^2 for Expt. 1; Δ , Q_c^1 or Q_c^2 for Expt. 2; \bullet , \blacktriangle , potential of the specimen just before the cathodic reduction experiment; \downarrow , potential changing fairly rapidly.

As can be seen in the above tables, the results obtained in both experiments are quite similar; Q_c^1 decreasing and Q_c^2 increasing with time. This could be interpreted simply as a decrease in the amount of defects and $\gamma-Fe_2O_3$ and an increase of the amount of Fe_3O_4 with time. However, as can be seen in Fig. 8, $|\Delta Q_c^1|$ increases rapidly in the first type of experiment after about 100 min when the potential has fallen to the region of the characteristic potential E_a^2 of about 0 mv where the commencement of Fe^{++} ion dissolution is to be expected. The change of Q_c^2 with time on the other hand appears to be unaffected by the presence of the solution.

Discussion

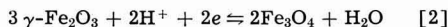
Previous Theories on the Passivation Potential

The anodic passivation of iron is characterized by the existence of a passivation potential above which passivity becomes stable, so that, in order to discuss the mechanism of passivity, it is quite essential to understand the significance of this potential. It has been observed for iron in an acidic solution that the passivation potential observed in a potentiostatic polarization experiment has almost the same value as the Flade potential-arrest which is observed just before the spontaneous activation of the passive specimen occurs (3, 4). Franck (5) measured the effect of pH on the Flade potential by using several kinds of buffer solutions at values of pH from 0.3 to 4 and obtained the empirical equation

$$E = 580 - 59 \text{ pH mv (vs. N.H.E.)} \quad [1]$$

Most previous theories of passivation more or less attempt to explain Eq. [1]. However, attempts to interpret the Flade potential as corresponding to the equilibrium potential of formation of any known oxide from metallic iron have been unsuccessful because the theoretical values are always far lower (by about 660 mv) than the experimental values. In order to avoid this difficulty, Beinert and Bonhoeffer (6) first assumed an oxygen-rich iron oxide of unknown structure as the passive film. Pryor (7)

recently proposed a somewhat continuous change of defect structure with thickness in a single phase γ - Fe_2O_3 film, the inner and the outer part of the film being a metal excess and an oxygen excess type of oxide, respectively. He suggested that the structure of the outermost part of film controls the behavior of the Flade potential. Göhr and Lange (8, 9) and later Vetter (10) pictured the system as being $\text{Fe}/\text{Fe}_3\text{O}_4/\gamma\text{-Fe}_2\text{O}_3/\text{H}_2\text{O}$ and explained the passivation potential as the equilibrium potential of the reaction



They considered that the chemical potential of iron in the magnetite layer decreases with the distance outward from the metal surface in accordance with the inner potential difference across the film when the electrode $\text{Fe}/\text{Fe}_3\text{O}_4/\text{H}_2\text{O}$ is anodically polarized; at the distance where the potential lowering comes to a value ($\Delta\phi = 660$ mv) corresponding to the change in the free energy of the reaction³ $3\text{Fe}_3\text{O}_4 \rightarrow 4\gamma\text{-Fe}_2\text{O}_3 + \text{Fe}$, the formation of $\gamma\text{-Fe}_2\text{O}_3$ occurs to give a duplex layer and resulting passivity. According to Vetter's concept, there is no further change of composition with thickness in the outer $\gamma\text{-Fe}_2\text{O}_3$ layer and growth of film occurs simply forced by the field strength set up across the layer. He also considered that, after the interruption of the circuit, once the outer $\gamma\text{-Fe}_2\text{O}_3$ was consumed by slow dissolution in an acid solution it was followed by an extremely rapid dissolution of the magnetite layer and resulting activation. Heusler, Weil, and Bonhoeffer (11, 12) observed that in neutral and alkaline solutions the values of passivation potentials were much more negative than that expected from Eq. [1]. They explained that the primary Fe_3O_4 film is sufficiently insoluble to produce "pseudopassivity," and that "real passivation" occurs when the potential is raised to the equilibrium potential of the formation of $\gamma\text{-Fe}_2\text{O}_3$ from Fe_3O_4 . Cartledge (13) interpreted the passivation potential in a similar way as Lange and Vetter by postulating an electrode system of $\text{Fe}|\text{FeO}|\text{Fe}_2\text{O}_3|\text{H}_2\text{O}$.⁴ In contrast to these workers Uhlig and King (14) have considered that the Flade potential is an equilibrium potential for the reduction of chemisorbed oxygen atoms and molecules on the surface of iron.

The data reported here show that the passivation potential and the static potential observed after the decay of the polarized anodic potential are essentially the same and is dependent on both $[\text{Fe}^{++}]$ and pH. Because the above considerations are inadequate for the explanation of these results a new mechanism is proposed for anodic passivity in neutral solutions.

Effect of Fe^{++} Ion on the Formation of the Passive Film

In the previous paper (1) it was observed that there was a region in the anodic passivation range (-550 mv to -200 mv) where Fe^{++} was found in

³ The value of the chemical potential of "oxide" is chosen so as to explain the Flade potential which was measured by Franck in acidic solutions.

⁴ See footnote 3.

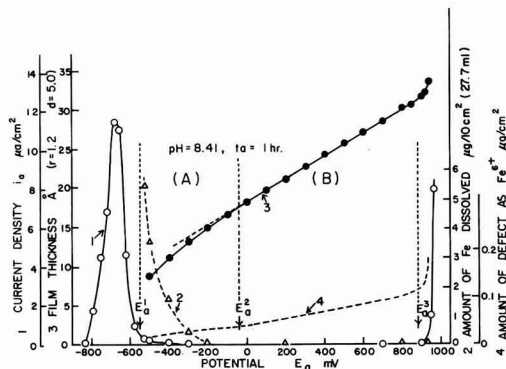


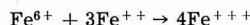
Fig. 9. Anodic polarization curve and effect of potential on the amount of Fe^{++} ion dissolution, film thickness, and on the amount of defects.

solution after 1 hr of polarization. This is shown in Fig. 9. When ferrous ion is added to a solution in which iron with the passive film is being anodically polarized (Fig. 1) it is converted to Fe_2O_3 at a rate dependent on the concentration of Fe^{++} and the applied potential. At sufficiently high applied potentials the rate of oxidation to Fe_2O_3 is simply diffusion controlled (Fig. 3). In the absence of an applied current and at constant pH the static potential is dependent on $[\text{Fe}^{++}]$. It was also observed that the decay rate of the potential of films formed at higher oxidation potentials was increased by the addition of Fe^{++} ion to the solution.

In the previous paper a characteristic potential (E_a^2) was observed at which there was an increase in the rate of formation of vacancies in the outer layer of oxide with potential (Fig. 9). On the basis of the above observation this potential would appear to correspond to a range in which the $[\text{Fe}^{++}]$ is so low that it cannot affect the rate of formation of vacancies by reaction with the outer layer of oxide. Thus, although E_a^2 is not a specific potential relating to a reaction, it is convenient to discuss the range of potentials in which passivity is obtained in two regions, "Region A" where Fe^{++} in solution is observed, and "Region B" where the $[\text{Fe}^{++}]$ is too low for analysis.

Behavior of Passive Iron in Region A

It is to be expected from the above that the defect concentration in the extreme surface of the oxide found previously (1) is maintained at almost zero in the potential region A because of the reaction of defects with Fe^{++} ion in the solution. If the defect is expressed as Fe^{6+} ion, the reaction will be



The rate of the reaction is assumed to be very high due to the relatively high concentration of Fe^{++} ion in this potential region; the rate must be a function of the concentration of the surface defects and of the $[\text{Fe}^{++}]$ in solution.

The possible change in the final composition of the oxide film with distance from the metal is shown schematically as curve A in Fig. 10; the film will consist of $\gamma\text{-Fe}_2\text{O}_3$, with a more or less defect

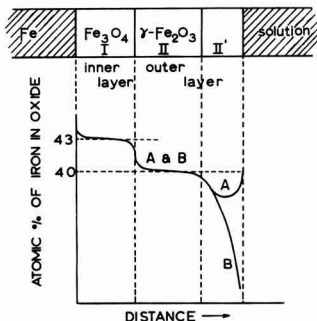


Fig. 10. Possible change of composition of the passive film with thickness: curve A, potential region A; curve B, potential region B.

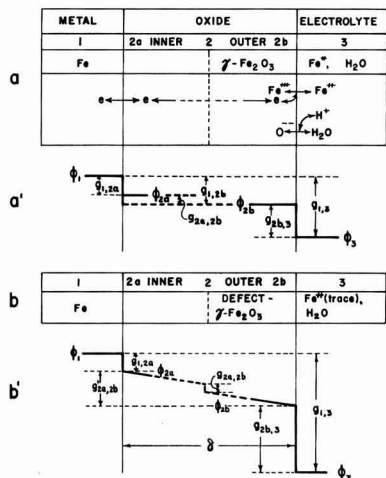


Fig. 11. Phase arrangement of the electrode system and the distribution of inner potential across the phases: a, a', potential region A; b, b', potential region B.

structure, and Fe₃O₄ layers, the latter being adjacent to the metal. In the initial period of passivation for a cathodically pretreated specimen the passive oxide film, whose change of composition with thickness is shown as curve B, is formed by the high potential gradient initially applied across the film. As Fe⁺⁺ ions are accumulated in the solution with time, the composition of the extreme surface of the oxide changes toward that of stoichiometric γ-Fe₂O₃. However, since the rate of migration of defects from the interior part of the film is quite small, the defects in the interior cannot be eliminated within the ordinary time of the experiment. Hence even in region A after 1-hr polarization a small number of defects is observed by analysis (Fig. 9).

If we assume here that the interior part of the oxide film, whatever composition it has, behaves merely as an electronic conductor, the passive iron would behave basically as an electrode system of Fe|γ-Fe₂O₃|Fe⁺⁺, H₂O, irrespective of the existence of an inner oxide layer having a different composition.

Derivation of Potential in Region A

Figure 11(a) shows the schematic phase arrangement of the electrode system and the possible partial reactions at interfaces. In a pseudoequilibrium condition⁵ of this electrode, the inner potential difference (*g*) across each interface can be expressed in terms of the chemical potential (*μ*) of the substances which participate in each partial reaction. Between the metal (phase 1) and the outer oxide (phase 2b), electron transfer reactions are



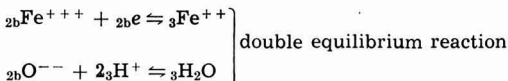
so that the inner potential difference between the metal and the outer oxide can be expressed as

$$g_{1,2b} = \phi_1 - \phi_{2a} + \phi_{2a} - \phi_2 + \phi_2 - \dots - \phi_{2b} = \phi_1 - \phi_{2b} = - ({}_1\mu_e - {}_{2b}\mu_e) / -F \quad [4]$$

where ϕ is the inner potential of a phase.

Thus, as far as the expression of $g_{1,2b}$ is concerned, the presence of the inner oxide layers having different compositions can be neglected.

At the oxide/solution interface



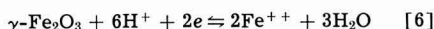
$$\therefore g_{2b,3} = \phi_{2b} - \phi_3 = - ({}_{2b}\mu_{Fe^{+++}} + {}_{2b}\mu_e - {}_3\mu_{Fe^{++}} - {}_3\mu_{H_2O} - {}_{2b}\mu_{O^{--}} - {}_3\mu_{H^+}) / 2F = - ({}_3\mu_{H_2O} - {}_{2b}\mu_{O^{--}} - {}_3\mu_{H^+}) / 2F \quad [5]$$

As can be seen in Eq. [5], the value of $g_{2b,3}$ is determined only by the chemical potential or the activity of H⁺ ion in solution if the composition of the surface oxide is constant, since in this condition ${}_3\mu_{H_2O}$, ${}_{2b}\mu_{Fe^{+++}}$ and ${}_{2b}\mu_{O^{--}}$ are expected to be constant. The chemical potential of the electron, ${}_{2b}\mu_e$, is considered to be a function of the chemical potential or the activity of Fe⁺⁺ ion in solution when the composition of the surface oxide and the activity of H⁺ ion are constant, so that, if the activity of Fe⁺⁺ ion is changed, $g_{1,2b}$ will be changed according to Eq. [4] because the value of ${}_1\mu_e$ is expected to be constant.

The electrode potential is the sum of the inner potential difference across the interfaces so that

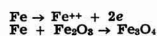
$$g_{1,3} = \phi_1 - \phi_3 = g_{1,2b} + g_{2b,3} = ({}_{2b}\mu_{\gamma-Fe_2O_3} + {}_3\mu_{H^+} + {}_{2b}\mu_e - {}_3\mu_{Fe^{++}} - {}_3\mu_{H_2O}) / 2F$$

This corresponds to the equilibrium potential of the net reaction of



If $g_{1,3}$ is measured against the normal hydrogen electrode as E_{H_2} , using the relation $\mu = \mu^\circ + RT \ln a$,

⁵ Strictly speaking one cannot use the term equilibrium in a system of this type. Obviously in the thermodynamic sense, iron is essentially unstable when anodically polarized in a water solution due to such reactions as



However, in that it is observed that these reactions take place only extremely slowly in this system, one can use the term equilibrium while meaning "pseudoequilibrium."

the dependence of E_h on $[\text{Fe}^{++}]$ and pH can be expressed as

$$E_h = \{(\mu^\circ_{\gamma\text{-Fe}_2\text{O}_3} + 6\mu^\circ_{\text{H}^+} - 2\mu^\circ_{\text{Fe}^{++}} - 3\mu^\circ_{\text{H}_2\text{O}})/2F\} + (3RT/F) \ln a_{\text{H}^+} - (RT/F) \ln a_{\text{Fe}^{++}} = E_h^\circ - 177 \text{ pH} - 59 \log a_{\text{Fe}^{++}} \text{ mv } (25^\circ\text{C}) \quad [7]$$

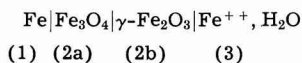
The equilibrium potential of the electrode is a function of only $[\text{Fe}^{++}]$ and pH, since the chemical potential of the outer $\gamma\text{-Fe}_2\text{O}_3$ is expected to be constant as far as it has constant stoichiometric composition. Thus, the change of the inner potential across the phases is shown schematically in Fig. 11a. Equation [7] is supported by the data shown in Fig. 4 and 5.

If passive iron in pseudoequilibrium at a constant pH is anodically polarized by ΔE in this potential region A, a flow of electrons across the film toward the metal/oxide interface occurs in accordance with the effective potential gradient $\Delta E/\delta^6$ (δ : film thickness) set up in the film, being accompanied by the oxidation of Fe^{++} ion to $\gamma\text{-Fe}_2\text{O}_3$ at the oxide/solution interface. The consumption of Fe^{++} ion in solution is continued slowly until the change of $g_{1,2b}$ compensates the polarization ΔE . In other words, at equilibrium obtained after an infinite passage of time the applied polarization will be off-set by a change of the potential difference between the outer oxide and metal $g_{1,2b}$ (the concentration polarization of Fe^{++} ion), and there will be no gradients of potential in the body of the oxide, such gradients existing only during electron flow in the approach to equilibrium. During the nonsteady state of polarization, growth of the film due to the migration of iron ions outward from the metal is also possible under the influence of the potential gradient that exists in the film. It should be emphasized here that, in ordinary times of experiment, such a pseudoequilibrium state is not attained, even though the changeable potential difference ΔE (effective potential gradient $\Delta E/\delta$) across the film is very small compared to the total potential difference $g_{1,3}$.

Significance of the Passivation Potential

The effect of $[\text{Fe}^{++}]$ and pH on the static passive potential (Flade potential), which was described above, is in fairly good agreement with Eq. [7]. Accordingly the passivation potential observed in neutral borate solutions can be interpreted as corresponding to the equilibrium potential for the reaction between $\gamma\text{-Fe}_2\text{O}_3$ and Fe^{++} ion in solution. Thus, in region A, it seems quite likely that the passive film obtained in this experiment behaves simply as an $\text{Fe}|\gamma\text{-Fe}_2\text{O}_3|\text{Fe}^{++}, \text{H}_2\text{O}$ electrode in the presence of Fe^{++} ion in solution, even though the composition of the interior part of the film is different from the nearly stoichiometric $\gamma\text{-Fe}_2\text{O}_3$ that exists at the surface of oxide. This behavior is expected for the passive film which has been shown to be a duplex type of oxide electrode which, by ignoring complications due to the variation of defect concen-

tration in the interior (cf. Fig. 9), can be simply expressed as



To get agreement in behavior it is necessary to assume that the oxide is a good electronic conductor and that the exchange rates of the partial reactions at the oxide/solution interface (${}_{2b}\text{Fe}^{++} + {}_{2b}\text{e} \rightleftharpoons {}_3\text{Fe}^{++}$ and ${}_{2b}\text{O}^{--} + {}_2\text{H}^+ \rightleftharpoons {}_3\text{H}_2\text{O}$) are much greater than that of the partial reaction at the oxide/oxide interface (${}_{2a}\text{Fe}^{8/3+} \rightleftharpoons {}_{2b}\text{Fe}^{++} + 1/3 \text{e}$). The exchange current of the latter reaction which is accompanied by the movement and the rearrangement of iron ions and oxygen ions in the oxide phase must be extremely small. It was shown previously in the cathodic reduction experiment (1) that the reduction of $\gamma\text{-Fe}_2\text{O}_3$ to Fe^{++} ion in solution begins to occur with almost 100% current efficiency when the potential is lowered to the region of passivation potential E_a^1 . It is seen, on the other hand, in the section on Effect of ferrous ion on the polarization curve, that the change of potential above E_a^1 causes the reaction from Fe^{++} to Fe_2O_3 to occur, again with almost 100% current efficiency. These experimental facts give clear evidence of the validity of the assumption that the oxide is a good electronic conductor and that the potential-determining reaction is the reaction at the oxide-solution interface.

Heusler, Weil, and Bonhoeffer (11) compared, in their measurements conducted in a borate solution (pH = 9.3), the value of the passivation potential E_a^1 obtained when active iron is anodically polarized by a stepwise potentiostatic method and that of the potential $E_a^{1'}$, at which a specimen completely passivated at relatively high potential begins to be reduced cathodically to the active state. As is indicated in Fig. 5 for purpose of comparison with the result of our static potential (Flade potential) measurements their potential E_a^1 is in the same region as ours, but $E_a^{1'}$ is much more positive (by about 500 mv) than E_a^1 . Their explanation was that E_a^1 and $E_a^{1'}$ correspond to the potentials of the formation of Fe_3O_4 and Fe_2O_3 which produce "pseudo-" and "real-passivity," respectively; the pseudopassivity is expected only in neutral and alkaline solutions in which the rate of dissolution of Fe_3O_4 is sufficiently small to produce passivity (cf. section on Previous Theories on the Passivation Potential). However, their explanation does not fit our previous experimental result (1) which shows that the formation of a substantial amount of $\gamma\text{-Fe}_2\text{O}_3$ begins to occur at the passivation potential corresponding to their potential E_a^1 , where they postulate the presence only of Fe_3O_4 . The above disagreement between E_a^1 and $E_a^{1'}$ should be interpreted in terms of Fe^{++} ion concentration which is in equilibrium with $\gamma\text{-Fe}_2\text{O}_3$, the passive oxide. In precise terms, the potential they measured as E_a^1 will correspond to a fairly high concentration of Fe^{++} ion because an initially active specimen is gradually passivated; the potential $E_a^{1'}$, on the other hand, is considered to correspond to a much lower concentration of Fe^{++} and consequently higher concentration of defects in the surface of oxide (cf. section on Deriva-

⁶ ΔE does not include the inner potential difference originally existing between different oxide phases.

tion of Potential in Region A) which is observed if the specimen has been maintained at a sufficiently high potential for a sufficient period of time.

As can be seen in Fig. 5, the results of our static potential measurements obtained over a pH range of 5-9 at various Fe^{++} ion concentrations on extrapolation to the acidic region do not agree with those obtained by Franck (5) for specimens passivated in acidic solutions. The cause of the disagreement is not clear at the moment. However, the nature of the passive film and the mechanism of passivity for iron in strongly acidic solution may be quite different, by judging from the fact that the addition of Fe^{++} ion to the solution and stirring of the solution do not change the size of anodic current i_a in the passive potential region (15).⁷ It may be that, in view of the high rate of autoreduction in acid solutions, the decay potential observed is a highly polarized mixed potential.

Behavior of Passive Iron in Region B

As has been described above, the concentration of Fe^{++} in the vicinity of the oxide/solution interface is considered to be extremely small when the potential of the passive iron is held in the higher potential region B. In this case, the change in the composition of film with thickness is expressed by curve B in Fig. 10 and the passive iron is assumed to behave essentially as an electrode system of $\text{Fe}|\text{defect } \gamma\text{-Fe}_2\text{O}_3|\text{Fe}^{++}$ (very dilute), H_2O , the phase arrangement being shown in Fig. 11b. The partial reactions occurring at the interfaces are considered to be essentially the same as those assumed for the electrode system in the potential region A (Fig. 11a'), except for the additional effect of the defects, which appear in the surface of the oxide in this potential region, on the reaction at the oxide/solution interface. At the pseudoequilibrium condition of this electrode, the total potential difference $g_{1,3}$ is much larger than that in region A because of the unusually low activity of Fe^{+++} ion (or the correspondingly high activity of O^{--} ion) in the oxide phase as well as the extremely low concentration of Fe^{++} ion in solution. The appearance of surface defects in potential region B provides a second form of concentration overpotential because the concentration of defects, as well as H^+ ions in solution, can also change the value of $g_{2b,3}$.

When the specimen is anodically polarized in the potential region B, a potential gradient is set up across the film and defects begin to be produced by the removal of electrons from Fe^{+++} ions at the oxide surface, accompanied by the transfer of the corresponding excess amount of O^{--} ion from the solution ($3\text{H}_2\text{O} \rightarrow 2\text{O}^{--} + 2\text{H}^+$). Simultaneously, growth of the film and a decrease of Fe^{++} ion in the vicinity of the oxide surface take place. However, since there is a tendency for migration of defects from the surface to the interior part of the film, it will take a very long time to attain a steady concentration of defects at the oxide surface under constant applied potential. At the pseudoequilibrium condition, the distribution of defects across

the film (cf. Fig. 10, curve B), the surface concentration of defects, and also the surface concentration of Fe^{++} ion remain unchanged with time, and the changes in the values of $g_{1,2b}$ and $g_{2b,3}$ almost completely compensate the applied polarization for the $\text{Fe}|\gamma\text{-Fe}_2\text{O}_3|\text{Fe}^{++}$, H_2O electrode. For the intermediate stage before equilibrium, the effective potential gradient across the film

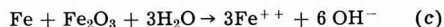
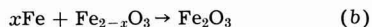
$$\Delta E/\delta = (g'_{2a,2b} - g_{2a,2b})/\delta$$

is shown schematically in Fig. 11b'.

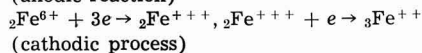
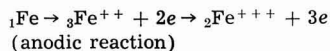
As can be expected from the above, the potential gradient across the film ΔE would be much greater if the defects were not produced under the same applied potential. Thus, the role of defects in the mechanism of passivity is simply to decrease the effective potential gradient across the film, which will be the driving force for film growth by the migration of cations through the oxide film. The decrease in slope of the film thickness-potential curve observed above the potential E_c^2 , that was described in the section on the Effect of Fe^{++} on the Formation of the Passive Film, can thus be explained as being due to the beginning of an increase in surface defect concentration with potential.

Mechanism of the Decay of the Polarized Potential

The characteristics of the decay of the polarized potential on open circuit in solutions initially free from ferrous ion can be explained in terms of the change in the pseudoequilibrium potential of the Fe defect $\gamma\text{-Fe}_2\text{O}_3|\text{Fe}^{++}$, H_2O electrode due to changes in both the concentration of defects and of Fe^{++} ion. As can be seen in Fig. 6 there is no major change in potential immediately after stopping the current. This observation is consistent with the view that the polarized potential is very close to the equilibrium potential of the defect oxide. The relatively slow decay of the potential to the static potential characteristic of $\gamma\text{-Fe}_2\text{O}_3$ is due to reactions, probably diffusion controlled, between the substrate metal and the oxide. The over-all reactions are as follows



Reaction (c) is only possible when the specimen is in contact with the solution. These reactions can be divided into the partial reactions



In the absence of solution iron diffuses from the metal into the oxide to give both reactions (a) and (b) as can be seen from Fig. 8. There is an increase in the amount of magnetite and a decrease in the amount of Fe_2O_3 . This reaction should take place by diffusion of ferrous ion and electrons and, if this is the only diffusion process taking place, the composition of the surface of the oxide, and hence the immersion potential, should not be changed until

⁷ This has been partially confirmed in our experiment for a borate-acetic acid solution at pH of 4. However, the effect of Fe^{++} ion on the static passive potential is observed even in this solution (cf. Table II).

practically the whole of the oxide is changed to Fe_3O_4 . Electron diffraction examination of the anodic oxide (1) gave patterns and spot sizes very similar to those observed previously (16). These patterns were interpreted to mean that the particle size in this highly oriented film is only 30–50Å, and hence there are a large number of grain boundaries. Grain boundary diffusion is much faster than bulk diffusion. One might therefore expect pipes of Fe_3O_4 at the grain boundaries which would allow more rapid access of Fe^{++} and electrons to the oxide surface. These would combine to reduce the concentration of defects at the surface and hence the immersion potential long before the body of the oxide is converted by simple bulk diffusion. This gradual conversion of the oxide to Fe_3O_4 was also noted in a previous study (16).

In the presence of solution the process of conversion of the surface of the oxide to stoichiometric oxide and finally the reductive dissolution of the $\gamma\text{-Fe}_2\text{O}_3$ is accelerated by reaction (c). Iron ions can be supplied both by diffusion through the magnetite pores and by reductive dissolution of any stoichiometric $\gamma\text{-Fe}_2\text{O}_3$. In region B any iron ion which gets into the solution will be consumed by reaction with nonstoichiometric oxide on the surface with a subsequent decrease in potential. When the potential reaches region A at about 0 mv (E_a^2), some iron should appear in the solution, and the potential will gradually approach the static potential for $\gamma\text{-Fe}_2\text{O}_3$ characteristic for this pH and $[\text{Fe}^{++}]$. As can be seen in Fig. 8, although the composition of the outer layer is changed more rapidly in the solution than in nitrogen, the rate of growth of magnetite is essentially the same. This indicates that bulk diffusion in both cases is equal. A considerable time will elapse before the steady state is attained because of the slow migration of defects from the interior to the surface of the oxide film. At a constant pH, the static potential is determined only by the existing Fe^{++} ion concentration whereas the potential during the decay is a function of the concentration of both defects and Fe^{++} ions. During the decay of potential in this region slight thinning of the film due to autoreduction is to be expected in spite of the thickening due to the migration of iron through the film. As a matter of fact, the amount of corrosion, $0.5 \mu\text{g Fe}^{++}/10 \text{ cm}^2$, estimated⁸ from the deviation of the Q_c /time curve for Expt. 1 from that for Expt. 2 (Fig. 8) is of the same order of magnitude as that obtained by an analysis of the solution which is indicated in Fig. 6. It should be pointed out here that Fe^{++} ion dissolution was detected only when the potential came down to about 0 mv (E_a^2) whereas no change in the solution was observed above this potential (Fig. 8).

The above conclusion is supported by the fact that a marked potential decay occurs very rapidly when the specimen is put in contact with a large number of Fe^{++} ions in solution (Fig. 6). The rise of potential observed after changing the solution containing Fe^{++} ion to the standard solution (Fig. 7') constitutes strong evidence for the migration of

defects from the interior to the surface of the oxide during the potential decay.

General Mechanism for Film Growth and Breakdown

On the basis of the above data and discussion it is now possible to propose a general mechanism for the formation, stability, and breakdown of the anodically formed oxide films (passive films) in neutral solutions.

When an anodic potential is first applied to a film-free iron specimen the iron is oxidized to form both a film of magnetite and ferrous ion in solution. When the applied anodic potential is above the range where $\gamma\text{-Fe}_2\text{O}_3$ is stable, $\gamma\text{-Fe}_2\text{O}_3$ is formed on top of the magnetite, and any excess ferrous ion in the solution over the equilibrium value is also oxidized at the oxide-solution interface to form $\gamma\text{-Fe}_2\text{O}_3$. In the initial stages the film is thin so that there is a high potential gradient across the film and thickening occurs rapidly. However as the potential gradient decreases with thickening the rate of migration also decreases and the anodic current drops. The second factor leading to a decrease in the film growth rate is a change in the composition of the outer layer of oxide. As the equilibrium concentration of Fe^{++} in the solution drops to a very low number (around E_a^2) it becomes possible to form an oxide with cation defects at the surface because of the strong oxidizing conditions. The higher equilibrium potential associated with this defect oxide leads to a further decrease in the potential gradient across the film which is finally almost independent of applied potential because of the combination of thicker films and increased cation vacancies (accompanied by a higher "equilibrium potential") at the higher applied anodic potential.

Only those films formed close to the passivation potential (E_a^1) will give equilibrium behavior with regard to $[\text{Fe}^{++}]$ and pH. Films formed at higher potentials tend to change to the equilibrium type film on cessation of anodic polarization. This decay of the potential can occur naturally by diffusion or autoreduction through "pores" and can be accelerated by the addition of ferrous ion to the solution or slight cathodic treatment. In the long run all of the oxide may be removed by autoreduction and the reaction of iron to give ferrous ion in solution will predominate. This latter condition, of course, is the active state.

Any discussion of this paper will appear in a Discussion Section to be published in the December 1963 JOURNAL.

REFERENCES

1. M. Nagayama and M. Cohen, *This Journal*, **109**, 781 (1962).
2. F. Flade, *Z. physik. Chem.*, **76**, 513 (1911).
3. U. F. Franck, *Z. Elektrochem.*, **55**, 154 (1951).
4. U. F. Franck and K. G. Weil, *ibid.*, **56**, 814 (1952).
5. U. F. Franck, *Z. Naturforsch.*, **4a**, 378 (1949).
6. H. Beinert and K. F. Bonhoeffer, *Z. Elektrochem.*, **47**, 536 (1941).
7. M. J. Pryor, *This Journal*, **106**, 557 (1959).

⁸ For the purpose of the calculation, the reactions were assumed to be $\text{Fe} \rightarrow \text{Fe}^{++} + 2e$; $\gamma\text{-Fe}_2\text{O}_3 + 6\text{H}^+ + 2e \rightarrow 2\text{Fe}^{++} + 3\text{H}_2\text{O}$.

8. H. Göhr and E. Lange, *Naturwiss.*, **43**, 12 (1956).
9. H. Göhr and E. Lange, *Z. Elektrochem.*, **61**, 1291 (1957).
10. K. J. Vetter, *ibid.*, **62**, 642 (1958).
11. Heusler, K. G. Weil, and K. F. Bonhoeffer, *Z. physik Chem., N.F.*, **15**, 149 (1958).
12. K. G. Weil and K. F. Bonhoeffer, *ibid.*, **4**, 175 (1955).
13. G. H. Cartledge, *J. Phys. Chem.*, **60**, 1571 (1956).
14. H. H. Uhlig and P. F. King, *This Journal*, **106**, 1 (1959).
15. K. J. Vetter, "Passivierende Film und Deckschichten," p. 87, Springer-Verlag, Berlin (1956).
16. P. B. Sewell, C. D. Stockbridge, and M. Cohen, *This Journal*, **108**, 933 (1961).

Valency Changes in the Surface Oxide Films on Metals

H. S. Isaacs and J. S. Llewelyn Leach

Metallurgy Department, Imperial College of Science and Technology, London, England

ABSTRACT

Two methods are described by which a square current pulse may be used to measure the surface capacity and resistance of metal electrodes immersed in an electrolyte. The methods have been applied to the study of electrodes of aluminum, tantalum, and zirconium, and to electrodes of titanium, niobium, vanadium, and uranium. The first group shows surface capacities which vary with the hydrogen content of the oxide but which are always less than those of the double layers. The second group shows surface capacities greatly in excess of those associated with double layers, and these have been interpreted in terms of reversible reactions occurring within the oxide layers.

It has been suggested that hydrogen, formed as a corrosion product, may influence the physical or chemical properties of the protective oxide, and the resulting change may give rise to enhanced corrosion (1, 2). A change in the valency of the metal ion has also been suggested as a cause of change in the corrosion rate. However, considerable difficulties are involved in directly examining the properties of these oxide films without altering their characteristics.

Of the indirect techniques available, a-c measurements are one of the most sensitive for determining the properties of metal electrodes in solutions, and the use of these methods has contributed substantially to the understanding of the properties of and processes occurring at electrode surfaces (3, 4). The results of such measurements can be described in terms of the surface capacity and resistance of the electrode. The values of the capacity of oxide layers on the valve metals are usually less than $15 \mu\text{F}/\text{cm}^2$, and the behavior of these oxides at anodic potentials is similar to that of the dielectric in a parallel plate condenser, the electrodes of which, in the case of the oxide layers, are formed by the metal on the one side and the solution on the other. Little is known about these oxide-covered electrodes at cathodic potentials besides the fact that electronic current flows producing rectification (5, 6).

Previous measurements on uranium (1) which rapidly forms an oxide layer, have shown high capacities (*ca.* $300 \mu\text{F}/\text{cm}^2$) in a restricted potential range. A similar observation has been made on iron by Hackerman (7). This would not be expected if the oxide behaved as a dielectric, and it was therefore decided to test a series of oxide-covered metals in order to investigate this phenomenon.

Experimental Methods

In principle the technique used examines the voltage response of an electrode on which a square current wave is imposed. This voltage change has been examined in two ways. In the first method the behavior of the electrode is compared with that of an analogue circuit consisting of a capacitor and a resistor in parallel. In the second method the voltage response is recorded as a function of time and analyzed mathematically.

The apparatus used in the first method was developed by Denholm (1). The voltage developed by the current wave (*ca.* 10 mv) is measured by comparing the voltage of the specimen with that of a silver wire reference electrode. This method overcame some of the difficulties involved in the use of more conventional impedance bridges which include, in the measured impedance, the impedance of the anode and the resistance of the solution. As virtually no current flows through the silver reference electrode the voltage response is independent of its impedance.

The a-c voltage of the test electrode was compared with the voltage response of an analogue circuit, consisting of a variable capacitor and resistor in parallel, to which was applied a square current wave in phase with that through the test electrode. An electronic integrator circuit eliminated the need for several decades of capacity and resistance in the analogue circuit. The two voltage responses, after amplification, were applied respectively to the X and Y plates of an oscilloscope, a correct balance being indicated by a straight line at 45° , Fig. 1a.

The use of square wave excitation enables series resistance to be examined separately, as a parallelogram, with one pair of sides at 45° and the other pair

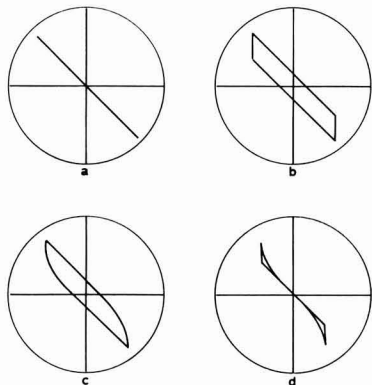


Fig. 1. Oscilloscope traces indicating (a) an ideal balance, (b) an ideal balance with uncompensated series resistance, (c) balance with distortion caused by a smaller time constant, (d) compensation for apparent series resistance in (c).

vertical, indicates the presence of series resistance associated with the test electrode (see Fig. 1b). Provision is made in the equipment to compensate for this series resistance which was shown to be associated, in most cases, with the resistance of the solution between the reference and test electrodes and was not measured. If, instead of a square wave, a sine wave of the same repeat frequency was used, values at balance were the same in both cases once all series resistance was compensated.

If the behavior of an electrode is more accurately represented by two analogue circuits with different time constants, one much smaller than the other, then the balance obtained which reflects the larger time constant is represented by a pseudoparallelogram with one pair of sides at 45° , but in this case the obtuse angles are rounded as in Fig. 1c. These curves are formed by the initial portion of the square wave (high frequencies) which, in the presence of two time constants, produces a more rapid voltage change in the circuit having the smaller value of time constant. When fully charged the voltage across this circuit is constant and the circuit behaves as a series resistance. The trace obtained on correcting for this as if for a series resistance is shown in Fig. 1d. As the difference between the two time constants decreases, the rounded portion occupies more of the trace and, under certain conditions, no balance can be obtained. As the time constants become more nearly the same the balance represents a mean value.

This equipment has limitations in that, although it is very sensitive to changes in parallel capacity, precise changes in parallel resistance are more difficult to determine. In addition, measurements at high repeat frequencies (>20 kc/sec) are complicated by the small signal and limitations of the amplifiers in the apparatus. The results appearing in Fig. 4-12 were obtained using this technique.

In the second method the voltage response of the test electrode to the square current wave is displayed directly on a measuring cathode-ray oscilloscope, as a function of time. The circuitry of the apparatus is shown in Fig. 2. The magnitude of the square current wave can be altered by varying the

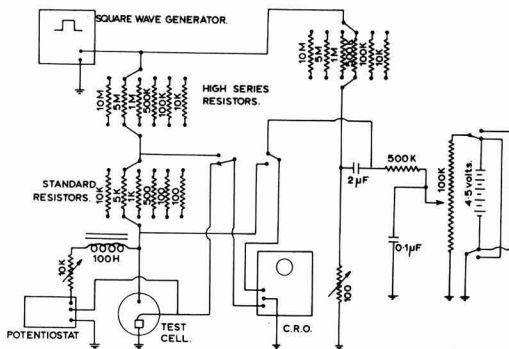


Fig. 2. Electrical circuit of apparatus for measuring the voltage response of a metal electrode to a square current wave.

values of the high series resistors or by changing the peak to peak value of the square wave voltage. The current is measured by displaying on the oscilloscope the potential developed across the standard resistors. This method also permits the shape of the current wave to be monitored. The rise time of the voltage wave (claimed to be 4×10^{-8} sec) could not be measured as the band width of the amplifiers of the oscilloscope is not sufficiently large. The minimum value of the band width which occurs at maximum gain (1 mv/cm) is of the order 0.5 Mc/sec. The apparatus thus enabled a voltage response at times greater than 2.10^{-6} sec to be observed. Compensation of the series resistance can be made and the d-c potential of the specimen can be measured in a manner similar to that adopted in the other equipment, i.e., by use of a differential amplifier on the oscilloscope. As the potential of the silver electrode tended to vary with time, it was standardized against a saturated calomel electrode using a valve voltmeter.

Assuming that the electrode behavior can be represented by a resistor, R , and capacitor, C , in parallel, with a constant current, I , flowing through the circuit, then the voltage across the circuit is given by

$$V = IR(1 - e^{-t/CR})$$

Differentiating gives

$$\frac{dV}{dt} = \frac{I}{C} e^{-t/CR}$$

which can be expressed as

$$\log \frac{dV}{dt} = \log \frac{I}{C} - \frac{t}{CR} \cdot \frac{1}{2.3}$$

A plot of $\log dV/dt$ against t should give a slope $1/2.3CR$ and an intercept at $t = 0$ of $\log I/C$. Alternatively the logarithmic scale may be normalized by plotting $\log 1/I dV/dt$ which allows direct comparison of results.

This analysis is correct for the case where the square current step is superimposed on steady-state conditions. In the present equipment the imposed current reverses periodically giving a zero net additional direct current. The frequency is such that in general steady-state conditions are not achieved

prior to each reversal, and the form of the voltage response is modified so that it is expressed

$$V = IR \left\{ 1 - \left(1 + \tanh \frac{T}{CR} \right) e^{-t/CR} \right\}$$

where $4T$ is the period of the square wave oscillation.

When T/CR is small $\tanh T/CR \ll 1$ and the equation reduces to that for a single step. The voltage response then indicates the value of the capacitor as nearly all the current flows into the capacitor and little leaks through the resistor. When T/CR is large (>10), $\tanh T/CR \approx 1$. The capacitor can then reach a fully charged state and all the current flows through the resistor. Generally $(1 + \tanh T/CR)$ will be neither one nor two but will be between these two values. As in the first case (a single step) the plot of $\log dV/dt$ against t will give a slope $1/2.3CR$. However, the intercept at $t = 0$ is $\log I/C(1 + \tanh T/CR)$ and this correction factor must be applied.

This method permits the calculation of the parallel capacity and resistance from the slope and intercept on the logarithmic axis when $\log dV/dt$ is plotted against t , as, for a single value of capacity and resistance, the plot is a straight line.

Where the measured values of C and R are a function of frequency, as is usually the case with oxide films, the relation between $\log dV/dt$ and t is not linear. The values of C and R for any frequency, f , can be derived by drawing the tangent to the curve at time t (where $t \times f = 1$). The behavior of the electrode may be approximated to any desired degree by a number of analogues in series, the components of each of which are frequency independent. This is done by taking the tangent to the curve at long times, giving the components of one analogue. The rate of voltage change arising from this analogue is then subtracted from the original curve and the remainder treated in the same way giving another set of components and so on. Figures 14 and 15 show results obtained by this method of analysis from data of the type given in Fig. 13.

Measurements of the electrode impedance were made at cathodic potentials, initially on changing the potential to more negative values and then with the potential increasing. The solutions, which were made

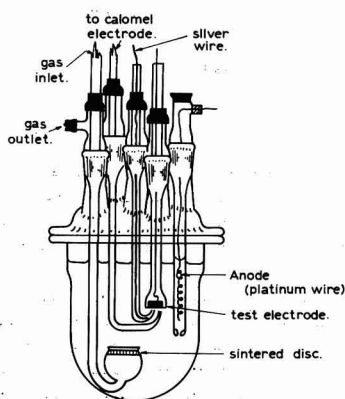


Fig. 3. Diagram of the cell

Table I. Metals tested

Metal	Percentage composition
Al	99.99 Al
Ta	99.8 Ta, 0.1 Nb, 0.01 C
Zr	99.9 Zr
Ti	99.9 Ti
Nb	99.5 Nb, 0.3 Ta, 0.05 Al, Fe, C, Si, O
V	99.7 V, 0.09 O, 0.05 C, Fe, N, Si
U	99.95 U, 0.009 Fe, O, N, C, Si, Al
Cr	99 Cr, 0.3 Fe, 0.2 Al, 0.1 Si, 0.06 C, Cu, S, P

from distilled water and Analar reagents, were a carbonate-bicarbonate buffer solution ($5/N \text{ NaHCO}_3 + 5/N \text{ Na}_2\text{CO}_3$) having a pH of 9.7 and a normal solution of sodium sulfate the pH of which was adjusted with sodium hydroxide or sulfuric acid. The cell used is shown in Fig. 3. Oxygen-free nitrogen was bubbled into the solution prior to testing to reduce the oxygen concentration.

The metals tested were aluminum, tantalum, zirconium, niobium, titanium, vanadium, uranium, and chromium (see Table I). The electrodes were prepared by mounting samples in a cold setting plastic followed by grinding on emery paper down to 600 grade. The resulting surface was either used in that state or anodized in a boric acid solution, adjusted to pH 9-10 by additions of ammonium hydroxide. The more detailed tests on titanium electrodes involved surfaces prepared by chemical etching in a hydrofluoric acid and hydrogen peroxide mixture (10 cc 40% HF + 90 cc 20 vols H_2O_2). This preparation was found to give more reproducible values of capacity, although the values were not strictly comparable with those for abraded surfaces due to the differences in true surface area.

Results

The variation of the capacity with potential for an aluminum electrode both when abraded and when

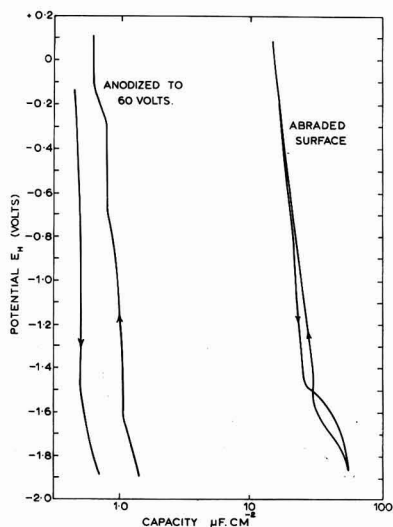


Fig. 4. Variation of the capacity of an anodized and an abraded electrode of aluminum with potential. Carbonate solution pH 9.7.

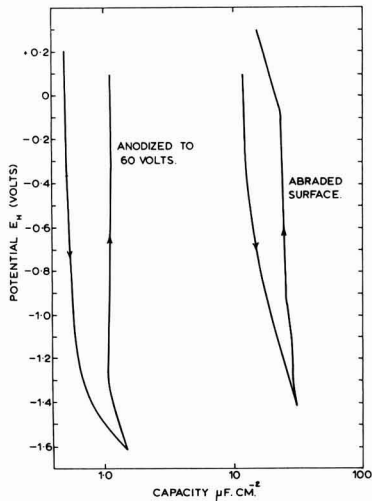


Fig. 5. Variation of the capacity of an anodized and an abraded electrode of tantalum with potential. Carbonate solution pH 9.7.

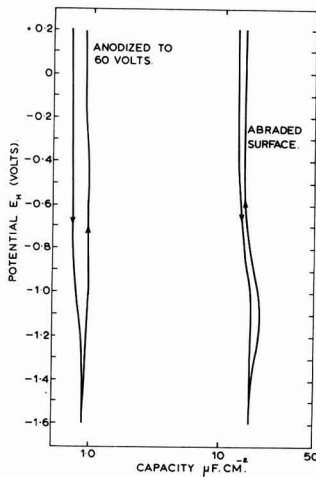


Fig. 6. Variation of the capacity of an anodized and an abraded electrode of zirconium with potential. Carbonate solution pH 9.7.

anodized to 60v is shown in Fig. 4. The results for similarly prepared specimens of tantalum, zirconium, niobium, and titanium are shown in Fig. 5, 6, 7, and 8, respectively.

From these results it can be seen that the capacities of the anodized specimens, measured prior to cathodic polarization, are lower than those for abraded surfaces. The subsequent behavior of niobium and titanium, which on decreasing the potential shows marked capacity maxima, differs significantly from that of aluminum, tantalum, and zirconium.

The capacities of vanadium, chromium, and uranium specimens, which had been abraded prior to testing, are shown in Fig. 9, 10, and 11. The vanadium specimen, on decreasing the potential, shows two capacity maxima. Chromium (Fig. 10) shows a capacity of the order of $25 \mu F/cm^2$ and has no marked maximum. Figure 11 shows the results for uranium

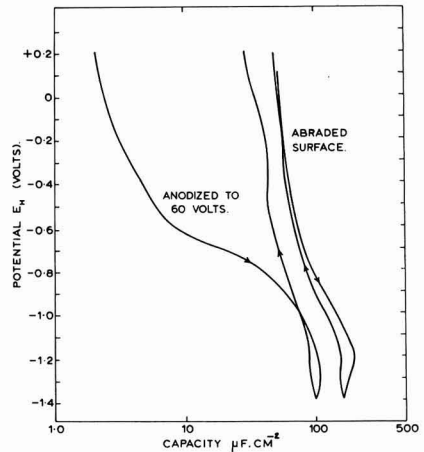


Fig. 7. Variation of the capacity of an anodized and an abraded electrode of niobium with potential. Carbonate solution pH 9.7.

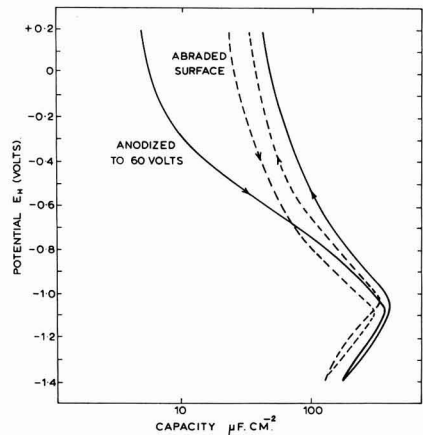


Fig. 8. Variation of the capacity of an anodized and an abraded electrode of titanium with potential. Carbonate solution pH 9.7.

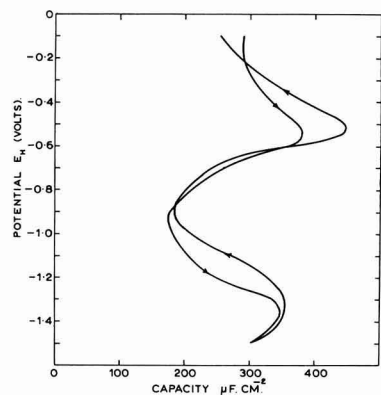


Fig. 9. Variation of the capacity of an abraded electrode of vanadium with potential. Carbonate solution pH 9.7.

in a sulfate solution of pH 9.8; the results are similar to those observed in a carbonate solution of similar pH (1).

Figure 12 shows, for a titanium electrode, the variation with pH of the potential of the capacity maximum in a sodium sulfate solution. The potential is independent of pH up to a value near 11 and then decreases by 0.06 v/pH unit. In the lower pH region below a pH of about 5, a second capacity maximum is present at a more positive potential than the one shown in Fig. 12 and appears to be dependent on pH but as yet has not been fully investigated.

Figure 13 shows the voltage response of an etched titanium electrode in the carbonate buffer solution

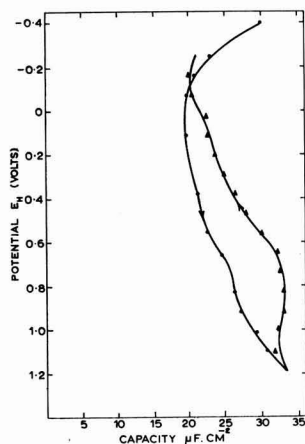


Fig. 10. Variation of the capacity of an abraded electrode of chromium with potential. Carbonate solution pH 9.7.

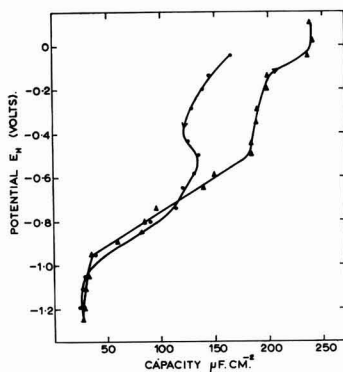


Fig. 11. Variation of the capacity of an abraded electrode of uranium with potential. Sulfate solution pH 9.8.

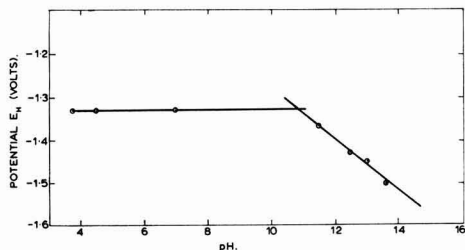


Fig. 12. Variation with pH of the potential of the capacity maximum for a titanium electrode. Sulfate solution.

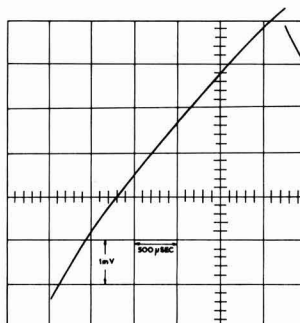


Fig. 13. Voltage response of an etched titanium electrode to a square current wave. Carbonate solution pH 9.7; electrode potential -0.03v SHE ; area of electrode 0.33 cm^2 .

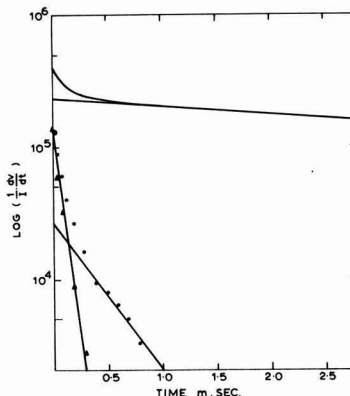


Fig. 14. Plot of $\log 1/I dV/dt$ vs. t for Fig. 13

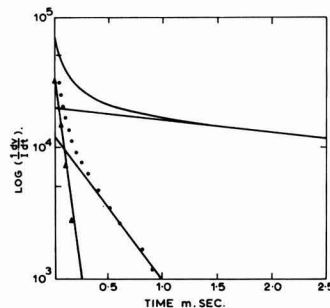


Fig. 15. Plot of $\log 1/I dV/dt$ vs. t for the titanium electrode at -1.055v SHE .

at a potential of -0.03v SHE . The repeat frequency was 200 c/sec , and the current was $\pm 12 \cdot 10^{-6}\text{ amp}$ for the curve shown. The graphically determined derivative of the curve is plotted logarithmically against time in Fig. 14. Figure 15 shows the same parameters for a titanium electrode at a potential of -1.055v SHE . The current pulse in this case was $\pm 58.1 \times 10^{-6}\text{ amp}$. Both measurements were made on decreasing the potential of the specimen.

Discussion

From an examination of the results it is possible to divide the oxide-covered metal electrodes into two

groups: the first consists of those metals the oxides of which behave as dielectrics, and the second group comprises those whose oxides show high capacity values, greater than the values usually accepted for the electrochemical double layer. Titanium shows both characteristics and, as a result, was studied in more detail than the other metals.

Normally oxide-covered metals would be expected to show capacities which correspond to the thickness of the oxide, decreasing with increased thickness as has been shown with the valve metals aluminum, tantalum, zirconium, and niobium, at anodic potentials.

The increase of capacity with decreasing potential for aluminum, tantalum, and zirconium could be attributed either to a thinning of the oxide, or, as appears more likely, to a change in the resistance of the oxide. If the oxide is considered to be composed of a series of layers, an increase in the conductivity of a layer could act as a shunt across that layer of oxide. This principle may be illustrated by considering the analogue shown in Fig. 16a. Reducing the high resistance in either of the parallel circuits to a low value will effectively short out the relevant capacitor and result in a larger measured value of capacity.

On increasing the potential, the values of the capacity and conductivity for the anodized specimens of aluminum, tantalum, and zirconium are larger than the values recorded on decreasing the potential. The magnitude of the increase (called hysteresis) appears to be dependent on the minimum potential reached. This has been the subject of a more detailed study which has confirmed the results shown here with other measurements on anodized zirconium (10) which had been subjected to more negative potentials. The hysteresis of the kind shown in that work has been reported previously (1, 5, 12) and in the present work has been observed on all the oxide-covered metals investigated. It was also shown in that work that the capacity decreased with time at 0v SHE (solution pH 9.7) to its original value. The capacities of the 60v oxide films, on aluminum, tantalum, and zirconium after hydrogen had been evolved from their surfaces, could be restored to a value approaching the original, prior to cathodic treatment, by anodizing to 10v. This treatment would not give rise to any oxide growth. These results suggest that hydrogen in the oxide increases its conductivity. The hydrogen can be introduced into the oxide by cathodic polarization accompanied by the evolution of hydrogen and removed by anodic polarization. These processes might provide a mechanism by which the rectification observed on these metals could occur. A similar mechanism has also been proposed by Schmidt (9).

The conductivity change does not appear to be uniform throughout the thick oxides as indicated by

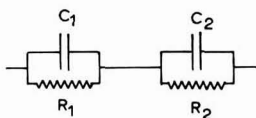


Fig. 16. Hypothetical analogue of an oxide composed of two layers

the value of the capacity change. A uniform decrease in the resistance of the oxide would not be accompanied by an apparent change in the capacity of the oxide unless its dielectric constant also increases.

These results are in many respects similar to those reported by Vermilyea (11) who found that the capacity of anodized films on tantalum increased after heating *in vacuo* above 300°C without any significant change in the interference colors of the films or their porosity. He attributed the increased capacity to an increase in the conductivity of the oxide resulting from loss of oxygen to the metal during vacuum heat treatment. Young (8) has interpreted his results on the variation of the impedance with frequency, as showing that the resistivity of the oxide on niobium varies with the depth below the oxide surface.

It should be stressed that, in all the effects so far discussed, the surface capacity of the electrodes of aluminum, tantalum, and zirconium at no time exceeded that corresponding to a clean surface, i.e., the capacity of the electrochemical double layer.

Considering the behavior of the capacity of titanium and niobium before and after cathodic polarization, it is seen that an increase in both the conductivity and capacity results from cathodically polarizing the anodized specimens, but to a very much greater extent than is found with the metals aluminum, tantalum, and zirconium. Subsequent anodic polarization to 10v restores the capacity to the original value prior to cathodic polarization (corresponding to a 60v film), indicating that little change in the thickness of the oxide occurred during cathodic treatment. The interference colors observed on the anodized specimens also remained apparently unchanged, supporting this interpretation.

The high values of the capacity obtained with titanium, vanadium, and niobium cannot be explained on the model of a parallel plate condenser as the value of the thickness of the oxide calculated on this basis would be less than 1Å at the potential of the capacity maximum.

Similar capacity maxima have been observed at the polarographic half-wave potential (3), where a species in the solution is depositing on the mercury surface, and by Breiter on platinum where adsorption processes are occurring (4). In the present work the solutions used for measuring contained no active species, other than those composing the water, which could be involved in an electrochemical reaction.

The basic requirement for a high Faradaic capacity is that the electrochemical reaction taking place must be reversible. The similarity between a reversible reaction and a capacitor has been drawn by Bryer and Gutmann (13). When the current is cathodic, deposition of a metal ion takes place, while on the reverse cycle dissolution occurs; the process thus involves the storage of charge, either metal ions in the solution or electrons by the metal to be released on the opposite half cycle of the current.

If a valency change occurred reversibly in the oxide, it could account for the high capacity values observed in the present work with the electrodes of titanium, niobium, and vanadium and those previously reported for uranium and iron. The capacity

Table II

Reaction	Potential		Remarks
	Calculated	Observed	
$V_2O_2 + H_2O = V_2O_3 + 2H^+ + 2e^-$	-1.393	-1.35	Carbonate soln. pH 9.7 Ref. (14)
$V_2O_3 + H_2O = V_2O_4 + 2H^+ + 2e^-$	-0.363	-0.5	
$NbO + H_2O = NbO_2 + 2H^+ + 2e^-$	-1.198	-1.21	Carbonate soln. pH 9.7 Ref. (15)
$2NbO_2 + H_2O = Nb_2O_5 + 2H^+ + 2e^-$	-0.862	NO	
$3Ti_2O_3 + H_2O = 2Ti_3O_5 + 2H^+ + 2e^-$	-1.063	-1.08	Carbonate soln. pH 9.7 Ref. (16, 18)
$3UO_2 + 2H_2O = U_3O_8 + 4H^+ + 4e^-$	-0.05	-0.5 to 0*	Sulfate and carbonate solns. pH 9.7 Ref. (17)
$U_3O_8 + H_2O = 3UO_3 + 2H^+ + 2e^-$	+0.32		

NO, no capacity maximum was observed around this potential.

* No sharp capacity maximum was observed although the values of the capacity were high (ca. 200 $\mu F/cm^2$).

maxima observed do occur in the vicinity of the potentials which may be calculated from thermodynamic data (see Table II). Aluminum, tantalum, and zirconium do not exhibit a change in valency, and no large capacities are observed with these metals.

The stability of trivalent chromium covers a large potential range, and no high capacity is observed within this range. If the high capacities resulted from an adsorption process, it would be expected that such a reaction would be seen with the chromium electrode, as the resistance of the oxide is relatively low and capacity relatively high.

The reaction occurring in the oxide is believed to be of the form



which only requires that protons and electrons are mobile species. The process therefore would depend on the concentration of hydrogen in the oxide, and this could explain the observed hysteresis in the capacity on potential cycling of titanium and vanadium. The presence of greater concentrations of protons would allow the reaction to proceed more rapidly, increase the value of the capacity measured, and move the potential of the capacity maxima to more positive values.

In order to get a clearer understanding of this phenomenon a more detailed study has been made of the behavior of a titanium electrode.

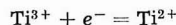
On the basis of a reaction such as $MO + H^+ + e^- \rightleftharpoons MOH$ it would be expected that the potential of the capacity maximum would depend on the pH of the solution, according to the equation

$$E = E_0 - 0.059 \text{ pH}$$

where E_0 is the reversible or equilibrium potential for the reaction. This variation with pH has been found to hold with titanium in a sodium sulfate solution above pH values of 11, as shown in Fig. 12. At lower pH values the potential of the capacity maximum is independent of pH.

There are two possible explanations for this behavior. The first is that the reaction occurring does not involve hydrogen ions and results from the

change in valency of some ions most probably in solution, e.g.



The other possible explanation is that the pH at the interface between the oxide and solution is independent of the solution pH up to a value of about 11. This could be due to the hydrogen evolution reaction associated with the d-c polarization which results in a high concentration of hydroxyl ion at the electrode-solution interface.

The potential of the capacity maximum of the titanium electrode depends on the composition of the solution, as can be seen from the comparison of the potentials at which the maximum occurs in the sulfate (Fig. 12) and carbonate (Fig. 8) solutions.

From the measured values of the capacity of the electrodes an estimate can be made of the number of ions changing valency. For the case of titanium a surface capacity of 150 $\mu F/cm^2$ corresponds to 4.7 $\times 10^{12}$ titanium ions per cm^2 changing valency from Ti^{2+} to Ti^{3+} . This is about 5×10^{-3} of the number of atoms in the surface. From this it might be concluded that this phenomenon is confined to the oxide surface. However, preliminary results show that, under certain conditions, the capacity exhibited by both uranium and titanium increases with increasing oxide thickness. This phenomenon appears to be dependent on the pH and on the nature of the anion in the solution, and more work is required to elucidate the details. It is reasonable to ask why so few ions change valency, and it seems likely that the number is limited by the availability of hydrogen in the oxide which might be expected to be in the range 10^{-6} – 10^{-3} mole fraction. A preliminary examination of the behavior of these high capacities shows that the measured values are time dependent in a way which adds additional support to the suggestion that this is not a surface phenomenon, but involves the bulk of the oxide.

The deviation from linearity of the derivative of the voltage response, as shown in Fig. 14 and 15, indicates that the analogue of a parallel capacitor and resistor chosen to represent the titanium specimen is only approximately correct. There is a closer ap-

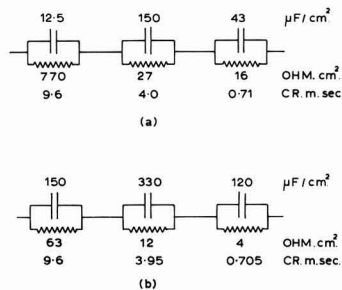


Fig. 17. Analogue circuit derived (a) from Fig. 14, (b) Fig. 15

proximation to a straight line when the oxide behaves as a dielectric (Fig. 14) than under those conditions where the oxide behaves as an electrolyte giving rise to an electrochemical reaction.

The deviation from linearity is larger with anodized specimens and on increasing the potential after hydrogen had been evolved from the oxide surface. These results suggest that the properties of the oxide are not homogeneous and that a high hydrogen activity does increase the heterogeneity of the oxide, which would account for the increased capacity.

As explained previously, by plotting the numerical values of the deviation from linearity in a manner similar to those of the derivative, two more time constants can be derived. The three series networks of capacitors and resistors in parallel equivalent to the three time constants, approximate closely to the voltage response of the electrode. Figure 17a shows such an analogue derived from Fig. 14 while Fig. 17b is derived from Fig. 15. At the present stage of development it is not possible to say whether such more complex analogues have any reality in a physical sense or whether this is merely a mathematical device for describing a frequency dependent process.

Conclusions

1. The surface capacity and conductivity of oxide-covered metal electrodes can be greatly changed by the presence of hydrogen.

2. The marked increase in capacity and conductivity observed on aluminum, tantalum, and zirconium electrodes after cathodic polarization has been explained in terms of a change in the oxide conductivity rather than in terms of mechanical damage to the oxide film. Nevertheless the oxide continues to behave like a dielectric, and the measured surface capacities do not exceed those corresponding to the double layer.

3. The behavior of the metals titanium, niobium, uranium, and vanadium which can show surface

capacities greatly in excess of the double layer capacity cannot be explained in terms of a dielectric oxide without implying a large and variable increase in the dielectric constant. The phenomena are discussed in terms of a Faradaic capacity arising from a change of valency of cations in the oxide by a reaction such as



which only involves the movement of electrons and protons.

4. Further work is required to clarify the relations between the measured values of capacity and such variables as frequency of measurement, oxide thickness, and nature of the solution all of which have been shown to be important.

Acknowledgments

The authors wish to thank Professor J. G. Ball in whose department the work is proceeding, the Central Electricity Generating Board for financial support, and the South African Atomic Energy Board from whom one of us (H.S.I.) is seconded. The authors also wish to acknowledge Imperial Chemical Industries Ltd. for supplying some of the materials.

Any discussion of this paper will appear in a Discussion Section to be published in the December 1963 JOURNAL.

REFERENCES

1. J. S. L. Leach, *J. Inst. Metals*, **88**, 24 (1959-60).
2. J. E. Draley and W. E. Ruther, *This Journal*, **104**, 329 (1957).
3. P. Delahay, "New Instrumental Methods in Electrochemistry," Interscience Publishers, Inc., London and New York (1954).
4. "Transactions of the Symposium on Electrode Processes," E. Yeager, Editor, John Wiley & Son, Inc., New York (1961).
5. W. G. L. van Geel, and C. A. Pistorius, *Philips Research Rept.*, **14**, 23 (1959).
6. H. E. Haring, *This Journal*, **99**, 30 (1952).
7. P. V. Popat and N. Hackerman, *J. Phys. Chem.*, **65**, 1201 (1961).
8. L. Young, *Trans. Faraday Soc.*, **51**, 1250 (1955).
9. P. F. Schmidt, *J. Appl. Phys.*, **28**, 278 (1957).
10. G. Fawkes, Private communication.
11. D. Vermilyea, *Acta Met.*, **5**, 113 (1957).
12. H. S. Isaacs, D.I.C. Dissertation, Imperial College, London (1960).
13. B. Bryer and F. Gutmann, *Discussions Faraday Soc.*, **1**, 19, (1957).
14. Cebelcor Technical Report 29 (1956).
15. Cebelcor Technical Report 53 (1957).
16. Cebelcor Technical Report 4 (1953).
17. Cebelcor Technical Report 31 (1956).
18. B. D. Tomashov, R. M. Al'Tovskii, and M. Ya. Kushnerev, *Doklady Akad. Nauk S.S.S.R.*, **141**, 193 (1961).

The Growth of Thin Passivating Layers on Metallic Surfaces

M. Fleischmann and H. R. Thirsk

Department of Chemistry, King's College, Newcastle upon Tyne, England

The Nature of the "Passivating Material"

The main problem in interpreting the passivation of metals in terms of a theoretical model lies in the nature of the "passivating material." Discussion repeatedly returns to this question [see for example (1-3)], and the answer usually takes one of two extreme forms, the first: passivation is due to a three-dimensional film of a definite chemical phase; the second: passivation is due to a disordered monomolecular array of adsorbed ions or molecules. In the light of the discussion given in this paper we might well add a third form: passivation is due to an ordered monomolecular, two-dimensional film of a definite chemical phase.

In many instances there can be little doubt that the first answer is correct (4). A new phase is formed at a potential close to a well-defined reversible potential, discrete centers can be seen to grow by microscopy or electron microscopy, and the electrode is passivated some time after these centers coalesce. Any adsorbed layer formed before the three-dimensional film clearly has little passivating effect. The growth of the centers is in general controlled by at least two potential dependent rate constants, the nucleation rate constant A^1 (nuclei $\text{cm}^{-2} \text{sec}^{-1}$) and the crystal growth constant (moles $\text{cm}^{-2} \text{sec}^{-1}$) (5-7). If the formation of the new phase is examined under constant potential conditions, the current-time transients obtained can be analyzed and the rate constants deduced. The concentration and potential dependence of these rate constants can then in turn be investigated and the mechanism of lattice formation deduced by methods familiar in the general field of electrochemical kinetics (5-7). The principles involved are referred to briefly in the next section. There can again be little doubt that a three-dimensional film is passivating the surface in cases where the formation of similar growth centers in a parent phase (itself formed from the substrate metal) can be followed potentiostatically such as in the oxidation of lead sulfate (8) or of silver sulfate (9).

In a large number of cases, notably of iron and stainless steel, the simple explanation of the blocking of the electrode by three-dimensional growth centers is insufficient. Passivation is much faster and the essential step is usually masked by side reactions such as the "active dissolution" of the metal. The only well-defined electrochemical step which can be observed for example on iron (10) as well as on metals such as aluminum and tantalum (11, 12) is the thickening of the passivating material by high field conduction (13-15). A three-dimensional film can be stripped from the underlying metal for ex-

ample with iron (16, 17) and stainless steel (18, 19), and the thickness can be measured in a variety of ways, for example by chemical estimation (20) or by measuring the change in rotation of plane polarized light (21). The thickness of the films has also been shown to depend on the applied potential, for example, on iron (22, 23). In view of these properties of the protected metal, passivation in these systems is also often attributed to the formation of a three-dimensional film. Many features of the passivation process are, however, more readily explained in terms of the effect of adsorbed layers on the metal (24, 25). The inhibition of corrosion by adsorption of carbon monoxide (26, 27), the oxygen uptake by stainless steel (28), and the effect of this adsorption on the dissolution of iron (29) and chromium and nickel (30) can all be explained in terms of such a model. The similarity of the passivation process to the inhibition of other reactions such as the ionization of hydrogen on platinum by the adsorption of anions (31) has also been taken to support the view that passivation is due to adsorption, particularly of hydroxyl ions (32).

A combination of the two views is sometimes advanced in specialized theories of adsorption followed by reaction leading to passivation (3, 33). It can be assumed for example that the "decision" for passivation may be taken at the monolayer adsorption stage (1). The relative role of adsorption and film formation in causing passivation is still uncertain, however. It has been suggested that the rapidity of the first adsorption stage precludes the formation of an ordered film and that passivation must be due to the formation of a random adsorbed layer (3). The purpose of this paper is to examine the initial stages of passivation in a number of systems by measurements of the kinetics at constant potential using potentiostats suitable for measurements at high frequencies (34) and to correlate the measurements with structural observations obtained by electron microscopy and electron diffraction. It will be shown that the problem can be treated, in favorable cases, as an example of the electrochemical kinetics of crystal growth.

Growth of Discrete Centers on Electrodes

Discrete centers can grow on electrodes in a number of ways (5-9). At constant potential the rate constants governing crystal growth are independent of time, and in general the current in amp/cm^2 into surface S will be given by

$$i = zFkS \quad [1]$$

This equation also holds for centers which expand in one dimension only, i.e., the current is independ-

ent of time. For centers growing in two or three dimensions the current may be expressed by using the linear dimensions of the particles, r

$$r = \frac{Mkt}{\rho} \quad [2]$$

where M is the molecular weight and ρ is the density. For cylinders and hemispheres we therefore obtain, respectively

$$i = \frac{2zF\pi Mhk^2t}{\rho} \quad [3]$$

and

$$i = \frac{2zF\pi M^2k^3t^2}{\rho^2} \quad [4]$$

where h is the height of the cylinders. These equations for the growth of a single center must be linked with the appropriate law giving the time dependence of the number of nuclei, N . If

$$i = f_1(t) \quad [5]$$

and

$$N = f_2(t) \quad [6]$$

then in the initial stages where there is no limitation of the area of the growing centers by overlap

$$i = \int_0^t f_1(u) \left(\frac{df_2}{dt} \right)_{t=t-u} du \quad [7]$$

If nucleation takes place at a number of preferred sites N_0 on the substrate and the probability of forming a nucleus is uniform with time

$$N = N_0(1 - \exp - At) \quad [8]$$

where A is in seconds⁻¹, Eq. [8] commonly reduces to two limiting forms: if A is large so that $At \gg 1$ for the bulk of the period of growth

$$N \approx N_0 \quad [9]$$

i.e., the nuclei appear to be formed instantaneously; on the other hand if A is small so that $At \ll 1$ during the period of growth

$$\begin{aligned} N &\approx AN_0t \\ &= A't \end{aligned} \quad [10]$$

where A' is nuclei cm⁻² sec⁻¹. Equation [10] also applies if there are no preferred sites for nucleation. Combination of [8] or [10] with the appropriate law for the growth of a single center according to [7] gives the over-all current-time transient in the initial stages of growth. For example, for two-dimensional centers with instantaneous formation of nuclei

$$i = \frac{2zF\pi MhN_0k^2t}{\rho} \quad [11]$$

and for progressive nucleation

$$i = \frac{zF\pi Mhk^2A't^2}{\rho} \quad [12]$$

while for three-dimensional centers with progressive nucleation

$$i = \frac{2zF\pi M^2k^3A't^3}{3\rho^2} \quad [13]$$

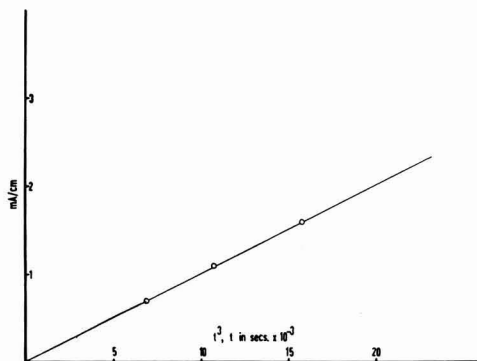


Fig. 1. Variation of current with cube of time for the electrodeposition of γ -manganese dioxide onto a platinum electrode at a potential $E_h = 1320$ mv. Solution composition: 0.01M $MnSO_4$, 1.0M Na_2SO_4 , 0.25M H_2SO_4 .

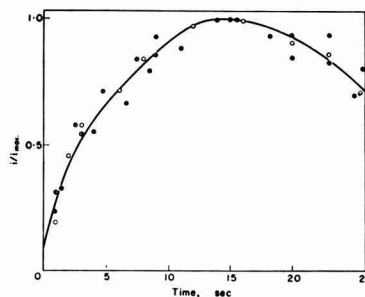


Fig. 2. Variation of (current/current at maximum) with the time for the oxidation of silver sulfate to argentic oxide in molal sulfuric acid at the following potentials with respect to the lead dioxide/lead sulfate electrode: solid circle + 0.325v, half opened circle, solid on right side + 0.350v, open circle + 0.0375v, half opened circle, solid on left side + 0.400v.

This equation is illustrated in Fig 1 by the initial stages of the electrodeposition of γ -manganese dioxide from manganous sulfate solutions onto platinum electrodes (35). It has also been found to apply for the electrodeposition of α - and β -lead dioxide (36, 5) as well as the oxidation of lead sulfate (8).

In the later stages of crystal growth the centers overlap, and the area available for electrodeposition becomes restricted. In the cases of interest in the context of this paper reaction must finally stop either when the electrode surface is "blocked" or when the parent phase has been completely converted into the new phase. The current must therefore pass through a maximum. This is illustrated in Fig. 2 by the oxidation of silver sulfate to silver oxide (9). In this system cylindrical centers grow from nuclei which are formed instantaneously, but it can be seen that the initial linear rise of the current with time is rapidly restricted by overlap. The extent of overlap of centers taken two at a time can be readily calculated for most growth geometries. In the present example the overlap area takes the particularly simple form

$$\begin{aligned} S_o &= 4\pi N_0^2 r h \int_0^{2r} a \cos^{-1} \frac{a}{2r} \cdot da \\ &= 4\pi^2 N_0^2 h r^3 \end{aligned} \quad [14]$$

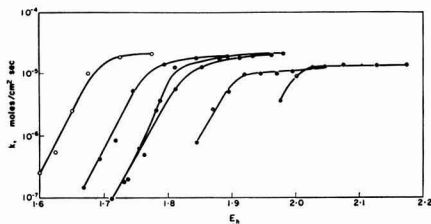


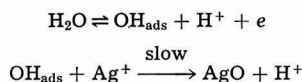
Fig. 3. Variation of the rate constant for the oxidation of silver sulfate with electrode potential and solution composition. Open circle, 0.001M sulfuric acid + M sodium sulfate; half open circle, solid on right side, 0.01M sulfuric acid + 0.99M sodium sulfate; solid circle, 0.1M sulfuric acid + 0.9M sodium sulfate; half opened circle, solid on left side, 0.1M sulfuric acid; half opened circle, solid on top, M sulfuric acid; half opened circle, solid on bottom, 5M sulfuric acid.

where a is the radius of an annular ring of thickness da surrounding the center of radius r . Combination with the freely growing area gives the current-time transient

$$i = \frac{2zF\pi MhN_0k^2t}{\rho} \left(1 - \frac{\pi N_0 M^2 k^2 t^2}{\rho^2} \right) \quad [15]$$

Equation [15] has been shown to hold for the oxidation of silver sulfate illustrated in Fig. 2. In general the equations derived by allowing for overlap of centers have a similar form and predict a maximum in the current-time curve. The time and current at the maximum can be obtained by differentiation, and the rate constants k^*A' or k^*N_0 may be derived from the experimental values or from the slope of the appropriate power law plot in the initial stages of growth. In favorable cases the nucleation and growth constants can be separately determined by detailed analyses of the current-time transients (8). The nucleation rate can also be obtained by counting the number of growth centers on micrographs (9) or electron micrographs (35) or by forming a large number of nuclei by means of a preliminary polarization for a short time at a high potential and thereby changing the transient from that for progressive to that for instantaneous nucleation, e.g., from Eq. [12] to Eq. [11] (36, 5, 7).

When the characteristics of the crystal growth processes have been found, the variation of the rate constants k and A' with solution composition and potential can be examined. This is again illustrated in Fig. 3 for the formation of silver oxide from silver sulfate (9). For this one electron oxidation the slope of the Tafel lines at low potentials is nearly 60 mv^{-1} , and the reaction is proportional to pH . At high potentials the rate constant is independent of potential and pH . These facts are all explained by a rate-determining formation of the lattice at the growth sites by a slow chemical reaction between argentous ions and adsorbed hydroxyl radicals formed by an electrochemical equilibrium



In other examples which have been examined lattice formation has also been found to be the slow step in

contrast to the assumptions frequently made in theories of crystal growth (see for example [7]).

Growth of Centers of Monomolecular Height

An important example of the kinetics of crystal growth is obtained if centers of monomolecular height grow two dimensionally on electrodes. If the new phase shows a definite orientation, the height of the growing centers is a definite spacing of the unit cell. If these centers are regarded as cylinders, Eq. [11] and [12] again apply for the initial stages of growth for instantaneous and progressive nucleation, respectively. If the nuclei are distributed over the surface in a completely random manner, it is possible in these cases to calculate the current-time transient completely, that is, to allow for all possible forms of overlap between growing centers (37-39, 7). If S is the area of substrate covered by the growth centers, $S_{1\text{ex}}$ is the extended area (37) of all the patches ignoring overlap then

$$S = 1 - \exp(-S_{1\text{ex}}) \quad [16]$$

Since the volume v of the new phase is given by

$$v = Sh \quad [17]$$

then

$$i = \frac{zF\rho}{M} \cdot \frac{dv}{dt} \quad [18]$$

The most important case is that of progressive nucleation according to Eq. [10]. Substituting in [16] and [18] one obtains

$$i = \frac{zF\pi Mh k^2 A' t^2}{\rho} \exp\left(-\frac{\pi M^2 k^2 A' t^3}{3\rho^2}\right) \quad [19]$$

while for instantaneous nucleation

$$i = \frac{2zF\pi Mh N_0 k^2 t}{\rho} \exp\left(-\frac{\pi N_0 M^2 k^2 t^2}{\rho^2}\right) \quad [20]$$

If the growing centers are not circular, the area covered by a single center may be written

$$s = \frac{\sigma M^2 k^2 t^2}{\rho^2} \quad [21]$$

where σ is a shape factor (e.g., $\sigma = 6 \tan \pi/6$) in the case of regular hexagons (40). With the expression one obtains for example instead of [19] the equation

$$i = \frac{\sigma z F M h k^2 A' t^2}{\rho} \exp\left(-\frac{\sigma M^2 k^2 A' t^3}{3\rho^2}\right) \quad [22]$$

These equations show that it is possible to distinguish the formation of crystallites of monomolecular height from adsorption by following the kinetics of the process. The equations are similar in form to those obtained by only considering the overlap of centers taken two at a time such as Eq. [15]. The approximate equation is in fact given by the first term of the expansion of the exponential. The current again has a maximum, but the value and position differ by a numerical factor from that derived from the appropriate approximate equation. At high times the predicted current however approaches zero asymptotically. These equations are also of interest as they express the current-time transient for the formation of a single layer ac-

ording to a mechanism similar to the classical mechanism of crystal growth (41-43). The differences lie in the assumption of growth from a large number of nuclei rather than from one nucleus, in the restriction of growth by the overlap of growth centers rather than by the boundaries of the substrate crystal plane, and in the slow stage being the lattice formation at the periphery of the growing centers rather than the diffusion of reacting entities to the points where the lattice is built up. A consequence of these changes in the assumptions is a complete change in the potential and concentration dependence of the rate of deposition in the event of the repeated deposition of monolayers (7). The classical mechanism of crystal growth demands the nucleation of growth centers which requires an appreciable supersaturation or the equivalent overpotential. It is to be noted that, since crystals will grow at low supersaturations, it has been suggested in recent years that the lattice is built up at the edges of self-perpetuating steps such as those produced by screw dislocations (44-46, 5), but it has been pointed out (5) that the rejection of the classical mechanism depends on an assumption of the frequency factor for nucleation which may not be justified.

Investigation of the Initial Stages of Passivation

Evidence for the formation of ordered crystals or for the validity of the classical mechanism of crystal growth has not been obtained in previous investigations. This has probably been due mainly to the use of solid substrate electrodes. Even for highly perfect single crystal faces it is likely that imperfections such as dislocations or even the presence of mosaic boundaries will lead to a lack of "synchronization" of the current-time transient between different parts of the surface so that the over-all current-time transient will be a superposition of transients of the type [19] and [20]. Even for the deposition of a single layer this superposition would give rise to a plateau on the current-time plot instead of a maximum. In the event of the deposition of several layers the observation of a plateau is still more likely, and this does not give any distinguishing feature as to the mechanism of formation of the layer. It is clear that it is important to avoid nucleation at preferred sites, and we have attempted this in the first place by measuring the kinetics of formation of layers on liquid mercury and amalgam electrodes. Although these surfaces are in no sense perfect we can regard them as perfectly random so that nucleation is likely to take place at a uniform rate over the whole surface. It is likely therefore that equations of the type [19] will apply for the formation of a single layer.

In all the kinetic measurements reported here the working electrode had the form of a segment of a sphere formed on the end of a wide bore capillary fed from a precision syringe controlled with a micrometer. The size of the electrode was set either by extruding a known volume or by adjusting the height while viewing through a cathetometer. The formation of the initial layers and the adsorption of anions preceding it have been found to be fast

processes (38, 39), and potentiostats suitable for measurements at short times have been used (34) the cells being also designed so as to minimize the effect of stray capacities at high frequencies (34). The potential to be applied to the working electrode by the potentiostat was controlled by means of pulse generators of fast rise time and accurate amplitude stability, and all current-time transients were measured oscillographically.

Examples of the kinetics of adsorption and of layer formation are shown in Fig. 4-10. If the potential of the working electrode is pulsed from a potential negative to that for the formation of the new phase to a second potential which is either less negative to the reversible potential or actually at the reversible potential and if this second potential is positive to the electrocapillary maximum of the substrate, then there will be a specific adsorption of anions in most systems. The implication of the term "specific" is that this is to some extent an activated process so that it will cover an appreciable period of time. An example is given in Fig. 4 for a 300 mv pulse negative to the reversible calomel potential on mercury in 0.1M hydrochloric acid (47). It would be expected that the current-time transients due to adsorption would usually have this form. It is of interest that the process is appreciably retarded although the time scale is such that the retardation

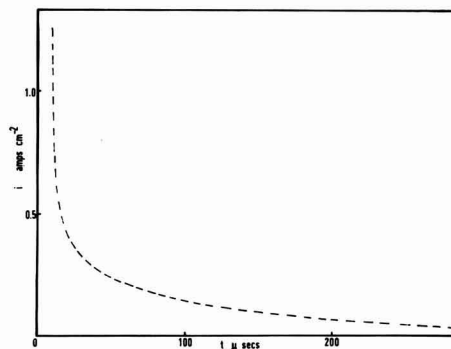


Fig. 4. Variation of current with time for the specific adsorption of chloride ions on mercury at the reversible calomel potential in 0.1M hydrochloric acid, 0 mv.

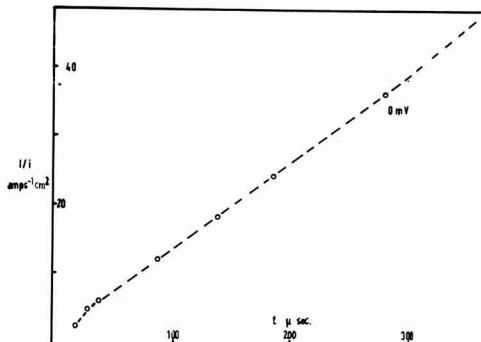


Fig. 5. Plot of $1/t$ against t for the specific adsorption of chloride ions on mercury at the reversible calomel potential in 0.01M hydrochloric acid.

would not normally be observed in measurements of the differential capacity (48). Estimates of the amount adsorbed agree with measurements derived from the differential capacity and indicate that the adsorption is following a Temkin isotherm. In consequence the time dependence of the adsorption follows the Elovich equation at low coverage which is best illustrated by a plot of $1/i$ against t , Fig. 5 (47). The adsorption of chloride ions on thallium amalgam is illustrated in Fig. 6 (50). At potentials more than 20 mv negative to the reversible thalious chloride potential the transient has the same form as for the adsorption of chloride ions on mercury, but at less negative potentials a plateau develops on the current-time curve. The significance of this plateau is discussed in the last section.

At potentials positive to the reversible potential the current-time curves in general develop a series of peaks (38). This is illustrated for calomel in Fig. 7. In this system up to seven maxima can be observed. It is natural to attribute the maxima to a successive deposition of layers on the surface according to the mechanism giving Eq. [19] for one layer. With increasing overpotential the amplitude of the peaks increases and the time scale contracts due to the increase of the rate constants. The area under each peak remains constant and approximates to a monomolecular layer of the {110} plane, the

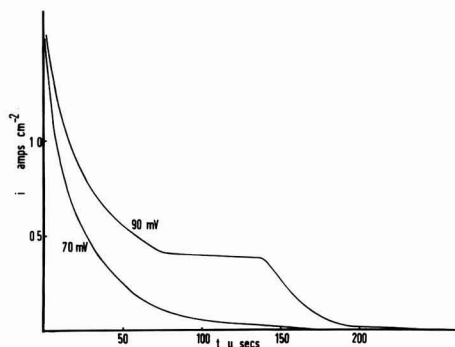


Fig. 6. Variation of current with time for the specific adsorption of chloride ions on thallium amalgam observed by applying a pulse of 70 mv and of 90 mv from an initial potential 100 mv negative to the thallium chloride potential.

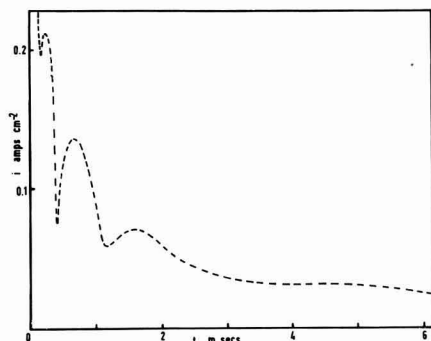


Fig. 7. Variation of current with time for the formation of calomel on mercury in 0.1M hydrochloric acid at an overpotential of 36 mv.

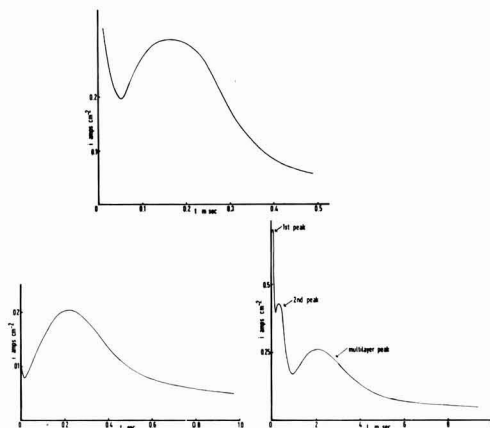


Fig. 8. Variation of current with time for the formation of thalious chloride on thallium amalgam in M hydrochloric acid: A (top) overpotential of 30 mv, first monolayer peak; B (bottom left) overpotential of 30 mv, multilayer peak; C (bottom right) overpotential of 75 mv, first and second monolayer and multilayer peaks.

adsorption transient being added to the first peak. The effect of the adsorption can obscure the first peak and can be largely eliminated by applying a first pulse up to the reversible potential and then a second pulse to a positive overpotential. The results in Fig. 7 and 8 have been taken in this way.

In the case of thalious chloride (50) two peaks are observed at low overpotentials, the first corresponding to the deposition of a single layer of the {100} plane parallel to the substrate (see next section), the second up to 100 layers, Fig. 8A, 8B. At higher overpotentials the second peak is split, and the formation of a second monomolecular layer can be detected. The quantity of electricity under the third multilayer peak decreases, about eight layers being deposited in the example shown. At still higher potentials the orientation changes, the prism face lying parallel to the substrate.

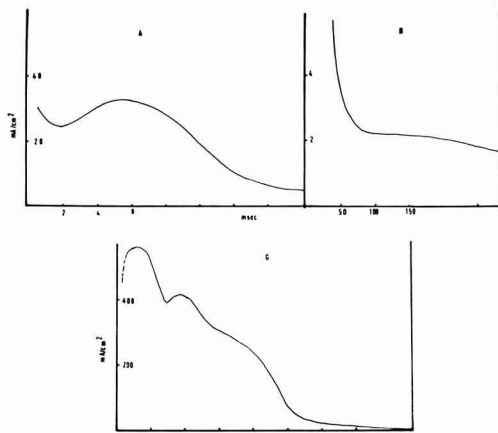


Fig. 9. Variation of current with time for the formation of cadmium hydroxide on cadmium amalgam in N sodium hydroxide: A, overpotential of 20 mv, first monolayer; B, overpotential of 20 mv, second monolayer; C, overpotential of 170 mv, first, second, and third monolayer.

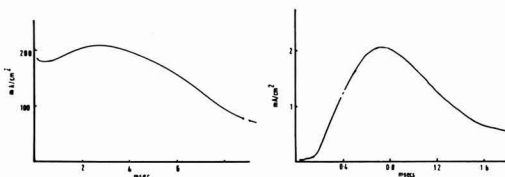


Fig. 10A (left) Variation of current with time for the formation of zinc oxide on zinc amalgam in 0.1N sodium hydroxide + 0.9M sodium nitrate at an overpotential of 185 mv; B (right) variation of current with time for the reduction of zinc oxide on zinc amalgam in borate buffer of pH 9.14 at an overpotential of 35 mv.

In the formation of cadmium hydroxide on cadmium amalgam (40) two peaks can be observed at low overpotentials which again occur at widely different times and which differ in amplitude, Fig. 9A and 9B. With increasing overpotential the second peak "catches up" on the first peak, and the amplitudes become nearly equal. At the same time a shoulder develops on the second peak. This may be attributed to the formation of a third layer since the total quantity of electricity used is somewhat in excess of that required for three layers of the {001} plane (see next section), whereas at low overpotentials the area under each peak approximates to one layer of this plane.

A final example is the formation of zinc oxide on zinc (51), Fig. 10A. In this case a single layer only is formed on the surface. The kinetics of reduction of this single layer are illustrated in Fig. 10B and can be seen to follow the same pattern as the formation of the layers, Fig. 7-10. This pattern must be attributed to the formation and growth of two-dimensional holes in the layer.

Investigation of the Structure of the Deposits

It is evident that for the analysis of the data in Fig. 7-10 the orientation and structure of the films must be determined. Since the layers are very thin this is best done by transmission electron microscopy and diffraction of films stripped from the surface. In the present investigation the following method was employed as a standard technique: the deposit was formed on a horizontal pool electrode fed from a syringe and connected in parallel to a second working electrode. The Luggin capillary was carried on a sleeve joint and after the formation of the film had been completed was placed opposite this second electrode. The solution level was lowered, the polarization interrupted, and the layer washed with water or alcohol and dried. The film was then coated with a drop of 0.1% Formvar in chloroform, and the composite layer was strengthened by the addition of a few drops of 2% collodion in ethyl acetate. At this stage the backed film could be removed in the form of a disk about 1 cm in diameter from the mercury or amalgam surface. Small areas near the center of the disk were cut out by means of a razor blade, and then pieces approximately 2 mm square were placed on E.M. grids using a drop of acetone to fix the films in position. The grids and attached films were placed in amylacetate vapor and then in the liquid for several hours to remove the collodion supporting film, and

finally placed in chloroform to reduce the thickness of the Formvar film.

Specimens were then studied at minimum beam intensity in the electron microscope and at the same time selected area electron diffraction patterns taken with a 10μ diameter selection area at the specimen. Calibration of the diffraction patterns was conveniently carried out by placing a grid carrying an evaporated gold film adjacent to the grid carrying the film in the specimen carrier of the microscope. Values of spacings in a direction perpendicular to the film were ascertained by transferring the grid to a Finch-type electron diffraction camera and rotating the specimen round a horizontal axis some 30° - 50° .

Cadmium hydroxide possesses a similar structure to cadmium iodide, that is a layer structure consisting of two plane hexagonal networks of hydroxide ions superimposed in such a way that the oxygen atoms of one rest on those of the other in alternate interstices with an hexagonal network of cadmium atoms separating the pair of layers of hydroxide ions but with the cadmium ion lying at the center of a line perpendicular to the layer plane and joining the center of a line perpendicular to the layer plane and joining the center of the triangles of hydroxide ions. The hexagonal layers of cadmium are arranged with the ions directly above those of the next lower layer.

The actual a_0, c_0 axial spacings of the hexagonal unit cell vary quite widely in the literature. Reasons for this variation may probably be the inclusion of water molecules in the "OH" layer. Indeed under the wide variety of conditions of formation it would not be unreasonable to seek for a CdCl_2 type of structure and for abnormalities in the stacking of the hexagonal nets giving rise to a doubling of the c_0 axis repetition unit corresponding to the suggestions made by Arnefelt (52). In this essentially kinetic investigation we have satisfied ourselves, by the methods described briefly below, that the structure of the hydroxides prepared are of the "normal" CdI_2 type, by using techniques which would disclose small changes in the a_0, c_0 parameters but have not sought as yet for the presence of systematic changes in lattice spacings with preparative conditions.

Selected films, prepared as described above from the layers deposited in the kinetic experiments, were first examined by electron microscopy. Electron diffraction was then used to confirm the orientation; this was invariably one with the [0001] axis perpendicular to the mercury surface as shown in Fig. 11a and showing therefore $hk, 0$ diffractions only. Fig. 11b shows a composite pattern with the gold diffraction calibrating rings. A cube edge parameter of $a_0 = 4.0786\text{\AA}$ (53) was used in the calibration of the $\text{Cd}(\text{OH})_2$ spacings. Selected area diffraction permitted the calculation in many cases of the actual number of crystals present in the given area from the resolution of the diffraction spots in the rings. This number is in approximate agreement with the number of hexagonal crystallites which can be counted on the micrographs, Fig. 11c. It is likely therefore that these crystallites are the basic units growing on the surface. Rotation of the specimen

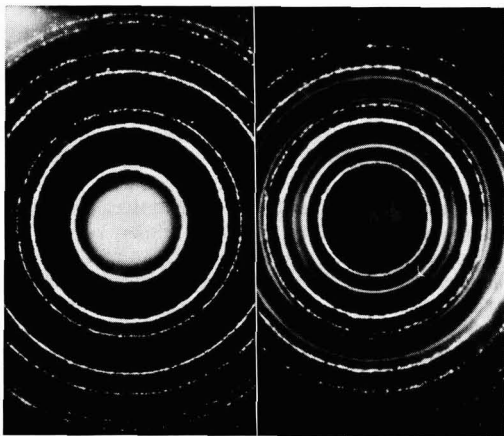


Fig. 11A (left) Electron diffraction pattern of cadmium hydroxide film formed on cadmium amalgam in 1N sodium hydroxide; beam \parallel to $\langle 001 \rangle$ axes of crystallites; B (right) composite pattern with gold for calibration.

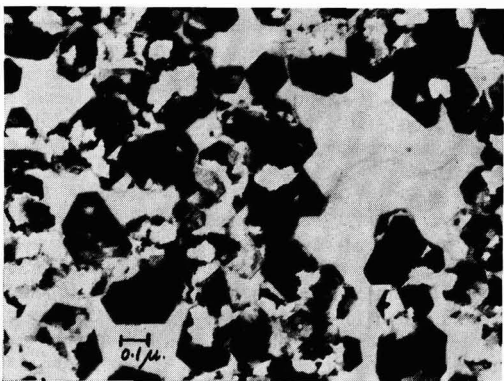


Fig. 11C. Electron micrograph of cadmium hydroxide crystals

in the electron beam gave rise to patterns similar to the example indexed in Fig. 12 where the $\{hk,l\}$ hexagonal indices (written as $\{hkl\}$ for convenience on the diagram) correspond to sharp and easily measured spots developing on the layer lines corresponding to a spacing of $\lambda L/c_0 \cos \theta$ where λ is the wave length, L the camera length, and θ the extent of rotation of the film from the position with the c_0 axis parallel to the beam.

The plane spacings can be internally calibrated from the a_0 value calculated from the $\{hk,0\}$ diffractions calibrated in turn with the gold. The axial ratio is then calculated by the expression

$$\frac{c_0}{a_0} = \frac{l}{\left[\frac{a_0^2}{d^2} - \frac{4}{3} (h^2 + k^2 + hk) \right]^{1/2}} \quad [23]$$

Typical data for the cadmium hydroxide films produced through three kinetic runs with 1% cadmium amalgam concentration in 1N sodium hydroxide are for an overpotential $\eta = 70$ mv $a_0 = 3.502 \text{ \AA}$ $c_0/a_0 = 1.339$; $\eta = 120$ mv $a_0 = 3.510 \text{ \AA}$ $c_0/a_0 = 1.323$ and $\eta = 220$ mv $a_0 = 3.489 \text{ \AA}$ $c_0/a_0 = 1.323$. These values should be compared with the A.S.T.M. index

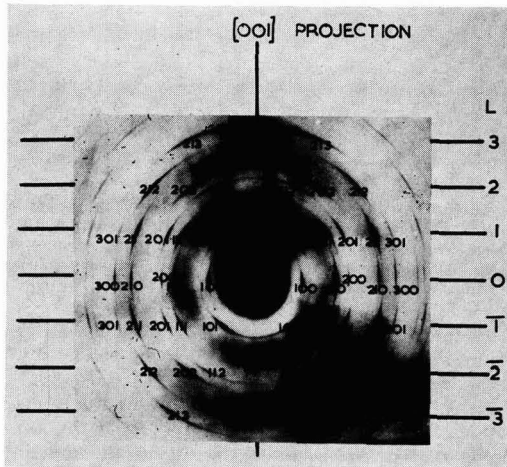


Fig. 12. Indexed electron diffraction pattern of cadmium hydroxide film tilted through 41° (hexagonal indices).

which gives for the unit cell $a_0 = 3.580$ $c_0/a_0 = 1.405$; $a_0 = 3.475$ $c_0/a_0 = 1.358$ (54); $a_0 = 3.47 \text{ \AA}$ $c_0/a_0 = 1.337$ (55).

A similar technique with mercurous chloride with the electron beam at an angle to the orientated plane parallel to the mercury surface yields patterns such as that shown in Fig. 13. The orientation with the c_0 axis of the tetragonal cell together with the end face diagonal is invariably followed under any condition of deposition. The patterns are most readily indexed by substituting as unit cell one of $\sqrt{2}a_0$ and c_0 as the parameters, this cell lying with the

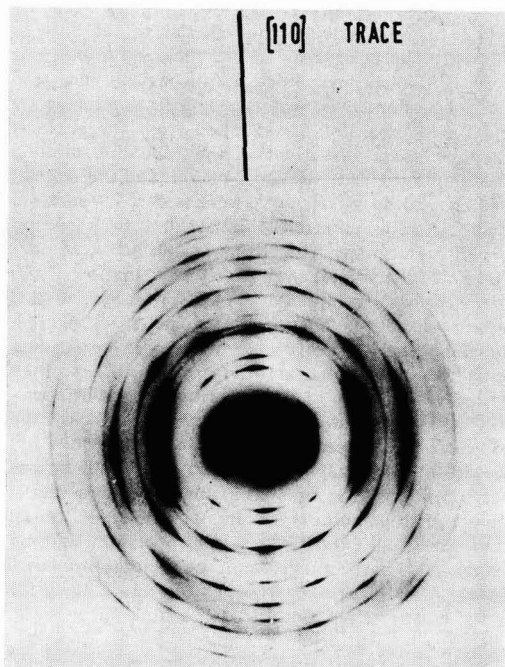


Fig. 13. Electron diffraction pattern of tilted calomel film

{100} face in the film and the layer lines developing from the $a_0\sqrt{2}$ plane spacings perpendicular to the film.

Thalious chloride (cesium chloride structure) crystallizes with spacings strictly in accordance with the massive material. At overpotentials up to about 80 mv the basal orientation is with a cube face parallel to the amalgam surface; at higher overpotentials a change in orientation is observed, and the larger crystals can be seen to have a {110} face parallel to the amalgam surface. This is clearly shown in Fig. 14A and B. With more finely crystalline material it is difficult to say if the {110} orientation is unique because there are no absent reflections as is the case with the finely crystalline material in the {100} orientation.

The confirmation of the structure of the extremely thin layers of zinc oxide has proved to be of considerable difficulty. Reasonably clear diffraction patterns were obtained with an Akashi Tronscope electron microscope after the removal of the pole pieces and on a Metropolitan Vickers type E.M.3. instrument. Attempts to use a Finch-type electron diffraction camera were without success. There was a close similarity between the patterns from the films which were clearly of very small particle size. Typical d spacings in Å are 2.821, 2.437, 1.623, 1.357 corresponding to diffractions from the {10,0}, {10,1}, {11,0}, and {20,1} planes of hexagonal zinc oxide. (The ASTM index gives 2.861, 2.476, 1.626, 1.354Å, respectively.) The {00,2} diffraction ring is completely missing as are the {10,2} and {10,3}. We consider that the evidence for a nearly unimolecular layer of finely crystalline zinc oxide with a predominantly basal orientation is thus quite strong.

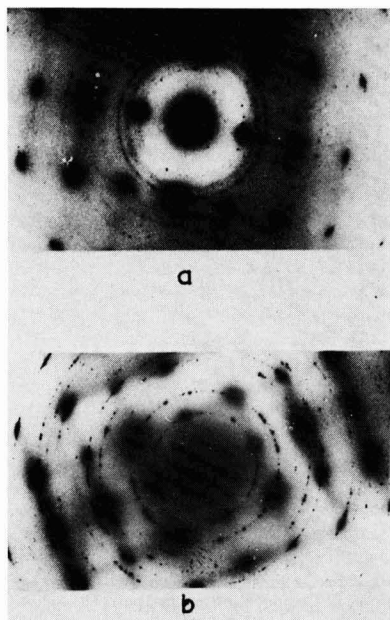


Fig. 14. Electron diffraction patterns of thallium chloride films formed on thallium amalgam in 1N hydrochloric acid. A, overpotential of 90 mv, [110] orientation; B, overpotential of 50 mv, [100] orientation.

Discussion of the Kinetics of the Initial Stages of Passivation

It has already been pointed out that the current-time transients obtained below the reversible potential can be explained by the slow adsorption of anions. In most systems the coverage at the reversible potential is already very high, of the order 0.5. At potentials above the reversible potential the shape of the current-time transient changes and this shape is clearly consistent with the mechanism of growth of two-dimensional centers. This mechanism is clearly favored by the highly condensed adsorbed layer which is formed at these potentials. In such a layer the formation of clusters leading to two-dimensional nucleation is very likely.

Detailed tests of the fit of the data to Eq. [19] can be carried out at low overpotentials where a single peak can be observed separately, for example, for cadmium hydroxide, Fig. 9A. For the reduction of the layer on zinc amalgam the initial part can be observed independently of other processes such as adsorption. In this region of time Eq. [19] reduces to Eq. [12]. A test of this equation is shown in Fig. 15. At longer times the exponential term, leading to a reduction in the current, must be taken into account. Equation [19] can be written

$$\ln \frac{i}{t^2} = \ln \frac{zF\pi M h k^2 A'}{\rho} - \frac{\pi M^2 k^2 A' t^3}{3\rho^2} \quad [24]$$

A test of this is shown in Fig. 16A. It can be seen that the fit is again good (40). On the other hand a similar test for the second layer, assuming this to grow on a uniform complete monolayer of the new phase, does not give a good fit, Fig. 16B. It is clear that layers after the first cannot be assumed to grow independently of each other. It is difficult to treat the problem of the deposition of a succession of monolayers algebraically, but it has been shown (38, 39) that transients of the kind in Fig. 7, 8c, and 9c can be obtained by direct simulation in a digital computer of the multilayer problem. It is possible in this way to obtain also a separate esti-

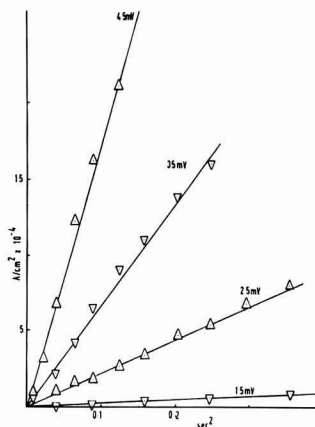


Fig. 15. Variation of the current with the square of time for the reduction of zinc oxide on zinc amalgam in borate buffer of pH 9.14 at the overpotentials shown (-ve values).

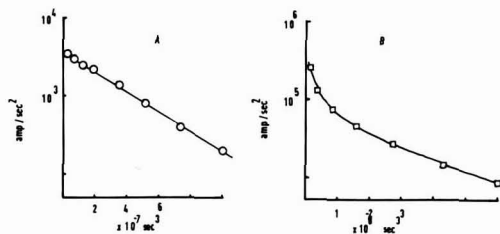


Fig. 16. Variation of $\log i/t^2$ with the cube of time for the formation of cadmium hydroxide on cadmium amalgam in 5N sodium hydroxide. A, first monolayer at an overpotential of 30 mv; B, second monolayer at an overpotential of 80 mv.

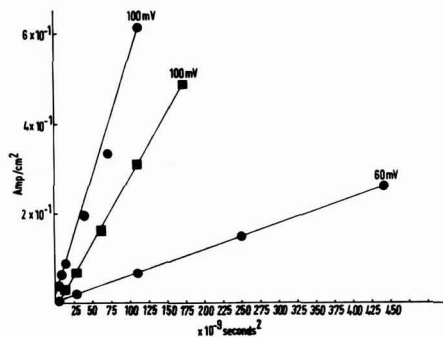


Fig. 17. Variation of the current with the square of time according to Eq. [25] for the growth of cadmium hydroxide on cadmium amalgam in N sodium hydroxide at the overpotentials shown: —●— first layer; —■— second layer.

mate of k and A' . The assumption that the succeeding layers grow independently of each other is most likely to hold in the vicinity of the current maximum and the validity of the model can alternatively be tested in this region for all the layers (7, 39, 40). Expansion about the maximum gives for small time displacements $\pm u$ using the general Eq. [22] for randomly orientated centers

$$i_u + i_{-u} \approx 2i_m - \frac{3 \exp\left(\frac{4}{3}\right) M^2 i_m^3 u^2}{2z^2 F^2 h^2 \rho^2} \quad [25]$$

provided $u^2/t^2 \gg u^4/t^4$. This equation can be tested in two ways. In the first place the current in the vicinity of the maximum should vary with the square of the displacement from the maximum. This is illustrated in Fig. 17 for the first and second peak observed during the formation of cadmium hydroxide. Second, the slope of these plots should be proportional to the cube of the current at the maximum, and this is illustrated in Fig. 18 again for the formation of cadmium hydroxide. The value of the intercept can be calculated furthermore from the observed orientation and gives the full line in Fig. 18. It can be seen that the agreement with this stringent test is reasonable and that there are no systematic differences between the first and second layers. The assumption that the first and second layers grow independently of each other in the vicinity of the current maximum is therefore justified (40). Similar agreement has been obtained for the first three

layers of calomel growing on mercury (39) and the first two layers of thallium chloride on thallium amalgam (50).

The fit of the current-time transients to the model assuming the growth and overlap of two-dimensional centers leads to further conclusions and results. Since the equations of the type [19] and [22] are derived assuming a uniform rate of deposition (k moles $\text{cm}^{-2}\text{sec}^{-1}$) it follows that the overlap of the centers cannot lead to a retardation of growth as it would, for example, if the rate of mass transfer of ions to the centers were reduced by the interaction of the diffusion fields. The slow stage of crystal growth must therefore take place at the edges of the growing centers so that lattice formation by an electrochemical reaction is rate-determining in the same way as in the growth of three-dimensional centers (5, 6, 8, 9, 35). The composite rate constant $k^2 A'$ can therefore be deduced from the parameters of the peaks, preferably the current at the maximum. The potential and concentration dependence of the composite rate constant $k^2 A'$ can then be examined in the usual way. The example for the first two peaks of cadmium hydroxide shown in Fig. 19 is typical of the results obtained. At high overpotentials the rate constants for the two peaks are equal. It follows that k and A' must separately be equal for the two layers. At low overpotentials the value of $k^2 A'$ for the second peak is much smaller than that for the first peak, and this has been attributed to a decrease in the nucleation rate constant for the second succeeding layers (7, 38, 39) as compared to the first. Formulation of the nucleation rate constant for the first layer according to the classical theory gives

$$A_1' = Kk_0 \exp - \frac{N\pi h^2 \sigma_1^2}{\left[\frac{h\rho z F \eta}{M} + (\sigma_3 - (\sigma_1 + \sigma_2)) \right] RT} \quad [26]$$

where σ_1 , σ_2 , and σ_3 are the surface energies between the nucleus and the solution, the nucleus and the

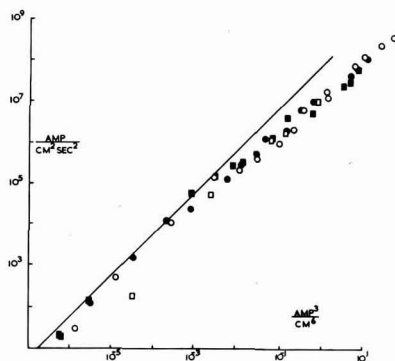


Fig. 18. Variation of the slope of plots such as those in Fig. 17 with the cube of the current at the maximum. The full line is drawn according to Eq. [25] with the crystallographic values of h and ρ . ○, first layer on 1% cadmium amalgam in 5N sodium hydroxide; □, second layer on 1% cadmium amalgam in 5N sodium hydroxide; ●, first layer on 1% cadmium amalgam in 1N sodium hydroxide; ■, second layer on 1% cadmium amalgam in 1N sodium hydroxide.

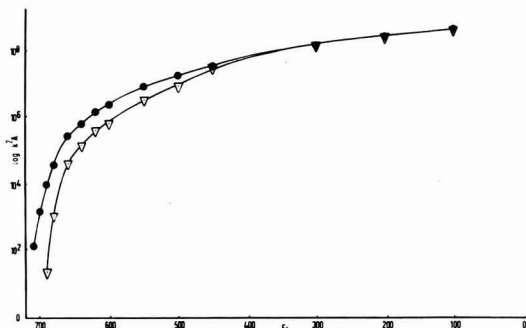


Fig. 19. Variation of rate constant k^2A with electrode potential for the growth of cadmium hydroxide on 1% cadmium amalgam in 1N sodium hydroxide. —●—, first layer; —▽—, second layer.

electrode, the electrode and the solution, k_o is the value of k at the reversible potential, and K is a constant containing the number of adsorbed species. For the second and succeeding layers it is likely that $\sigma_3 - (\sigma_1 + \sigma_2)$ is small so that the usual expression for two-dimensional nucleation is obtained.

$$A_2' = Kk_o \exp - \frac{NM\pi h\sigma_1^2}{\rho z F \eta RT} \quad [27]$$

Since $\ln \frac{k^2 A_2'}{k^2 A_1'}$ can be shown to vary linearly with

$1/\eta$ it has been suggested (39, 40, 50) that $\sigma_3 - (\sigma_1 + \sigma_2)$ is large for the first layer giving a nucleation rate nearly independent of potential (neglecting the variation of σ with ϕ). The large value of the surface energy between the metal and solution in fact drives the nucleation in the first layer and in favorable cases could lead to incipient crystal growth below the reversible potential. This behavior is analogous to the formation of condensed layers on adsorbents below the saturation vapor pressure and is the most likely explanation for the plateau developing on the current-time curves for the specific adsorption of chloride ions on thallium amalgam, Fig. 6.

With the assumption of a constant nucleation rate in the first layer the variation of k with composition and potential can be examined. In favorable cases (39) the nucleation rate can also be estimated giving absolute values of k and k_o . These are large, of the order $k_o = 4 \times 10^{-3}$ moles $\text{cm}^{-2} \text{sec}^{-1}$ in the case of the crystal growth of calomel. These large values in the particular crystallographic directions along the plane undoubtedly again favor the classical mechanism of crystal growth. It is of interest that the values of k when corrected for the effects of the reverse reaction give simple Tafel slopes near the reversible potential, Fig. 20, which imply a rate-determining formation of the lattice from ions "discharged" onto the edge. From an examination of the potential and concentration dependence it has been suggested that in the case of calomel (39) this is the incorporation of a simple Hg^+ ion, for cadmium hydroxide a rate-determining rearrangement of two OH^- ions into the layer planes (40), and for thallos chloride a succession of two first order deposition steps (50) possibly analogous to the

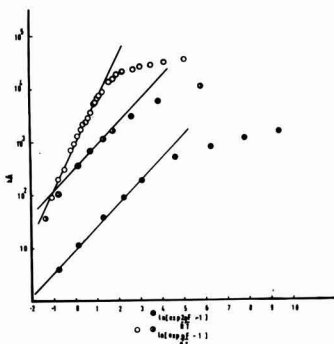


Fig. 20. Variation of the rate constant $k\sqrt{A}$ for the growth of the first monolayer of calomel, cadmium hydroxide, and thallos chloride with overpotential at low overpotentials. —●—, cadmium hydroxide; half open circle, solid on right side, calomel; —○—, thallos chloride. The full lines are drawn with the theoretical slopes according to the mechanisms suggested in the text.

nucleation of kinks at steps (56) followed by growth at these kinks. It must be noted that since lattice growth is the slow stage, the results do not give any indication as to the mechanism of ion transport to the growth sites.

The systems which have been examined already show a wide variety of behavior. In the case of cadmium amalgam in alkaline solution and of mercury in chloride solutions passivation sets in after a defined number of monolayers have been formed. For thallium amalgam in chloride solutions a multimolecular layer succeeds the formation of two monolayers before the electrode is passivated, while for the case of zinc amalgam in alkaline solutions a single layer only is found. The results show that a monomolecular film of a definite chemical phase is formed from the adsorbed layer and that the processes of adsorption and lattice formation can be kinetically distinguished and examined structurally. It seems likely that the process of passivation will usually be easy when there is a favorable crystal type and habit such as a layer structure. In the examples so far studied it appears that the kinetics of the initial stages of passivation can be regarded as a problem in electrocrystallization, the process of crystal growth being sterically defined.

Any discussion of this paper will appear in a Discussion Section to be published in the December 1963 JOURNAL.

REFERENCES

- U. R. Evans, *Z. Elektrochem.*, **62**, 619 (1958).
- H. H. Uhlig, *ibid.*, **62**, 626 (1958).
- N. Hackerman, *ibid.*, **62**, 632 (1958).
- W. J. Müller, "Die Bedeckungstheorie der Passivität der Metalle und ihre experimentelle Begründung," Verlag Chemie, Berlin (1933).
- M. Fleischmann and H. R. Thirsk, *Electrochim. Acta.*, **2**, 146 (1959).
- M. Fleischmann and H. R. Thirsk, *ibid.*, **2**, 22 (1960).
- M. Fleischmann and H. R. Thirsk, in "Advances in Electrochemistry," P. Delahay, Editor, Interscience, New York, To be published.
- M. Fleischmann and H. R. Thirsk, *Trans. Faraday Soc.*, **51**, 71 (1955).
- I. Dugdale, M. Fleischmann, and W. F. K. Wynne-Jones, *Electrochim. Acta.*, **5**, 229 (1961).

10. K. J. Vetter, *Z. Elektrochem.*, **58**, 230 (1954); **62**, 643 (1958).
11. A. Güntherschulze and H. Betz, *Z. Physik.*, **91**, 70 (1934); **92**, 367 (1934).
12. D. A. Vermilyea, *Acta Met.*, **1**, 282 (1953); **2**, 476, 482 (1954); **3**, 106, (1954). *This Journal*, **102**, 655 (1955).
13. E. J. W. Verwey, *Physica*, **2**, 1059 (1935).
14. N. Cabrera and N. F. Mott, *Rept. Progr. Phys.*, **12**, 163 (1949).
15. L. Young, "Anodic Oxide Films," Academic Press, London and New York (1961).
16. U. R. Evans, *J. Chem. Soc.*, **1927**, 1020.
17. J. E. O. Mayne and M. J. Pryor, *ibid.*, **1949**, 1831.
18. W. H. Vernon, F. Wormwell, and T. J. Nurse, *J. Iron Steel Inst.*, **150**, 281 (1944).
19. E. M. Mahla and N. A. Nielsen, *J. (and Trans.) Electrochem. Soc.*, **93**, 1 (1948).
20. W. Schwarz, *Z. Elektrochem.*, **55**, 170 (1951).
21. L. Tronstad and L. W. Borgmann, *Trans. Faraday Soc.*, **30**, 349 (1934); L. Tronstad, **29**, 502 (1933).
22. K. J. Vetter, *Z. Elektrochem.*, **58**, 230 (1954).
23. K. G. Weil, *ibid.*, **59**, 11 (1955); U. F. Franck and K. G. Weil, *ibid.*, **56**, 814 (1952).
24. I. Langmuir, *J. Am. Chem. Soc.*, **38**, 2267 (1946).
25. B. V. Ershler, *Doklady Akad. Nauk S.S.S.R.*, **37**, 258 (1946).
26. H. H. Uhlig, *Ind. Engng. Chem.*, **32**, 1490 (1940).
27. C. V. King and E. Rau, *This Journal*, **103**, 331 (1956).
28. H. H. Uhlig and S. S. Lord, *ibid.*, **100**, 216 (1956).
29. R. Ch. Burshtein, N. A. Shumilova, and K. Golbert, *Acta Physicochim. U.R.S.S.*, **21**, 785 (1956); N. A. Shumilova and R. Ch. Burshtein, *Doklady Akad. Nauk. S.S.S.R.*, **41**, 475 (1948); R. Ch. Burshtein, *Z. Elektrochem.*, **62**, 655 (1958).
30. Y. M. Kolotyrkin and W. M. Knasheva, *Zhur. fiz. Khim.*, **30**, 1990, (1956).
31. E. A. Aykasjan and A. J. Fedorova, *Doklady Akad. Nauk. S.S.S.R.*, **86**, 1137 (1952); A. N. Frumkin and E. A. Aykasjan, *ibid.*, **100**, 315 (1955).
32. Y. M. Kolotyrkin, *Z. Elektrochem.*, **62**, 665 (1958).
33. L. V. Vanyukova and B. N. Kabanov, *Zhur. fiz. Khim.*, **28**, 1025 (1954).
34. A. Bewick, A. Bewick, M. Fleischmann, and M. Liler, *Electrochim. Acta*, **1**, 83 (1959); A. Bewick and M. Fleischmann, *ibid.*, **8**, 89 (1963).
35. M. Fleischmann, H. R. Thirsk, and I. Tordesillas, *Trans. Faraday Soc.*, **58**, 1865 (1962).
36. M. Fleischmann and M. Liler, *Trans. Faraday Soc.*, **54**, 1370 (1958).
37. M. Avrami, *J. Chem. Phys.*, **7**, 1103 (1939); **8**, 212 (1940); **9**, 177 (1941).
38. A. Bewick, Ph.D. Thesis, University of Durham (1961).
39. A. Bewick, M. Fleischmann, and H. R. Thirsk, *Trans. Faraday Soc.*, **58**, 2200 (1962).
40. M. Fleischmann, K. S. Rajagopalan, and H. R. Thirsk, *ibid.*, **59**, 741 (1963).
41. I. N. Stranski, *Z. phys. Chem.*, **136**, 259 (1928).
42. I. N. Stranski and R. Kaishev, *Physikal. Z.*, **36**, 393 (1935).
43. M. Volmer, "Die Kinetik der Phasenbildung," Steinkopf, Dresden und Leipzig (1939).
44. W. K. Burton, N. Carbrera, and F. C. Frank, *Phil. Trans.*, **A243**, 299 (1951).
45. W. Lorenz, *Z. Naturf.*, **9A**, 716 (1954); *Z. phys. Chem.*, **17**, 136 (1958).
46. D. A. Vermilyea, *J. Chem. Phys.*, **25**, 1254 (1956).
47. A. Bewick, M. Fleischmann, and H. R. Thirsk, To be published.
48. D. C. Grahame, *Chem. Revs.*, **41**, 441 (1947). R. Parsons, Chap. 3 in "Modern Aspects of Electrochemistry," J. O'M. Bockris, Editor, Butterworths, London (1954).
49. D. C. Grahame and R. Parsons, *J. Am. Chem. Soc.*, **83**, 1291 (1961).
50. M. Fleischmann, J. Pattison, and H. R. Thirsk, To be published.
51. M. Fleischmann, K. S. Rajagopalan, and H. R. Thirsk, To be published.
52. H. Arnefelt, *Arkiv. f. Mat. Astron. Fysik. B.*, **23**, No. 2 (1932).
53. H. E. Swanson and E. Tatge, N.B.S. Circular 539, **1**, 33 (1953).
54. Strukturberichte II 258.
55. Strukturberichte I 161.
56. R. Becker and W. Döring, *Ann. Phys.*, **24**, 719 (1935).

Throwing Power of the Current in Anodic and Cathodic Protection

W. A. Mueller

Pulp and Paper Research Institute of Canada, Montreal, Quebec, Canada

ABSTRACT

Based on Ohm's and Kirchhoff's laws, a differential equation is derived relating the changing potential slope in the length direction of a pipe to the current density at the inner pipe surface. The extension of the pipe that can be passivated or maintained in the passive state by supplying current with one cathode is formulated for linear as well as exponential types of polarization curves and for pipes of finite and infinite length. Completely passivated pipes can be kept in the passive state over a much greater distance from the cathode than partly passive pipes. Agreement is found with reported experimental data on the throwing power of anodic protection. The same basic equations are valid with respect to the throwing power of cathodic protection, which is much smaller than that of anodic protection at comparable corrosiveness. On the application of anodic protection redox reactions of substances produced on cathodes, anodes on corroding metals and alloys can strongly influence the behavior.

For the application of anodic protection (1-6) in any lengthy vessel the throwing power (4) of the current is of primary importance. Evidently passivity is reached very rapidly in a vessel when the current density on its whole surface surpasses the

maximum value of the polarization curve. However, even at lower average current densities, formation and expansion of passivity occur when the current density locally surpasses the maximum value of the polarization curve. After the area of best current

supply has been passivated, more distant areas receive an increasing fraction of current.

A study of this problem has been carried out by Edeleanu and Gibson (7). They developed an experimental arrangement for the derivation of the throwing power of anodic protection. To this end a wire fed into a glass tube which was filled with an electrolyte was used as anode. From the wire the current flowed through the electrolyte to the cathode which was attached to the opening of the glass tube. From the length of the passivated area in the glass tube and from the current supplied, conclusions were made about the length of a pipe (made of the same metal as the tested wire) that can be passivated by current supply from one end. In this paper the throwing power of the current in anodic and cathodic protection is derived theoretically from polarization curves without the requirement of any other experimental data.

For the practical application of anodic protection a rough estimation of the required current is often possible without extended calculation. The high current required for initial passivation is equal to, or smaller than the product of the exposed surface area and the maximum current density of the pertinent polarization curve. In a vessel of lengthy shape, stepwise passivation can reduce the necessary current to a fraction of the amount required for simultaneous passivation. Also passivation from properly distributed cathodes or from both ends of tubes reduces the required current. The reader who is interested in practical application only, may omit the study of the complicated derivations to find most practical suggestions in the discussion.

Basic Derivation

This derivation refers to a pipe filled with an electrolyte of the specific resistance ρ ohm x cm. For the sake of simplicity a constant cross section of the pipe and a clean inner surface are assumed. Irregularities in the metal composition and deposits of foreign material are excluded.

The potential slope in the length direction of the pipe is according to Ohm's law

$$\frac{dE}{dx} = -\rho I_L \quad [1]$$

where E is the potential, x the length coordinate of the pipe, and I_L the current density in the length direction of the pipe.

Kirchoff's law may now be applied to calculate the change of the current in the length direction occurring when a fraction of it is branched off to the pipe surface. The current in the length direction of the pipe is $I_L \pi R^2$ where R is the radius of the pipe. The current exchange with the pipe surface between x and $x + dx$ amounts to $2\pi R I_S dx$, where I_S is the current density at the pipe surface. Hence

$$\frac{dI_L}{dx} = -\frac{2}{R} I_S \quad [2]$$

dI_L/dx can be derived from Eq. [1]. Thus a differential equation of general validity is derived (8)

$$\frac{d^2E}{dx^2} = \frac{2\rho}{R} I_S \quad [3]$$

Equation [3] can be used for the derivation of $E = f(x)$ if the polarization curve is known, i.e., the current density I_S as a function of the potential difference between pipe surface and electrolyte. It serves to derive the throwing power of the current in anodic and cathodic protection. In the present derivation the throwing power of the current with respect to anodic protection is expressed in two different ways: (a) as the maximum length of a pipe that can be passivated by current supplied from one end of the pipe which was originally in the active state, and (b) the maximum length of an originally passive pipe which can be maintained passive by supplying current. With respect to cathodic protection, the throwing power of the current is the maximum length of the pipe within which the corrosion rate is substantially reduced by cathodic protection. The values of R , ρ , and of the length of the pipe are required for the calculation. Equation [3] can be applied to any form of the polarization curve. Winsel (9) treated a similar problem, the distribution of current in porous electrodes. He limited the derivation to exponential polarization curves only, whereas in this paper the cases of linear current-density-potential relation and of potential-independent current density are also discussed.

Application to an Exponential Polarization Curve in the Active State with Respect to Anodic Protection

Initially the whole pipe may be in the active state. It is then passivated by anodic protection up to a certain distance from the cathode. The active state is assumed to be stable as indicated by a positive current density at the maximum of the polarization curve (1, 3, 10). The passive state may be stable or unstable, but in any case the current density in the passive state should be negligibly low in comparison to the current density in the active state.

For example, the polarization curve may be of the form given in Fig. 1 (12). For the slope of the polarization curve in the active state the decline of the current density may follow approximately the equation (12).

$$I_S = 2I_{SM} \exp \beta(E - E_M) \quad [4]$$

where I_{SM} is the maximum value of I_S , β the exponent (12) (volt⁻¹), and E_M the potential at which I_S is equal to I_{SM} . The numerical factor 2 in Eq. [4] is only an approximate value (12); it equals unity at $E = E_M$.

After substituting I_S from Eq. [4] into Eq. [3]

$$\frac{d^2E}{dx^2} = \frac{4\rho}{R} I_{SM} \exp \beta(E - E_M) \quad [5]$$

which is valid for $E_M - E > 0$.

For $E = E_M$, $\exp \beta(E - E_M) = 1$ and therefore

$$\left(\frac{d^2E}{dx^2} \right)_{(E=E_M)} = \frac{4\rho}{R} I_{SM} \quad [6]$$

The apparent deviation of Eq. [6] from Eq. [3] by the factor 2 is caused by the deviation of the

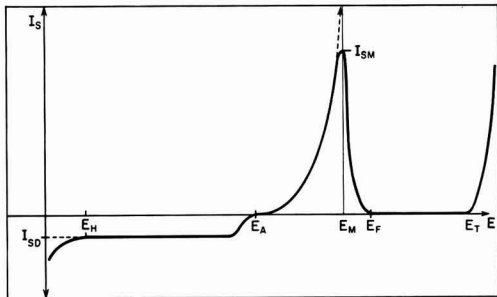


Fig. 1. Schematic diagram of a polarization curve composed of an exponential branch of the anodic dissolution current (10) leading to the constant very low current density in the passive state and of the diffusion current I_{SD} in the active state.

polarization curve from the exponential course when approaching I_{SM} (see definition of E_M).

It is easily shown that

$$\frac{dE}{dx} = - \left(\frac{4\rho}{R} I_{SM} \frac{2}{\beta} \exp \beta (E - E_M) + C \right)^{1/2} \quad [7]$$

is the solution of the differential Eq. [5], because Eq. [5] results from differentiation of Eq. [7]. It is understood from the derivation that Eq. [7] is valid for $E < E_M$. As the polarization curve reaches the maximum value of I_S at E_M , the deviation of dE/dx from Eq. [7] becomes very pronounced.

With respect to pipes of various lengths the value of C can be derived from the assumption $dE/dx = 0$ at the closed end of the pipe. Of course, the limits of the validity of Eq. [4] are to be considered. For a pipe of finite length

$$C = - \frac{8\rho I_{SM}}{R\beta} \exp \beta (E_E - E_M) \quad [8]$$

where E_E is the potential reached at the closed end of the pipe.

After substitution into Eq. [1], I_L is derived by integration

$$I_L = \left(\frac{8 I_{SM}}{\rho R \beta} \right)^{1/2} \left((\exp \beta (E - E_M) - \exp \beta (E_E - E_M))^{1/2} \right) \quad [9]$$

For the potential $E = E_M$, Eq. [9] becomes

$$I_{LM} = \left(\frac{8 I_{SM}}{\rho R \beta} \right)^{1/2} (1 - \exp \beta (E_E - E_M))^{1/2} \quad [10]$$

I_{LM} is the current density flowing in the length direction of the pipe where the potential is E_M .

In an analogous manner the behavior in the range of the conversion from active to passive states can be derived, assuming an exponential decrease of the current density (10) according to

$$I_S = 2I_{SM} \exp \gamma (E_M - E) \quad [11]$$

where γ is a constant. Close to $I_S = I_{SM}$ a deviation occurs as discussed with respect to Eq. [6] and [7].

The current density in the length direction is de-

rived for the potential range between E_M and the Flade potential E_F

$$I_L = - \left(\frac{8 I_{SM}}{\rho R \gamma} \right)^{1/2} (+ \exp \gamma (E_M - E) - \exp \gamma (E_M - E_F))^{1/2} + I_{LF} \quad [12]$$

where I_{LF} is the current density flowing from the passive to the active range of the pipe.

Usually the term $\exp \gamma (E_M - E_F)$ can be neglected and I_{LM} is given by

$$I_{LM} = - \left(\frac{8 I_{SM}}{\rho R \gamma} \right)^{1/2} + I_{LF} \quad [13]$$

I_{LF} results from Eq. [10] and [13]

$$I_{LF} = \left(\frac{8 I_{SM}}{\rho R \gamma} \right)^{1/2} + \left(\frac{8 I_{SM}}{\rho R \beta} \right)^{1/2} (1 - \exp \beta (E_E - E_M))^{1/2} \quad [14]$$

Equation [14] is valid for a pipe in which the potential $E_E < E_M$ is reached at the end located distant from the current supply.

The density of the current which flows from the cathode to the active range of the pipe is I_{LF} . If I_S in the passive state can be neglected, I_L in the passive state equals I_{LF} and the slope of the potential in the passive range is ρI_{LF} . The current supplied to the cathode can be increased so as to reach the potential of the borderline E_T between passive and transpassive range at the pipe surface close to the cathode. Then in agreement with Edeleanu and Gibson (7) the passive length L_P of the pipe is derived from Eq. [1]

$$L_P = \frac{E_T - E_F}{I_{LF} \rho} \quad [15]$$

By substitution in Eq. [14] L_P is derived for a pipe of finite length

$$L_P = \frac{(E_T - E_F)}{\left(\frac{8\rho I_{SM}}{R\gamma} \right)^{1/2} + \left(\frac{8\rho I_{SM}}{R\beta} \right)^{1/2} (1 - \exp \beta (E_E - E_M))^{1/2}} \quad [16]$$

If the whole pipe is initially in the active state, the current density at the pipe surface close to the cathode may initially be greater than I_{SM} . Hence the potential of that area of the pipe shifts rapidly to the passive range. The increasing extension of the passive range can be calculated from Eq. [16] if the changing polarization curve is known with respect to a surface that is active before the passivating current is switched on. For a pipe of limited length the passive area becomes somewhat further extended than for a pipe of infinite length. If two cathodes of distance D apart are used, D can be chosen twice the length of a tube with closed ends that can be passivated by applying current at one point only. For the calculation of L_P the value of E_E in Eq. [16] is required.

Hence the change of the potential with the distance from the source of current is of interest. Across the passive region of the pipe, dE/dx equals

— $I_{LF}\rho$. As in the active range an increasing fraction of I_L passes to the pipe surface, dE/dx decreases with increased distance from the source of current. According to Eq. [7] and [8] the relation between potential and the distance $x - x_M$ from the point where $E = E_M$ is given by

$$x - x_M = - \left(\frac{R \beta}{8 \rho I_{SM}} \right)^{1/2} \int_{E_M}^E \frac{dE}{\left(\exp \beta (E - E_M) - \exp \beta (E_E - E_M) \right)^{1/2}} \quad [17]$$

Equation [17] can be integrated by applying the standard integral

$$\int \frac{dx}{(a + \exp px)^{1/2}} = \frac{-2}{p \sqrt{-a}} \arcsin (-a)^{1/2} \exp - \frac{p}{2} x + C \quad [18]$$

to Eq. [17], giving

$$x - x_M = \left(\frac{R}{2 \beta \rho I_{SM}} \right)^{1/2} \frac{\arcsin \exp \frac{\beta}{2} (E_E - E_M) \left(\exp - \frac{\beta}{2} (E - E_M) - 1 \right)}{\exp \frac{\beta}{2} (E_E - E_M)} \quad [19]$$

Equation [19] represents the relation between the metal-electrolyte potential difference and the distance $(x - x_M)$ from the point where $E = E_M$. For the application of Eq. [19] $(x - x_M)$ might be calculated as a function of $(E - E_M)$ for a variety of $(E_E - E_M)$ values.

For a pipe of infinite length $\exp \frac{\beta}{2} (E_E - E_M)$

can be neglected. Hence the relation is considerably simplified and can be formulated

$$x - x_M = - \left(\frac{R}{2 \beta \rho I_{SM}} \right)^{1/2} \left(\exp - \frac{\beta}{2} (E - E_M) - 1 \right) \quad [20]$$

From Eq. [20] the potential difference $E - E_M$ is given by

$$E - E_M = - \frac{\beta}{2} \log \text{nat} \left[\left(\frac{x_M - x}{\left(\frac{R}{2 \beta \rho I_M} \right)^{1/2}} + 1 \right) \right] \quad [21]$$

The potential changes approximately proportionally to the logarithm of the distance from the point where $E = E_M$. These equations hold only in the potential range where anodic dissolution produces the main fraction of the current (Eq. [4]). For instance, the equations no longer apply when H_2 development causes the flow of current at an amount comparable to that caused by the dissolving metal.

The polarization curve does not always follow the model course assumed in the above derivation. For instance, it may follow a straight line from the

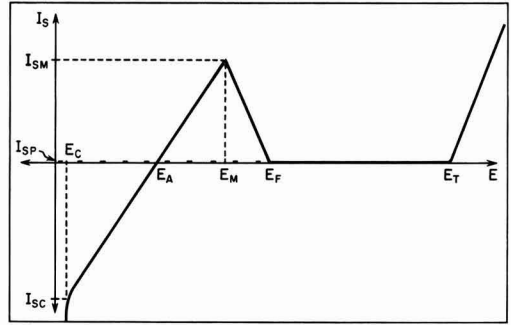


Fig. 2. Schematic diagram of a polarization curve composed of branches which change linearly with the potential.

maximum value I_M at E_M to the stable potential in the active state E_A (Fig. 2)

$$I_S = I_{SM} \frac{E - E_A}{E_M - E_A} \quad [22]$$

According to Eq. [3] the corresponding differential equation is

$$\frac{d^2(E - E_A)}{dx^2} = \frac{2 \rho I_{SM}}{R} \frac{E - E_A}{E_M - E_A} \quad [23]$$

In a manner analogous to the above derivation the potential-distance relation is derived to

$$\frac{E - E_A}{E_M - E_A} = \exp \sqrt{\frac{2 \rho I_{SM}}{R(E_M - E_A)}} (x - x_M) \quad [24]$$

where $(x - x_M)$, the distance of the point of the potential E from that of the potential E_M , is zero or negative. This equation shows that the potential approaches the stable active potential with an exponential curve. It applies to the potential range $E_A \leq E \leq E_M$.

Application to the Conditions of the Passive State

It has been proven (4) that excellent throwing power is obtained with respect to anodic protection of a lengthy tube even if the current is supplied only at one open end. This is possible because the density of the anodic dissolution current in the demonstrated case is almost negligible. To investigate this effect, assumptions have to be made with respect to the current-density-potential relation. For the sake of simplicity a constant current density ($I_S = I_{SP}$) may be assumed. Equations [1] to [3] are the basis of any such derivation. Integration of Eq. [3] results in

$$\frac{dE}{dx} = \frac{2\rho}{R} \int I_{SP} dx \quad [25]$$

At the end of the pipe $dE/dx = 0$ and $(x - x_0)$ may be the distance from the closed end, hence

$$\frac{dE}{dx} = - \frac{2\rho}{R} I_{SP} (x - x_0) \quad [26]$$

The potential is derived by another integration

$$E - E_0 = \frac{\rho I_{SP}}{R} (x - x_0)^2 \quad [27]$$

where E_o is the potential at $x = x_o$. If the potential of the pipe at the point which is closest to the cathode is E_T and the potential at the end of the Flade potential E_F , $(x - x_o) = L_M$, which is the maximum length that can be kept in the passive state by means one cathode, then

$$L_M = \left(\frac{(E_T - E_F)R}{\rho I_{SP}} \right)^{1/2} \quad [28]$$

Of course for safety reasons the total difference $(E_T - E_F)$ cannot be used; the potential at the end has to be higher than E_F to make sure no shift to the active state can occur even when conditions are changed temporarily.

Equation [28] may now be compared with the data given by Sudbury and co-workers (4) with respect to the passivation of a tube of 60 ft (1820 cm). The tube radius was $\frac{3}{4}$ in. (1.91 cm). The potential drop was 0.4v; the specific resistance of 67% by weight H_2SO_4 is about 1.54 ohm x cm at 75°F (13). The current density is therefore calculated to

$$I_{SP} = 0.15 \mu\text{a}/\text{cm}^2 \quad [29]$$

if the current was supplied only from one end of the tube, and to

$$I_{SP} = 0.60 \mu\text{a}/\text{cm}^2$$

if the current was supplied from both ends of the tube, i.e., through the back flowing acid as well as through the acid entering the pipe.

Shock and others (5) found at 304 stainless steel immersed in 67% H_2SO_4 by weight a decreasing current density which attained 0.6 $\mu\text{a}/\text{cm}^2$ after 1-2 hr. On the other hand, it is known that the decrease of the current density continues for days and weeks (11), and the calculated value of 0.15 $\mu\text{a}/\text{cm}^2$ may have been reached during the operation of anodic protection. In any case, the calculations give the right order of magnitude.

Throwing Power of Cathodic Protection

The equations of general validity, viz., Eq. [1]-[3], can also be applied to derive the throwing power of cathodic protection with respect to pipes. In this application the form of the polarization curve in the cathodic range is of decisive importance. If the negative current density in the cathodic range follows the same trends as the positive current density in the anodic range, the same equations apply to the current-density-potential-distance relation. For instance, the polarization curve may follow a straight line from the current density I_{SC} (Fig. 2) attained at the most cathodic potential to zero at the potential E_A . Then the current density I_S amounts to

$$I_S = I_{SC} \frac{E - E_A}{E_C - E_A} \quad [30]$$

Equation [30] is equal to Eq. [22] except for the constants. In an equation analogous to Eq. [24] the potential distance relation can be formulated

$$\frac{E - E_A}{E_C - E_A} = \exp \sqrt{\frac{2\rho I_{SC}}{R(E_C - E_A)}} (x - x_c) \quad [31]$$

where $x = x_c$ at the potential $E = E_C$. From Eq. [31] the corrosion rate in a pipe can be calculated as a

function of the distance from the anode, provided the current-density-potential relation follows Eq. [30].

There is another group of polarization curves in which the negative current density maintains a constant level over an extended range. For instance, this type of polarization curve is formed when the total depolarization current is diffusion-controlled. Under these conditions Eq. [25]-[27] apply when I_{SP} is replaced by the diffusion current I_{SD} (Fig. 1) and E_o by E_A . Analogous to Eq. [27] the current density-potential-distance relation is formulated

$$E - E_A = \frac{\rho I_{SD}}{R} (x - x_c)^2 \quad [32]$$

If the part of the pipe which is closest to the anode is kept at the potential E_H at which the negative current begins to increase rapidly (because of H_2 development) the range covered by cathodic protection is

$$L_M = \left(\frac{(E_H - E_A)R}{\rho I_{SD}} \right)^{1/2} \quad [33]$$

I_{SD} is greater than or equal to the density of the corrosion current I_{corr} . Hence under the conditions of Eq. [33] the distance from the anode at which cathodic protection would begin to reduce the corrosion rate in a pipe is equal to, or lower than

$$\left(\frac{(E_H - E_A)R}{\rho I_{corr}} \right)^{1/2}. \text{ For an effective protection of}$$

the pipe the distance from the anode should be considerably smaller. Equation [28] equals Eq. [33] except for the definition of the current densities. However, when the range protected by cathodic protection becomes large because of a very small value of I_{SD} , the corrosion rate found at that small value of I_{SD} which is reduced by cathodic protection is very small. But in anodic protection I_{SP} can be many orders of magnitude smaller than the corrosion current in the active state. Hence a high throwing power of the current in anodic protection can be attained even if the corrosion rate in the active state is high.

Discussion

The present derivation is based on the assumption that the actual polarization curve is known for the conditions under consideration. In addition to the polarization curve, only Ohm's and Kirchhoff's laws are used in Eq. [1]-[3]. Detailed equations are derived with respect to a polarization curve that can be formulated as a Tafel relation. For the application of the derived equations an exact knowledge of actual polarization curves is of fundamental importance. Swinging potentials and time-dependent polarization curves require particular attention. Also differences in the supply of chemicals to the metal surface may have a considerable influence. In this respect the strong influence of reagents produced by corrosion and by the applied current may be mentioned. The rapid dissolution of the metal in the boundary region between active and passive areas causes a rapidly increasing concentration of the produced metal ions. The partial current originating from redox reactions of these ions has to be con-

sidered in the calculations. For instance, if in an iron pipe the electrolyte flows from active to passive areas (14), bivalent iron ions formed in the active range would react with the passive fraction of the pipe to form trivalent iron ions. The anodic current caused by this redox reaction would decrease the current supplied to the active fraction of the pipe, thus strongly reducing the throwing power of anodic protection. In an analogous manner an electrolyte flowing from passive and transpassive to active areas might carry oxidizing reagents which would initiate a cathodic partial current in the active area thus reducing the total current density, i.e., the throwing power of the current in anodic protection would be increased. On the other hand, reducing reagents produced at the cathode and carried by the flowing electrolyte would have the opposite effect. Evidently redox reactions and their dependency on the flow direction of the electrolyte can strongly influence the throwing power of anodic and cathodic protection. These conclusions suggest methods to improve the throwing power of electrochemical protection, and they may explain some important phenomena (14). No experiments have been carried out to corroborate the derived equations, which appear to be reliable because no arbitrary assumptions had to be made in the basic derivations of Eq. [1]-[3]. The comparison with the experimental data of Sudbury and co-workers shows a reasonable agreement.

A striking result of these derivations is the great difference between the excellent throwing power of the anodic current in a completely passivated system and its fairly limited throwing power in a pipe which is partly in the active state. This result can be expressed by the ratio L_M/L_{P_s} , where L_{P_s} is the length of the passivated fraction of the pipe of infinite length which is in the active state except for the passivated fraction close to the cathode. From Eq. [16] and [28] is derived

$$\frac{L_M}{L_{P_s}} = \left(\frac{I_{SM}}{I_{SP}} \right)^{1/2} \left(\frac{8}{E_T - E_F} \right)^{1/2} \left[\left(\frac{1}{\beta} \right)^{1/2} + \left(\frac{1}{\gamma} \right)^{1/2} \right] \quad [34]$$

$$\text{The factor} \quad \left(\frac{8}{E_T - E_F} \right)^{1/2} \left[\left(\frac{1}{\beta} \right)^{1/2} + \left(\frac{1}{\gamma} \right)^{1/2} \right]$$

is usually close to unity. As the ratio I_{SM}/I_{SP} is in the range 10^4 to 10^8 in most cases, the protection in a completely passivated system covers about 10^2 to 10^4 times the length protected in a system which is partly in the active state. The initial passivation of an originally active pipe requires special methods to attain the extremely high throwing power known for completely passivated systems. The pipe might be passivated by filling with a passivating solution at low temperature (7, 15). Once passivity has been attained in the total length of the pipe, current is required only to maintain passivity when replacing the passivating solution by the solution to be conducted in the pipe. If the passive state is unstable, reactivation is caused by interruption of the current. With respect to a portion of a tube which is just being reactivated, the current required for repassivation is much less than the current required for the initial passivation.

Any discussion of this paper will appear in a Discussion Section to be published in the December 1963 JOURNAL.

REFERENCES

1. C. Edeleanu, *Nature*, **173**, 739 (1954); *Metallurgia*, **50**, 113 (1954); *Corrosion Technol.*, **2**, 204 (1955).
2. Milan Prazak, *Hutnické listy*, **11**, 644 (1956).
3. W. A. Mueller, *Can. J. Technol.*, **34**, 162 (1956); *Tappi*, **40**, [3], 129 (March 1957); *Pulp Paper Mag. Can.*, **60**, T3 (January 1959); *Tappi*, **42**, [3], 179 (March 1959).
4. J. D. Sudbury, O. L. Riggs Jr., and D. A. Shock, *Corrosion*, **16**, 91 (1960).
5. D. A. Shock, O. L. Riggs Jr., and J. D. Sudbury, *ibid.*, **16**, 99 (1960).
6. O. L. Riggs, Jr., Merle Hutchinson, and N. L. Conger, *ibid.*, **16**, 102 (1960).
7. C. Edeleanu and J. G. Gibson, *Chemistry and Industry*, **10**, 301 (March 1961).
8. W. A. Mueller, *Corrosion*, **18**, 359t (1962).
9. A. Winsel, *Z. Elektrochem.*, **66**, 287 (1962).
10. K. J. Vetter, in "Passivierende Filme und Deckschichten," H. Fischer, K. Hauffe, and W. Wiederholt, Springer Verlag (1956).
11. W. A. Mueller, *Corrosion*, **18**, 73t (1962).
12. W. A. Mueller, *This Journal*, **107**, 157 (1960).
13. A. N. Campbell, E. M. Kartzmark, D. Bisset, and M. E. Bednas, *Can. J. Chem.*, **31**, 303 (1953).
14. J. D. Sudbury and O. L. Riggs, Private communication.
15. W. A. Mueller, *Corrosion*, **17**, 557t (1961).

On the Passivity of Manganese in Acid Solutions

K. E. Heusler

Max-Planck-Institut für Metallforschung, Abteilung Sondermetalle, Stuttgart, Germany

A review of the literature concerning the anodic behavior of manganese gives some indication that manganese can be passivated. Passing sufficiently large anodic currents through a manganese electrode ennobles the potential until oxygen is evolved and permanganate is formed (1). One would expect (2) the passive manganese to be covered by a thin, invisible, and electron conducting oxide layer similar to the layers known to exist on iron and chro-

mium. However, in most of the earlier experiments with manganese passivity was accompanied with formation of a thick, visible deposit of manganese dioxide. The thick deposits could have been formed by oxidation of manganous ions or by decomposition of permanganate from the solution.

Detailed information on passive manganese is lacking. Polarization curves of passive manganese have not yet been measured, and it is an open ques-

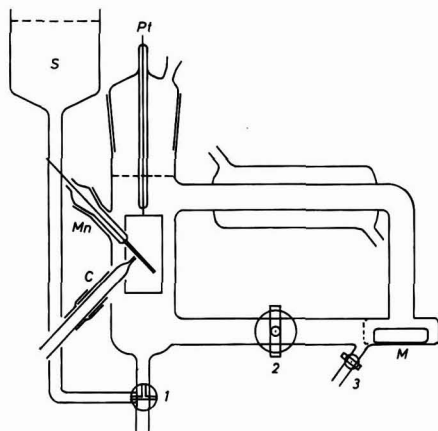


Fig. 1. Electrolytic cell with Mn, manganese electrode; Pt, platinum counter electrode; C, Haber-Luggin capillary; S, supply of electrolyte; M, magnetic stirrer. In order to renew the electrolyte, stopcock 2 was closed and stopcock 3 was opened. After removing from the cell about 2/3 of the electrolyte, stopcock 1 was opened to fill the cell.

tion whether an activation potential of the type first discovered by Flade (3) on iron can also be found on manganese. An attempt to clarify some of these problems is presented in this paper.

Experimental

Smooth manganese electrodes were produced by cathodic deposition of manganese on platinum wire electrodes from a solution of 1M MnSO_4 and 1M $(\text{NH}_4)_2\text{SO}_4$ adjusted to $\text{pH} = 2.2$ by addition of H_2SO_4 . The current density was 50 ma/cm^2 . The solution was kept at about 22°C .

Most of the experiments were performed in 0.5M orthophosphoric acid solutions which had been partially neutralized by addition of sodium hydroxide until the desired pH value was reached. All solutions were prepared from Merck analytical grade chemicals and triple distilled water.

The cell (Fig. 1) was designed to allow for effective renewal of the solution, which could be circulated by a magnetic stirrer. Experiments were performed at about 22°C .

A Wenking potentiostat was used in the potentiostatic circuit. Currents could be measured by feeding the voltage drop across a precision resistor to the input of a Cary 32 vibrating reed amplifier connected to a Siemens Linecomp recorder. The vibrating reed amplifier also served to determine time dependences of the potential in galvanostatic experiments. Potentials were measured *vs.* a saturated calomel electrode (SCE).

Results

Passivation.—The manganese could be passivated in phosphoric acid solutions by applying an anodic current density of several hundred ma/cm^2 . Passivation usually started from a certain point of the electrode apparently corresponding to the highest local current density and spreading from there over the rest of the electrode. During passivation a zone where permanganate and small bubbles of oxygen

were produced moved across the electrode surface replacing the zone where active manganese dissolved with hydrogen evolution. After completion of the passivation the electrode was covered by a brown deposit which was easily swept away on renewing the solution. In the solution free of manganese ions the manganese was kept potentiostatically at a potential in the region between the potentials of oxygen evolution and of activation. The metallic appearance of the manganese was retained even after days.

Polarization curves.—A polarization curve measured under potentiostatic conditions in 0.5M orthophosphate solution at $\text{pH} = 1.9$ one day after passivation is shown in Fig. 2. The Tafel line at noble potentials corresponds to oxygen evolution. The region of formation of permanganate at very high potentials was avoided during the experiments. At more negative potentials the current density was almost potential independent. Such behavior is characteristic of passive metals (4). The current density corresponding to the corrosion rate of the passive metal increased at lower potentials, and the manganese finally became active.

The points on the polarization curve were taken by changing the potential stepwise and waiting for 1 to 2 hr until the current density became approximately independent of time. Immediately after shifting the potential in the negative direction a cathodic current or an anodic current smaller than the steady-state current flowed. If the potential was made more noble, the anodic current at first was larger than in the steady state. These observations indicate that after a shift of the potential certain electric charges, which are large compared to those expected for charging the double layer capacity, are stored in the electrode and serve to change the thickness or the state of oxidation of the passive layer.

The potential independent corrosion rate of the passive manganese was still decreasing slowly after

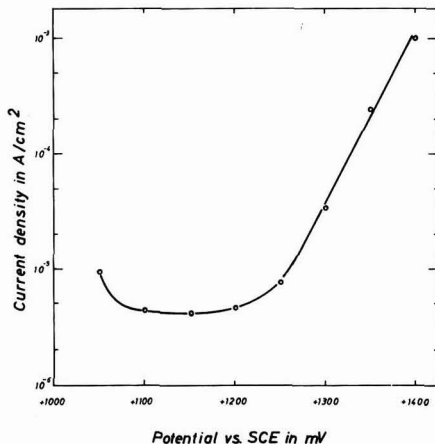


Fig. 2. Polarization curve of passive manganese in 0.5M sodium orthophosphate solution, $\text{pH} = 1.9$, measured after having maintained a potential of about $E_{\text{SCE}} = +1300$ mv for one day after passivation.

several days. The corrosion current densities found after four days were about $1 \mu\text{a}/\text{cm}^2$ at $\text{pH} = 1.0$ and about $0.1 \mu\text{a}/\text{cm}^2$ at $\text{pH} = 4$ (5). These values taken in unstirred solutions at 22°C were three to four times lower than the corrosion current densities at 42°C .

It was difficult for two reasons to evaluate the corrosion current density quantitatively: In rapidly stirred solutions the current densities were a few tenths of a $\mu\text{a}/\text{cm}^2$ larger than in unstirred solutions. This pH-independent, additional current density apparently resulted from the oxidation of traces of manganous ions, phosphorous acid, or hydrogen diffusing to the electrode. Although the diffusion current density must be quite small in unstirred solutions, measurements of the corrosion current density were made uncertain at high pH values where the corrosion is very slow. Another difficulty arose at low pH values close to $\text{pH} = 1$, where only a minimum of the current density and no region of potential independent current density was observed. The reason for this effect is that the pH dependence of the potential of activation (see section on The Flade potential of Mn) is much larger than the pH dependence of the oxygen evolution reaction. The corrosion current density at about $\text{pH} = 1$ must be evaluated from the deviations from the Tafel line at low current densities.

The Flade potential of manganese.—To determine the Flade potential of manganese Flade's original method (3a) of self-activation was used. The manganese was kept passive for at least several hours at a fixed potential. The potentiostatic circuit then was interrupted and the time dependence of the potential was recorded (Fig. 3). At first the rate of decrease of the potential slows down, increasing again after a certain point of inflection has been passed. The point of inflection was taken as the Flade potential. The Flade potential is a function of the pH value of the solution, and it is not signifi-

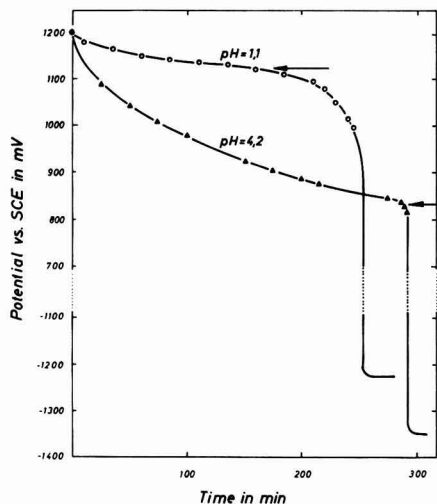


Fig. 3. Potential decay during self-activation of passive manganese in 0.5M sodium orthophosphoric acid solutions at different pH values.

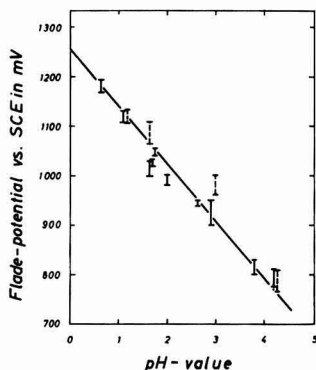


Fig. 4. Flade potential of manganese as a function of the pH value of sodium orthophosphoric acid solutions. (I) from potential decays; (II) from polarization curves.

cantly influenced by the prehistory of the electrode. From Fig. 4, the pH dependence of the Flade potential of manganese (vs. S.H.E.) can be described by

$$E_{F(\text{Mn})} = 1.50 - 0.118 \text{ pH} \quad [1]$$

The Flade potential, as determined by the galvanostatic method of self-activation, must be expected to coincide with the potential corresponding to the first increase of the anodic current density when measuring the polarization curve under potentiostatic conditions from noble toward less noble potentials. In fact, within the experimental limits the same values of the Flade potential have been measured by both methods.

Factors influencing potential decay.—A manganese electrode covered by manganese dioxide obtained by keeping the manganese passive in a solution containing manganous ions, exhibited the same Flade potential as a passive manganese electrode of metallic appearance. The manganese dioxide slows down the potential decay, but it does not affect the value of the point of inflection corresponding to the Flade potential. In Fig. 3 the potential decay shown for $\text{pH} = 1.1$ is characteristic for an electrode covered with a visible deposit of manganese dioxide, whereas the potential decay shown for $\text{pH} = 4.2$ is characteristic for the normal case of a clean passive manganese electrode.

The time of activation, the interval from interrupting the potentiostatic circuit until the Flade potential is reached, increases with increasing pH of the solution and with ennobling of the potential at which the manganese had been kept potentiostatically.

The potential of the point of inflection and the time of activation are influenced by additions of manganous ions or ferrous ions to the solution, or by cathodic currents. The action of manganous and ferrous ions was tested in the following way: The potential decay was observed in a solution containing no manganese ions. When the potential approached the region close to the Flade potential the solution was replaced by an almost identical solution, but containing some manganous or ferrous salt. Figure 5 shows that the potential of the point

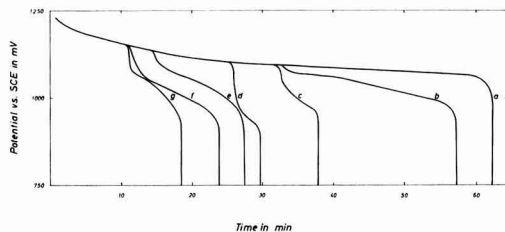


Fig. 5. Influence of reducing agents or cathodic currents on the potential decay during the activation of manganese in 0.5M orthophosphoric acid solution of pH = 1.95. a, normal potential decay; b, $c_{(\text{Mn}^{++})} = 10^{-5}\text{M}$; c, $c_{(\text{Mn}^{++})} = 10^{-4}\text{M}$; d, $c_{(\text{Mn}^{++})} = 10^{-3}\text{M}$; e, $j = -1.0 \mu\text{a}/\text{cm}^2$; f, $c_{(\text{Mn}^{++})} = 10^{-4}\text{M}$; g, $c_{(\text{Fe}^{++})} = 10^{-4}\text{M}$.

of inflection is made more negative than the Flade potential found in solutions free of Mn^{++} for concentrations $c_{(\text{Mn}^{++})} > 10^{-5}\text{M}$. The time of activation is markedly decreased.

Addition of Fe^{++} caused almost identical decay curves, if the Fe^{++} concentration was about one tenth of the Mn^{++} concentration. The same effects could be produced by applying cathodic currents. A current density of $1.0 \mu\text{a}/\text{cm}^2$ corresponded to about $c_{(\text{Mn}^{++})} = 10^{-4}\text{M}$, a current density of $10 \mu\text{a}/\text{cm}^2$ to about $c_{(\text{Mn}^{++})} = 10^{-3}\text{M}$.

Current impulses applied to the passive manganese during the potential decay should yield information on the state of oxidation of the passive layer. A linear relationship between the logarithm of the charge necessary to polarize the manganese to a given potential and the potential reached during the potential decay was observed (Fig. 6). If the potential decay had passed the Flade potential, the charge increased even more than exponentially. This is easily explained by the fact that the corrosion current density increases below the Flade potential. Only the difference of the applied current density to the corrosion current density can contribute to the charge stored in the passive layer.

If the pH value of the solution was suddenly changed during the potential decay, the potential

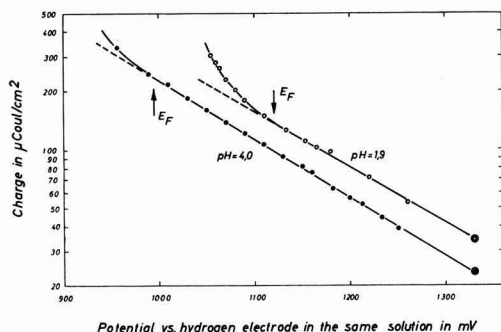


Fig. 6. Charge stored in the passive manganese as a function of the potential E_{HSS} vs. the hydrogen electrode in the same solution. By applying an anodic current density of $10 \mu\text{a}/\text{cm}^2$ the potential was brought back to $E_{\text{HSS}} = +1330 \text{mv}$. Curves are corrected by adding a charge Q_0 (dotted circle, circle within a circle) to the charges determined experimentally. Q_0 is the charge which would be necessary to shift the potential of the passive manganese from $E_{\text{HSS}} = +1330 \text{mv}$ further to $E \rightarrow +\infty$.

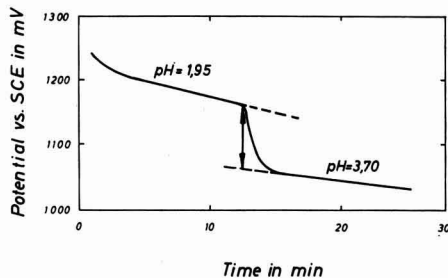


Fig. 7. Change of the potential of passive manganese in 0.5M orthophosphoric acid solution after replacing a solution of pH = 1.95 by a solution of pH = 3.70.

shifted by about $(\partial E/\partial \text{pH}) = -57 (\pm 5) \text{mv}$ (Fig. 7).

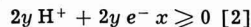
Influence of anions on the passivity of manganese.—Some experiments conducted at various phosphate concentrations between 0.1 and 1.0M and in orthoarsenic acid solutions did not show any effect on the behavior of the passive manganese.

It was very difficult to passivate or keep the manganese passive in acid sulfate, perchlorate, or acetate solutions. This is connected, evidently, with the fact that the manganous salts of these anions are extremely soluble. Experiments by Agladze *et al.* (1) have demonstrated that manganese is more and more easily passivated in sulfuric acid solutions at concentrations from 10 to 22N, where the solubility of manganous sulfate is relatively low.

Discussion

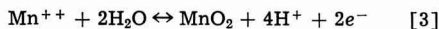
The experiments described above are in accord with the assumption that a continuous oxide layer governs the electrochemical behavior of passive manganese in a way similar to that known for other passive metals. The Flade potential, in particular, is determined by properties of the oxide layer. Therefore it has to be decided whether the Flade potential is an equilibrium potential or whether it is determined by kinetic parameters.

The pH dependence of the Flade potential given by Eq. [1] cannot be explained as an equilibrium potential between two oxides or between an oxide and the metal:



All reactions of the type given by Eq. [2] have equilibrium potentials with the same pH dependence of 59 mv/pH as the reversible hydrogen electrode.

If the Flade potential corresponds to an equilibrium potential at all, the reaction must involve twice as many hydrogen ions as electrons and, consequently, manganese ions from the solution. The most probable reaction of that type is given by Eq. [3]



An equilibrium involving trivalent manganese ions in the solution is highly improbable, since this ion is unstable in orthophosphoric acid solutions. The standard potential of reaction [3] is $E_N = 1.23\text{v}$ (6).

The Flade potential normalized to $pH = 0$ of $E_F = 1.50v$ would be the reversible potential of reaction [3] at a manganous ion activity of $10^{-4.5}M$. The Flade potential should depend on the manganous ion activity by $\partial E/\partial \log a_{(Mn^{++})} = -29 \text{ mv/decade}$. The effect found experimentally is about twice this value.

In addition, it is difficult to understand that the time of activation is considerably shortened by an increase of the manganous ion concentration. The manganous ions seem to act on the passive manganese as a reducing agent (7). This view is supported by the observation that the activation of passive manganese is affected by ferrous ions or by suitable cathodic currents in the same way as by manganous ions.

Very probably the Flade potential of manganese, as for iron, must be explained as resulting from the kinetics of dissolution of the passive oxide.

According to Vetter (2) the composition of an oxide at the oxide solution interface in solutions of different pH values is the same at equal potentials *vs.* the hydrogen electrode in the same solution. The conditions are that the oxide is a good electron conductor, and that the corrosion rate is small compared to the rate of exchange of oxygen ions between the oxide and the water of the solution. Both of these conditions are fulfilled: Oxygen evolution or any other redox reaction proceeds at normal overvoltages. Therefore the passive oxide must be a good electron conductor. Figure 7 shows that, on sudden change of the pH , the potential of the passive manganese responds by a potential change of about

$$(\partial E/\partial pH) = -RT/F \quad [4]$$

which is expected for an equilibrium between the oxygen ions in the oxide and in the water (2). No appreciable change of the state of oxidation can occur in the passive layer during this experiment.

Measured against the hydrogen electrode in the same solution the Flade potential of manganese is

$$E_{F(HSS)} = 1.50 - 0.059 \text{ pH (v)} \quad [5]$$

Relation [5] means that at the Flade potential the passive oxide is in a lower state of oxidation at high pH values than at low pH values. The results given in Fig. 6 verify this conclusion. More charge must be stored in the passive layer at high pH values than at low ones in order to oxidize the layer existing at the Flade potential to a given state of oxidation. The proportionality between the logarithm of the charge and the potential reached during the potential decay indicates that the charge is stored by changing the state of oxidation of the passive oxide rather than the thickness. A change of thickness at constant composition of the oxide would yield a linear relation between charge and potential (8). The charge is only a measure of the amount of the reduced oxide reoxidized during the anodic pulse. Nothing is known about the distribution of the concentrations as a function of time and of the distance from the oxide-solution interface, nor about the activity coefficients as a function of the composition of the oxide. Therefore an explanation

of the slope of the curve in Fig. 6 cannot be given without more experiments.

At the noble potentials where the manganese dioxide can exist thermodynamically. Since $\gamma\text{-MnO}_2$ can be reduced through a wide range of composition to $\alpha\text{-MnOOH}$ in a homogeneous phase (9), the reduced form of the oxide will be denoted as $MnOOH$ and the oxidized form as MnO_2 without excluding other possibilities. It follows from thermodynamic considerations that

$$\partial E_{(HSS)}/\partial \log \left\{ \frac{a_{(MnOOH)}}{a_{(MnO_2)}} \right\} = -RT/F \quad [6]$$

The ratio of the activities $a_{(MnOOH)}/a_{(MnO_2)}$ at the oxide solution interface should increase by one decade per pH at the Flade potential, as now can be concluded from Eq. [5]. Thus, the observed pH dependence of the Flade potential is caused by two effects, given by Eq. [4] and [6].

The kinetics of the dissolution of the passive oxide must be such that at noble potentials the oxide dissolves at a potential independent rate. If at less noble potentials a certain state of oxidation corresponding to the pH value of the solution is reached, the rate of dissolution increases as the potential is shifted into the negative direction. The mechanism of the reduction of manganese dioxide is not known sufficiently well. At potentials negative to the Flade potential of the manganese, a potential dependent reductive dissolution of manganese dioxide influenced by pH and composition of the oxide has been observed (9b, 10). This process may correspond to the increase of the corrosion rate of the manganese just below the Flade potential.

The activation of the passive manganese appears to be a process very similar to the activation of iron in neutral and alkaline solutions. The Flade potential, defined as the potential where the corrosion current density starts to increase when making the potential more negative, has a much greater pH dependence for iron in neutral and alkaline solutions than in acid solutions below $pH = 4$. The pH dependence of 59 mv/pH observed in acid solutions (3b) means that the Flade potential always corresponds to the same composition of the passive oxide. At $pH > 4$ the passive oxide on iron must be reduced more the higher the pH , in order to obtain a rate of the potential dependent, reductive dissolution exceeding the rate of the potential independent, nonreductive dissolution. In alkaline solutions at potentials negative to the Flade potential expected from the measurements in acid solutions, the passive layer has to be reduced from Fe_2O_3 to Fe_3O_4 almost completely before the actual Flade potential is reached at relatively negative potentials (11). Vetter and Klein (12) were able to detect the reduced form of the passive layer on iron in solutions of $pH = 4$ to $pH = 7$. At these low pH values the reduced form of the passive layer was found to dissolve very rapidly.

Acknowledgment

The author appreciates helpful discussions with Dr. H. Schurig of this Laboratory. Financial support

of the Arbeitsgemeinschaft Korrosion der Gesellschaft Deutscher Chemiker is gratefully acknowledged.

Any discussion of this paper will appear in a Discussion Section to be published in the December 1963 JOURNAL.

REFERENCES

1. a, W. J. Müller, *Z. Elektrochem.*, **10**, 518 (1904); b, G. Grube and H. Metzger, *ibid.*, **29**, 17 (1923); c, R. I. Agladze and G. M. Domanskaja, *Zhur. Priklad. Khim.*, **24**, 787, 915 (1951); d, R. I. Agladze and M. Ya. Gdzlishvili, *Elektrochim. Margantsa, Akad. Nauk Gruz. SSR*, **1**, 139 (1957); quoted in *C. A.*, **53**, 19625 (1959); e, R. I. Agladze and N. I. Khabaradze, *ibid.*, **1**, 235, 253, 279 (1957); quoted in *C. A.*, **54**, 100 (1960).
2. K. J. Vetter, *Z. Elektrochem.*, **66**, 577 (1962).
3. a, F. Flade, *Z. physik. Chem.*, **76**, 513 (1911); b, U. F. Franck, *Z. Naturforschung*, **4a**, 378 (1949).
4. K. J. Vetter, "Elektrochemische Kinetik," p. 608 ff, Springer (1961).
5. An analogous dependence has been observed on passive iron: K. J. Vetter, *Z. Elektrochem.*, **59**, 67 (1955).
6. K. H. Maxwell and H. R. Thirsk, *J. Chem. Soc.*, **1955**, 4054, 4057, with review of older literature.
7. A reaction of manganous ions with manganese dioxide was observed by J. M. Cowley and A. Walkley, *Nature*, **161**, 173 (1948).
8. a, D. A. Vermilyea, *Acta met.*, **1**, 282 (1953); b, K. J. Vetter, *Z. Elektrochem.*, **58**, 230 (1954); c, K. G. Weil, *ibid.*, **59**, 711 (1955).
9. a, H. Bode, A. Schmier, and D. Berndt, *Z. Elektrochem.*, **66**, 586 (1962), with review of older literature; b, J. Reynaud and J. Brenet, *Electrochim. Acta*, **6**, 1 (1962).
10. M. Fleischmann, H. R. Thirsk, and J. M. Tordesillas, *Trans. Faraday Soc.*, **58**, 1865 (1962).
11. K. E. Heusler, K. G. Weil, and K. F. Bonhoeffer, *Z. physik. Chem., N.F.*, **15**, 149 (1958).
12. K. J. Vetter and G. Klein, *ibid.*, **31**, 405 (1962).



The Electrochemical Society

INSTRUCTIONS TO AUTHORS OF PAPERS

(Revised as of 1/1/61)

Address all correspondence to the Editor,
JOURNAL OF THE ELECTROCHEMICAL SOCIETY,
30 EAST 42 St., New York 17, N. Y.

GENERAL

Manuscripts must be submitted in triplicate to expedite review. They should be typewritten, double-spaced, with 2½-4 cm margins.

Title should be brief, followed by the author's name and business or university connection. Authors should be as brief as is consistent with clarity and should omit introductory or explanatory material which may be regarded as familiar to specialists in the particular field. Proprietary and trade names should be avoided if possible; if used, they should be capitalized to protect the owners' rights.

Authors may suggest qualified reviewers for their papers, but the JOURNAL reserves the right of final choice.

TYPES OF ARTICLES

Technical Articles must describe original research of basic nature and must have adequate scientific depth. Articles of wide diversity of interest are appropriate, but subjects primarily covered in other specialized journals (e.g., analytical or nuclear chemistry) are not considered appropriate. An **Abstract** of about 100 words should state the scope of the paper and summarize its results. Suitable headings and subheadings should be included, but sections should not be numbered. Articles in recent issues of the JOURNAL should be consulted for current style.

Technical Notes are used for reporting briefer research, developmental work, process technology; new or improved devices, materials, techniques, or processes which do not involve more basic scientific study. No abstract is required.

Brief Communications are used only to report new information of scientific or technological importance which warrants rapid dissemination.

ILLUSTRATIONS

Drawings and Graphs ordinarily will be reduced to column width, 8.3 cm, and after such reduction should have lettering no less than 0.15 cm high. Lettering must be of letter-guide quality. India ink on tracing cloth or paper is preferred, but India ink on coordinate paper with blue ruling is acceptable. The sample graph shown on the reverse page conforms to suggestions of the American Standards Association (ASA Report Y15.1-1959).

Photographs should be used sparingly, must be glossy prints, and should be mailed with protection against folding. **Micrographs** should have a labeled length unit drawn or pasted on the picture.

Captions for figures (including photographs) must be included on a separate sheet. Captions and figure numbers must *not* appear in the body of the figure; they will be removed if they do.

Numerical Data should not be duplicated in tables and figures.

EQUATIONS

Mathematical Equations should be written on a single line if possible, and parentheses, brackets, the solidus (/), negative exponents, etc., may be used freely for this purpose. Authors are urged to consult Chapter VI of the "Style Manual" of the American Institute of Physics (available for \$1.00 at American Institute of Physics, 57 East 55 St., New York 22, N. Y.) and to follow the patterns described there.

SYMBOLS

If more than a few **Symbols** are used, they should be defined in a list at the end of the paper, with units given. For example:

$a, b \dots =$ empirical constants of Brown equation

$f_i =$ fugacity of pure i th component, atm

$D_v =$ volume diffusion coefficient, cm²/sec

ABBREVIATIONS

UNITS

POTENTIAL
SIGNS

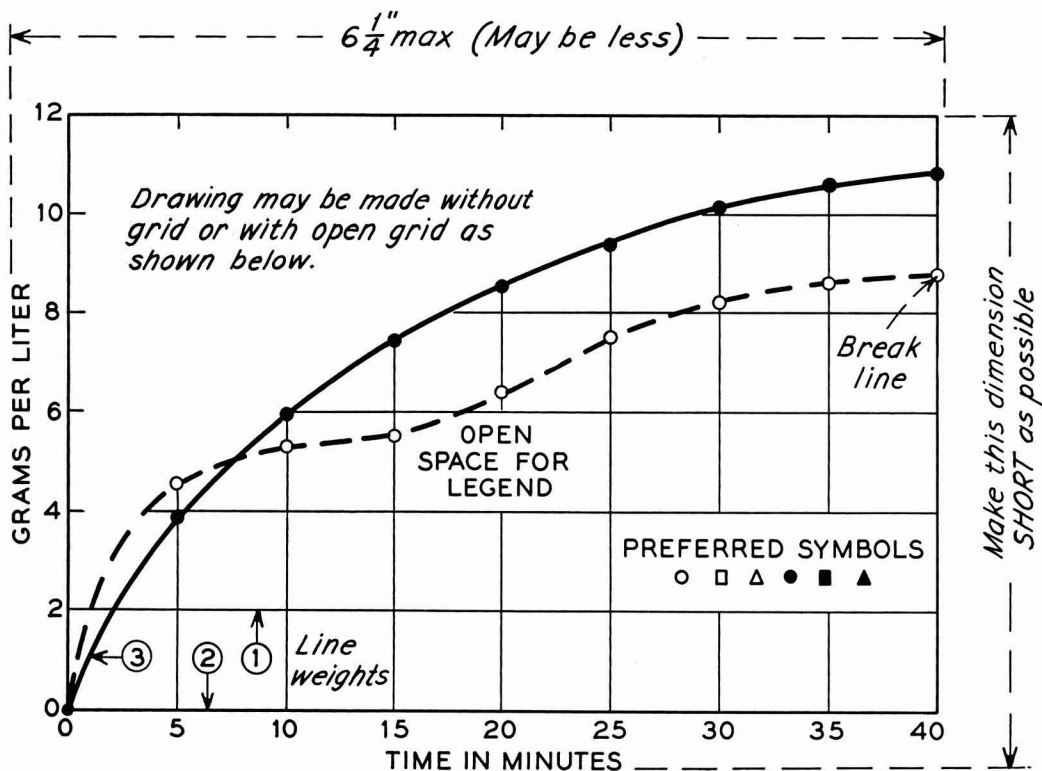
REFERENCES

The AIP "Style Manual" referred to here gives a suitable list of common *Abbreviations*. Units usually will be abbreviated without periods throughout the text, as sec, min, hr, cm, mm, etc.

Metric Units should be used throughout, unless English units are clearly more appropriate in the area of discussion.

Electrode Potentials: Authors are urged to state and make use of the polarity of test electrodes with respect to the reference electrode used, i.e., Zn is normally negative, Cu normally positive with respect to the standard hydrogen electrode. The sign for the emf of a cell should conform to the free energy change of the chemical reaction as written or implied, in accordance with the definition $\Delta G = -nFE$. These suggestions agree with the IUPAC conventions adopted in 1953. If any other convention is used, it should be stated clearly and used consistently throughout the manuscript.

Literature References should be listed on a separate sheet at the end of the paper in the order in which they are cited in the text. Authors' initials must be given, and the style and abbreviations adopted by *Chemical Abstracts* should be used. Any recent issue of the *JOURNAL* may be consulted.



Remarks: Line weight 2 is used for borders and zero lines. When several curves are shown, each may be numbered and described in the caption. Lettering shown is approximately $\frac{1}{8}$ in. In plotting current or potential as ordinate, increasing negative values should go down.

SAMPLE CURVE DRAWING FOR REDUCTION TO $\frac{1}{2}$ SIZE

The Electrochemical Society

Patron Members

Aluminum Co. of Canada, Ltd.,
Montreal, Que., Canada
International Nickel Co., Inc.,
New York, N. Y.
General Electric Co.
Capacitor Dept., Hudson Falls, N. Y.
Chemical Laboratory, Knolls Atomic Power
Laboratory, Schenectady, N. Y.
Chemical and Materials Engineering La-
boratory, Advanced Technology Labora-
tories, Schenectady, N. Y.
Chemistry Research Dept., Schenectady,
N. Y.
Direct Energy Conversion Operation, West
Lynn, Mass.
Lamp Division, Cleveland, Ohio
Materials & Processes Laboratory, Large
Steam Turbine-Generator Dept., Sche-
nectady, N. Y.
Metallurgy and Ceramics Research Dept.,
Schenectady, N. Y.
Olin Mathieson Chemical Corp.,
Chemicals Div., Industrial Chemicals
Development Dept., Niagara Falls, N. Y.
Union Carbide Corp.
Divisions:
National Carbon Co., New York, N. Y.
Union Carbide Consumer Products Co.,
New York, N. Y.
Westinghouse Electric Corp., Pittsburgh, Pa.

Sustaining Members

Air Reduction Co., Inc., New York, N. Y.
Ajax Electro Metallurgical Corp.,
Philadelphia, Pa.
Allen-Bradley Co., Milwaukee, Wis.
Allied Chemical Corp.
Solvay Process Div., Syracuse, N. Y.
General Chemical Div., Morristown, N. J.
Alloy Steel Products Co., Inc., Linden, N. J.
Aluminum Co. of America,
New Kensington, Pa.
American Metal Climax, Inc.
New York, N. Y.
American Potash & Chemical Corp.,
Los Angeles, Calif.
American Smelting and Refining Co.,
South Plainfield, N. J.
American Zinc Co. of Illinois,
East St. Louis, Ill.
American Zinc, Lead & Smelting Co.,
St. Louis, Mo. (2 memberships)
M. Ames Chemical Works, Inc.,
Glens Falls, N. Y.
Armco Steel Corp., Middletown, Ohio

Basic Inc., Maple Grove, Ohio
Bell Telephone Laboratories, Inc.,
New York, N. Y. (2 memberships)
Bethlehem Steel Co., Bethlehem, Pa.
(2 memberships)
Boeing Co., Seattle, Wash.
Burgess Battery Co., Freeport, Ill.
(2 memberships)
Burndy Corp., Norwalk, Conn.
Canadian Industries Ltd., Montreal,
Que., Canada
Carborundum Co., Niagara Falls, N. Y.
Consolidated Mining & Smelting Co. of
Canada, Ltd., Trail, B. C., Canada
(2 memberships)
Continental Can Co., Inc., Chicago, Ill.
Cooper Metallurgical Associates, Cleveland,
Ohio
Corning Glass Works, Corning, N. Y.
Diamond Alkali Co., Painesville, Ohio
Dow Chemical Co., Midland, Mich.
Wilbur B. Driver Co., Newark, N. J.
(2 memberships)
E. I. du Pont de Nemours & Co., Inc.,
Wilmington, Del.
Eagle-Picher Co., Chemical and Metals Div.,
Joplin, Mo.
Eastman Kodak Co., Rochester, N. Y.
Thomas A. Edison Research Laboratory, Div.
of McGraw-Edison Co., West Orange, N. J.
Electric Auto-Lite Co., Toledo, Ohio
C & D Div., Conshohocken, Pa.
Electric Storage Battery Co., Yardley, Pa.
Engelhard Industries, Inc., Newark, N. J.
(2 memberships)
The Eppley Laboratory, Inc., Newport, R. I.
(2 memberships)
Exmet Corp., Tuckahoe, N. Y.
Fairchild Semiconductor Corp., Palo Alto,
Calif.
FMC Corp.
Inorganic Chemical Div., Buffalo, N. Y.
Chlor-Alkali Div., South Charleston, W. Va.
Foote Mineral Co., Exton, Pa.
Ford Motor Co., Dearborn, Mich.
General Motors Corp.
Allison Div., Indianapolis, Ind.
Delco-Remy Div., Anderson, Ind.
Research Laboratories Div., Warren, Mich.
General Telephone & Electronics
Laboratories Inc., Bayside, N. Y.
(2 memberships)
Globe-Union, Inc., Milwaukee, Wis.
B. F. Goodrich Chemical Co.,
Cleveland, Ohio
Gould-National Batteries, Inc.,
Minneapolis, Minn.

(Sustaining Members cont'd)

- Great Lakes Carbon Corp., New York, N. Y.
Hanson-Van Winkle-Munning Co.,
Matawan, N. J. (2 memberships)
Harshaw Chemical Co., Cleveland, Ohio
(2 memberships)
Hercules Powder Co., Wilmington, Del.
Hill Cross Co., Inc., West New York, N. J.
Hoffman Electronics Corp., Semiconductor
Div., El Monte, Calif. (2 memberships)
Hooker Chemical Corp., Niagara
Falls, N. Y. (3 memberships)
HP Associates, Palo Alto, Calif.
Hughes Research Laboratories, Div. of
Hughes Aircraft Co., Malibu, Calif.
International Business Machines Corp.
New York, N. Y.
International Minerals & Chemical
Corp., Skokie, Ill.
International Resistance Co., Philadelphia,
Pa.
ITT Federal Laboratories, Div. of
International Telephone & Telegraph
Corp., Nutley, N. J.
Jones & Laughlin Steel Corp.,
Pittsburgh, Pa.
K. W. Battery Co., Skokie, Ill.
Kaiser Aluminum & Chemical Corp.
Div. of Chemical Research,
Permanente, Calif.
Div. of Metallurgical Research,
Spokane, Wash.
Kawecki Chemical Co., Boyertown, Pa.
Kennecott Copper Corp., New York, N. Y.
Leesona Moos Laboratories, Div. of Leesona
Corp., Jamaica, N. Y.
Libbey-Owens-Ford Glass Co., Toledo, Ohio
Lockheed Aircraft Corp.,
Missiles & Space Div., Sunnyvale, Calif.
Mallinckrodt Chemical Works, St. Louis, Mo.
P. R. Mallory & Co., Indianapolis, Ind.
Martin-Marietta Corp., Baltimore, Md.
Melpar, Inc., Falls Church, Va.
Merck & Co., Inc., Rahway, N. J.
Miles Chemical Co., Div. of Miles
Laboratories, Inc., Elkhart, Ind.
Minneapolis-Honeywell Regulator Co.,
Minneapolis, Minn.
Minnesota Mining & Manufacturing Co.,
St. Paul, Minn.
Monsanto Chemical Co., St. Louis, Mo.
M&T Chemicals Inc., Detroit, Mich.
National Cash Register Co., Dayton, Ohio
National Lead Co., New York, N. Y.
National Research Corp., Cambridge, Mass.
National Steel Corp., Weirton, W. Va.
North American Aviation, Inc., Rocketdyne
Div., Canoga Park, Calif.
Northern Electric Co., Montreal, Que.,
Canada
Norton Co., Worcester, Mass.
Owens-Illinois Glass Co., Toledo, Ohio
Pennsalt Chemicals Corp.,
Philadelphia, Pa.
Phelps Dodge Refining Corp., Maspeth, N. Y.
Philco Corp., Research Div., Blue Bell, Pa.
Philips Laboratories, Inc., Irvington-on-
Hudson, N. Y.
Pittsburgh Plate Glass Co., Chemical Div.,
Pittsburgh, Pa.
Potash Co. of America,
Carlsbad, N. Mex.
The Pure Oil Co., Research Center,
Crystal Lake, Ill.
Radio Corp. of America
Tube Div., Harrison, N. J.
RCA Victor Record Div., Indianapolis,
Ind.
Ray-O-Vac Co., Madison, Wis.
Raytheon Co., Waltham, Mass.
Remington Rand, Div. of Sperry Rand Corp.,
New York, N. Y.
Reynolds Metals Co., Richmond, Va.
Shawinigan Chemicals Ltd., Montreal, Que.,
Canada
Socony Mobil Oil Co., Inc.,
Dallas, Texas
Speer Carbon Co.
International Graphite & Electrode
Div., St. Marys, Pa.
Sprague Electric Co., North Adams, Mass.
Stackpole Carbon Co., St. Marys, Pa.
Stauffer Chemical Co., New York, N. Y.
Tennessee Products & Chemical Corp.,
Nashville, Tenn.
Texas Instruments, Inc., Dallas, Texas
Metals and Controls Corp.,
Attleboro, Mass.
Titanium Metals Corp. of America,
Henderson, Nev.
Udylite Corp., Detroit, Mich.
(4 memberships)
United States Borax & Chemical Corp.,
Los Angeles, Calif.
United States Steel Corp., Pittsburgh, Pa.
Universal-Cyclops Steel Corp.,
Bridgeville, Pa.
Upjohn Co., Kalamazoo, Mich.
Western Electric Co., Inc., Chicago, Ill.
Wyandotte Chemicals Corp.,
Wyandotte, Mich.
Yardney Electric Corp., New York, N. Y.

